VIRTUAL ENVIRONMENT FOR DYNAMIC AFM
Version 2.2

Comprehensive Manual

John Melcher, Daniel Kiracofe, Sudharsan Balasubramaniam, Shuiqing Hu, Steven Johnson, and Arvind Raman
School of Mechanical Engineering and Birck Nanotechnology Center
Purdue University, West Lafayette, IN 47907

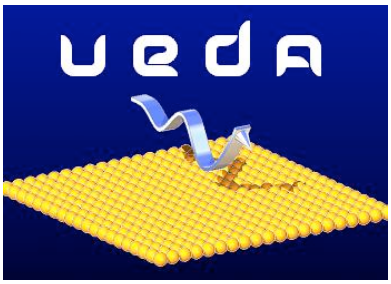

Copyright 2009-2020 John Melcher, Daniel Kiracofe, Shuiqing Hu, Steven Johnson, Arvind Raman

Contents

I. Why VEDA? 6

II. Basic concepts and terminology 8

A. Basic AFM design 8

B. Imaging modes 8

C. Excitation methods 10

D. Photodiode output 11

III. Tools 13

A. Amplitude Modulated Approach Curves (AMAC, basic) 13

1. Example 1: Attractive and repulsive regimes of oscillation 15
2. Example 2: Retraction curves 19
3. Example 3: Effects of viscoelastic damping in polymer samples 22

B. Amplitude Modulated Scanning (basic) 24

1. Example 1: Silicon trench 27
2. Example 2: Phase contrast in polymer blends 33
3. Example 3: Effects of adhesion, Jumps between regimes 38
4. Example 4: Effect of controller gains 44
5. Example 5: Controller Instability 44

C. Amplitude Modulated Approach Curves: Advanced 46

1. Example 1: Multiple impact regimes for a Biolever in liquid 49
2. Example 2: Bimodal excitation of a Biolever in a liquid environment 49
3. Example 3: Internal resonance of a stiff cantilever in air 53
4. Example 4: Bimodal excitation in air 55
5. Example 5: Phase spectroscopy in Bimodal AFM 57

D. Amplitude Modulated Scanning (Advanced) 59

1. Material Contrast in Bimodal AFM 60

E. Amplitude Modulated Approach curves, steady state solution 61

F. Frequency Sweep 62

1. Example 1: Examining the nonlinear resonance response of a microcantilever near HOPG in air 62
2. Example 2: Effect of sample Stiffness on non-linear response 64
3. Example 3: Sweep up versus sweep down 65

G. Force Distance Curves 67

1. Example 1: Approaching and retracting from a sample modeled using DMT contact 71
2. Example 2: Approaching and retracting from a sample modeled using JKR 72
3. Example 3: Approaching and retracting from a sample using Attard's model 73
H. Force Viewer 79
1. Example 1: DMT Model 79
2. Example 2: Viscoelastic Material Models 79
3. Example 3: Attard's model 83
I. FM Approach Curves 84
1. Approach to a Si facet in UHV 84
2. Approach to mica in liquid 87
J. FM Scanning 87
K. Contact Mode Scanning 88
1. Example 1: Tip-sample geometry convolution 88
L. Peak force tapping tool 88
1. Example 1: Peak force tapping on sinusoidal feature, modeled with Hertz contact 90
2. Example 2: Flat sample with two different materials, using Attard's model 90
M. Jump mode tool 91
N. Single point tool 91

IV. Theory 93
A. Models for tip-sample interaction 93
1. Piecewise linear contact 93
2. Piecewise linear attractive/repulsive contact 93
3. Hertz contact 95
4. Hertz contact conical tip 96
5. Derjaguin-Müller-Toporov (DMT) contact model 96
6. Derjaguin-Landau-Verwey-Overbeek electrostatic double layer forces 96
7. Johnson-Kendall-Roberts (JKR) contact model 97
8. Chadwick theory for thin membranes 98
9. Hertz contact with bottom effect correction for thin samples, (Dimitriadis et al, Gavara & Chadwick) 99
10. Lennard-Jones Potential + van der Waals 100
11. Viscoelastic contact models 101
12. Morse Potential 101
13. Long range electrostatic forces (noncontact) 101

14. Capillary forces 103
15. Molecular recognition forces: Worm like chain model 103
16. Solvation forces: conservative 104
17. Solvation forces: non-conservative 106
18. Magnetic dipole-dipole interactions 106
19. Tip-sample squeeze film damping 106
20. Surface Energy Hysteresis 107
21. Non-smoothness of the interaction force models 108
B. Tip samples interaction: Viscoelasticity 108
1. Viscoelasticity based on Linear Contact 109
2. Hertz contact based viscoelasticity, Kelvin-Voigt 111
3. Viscoelasticity conical tip 114
4. Maxwell viscoelasticity 114
5. Three element model 115
6. Generalized Maxwell Model. Prony Series 117
7. Dynamic elastic modulus 118
8. Spatial discretization models (Attard) 118
C. Models for cantilever dynamics 122
1. The equivalent point-mass model 122
2. Bernoulli-Euler beam model 124
3. The dispersion relationship and normal eigenmodes 125
4. The Galerkin discretization 127
5. The non-dimensional multiple degree-of-freedom model 129
6. The photodiode signal 129
7. Excitation sources and schemes 130
8. Self-excitation models (BETA testing) 132
9. Extensions to triangular and other non-standard geometries 133
D. Models for lock-in amplifiers and noise 133
E. Models for AM controller dynamics 134
F. Models for FM controller dynamics 135
G. Numerical integration scheme 136
H. Tip-sample geometry convolution 137
I. Energy outputs 137

V. How get help 140

VI. Changelog 141

VII. Acknowledgements 141

VIII. Appendix: Input parameters and options 142

IX. Appendix: Installing and Using VEDA on your local machine 151

A. Installing Rappture on your machine 151

B. Installing VEDA on your local machine: pre-compiled binaries 151

C. Installing VEDA on your local machine: Compiling from source 152

D. Using VEDA on your local machine 152

E. Running batch simulation / parameter studies 154

1. Running multiple jobs in serial on a single machine. 154

2. Running multiple jobs in parallel on several machines 155

X. Appendix: Using VEDA on a Windows Machine 156

A. Compiling the rappture libraries on Windows 156

B. Compiling VEDA on Windows 157

C. Using VEDA on Windows 158

References 159

I. WHY VEDA?

Since its debut in 1986, atomic force microscopy (AFM) invented by Rohher, Binnig et al. [1] has emerged as a powerful tool in nanotechnology. In particular, dynamic atomic force microscopy (dAFM) [2, 3] has proven to be an invaluable tool that has enabled the imaging, measurement and manipulation of matter at the molecular and atomic scale. As the ability for AFM to measure and manipulate properties at the nanoscale has increased, so too has the importance of understanding the tip dynamics as the oscillating AFM probe interacts with nonlinear tip-sample interaction forces [4–11]. Thus the topographic images generated in dAFM scans are actually a cumulative result of nonlinear interaction forces between the probe tip and the sample [4–11], cantilever probe mechanics [8, 12–14], tip-sample geometry convolution [15–18], and the AFM feedback control system [19–21]. Ultimately the limits of dAFM nanometrology depend on the ability to correctly "deconvolve" or eliminate such spurious effects in some manner. From an experimentalist's point of view, operating an dAFM can often be quite non-intuitive due to the underlying nonlinear dynamics. As a result the choice of operating conditions and cantilevers for a specific experiment can involve much trial and error. Where intuition fails, simulations can provide powerful insights into the fundamental physics of this instrument. With the aid of simulation tools like VEDA (Virtual Environment for Dynamic AFM), students and researchers can develop a deeper quantitative understanding of dAFM.

This document attempts to provide the user with the necessary information about the theory, modeling, and computational approach that are present in the VEDA simulation tools, and the inputs required to perform simulations. Additionally, several demonstration examples are provided that point out some of the nonlinear phenomena that underpin the operation of dynamic AFM. User are encouraged to use these examples as a starting point to explore the vast parameter space and variety of nonlinear phenomena present in dAFM.

VEDA [22, 23] currently includes many different tools. Each tools corresponds to a different type of AFM experiment. This includes

The F-Z Curves tool (FZC) uses the equations and solution procedure developed for the other Approach Curves tools to simulate an the mechanics of an undriven microcantilever approaching or retracting from a sample. This tool is useful for observing bi-stabilities in equilibria and the related "snap-in" and "pull-off" phenomena.

The Frequency Sweep tool (FS) simulates the nonlinear response of a driven cantilever swept across resonance. Simulations of single or multiple eigenmodes are possible.

Dynamic Approach Curves simulates an AFM cantilever excited near resonance and brought towards a sample surface. Several different versions are available: Amplitude modulation (i.e. tapping mode) and Frequency modulation. The AM tool has both a basic and advanced version. The basic tool is suitable for simulating either ambient conditions or ultra high vacuum (UHV). The advanced tool is an expanded version of the basic tool allowing both multiple eigenmode simulations as well as multiple excitation frequencies. This tool

is designed specifically for simulating approach/retraction curves in liquids, bimodal excitations, and internal resonance (harmonic cantilevers) applications. The model for cantilever dynamics includes a general number of eigenmodes and users are able to specify either acoustic (base) and magnetic excitation sources with single or multiple frequencies. The frequency modulated version simulates the situation where the AFM cantilever is excited at a frequency that is tuned to the nonlinear natural frequency through the use of a phase locked loop (PLL) and amplitude is maintained constant with an active feedback loop.

Scanning tools simulates scans over specified geometric features with heterogeneous material properties. Several different version are available corresponding to contact mode, amplitude modulated (i.e. tapping mode), and frequency modulation. Both basic and advanced versions of the Amplitude Modulated tool are also available, corresponding to the same feature sets as the basic and advanced Amplitude Modulated Approach Curves tools, respectively.

II. BASIC CONCEPTS AND TERMINOLOGY

In this section we will introduce basic AFM concepts and terminology for the benefit of beginning AFM users. Additionally, schematics are provided to illustrate relevant coordinates and reference frames.

A. Basic AFM design

A schematic of the standard AFM is shown in Figure 1. A microcantilever probe with a sharp tip (Figure 2) interacts with a sample. The position of the sample is controlled by a stage with piezo actuators. To create an image, the sample is moved so that the microcantilever probe tip rasters over the sample. The precise method by which an image of the sample's surface is generated from the raster depends on the imaging mode. However, in general, creating an image of the surface topography in AFM involves monitoring some characteristic measure (deflection, amplitude, phase, etc.) of the cantilever deflection caused by the interactions forces between the tip and the sample. Measurements of the microcantilever deflection have been made in a variety of ways. In the most common method, the optical-lever technique, a laser beam is reflected off of the cantilever and detected by a quadrature photodetector. For small deflections of the probe, signal of the photodetector is proportional to the change in slope (angle) of the microcantilever.

Components of the AFM along with relevant coordinates are shown in Figure 1. Simulations approaching the sample, either statically (F-Z curves) or with an oscillating probe are achieved through extensions of the Z-piezo to reduce the Z distance $Z(t)$. While the cantilever is approaching the sample, the stage is fixed (X_{scan} is constant). While cantilever is scanning over the sample, the stage moves the sample at a constant rate $X_{scan}(t)$ at a constant rate $V_{scan} = dX_{scan}(t)/dt$.

B. Imaging modes

There are myriad different AFM operating modes, all of which are built on the basic design above. These different modes have different strengths and weaknesses, and a particular task may be better served by one mode than another. A taxonomy of the major AFM modes is shown in Figure 3. There is a major division between static modes and dynamic modes. In dynamic modes, the cantilever probe is excited (typically at resonance) as it is scanned over the surface. In static modes, the probe is not excited. Within static modes, two of the major modes are contact mode and force-volume mode. In contact mode, the probe is essentially in contact with the sample at all times. In force-volume mode and the related jump mode, the probe touches a point, retracts, moves to the next point, approaches, and touches the next point. Both of these modes are built upon force-distance curves, also known as F-Z Curves. In dynamic modes, two of the main modes are amplitude modulated (AM) and frequency modulated (FM). These names can be confusing because in both AM and FM modes a feedback controller is used to keep the vibration

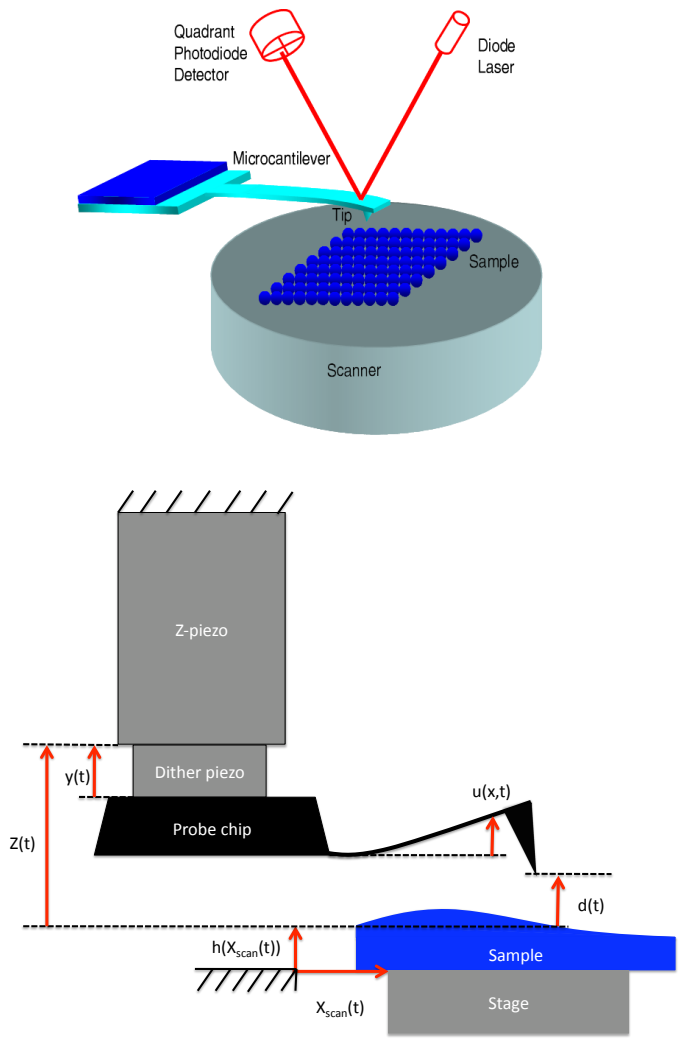

FIG. 1: A schematic of basic AFM operation (top [24]) and important coordinates (bottom). The Z-piezo expands or contracts in order to modify the Z distance $Z(t)$. The dither piezo is used to excite the cantilever by shaking the base (acoustic excitation) by $y(t)$. The transverse deflection relative to the base is $u(x,t)$, where x is the axial displacement from the base. Scanning is achieved by varying $X_{scan}(t)$ by a constant scanning velocity $V_{scan} = X_{scan}(t)/dt$. The instantaneous gap between the tip and the sample is $d(t) = Z(t) + y(t) + u(L,t)$, where the Z distance $Z(t)$ is modified by the Z-piezo extension/displacement or variations in the sample height $h(t)$.

amplitude constant during a scan. In AM mode, the height of the probe above the sample is what is used to keep the vibration amplitude constant, while in FM mode, a more complicated feedback scheme is used that attempts to keep the oscillation amplitude, phase, and frequency shift constant while scanning the sample.. These feedback schemes are described in more detail in Section IV.

A diagram of the operation of contact mode, AM, and FM modes is shown in Figure 4. Note that FM-AFM (Figure 4b) is shown scanning far away from the sample to indicate operation in the attractive regime, and that AM-AFM (Figure 4c) is shown closer to the sample to indicate intermittent contact or repulsive regime. Although this is usually the way the two modes are used in practice, it is not the distinguishing characteristic. AM-AFM can be used in the

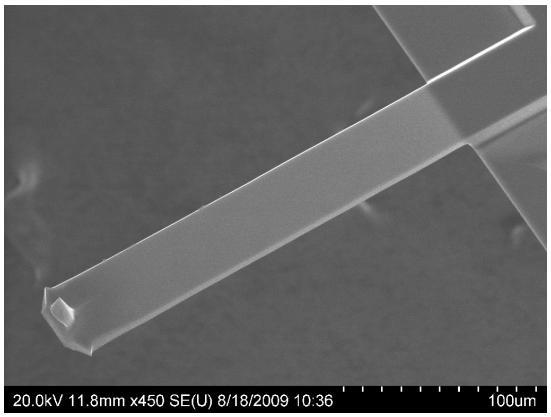

FIG. 2: SEM image of a typical AFM cantilever. The imaging tip is in the lower right.

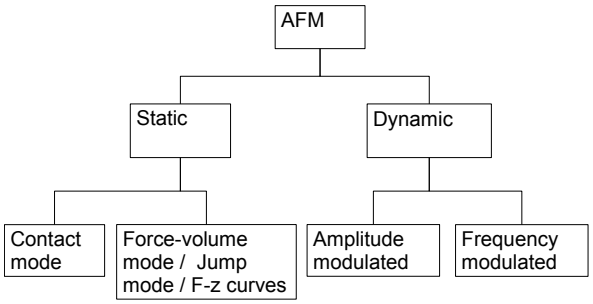

FIG. 3: A taxonomy of some major AFM modes.

attractive regime and FM-AFM can be used in the repulsive regime. The distinguishing characteristic between the two modes is the feedback scheme.

VEDA was originally written with AM-AFM in mind. Later expansions have allowed simulations of F-Z/F-d Curves and FM methods.

C. Excitation methods

With dynamic modes, there are many different methods by which the cantilever can be vibrated. Two of the most common are acoustic mode and magnetic mode. Figure 5 shows these two methods schematically. In the magnetic mode, a magnetic coating (or magnetic particles) is applied to the cantilever and a solenoid provides an alternating magnetic field that drives the cantilever. In acoustic mode, a so-called dither piezo vibrates up and down. which moves the base of the cantilever up and down. Note that due to the readout scheme used in most AFMs, the absolute deflection of the cantilever cannot be accessed but only the deflection relative to the base (bending). This can cause

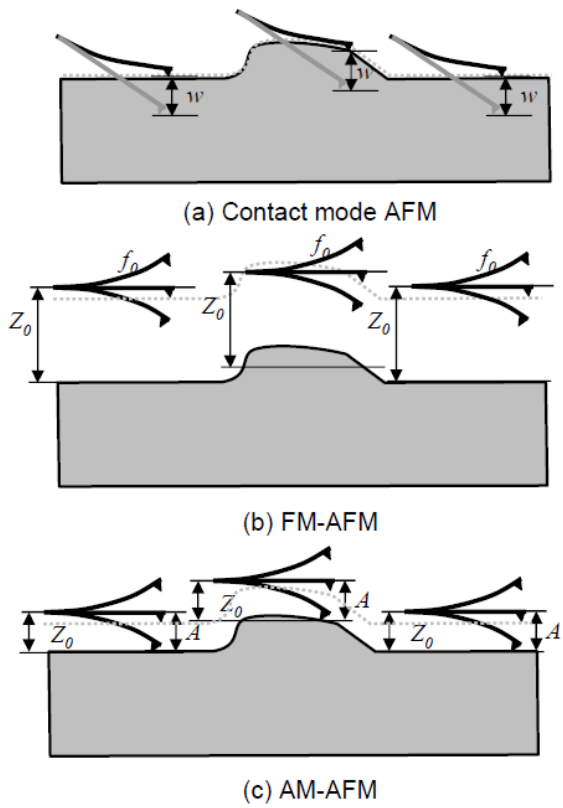

FIG. 4: Schematic diagrams of the operation mechanisms for (a) contact mode AFM, (b) FM-AFM, and (c) AM-AFM. Taken from [24]

significant complications for acoustic mode in low Q (e.g. liquid) operation. More details on the difference between these excitations can be found in [25]

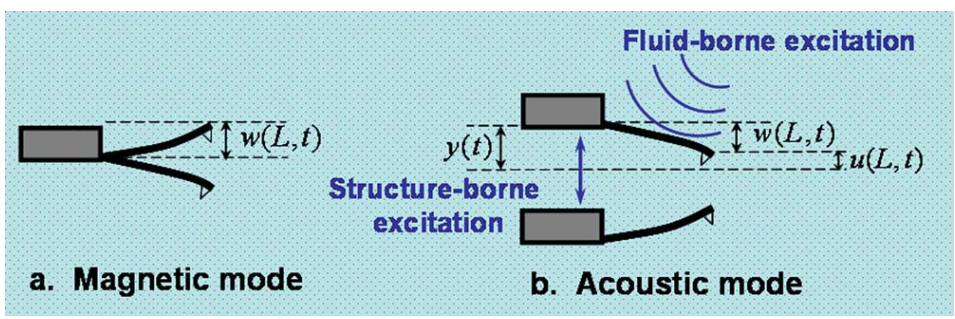

FIG. 5: A schematic showing the different tip motions measured in the magnetic mode and acoustic mode. In magnetic mode the measured tip motion is the absolute tip motion $w(x,t)$. While in the acoustic mode the measured motion $w(x,t)$ (transverse cantilever deflection) is the motion $u(x,t)$ relative to the base motion $y(t)$. Reproduced from [25]

D. Photodiode output

In this section, we demonstrate why the photodiode is more sensitive to slope than displacement.

In 6, we see that if a flat mirror is moved down, the laser spot will move on the photodiode. Similarly, if a flat

mirror is rotated, the laser spot will move on the photodiode. Now for a cantilever, there will be some displacement at the end and some slope. There will be contributions from both. But which is more sensitive?

The static bending shape of a cantilever is given by $g(x) = 1 - 0.5(x/L)^2(3(x/L))$, where L is cantilever length. This means that the slope $g'(L) = -1.5/L$. In other words, for a bending displacement of h, the cantilever has a slope at the end of $1.5h/L$, which means the rotation angle is $d\theta = \arcsin(1.5h/L)$. Because the angles are small, $\sin(d\theta) \approx d\theta$. So, for bending displacement of h, the laser spot moves $H * 2 * 1.5h/L$.

For example assume H = 1 cm, θ=45 deg, h=1e-9, L=100e-6 Then the displacement contribution to spot movement is 1.4e-9 = 1.4 nm and the rotation contribution is H*2*1.5h/L = 2e-7 = 200 nm. In other words, the displacement contribution is less than 1 percent of the rotation contribution. For this reason, we typically ignore the displacement contribution.

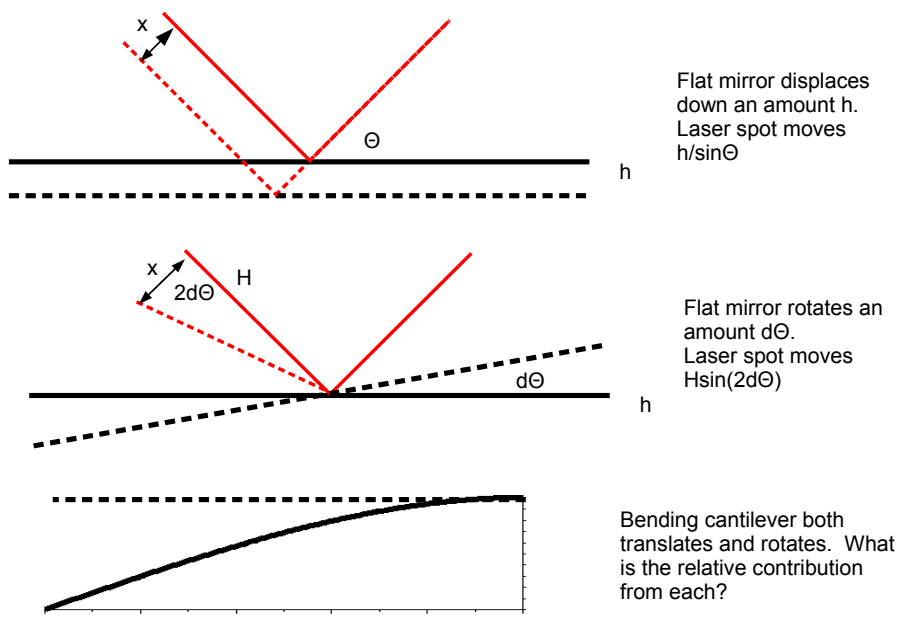

FIG. 6: A schematic explaining why the photodiode measures slope and not true deflection

III. TOOLS

A. Amplitude Modulated Approach Curves (AMAC, basic)

At the backbone of dAFM is the assumption that the microcantilever's oscillations are affected by nonlinear interactions between the tip and sample. In particular, in AM-AFM, the amplitude of the microcantilever is affected by of both attractive and repulsive forces interactions between the tip and the sample. This occurs primarily because of the detuning on the nonlinear natural frequency from the fixed excitation frequency as the probe approaches the sample. However when the oscillation amplitude is much smaller than the decay length of the interaction forces, there is also a shift in linear frequency of the oscillator which can reduce the driven oscillation amplitude. Monitoring characteristics of the microcantilever's oscillation while approaching a sample reveals information about the mechanical properties of the sample and of tip-sample interaction (imaging) forces. Additionally, an appropriate set-point amplitude for use in AM-AFM scanning (and simulated by the AMS tool) can be determined. The Amplitude Modulated Approach Curves (AMAC) tool can be utilized to simulate the response of a microcantilever excited near it's fundamental resonance and gradually introduced to the sample by extending the Z-piezo and reducing the Z distance between the base and the sample. Input parameters for AMAC (basic) include the properties of the cantilever and the tip-sample interactions, as well as operating conditions and simulation parameters.

The following assumptions have been made in the AMAC tool (in addition to the assumptions made in the models):

1. Cantilever dynamics are modeled by a single eigenmode model (Eq. 101 for $i = 1$).
2. Interactions between the tip and the sample are modeled by any one of the models given in Sec. IV A.
3. The cantilever is either acoustically or magnetically excited with a single frequency.
4. The Z distance between the sample can be reduced or increased, but the cantilever does not move laterally. Inertial and hydrodynamic forces caused by the Z motion are negligible.

This section provides an overview of the outputs of the Amplitude Modulated Approach Curves (AMAC) tool in the form of three example simulations.

TABLE I: Input parameters for AMAC examples.

PARAMETER	EXAMPLE 1	EXAMPLE 2	EXAMPLE 3
Operating conditions and cantilever properties			
Unconstrained amplitude (nm)	30	30	60
k (N/m)	40	40	3
Q	400	400	150
f (kHz)	350	350	75
f_d (kHz)	350	350	75
Z approach velocity (nm/s)	200	200	200
Z range Determination	Autocalc	Specify	Autocalc
Initial Z separation (nm)	NA	0	NA
Final Z separation (nm)	NA	35	NA
Tip-sample interaction properties			
Tip-sample interaction model	DMT contact	DMT contact	Hertz contact
Tip radius (nm)	20	20	10
Young's modulus of tip (GPa)	130	130	130
Poisson's ratio of the tip	0.3	0.3	0.3
Auto calculate intermolecular distance?	no	no	n/a
Intermolecular distance (nm)	0.164	0.164	n/a
Hamaker constant (J)	$7.1 \cdot 10^{-20}$	$7.1 \cdot 10^{-20}$	n/a
Young's modulus of sample (GPa)	1.2	1.2	1
Poisson's ratio of the sample	0.3	0.3	0.3
Sample visco-elastic forces?	none	none	Kelvin-voigt
Sample viscosity ($Pa \cdot s$)	NA	NA	500
Simulation parameters			
Number of points plotted	500	500	500
Deflection points per cycle	400	1000	1000
Include time histories	yes	no	yes
Number of time histories	1	NA	1
Choose amplitude ratio(s)	0.55	NA	0.55
Number of cycles	5	NA	5
Choose X-axis variable	Z-distance (nm)	Z-distance (nm)	Z-distance (nm)

1. Example 1: Attractive and repulsive regimes of oscillation

In this example, two different regimes of oscillation are explored. The attractive regime refers to oscillations where the interaction forces between the tip and sample are primarily attractive. Likewise, the repulsive regime refers to oscillations where the interactions with the sample are primarily repulsive contact forces. Proper identification of the attractive and repulse regimes is critical for an AFM experimentalist for improving imaging resolution, avoiding imaging bi-stabilities and correctly interpreting of phase contrast images. This first example is aimed at reproducing some of the key results from Garcia and San Paulo [5].

After opening VEDA, select *Amplitude Modulated Approach Curves (basic)* from the pull-down menu labeled *Application*. Once the interface for the AMAC tool is loaded, there is a second pull-down menu titled *Example loader*. Select *Example 1: Attractive and repulsive regimes of oscillation* and the inputs for this example listed in Table I will be loaded automatically into the interface. Take a moment to peruse the three input panels.

The first tab is *Operating conditions and cantilever properties* and it contains the following input parameters:

Unconstrained amplitude this is the amplitude when the cantilever is very far from the sample, sometimes called free amplitude or initial amplitude.

k (N/m) represents the cantilever stiffness of the fundamental eigenmode.

Q represents the quality factor of the resonance. The quality factor is a measure of the sharpness of the resonance peak and is easily determined experimentally from a frequency sweep or "tuning curve".

Nat. Freq (kHz) represents the fundamental natural frequency in kilohertz.

Driving Freq. (kHz) represents the drive frequency, or excitation frequency applied by the excitation source (acoustic or magnetic) to the microcantilever.

Z approach speed (nm/s) represents the average speed of the Z piezo (i.e. the speed at which the base of the microcantilever approaches the sample) in nanometers per second.

Z range determination allows a few different options to specificy the initial and final Z displacements of the base of the microcantilever. For the purposes of this example, the autocalculated values will be fine (in this case it will 5 nm above where the tip contacts the sample, which is Z=35 nm because the unconstrained amplitude is 30 nm)

The second tab is *Tip-sample interaction properties*. There are several input parameters on this tab; however, the user required only to input parameters relevant to the choice of tip-sample interaction model. In this example, we choose the DMT contact model, which is selected from the pull-down menu at the top of this panel. The DMT contact model requires the following inputs:

Tip radius (nm) represents the radius of the cantilever tip, in nanometers, which will come into contact with the sample.

Young's modulus of tip (GPa) represents the stiffness of the elastic tip material. More precisely, the Young/s modulus is a relationship between stress and strain for an elastic element according to Hooke's law. For silicon (Si), $E \approx 130$ GPa.

Poisson's ratio of the tip represents the Poisson's ratio of the material used in the cantilever's tip. This parameter is used in all tip-sample interaction models except for the two linear-contact models. The Poisson's ratio is a material property that relates a uniaxial strain induced in a specific direction due to a stress applied in the orthogonal direction.

Auto calculate intermolecular distance gives the user the opportunity to have the intermolecular distance a_0 automatically calculated. If the box is checked ("yes"), a_0 will be calculated for the DMT and DMT+DVLO models using the van der Waals adhesion force, the tip radius, and the Hamaker constant. If unchecked ("no"), the van der Waals adhesion force will be calculated from a_0, the tip radius, and the Hamaker constant. This option is provided solely for convenience. In either case, the component of the adhesion resulting from the van der Waals forces is $F_{ad,vdW} = HR/6a_0^2$ (see tip-sample interaction models in the theory in Section IV A).

van der Waals adhesion force (nN) represents the component of adhesion force, measured in nanonewtons, attributable to attractive van der Waals forces. If the DMT contact model is applicable, the adhesion forces is the "pull-off" force that can be found experimentally from a static force-distance curve

$$F_{ad} = |k_c \times w^*|, \tag{1}$$

where k_c is the static bending stiffness of the cantilever, and w^* is the deflection of the tip at the "pull-off" location as the cantilever is withdrawn from the surface.

Hamaker constant (J) represents the value used to predict the attractive van der Waals forces between the tip and the sample. This parameter depends on the material of both the tip and the sample, as well as the surrounding material.

Young's modulus of the sample (GPa) represents the stiffness of the sample material.

Poisson's ratio of the sample: see Poisson's ratio of the tip above.

Solvation forces this is applicable only for liquids, and thus is not relevant to this example.

Nonconservative forces Allows users to include non-conservative interaction forces between the tip and the sample. Non-conservative dissipate mechanical energy of the probe during interaction. This example does not call for including such forces.

The third and final tab is *Simulation parameters*, which contains input parameters relating to the simulation, but not the physics of the problem. Relevant inputs in this example are:

Number of points plotted: This is the number of points contained in each plot. This values of this parameter may be increased if the user is interested in abrupt features in the results.

Speed versus accuracy tradeoff: This controls the number points that the differential equation solver computes in each drive cycle. Using more points will give a more accurate result, but will take longer to compute.

Include time histories: The default outputs of VEDA are quantities such as amplitude and phase that are averaged over several drive cycles (similar to a real AFM). This option allows the user to examine the raw data of each individual cycle (similar to hooking up an oscilloscope to the AFM and viewing the raw voltage traces).

Choose X-axis variable: Choose whether to plot simulation data against Z distance or against amplitude ratio (A_1/A_0)

After reviewing that the input parameters, click on the Simulate button. The simulation results for the input parameters are available by selecting a result from the pull-down menu once the simulation has concluded. The following provides a brief discussion of each result.

A few minutes after pressing the simulation button, the plot in Figure 7 should appear. Simulations running much longer than a few minutes are likely due to erroneous or non-physical input parameters. If these occurs even though the inputs parameters are correct, please submit a support ticket by selecting the Help! button.

Figure 7 shows that, as the cantilever approaches the sample from right to left, there is first a reduction in amplitude due to the attractive van der Waals interaction [5]. This reduction is due to the attractive interaction forces detuning the nonlinear resonance frequency of the probe tip from the fixed excitation frequency. This detuning also causes the phase of the first harmonic to increase above 90 degrees, as shown in Figure 8. The onset of repulsive regime is marked by a jump in amplitude and corresponding jump in phase to a value less than 90 degrees.

While approaching the sample, the first harmonic phase first increases about 90 degrees in the attractive regime of oscillations due to the softening of the nonlinear natural frequency. At this point, the nonlinear natural frequency has been detuned (decreased in this case) from the fixed excitation frequency applied to the probe. This results in a phase greater than 90 degrees. Continuing to approach the sample, a jump from the attractive to the repulsive regime occurs at a Z distance around 27 nm. This jump is marked by a phase less than 90 degrees in Figure 8. In the repulsive regime, the nonlinear natural frequency stiffens, and is now greater than the fixed excitation frequency applied to the probe. If the user repeats the simulations for an excitation frequency f_d not equal to the natural frequency f (say 200 Hz above or below) the results will be slightly different because the detuning effects of the attractive and repulsive regimes will accomplish different results.

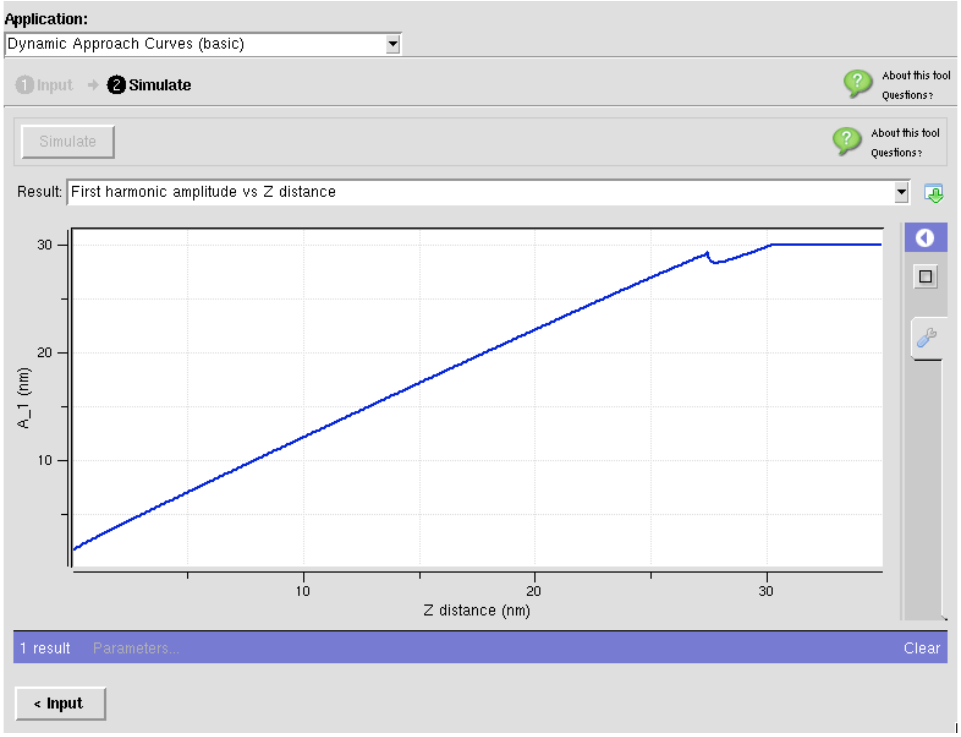

FIG. 7: Amplitude of the first harmonic vs. Z distance during approach to the sample. The abrupt change in amplitude marks the transition from the attractive to the repulsive regime of oscillations. (AMAC Ex 1)

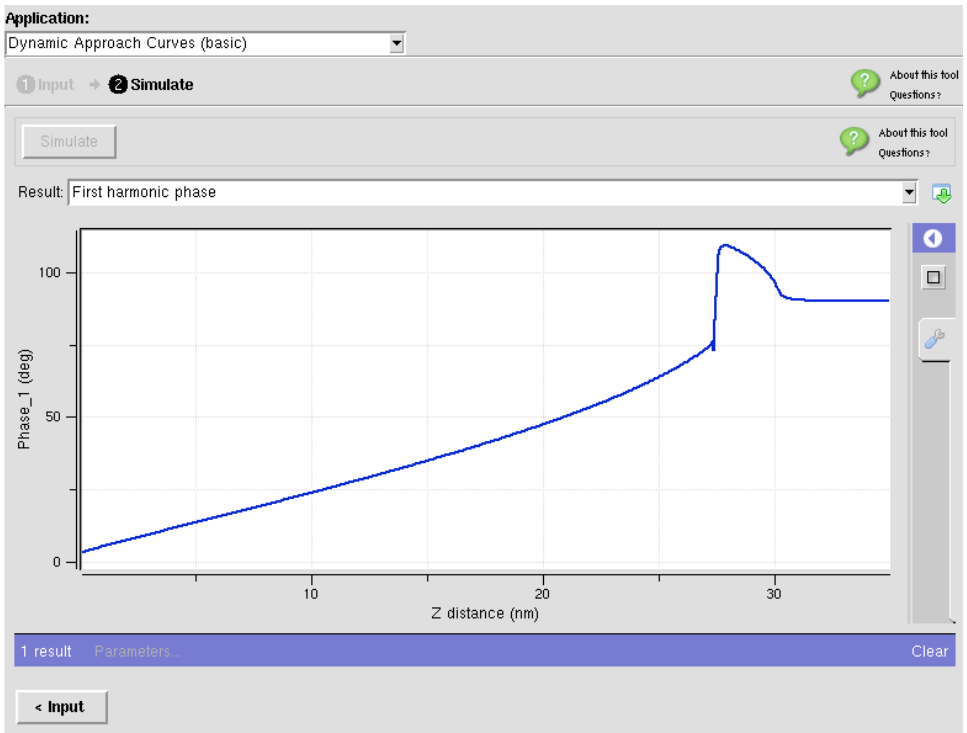

FIG. 8: Phase of the first harmonic vs. Z distance during approach to the sample. A phase greater than 90 degrees indicates the attractive regime while a phase of less than 90 indicates the repulsive regime. (AMAC Ex 1)

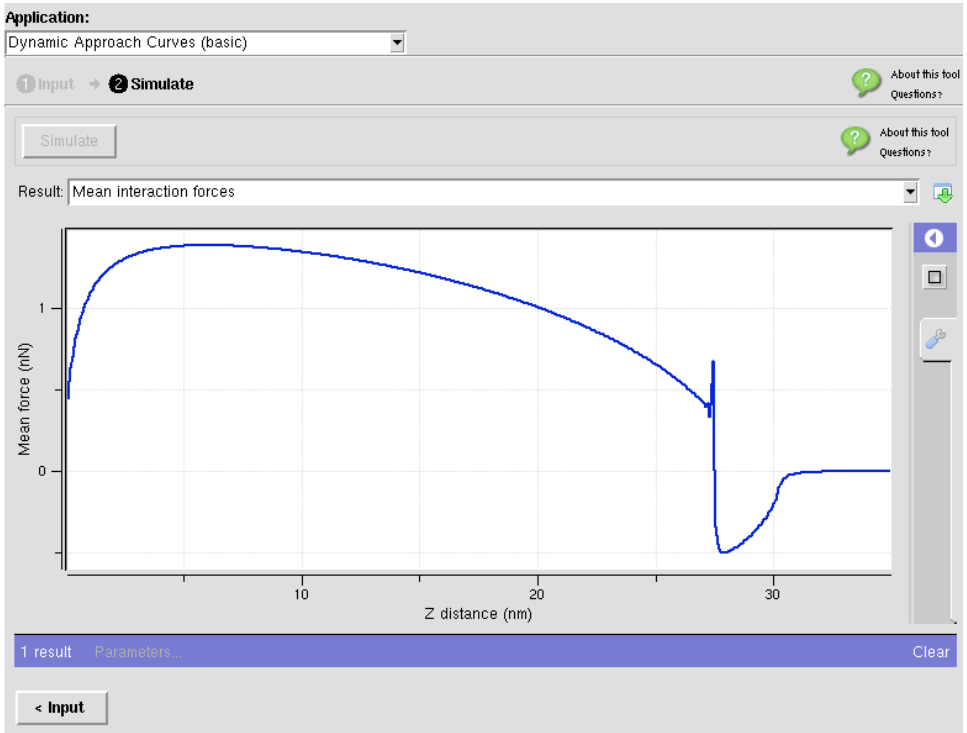

FIG. 9: Mean (oscillation cycle averaged) tip-sample interaction forces during approach. Mean forces are negative in the attractive regime and positive in the repulsive regime. (AMAC Ex 1)

As the cantilever proceeds through the attractive regime, there is eventually a sharp change in amplitude as the probes transitions from the attractive to the repulsive regime. By comparing the mean forces (Figure 9) to the amplitude (Figure 7) and phase (Figure 8), the user will find that the jumps in amplitude and phase occur precisely when the mean forces change abruptly from negative (attractive) to positive (repulsive). In this example, the change occurs around Z = 27 nm. Hence, the two regimes have been dubbed the attractive regime and the repulsive regime according to the mean interaction force observed during oscillation.

Figure 10 contains a sample of photodiode deflection signal $u_p(t)$ and interaction force histories containing five complete cycles. The histories shown in Figure 10 correspond to 1000 points per cycle. This number is likely to be sufficient for most simulations. To accurately record very small time-scale interactions, however, the user may wish to increase the value of the parameter. It is important to note that the tip-sample interactions are not directly measured in dAFM.

2. *Example 2: Retraction curves*

In this example, we investigate the tip dynamics during cantilever retraction from the surface. The cantilever/sample parameters used are the same in AMAC Example 1 (Section III A 1). Retraction curves are particularly interesting when the approach curves show a discontinuous amplitude jump from attractive to repulsive regimes of oscillation. In fact it can be shown [5] that there is a noticeable amplitude hysteresis between approach and retraction curves.

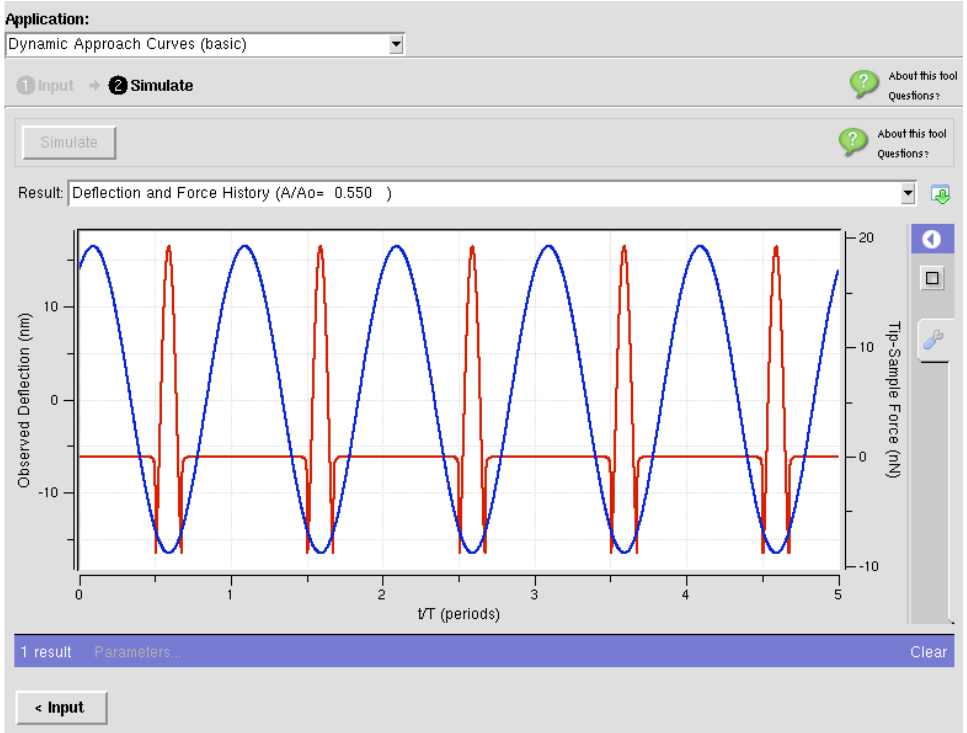

FIG. 10: Deflection signal from the photodiode accompanied by the corresponding tip-sample interaction force (setpoint = 0.55 %). (AMAC Ex 1)

We recommend completing AMAC Example 1 before proceeding to this example so the user can will be able to study the hysteresis due to the bi-stable oscillation regimes. The physical parameters, such as the cantilever properties and tip-sample interaction parameters, of this simulation are identical to the first example; however, we have changed the operating and simulation parameters to simulate retraction from the sample. The retraction is achieved by changing *Z range determination* to *Specify Z range* and change the initial Z separation to 0 nm and the final Z distance to 35 nm. The default Z range for the simulation is from 5 nm greater than the unconstrained amplitude (30 nm) to 0 nm. For this simulation we have simply inverted the default Z range.

If you have not already run AMAC Example 1, then follow these instructions: open the **AMAC** (basic) tool from the **VEDA** tools selection. Wait for the user input window to open. Under the *Operating conditions and cantilever properties* tab, set the *Unconstrained amplitude (nm)* to 30, and set k_i *(N/m)* to 40. Change Q to 400, change both f *(kHz)* and f_d *(kHz)* to 350, and change *Z approach velocity (nm/s)* to 200. Next, click the *Tip-sample interaction properties* tab. Under this tab, be sure that the *Tip-sample interaction model* is *DMT contact*. Change the rest of the input parameters under this tab and under the *Simulation parameters* tab to match those shown in Table I Example 2. Once all of the inputs have been correctly modified, click the *Simulate* button in the lower right-hand corner. This simulation generally takes about 4 minutes to run to completion.

The results of the retraction simulation are shown in Figures 11-13. We find that there is noticeable amplitude and phase hysteresis for Z distances between 27 to 30 nm. If the simulations for approaching the sample and retracting

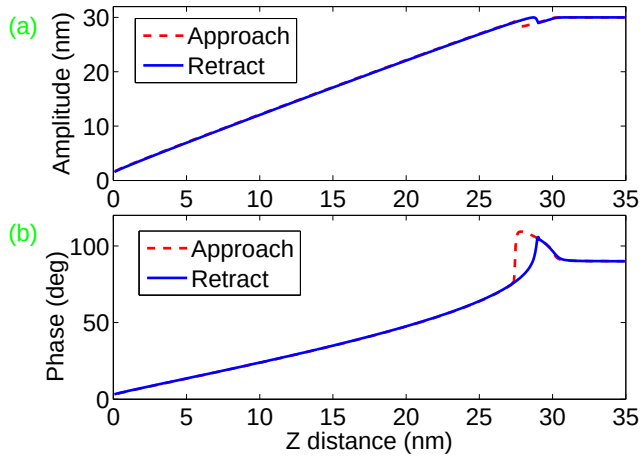

FIG. 11: (a) Amplitude (nm) vs. Z distance for retraction. The jump between attractive and repulsive regime oscillations occurs at a slightly different location when retracting from the sample. (b) Phase (deg) vs. Z distance for retraction from the sample. (**AMAC** Example 2)

from the sample are performed successively, the user will be able to plot both sets of results for comparison. We encourage users who are interested in hysteresis to download the actual data for plotting purposes.

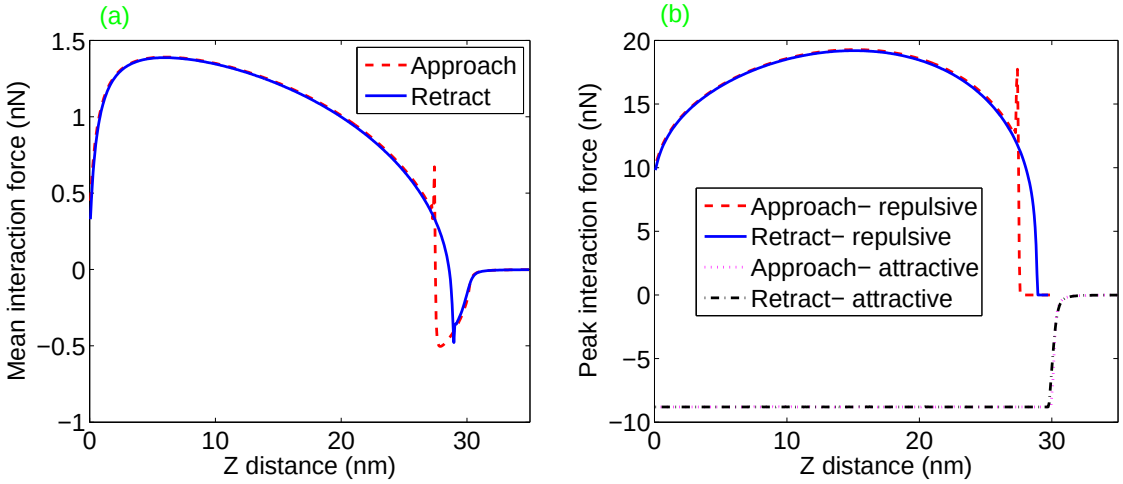

FIG. 12: (a) Mean interaction force (nN) vs. Z distance (nm) while retracting from the sample. (b) Peak attractive and repulsive interaction forces (nN) vs. Z distance (nm) while retracting from the sample. (**AMAC** Example 2)

Important note: For these operating parameters there is a range of Z distances where there are two amplitude branches, hence the hysteresis. If the user is interested in studying approach/retraction hysteresis, the cantilever must start in the repulsive regime during retraction curves and the attractive regime during approach. In this simulation, the initial Z separation was chosen to be 0 assuring with a high degree of confidence that the cantilever will start in the repulsive regime. This is confirmed in Figure 12. Had we chosen an initial Z separation closer to 25 nm, where there are two amplitude branches, this may not have been the case.

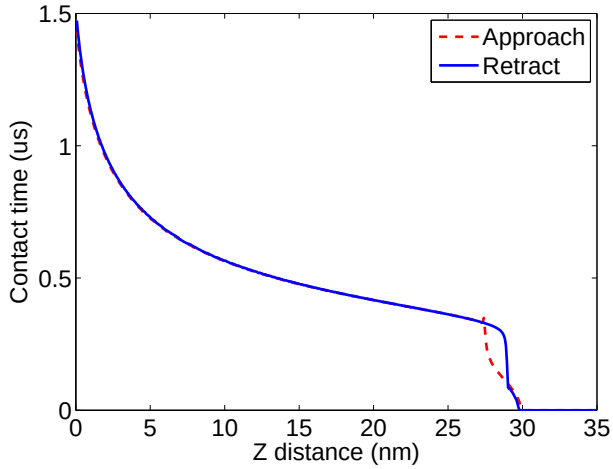

FIG. 13: Contact time (μs) vs. Z distance (nm) while retracting from the sample. (**AMAC** Example 2)

3. *Example 3: Effects of viscoelastic damping in polymer samples*

Our final example focuses on the effects of sample viscoelastic damping on the amplitude modulated approach curves and the resulting power dissipation curve resulting from this particular form of non-conservative tip-sample interaction. For this simulation, we choose sample properties that are characteristic of typical polymers including a sample viscosity of 500 Pa s (Table I).

To begin this example, open the **AMAC** tool from the **VEDA** tools selection. Wait for the user input window to open. Under the *Operating conditions and cantilever properties* tab, set the *Unconstrained amplitude (nm)* to 60, and set k_i *(N/m)* to 3. Change Q to 150, change both f *(kHz)* and f_d *(kHz)* to 75, and change *Z approach velocity (nm/s)* to 500. Next, click the *Tip-sample interaction properties* tab. Under this tab, be sure that the *Tip-sample interaction model* is *Hertz contact*. At the bottom under "non-conservative forces", change "Include sample viscoelastic forces" to the "Kelvin-voigt" model. Change the rest of the input parameters under this tab and under the *Simulation parameters* tab to match those shown in Table I Example 3. Once all of the inputs have been correctly modified, click the *Simulate* button in the lower right-hand corner. This simulation generally takes about 1.25 minutes to run to completion. After the simulation is finished, click back to tab 2 and change the "Include sample viscoelastic forces" to "None". Run this simulation and then compare the results with and without the viscoelastic forces.

The results of this simulation are shown in Figures 14 - 17.

First, in Fig. 14, we see that the amplitude does not change very much with the addition of the viscoelastic forces, but the phase changes significantly. The change in phase can be related to the fact that viscoelastic forces are non-conservative. That is, they dissipate energy. This is seen in Fig. 15. Additional effects of the viscous interaction are seen in the mean (Figure 15a) and peak (Figure 15b) interaction forces. The viscoelasticity significantly raises the peak force, although the mean force decreases slightly.

To have a better look at the forces, we can examine the interaction force time histories shown in Figure 16. During most of the cycle, the tip is not in contact with the sample. This figure shows just the small portion where they are in contact. Again, the peak value of the force is higher with the viscoelasticity, although the total area under the curve (the mean force) is approximately the same. Most notable, the shape of the force curve is asymmetric due to the viscous contribution.

Many additional details about viscoelasticity can be found under the viscoelasticity part of the theory section of this manual.

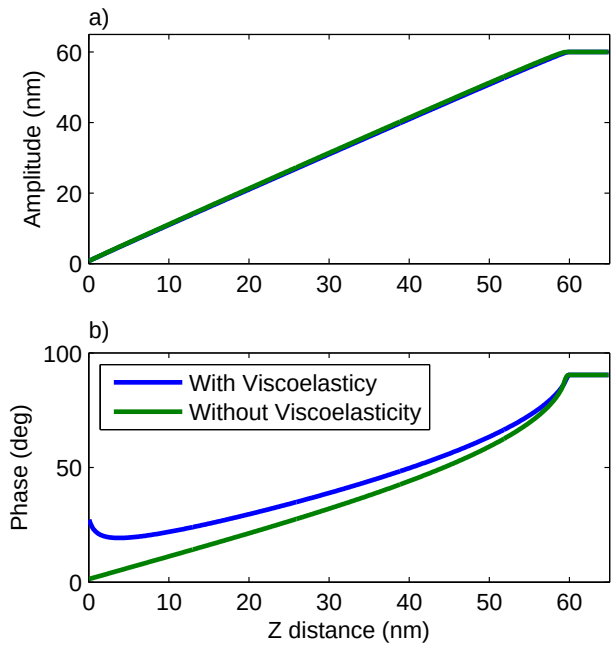

FIG. 14: (a) Amplitude (nm) vs. Z distance. (b) Phase (deg) vs. Z distance.(**AMAC** Example 3).

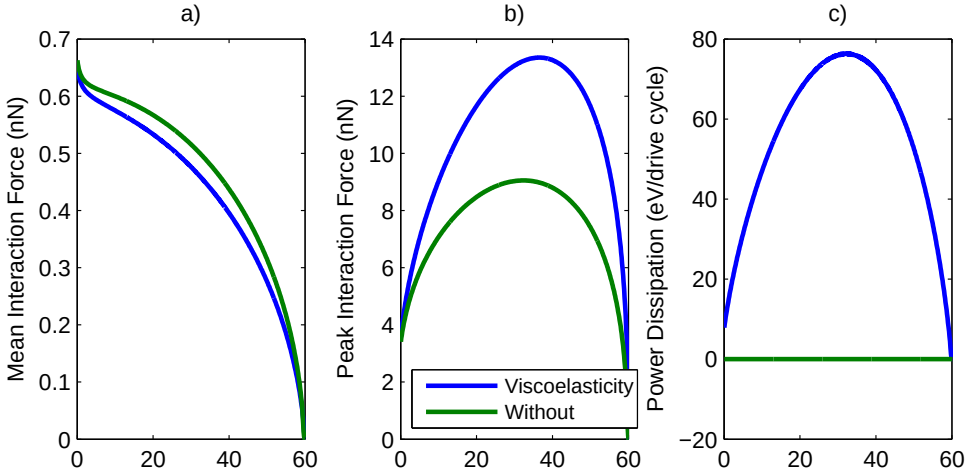

FIG. 15: (a) Mean interaction force (nN) vs. Z distance. (b) Peak interaction force (nN) vs. Z distance. (c) Power dissipated (pW) vs. Z distance. The power dissipated by viscoelastic damping depends on both the indentation and rate of indentation (**AMAC** Example 3).

B. Amplitude Modulated Scanning (basic)

A microcantilever is commonly used to image nano-scale surfaces by tapping along the surface while monitoring the location of the cantilever base as well as the tip deflection amplitude. The Amplitude Modulated Scanning tool (AMS) was created to simulate the response of a microcantilever excited near its first flexural natural frequency and in contact with a sample while being moved along the surface of the sample as a controller attempts to keep the cantilever tip deflection amplitude constant.

The following assumptions are unique to the basic Amplitude Modulated Scanning tool:

1. Cantilever dynamics are modeled by a single eigenmode model (Eq. 101, $i = 1$).
2. The cantilever is acoustically or magnetically excited with a single frequency.
3. The Z separation between the sample can be reduced or increased, but the cantilever does not move laterally.
4. The AFM controller is modeled as a simple proportional-integral (PI) controller.
5. Inertial and hydrodynamic forces acting on the cantilever due to the controller's Z adjustment of the base while scanning are negligible.

This section provides an overview of the outputs of the basic Amplitude Modulated Scanning (AMS) tool in the form of several example simulations.

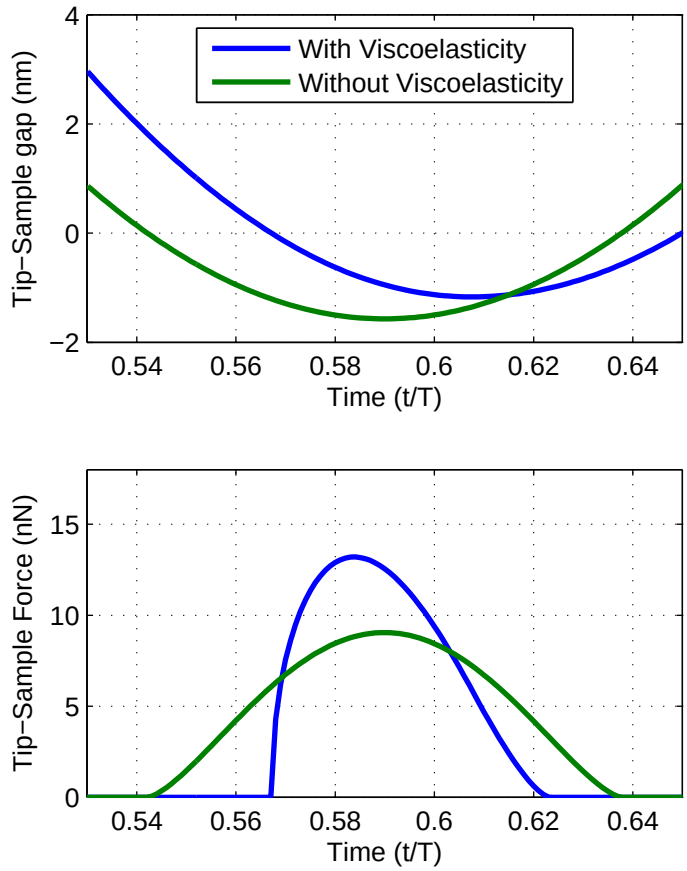

FIG. 16: Tip-sample gap and interaction force histories corresponding to $A/A_0 = 0.55$. The viscoelastic forces cause the interaction force history to be asymmetric. (**AMAC** Example 3).

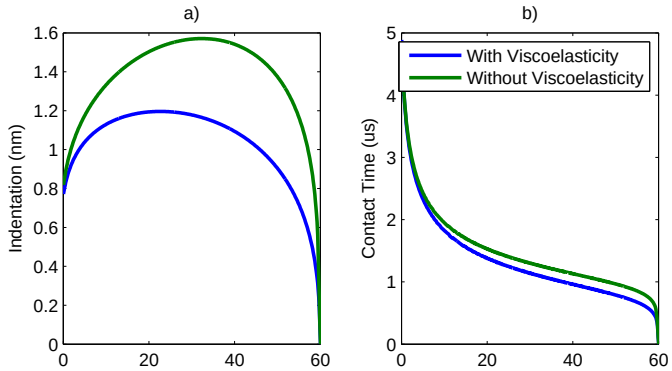

FIG. 17: (a) Indentation (nm) vs. Z distance (nm). (b) Contact time (μs) vs. Z distance (nm). (**AMAC** Example 3)

TABLE II: Input parameters for AMS examples.

PARAMETER	EX. 1	EX. 2	EX. 3	EX. 4	EX. 5
Operating cond. + Cantilever prop.					
Choose excitation source	Acoustic	Acoustic	Acoustic	Acoustic	Acoustic
Unconstrained Amplitude (nm)	30	30	13	10	6
k (N/m)	40	1	0.3	0.3	1
Q	400	200	100	100	10
f (kHz)	350	30	150	150	40
f_d (kHz)	350	350	150	150	40
Tip mass, (m_{tip}/m_c)	0	0	0	0	0
Set point ratio	0.9	0.9	0.98	0.85	0.7
Signal/Noise ratio (dB)	20	80	30	30	60
Scan Lines per second	13.33	33.33	33.33	33.33	10
Proportional gain	0.002	0.002	0.008	0.001	0.04
Integral gain	0.002	0.0015	0.004	0.004	0.1
Sampling frequency (Mhz)	1	1	1	1	1
Lock-in filter order	2nd	2nd	2nd	2nd	2nd
Lock-in time constant (μs)	50	50	50	50	200
Tip-sample int. prop: substrate					
Tip-sample interaction model	DMT contact	DMT contact	DMT contact	DMT contact	Hertz
Tip radius (nm)	10	10	10	10	10
Young's modulus of tip (GPa)	130	130	130	130	130
Poisson's ratio of the tip	0.3	0.3	0.3	0.3	0.3
Auto Calculate intermolecular distance?	yes	yes	no	yes	NA
van der Waals Adhesion force (nN)	3.2	3.4	N/A	1.4	NA
Intermolcular distance (nm)	N/A	N/A	0.2	N/A	NA
Hamaker constant (J)	$1.8 \cdot 10^{-19}$	$2.96 \cdot 10^{-19}$	$3.4 \cdot 10^{-20}$	$3.4 \cdot 10^{-20}$	NA
Young's modulus of sample (GPa)	130	10	60	60	1
Poisson's ratio of the sample	0.3	0.3	0.3	0.3	0.3
Include sample visco-elastic forces	None	3 element	None	None	None
Sample E2 modulus (GPa)	NA	0.1	NA	NA	NA
Sample Viscosity ($Pa \cdot s$)	NA	100	NA	NA	NA
Simulation parameters					
Number of points plotted	1000	1000	1000	1000	1000
Maximum number of deflection points per cycle	1000	1000	1000	1000	1000
Scan size (length) (nm)	150	30	30	30	100
Feature properties					
Select a geometric feature	Trapezoid	Step	Step	Step	Step
Feature height (nm)	-40	0	1	1	0
Length of feature (nm)	110	10	10	10	50
Length of trapezoid top (nm)	50	NA	NA	NA	NA
Include geometric convolution	no	no	no	no	no
Specify material properties	no	yes	yes	no	yes
Tip-sample interaction model	NA	DMT contact	DMT contact	NA	DMT contact
Auto Calculate intermolecular distance?	NA	yes	no	NA	yes
Intermolecular distance	NA	NA	0.2	NA	NA
van der Waals Adhesion force (nN)	NA	4.4	N/A	NA	15
Hamaker constant (J)	NA	$7.1 \cdot 10^{-20}$	$3.0 \cdot 10^{-20}$	NA	1e-19
Young's modulus of sample (GPa)	NA	1.2	60	NA	1
Poisson's ratio of the sample	NA	0.3	0.3	NA	0.3
Include sample visco-elastic forces	None	3 element	None	None	None
Feature E2 modulus (GPa)	NA	0.1	NA	NA	NA
Feature Viscosity ($Pa \cdot s$)	NA	10	NA	NA	NA

1. Example 1: Silicon trench

In the first example, we choose to simulate an amplitude modulated AFM scan of a silicon trench, representing a critical feature of a semiconductor device.

Prior to performing the scanning simulation, we first explore the dynamics between the cantilever probe and the sample with the Amplitude Modulated Approach Curves tool. The necessary inputs for this simulation are all also present in Table II with the exception of the Z approach velocity, which was chosen as 200 nm/s. To begin this example, open the **AMAC** tool from the **VEDA** tools selection. Enter the proper user inputs as shown in the Table II, then click the *Simulate* button in the lower right-hand corner. After this simulation is complete, open the **AMS** tool from the **VEDA** tools selection. After the user input window has opened, change the input values to those shown in Table II, and click the *Simulate* button in the lower right-hand corner.

From the results of AMAC simulation (Figure 18), we find that the transition from attractive to repulsive regime is more subtle (See Example 1 (III A 1) of AMAC for a contrasting example). To ensure that the cantilever will be tapping on the sample at the chosen set point ratio, we look at the phase vs. Z distance curve (Figure 18). When exciting the cantilever at resonance, a negative phase shift confirms that the cantilever is oscillating in the repulsive regime or "tapping" on the sample as long as the interaction is conservative. Finally, larger set point ratios are generally preferred to reduce peak repulsive interaction forces (Figure 19). With this in mind, we choose a set point ratio of 0.90 for this simulation.

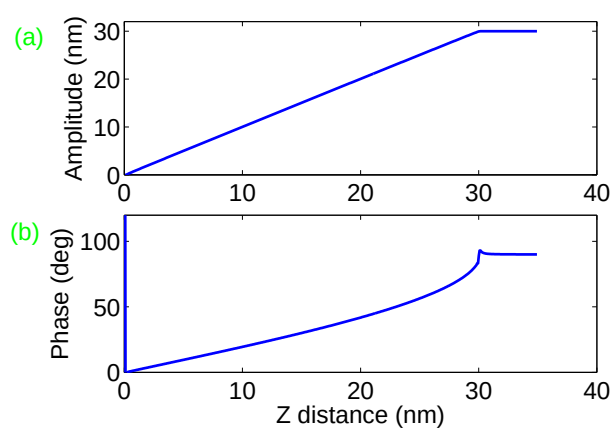

FIG. 18: (a) Amplitude (nm) vs. Z distance (b) Phase (deg) vs. Z distance (nm). (**AMS** Example 1)

Next, we need to determine the proportional gain and integral gain of the controller. To do so, we can apply the following methodology. The default gains should provide a good starting point, however these values may need to be adjusted for different cantilever and tip-sample properties and lock-in time constant. In general, if the system is unstable, or if there is a large ringing effect, these gains should be decreased. If the system is stable and there is no ringing, then these gains may be increased if there is a slow response time. Note that the controller is active during

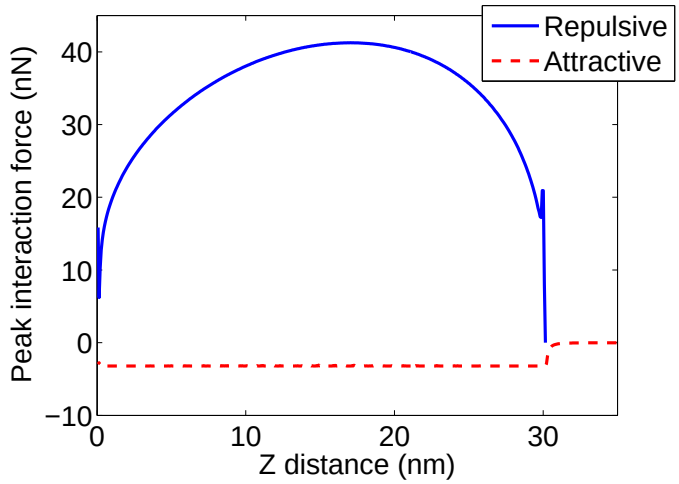

FIG. 19: Peak repulsive and attractive interaction forces (nN) vs. Z distance (nm). (**AMS** Example 1)

the transient computations so if the simulation progress bar stays on transient for a very long time, you may have an unstable controller and should probably decrease your gains.

Through some experimentation, we choose 0.002 as the proportional gain and 0.002 as the integral gain. Finally, the sample geometry is constructed by choosing the trapezoidal feature type and entering a negative feature height. All other inputs for this example are shown in Table II.

The results of the scanning simulation are shown in Figures 20 - 23. The measured topography (Figure 20a) refers to the sample height imaged by the AFM. This is determined by first allowing the simulation to reach steady state oscillations at the specified set point ratio, and then as the cantilever begins to scan over the sample and the change in Z distance based on the lock-in (Eq. 117) is recorded as the sample topography. The measurement error (Figure 21) represents the difference between the actual sample height and the measured topography. The amplitude error (Figure 21) represents the difference between the computed amplitude and the amplitude that satisfies the set point ratio. The amplitude is calculated two ways. First, by the lock-in and second by a Fourier transform. The controller uses the lock-in's calculation, the Fourier transform is provided as a reference so that you can check the performance of the lock-in. The phase (Figure 20) is computed is the same manner. Finally, the mean and peak interaction forces (Figure 22) and indentation (Figure 23) are found from the tip oscillation waveform (without noise).

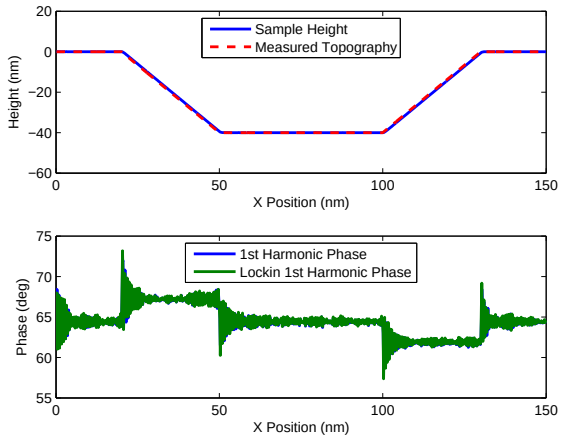

FIG. 20: (top) Measured topography and true sample height vs. X distance (nm) over which the AFM scans. (bottom) The phase (deg) vs. X distance (nm). (**AMS** (basic) Example 1)

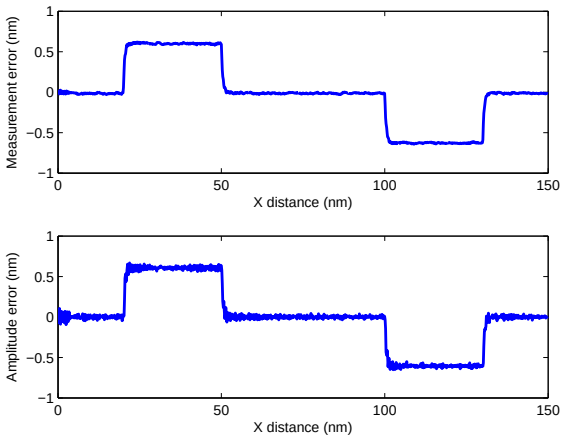

FIG. 21: (a) The measurement error (nm) vs. X distance (nm) plotted represents the difference between the measured topography and the sample height (see Figure 20). (b) Amplitude error (nm) vs. X distance (nm). The amplitude error is defined in Eq. 116 and differs from the measurement error due to the integral feedback term (Eq. 117). (**AMS** Example 1)

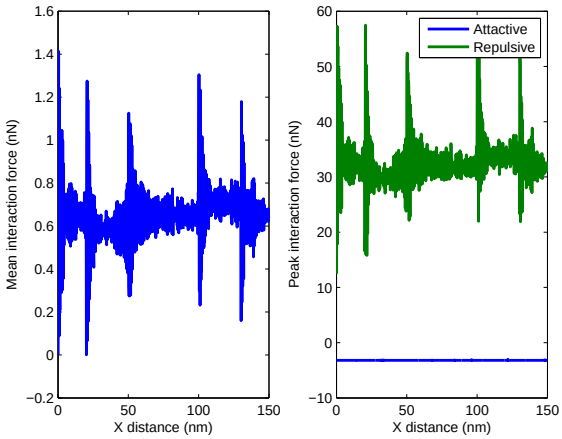

FIG. 22: (a) The mean interaction force (nN) vs. X distance (nm) is calculated based on the clean, padded tip oscillation waveform. (b) Peak attractive and repulsive interaction forces (nN) vs. X distance. Peak forces are calculated based on the clean tip oscillation waveform. (**AMS** Example 1)

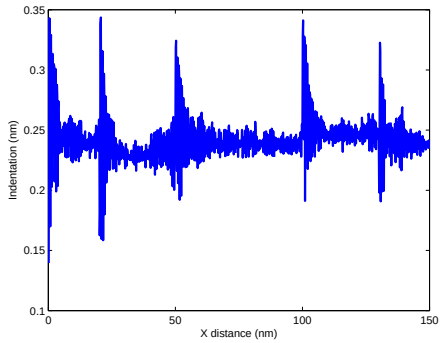

FIG. 23: The indentation (nm) vs. X distance (nm) corresponds to the peak repulsive force for the DMT contact force model. Indentation is calculated from the clean tip oscillation waveform. (**AMS** Example 1)

2. Example 2: Phase contrast in polymer blends

In this example we simulate scanning over a flat (no change in actual topography), heterogeneous sample composed of two different polymers. The total sample is 30 nm long and there is a 10 nm patch in the center that has different visco-elastic properties than the rest. We choose a smooth sample (Figure III B 2) to investigate the spurious topography imaged by the AFM due to different tip-sample interaction properties for the two materials. Finally, we choose similar input parameters as the previous example (Table II), but with a cleaner signal (60 dB) to reduce measurement error due to signal noise.

To run this simulation, choose "Example 2" from the example loader drop down box. Looking at the material properties tab for the substrate versus the feature, we see that we are modeling the contact with a Hertz contact based model (sec IV B 2) and modeling the viscoelastic properties with a three element model (sec IV B 5) The two modulii E_1 and E_2 are the same, but the viscosity is different. A better understanding of what this means can be gained by using equations (50) and (51) to calculate the storage and loss modulus for each material. This is shown in Figure . Because E_1 and E_2 are the same, the static modulus (i.e. the modulus that would be probed by a slow F-z curve) are the same, as are the high frequency behaviors. However, because the viscosity is not the same, the dynamic behavior at intermediate frequencies is different. Specifically, near the drive frequency of 30 kHz (dashed line), the red curve (the feature in the center) is significantly *softer* than the blue curve (the substrate). The loss modulus is significantly higher on the blue material, so we expect more energy dissipation there.

The results for this simulation are shown in Figure III B 2-III B 2. Figure III B 2 shows the topography imaged by the AFM. There is a step between the materials, but the sample is actually flat, so this is a measurement error of around -0.8 nm. Looking as the indentation (c) we see that there is also a 0.8 nm difference in indentation and we conclude that the measurement error is largely due to the difference in indentation of the (dynamically) softer sample. Thus topography errors can be expected due to changes in local viscoelasticity of the sample.

If we were to repeat this simulation with a cantilever natural frequency that was significantly lower, there would be a reverse in phase contrast because there would be significantly more energy dissipation on the blue material than on the red. (try it yourself: for example 35 kHz nat. freq. and drive frequency. Also use a lockin time constant 2 kHz and 3.33 line/s).

There is also clear phase contrast for the two different regions (d). In particular, the red material has a lower phase. This corresponds to less energy dissipation on the red material, as expected from the lower loss tangent at the driving frequency.

This simulation was relatively straighforward. Now let us repeat the simulation for a case that is not so easy to interpret. Increase the natural frequency and driving frequency to 200 kHz and increase the cantilever stiffness to 40 N/m. You may also want to increase the Scan lines per second to 36 so that the simulation runs in a similar amount of time. Repeat the simulation for both a setpoint of 0.9 and a setpoint of 0.3.

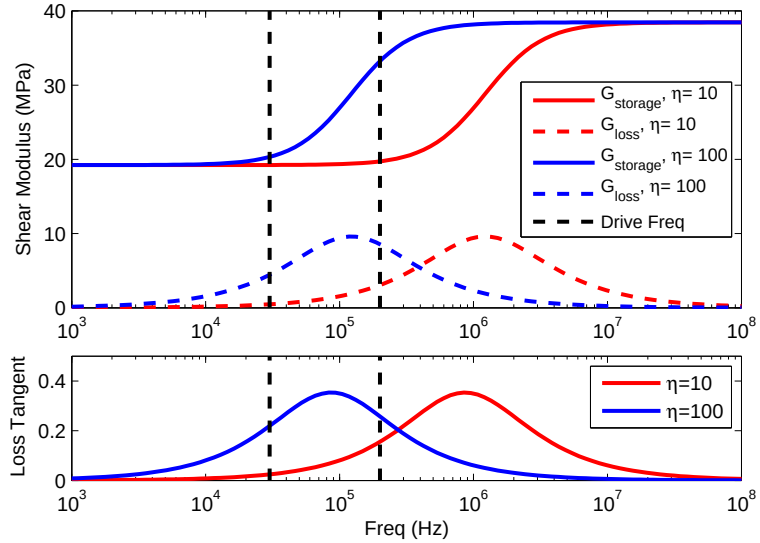

FIG. 24: Dynamic Storage and Loss modulus for the two materials used in this example. (**AMS** Example 2)

The result is shown in Figure 27. We see that now, the red material has a *higher* phase at 90\% setpoint, but a *lower* phase at 30% setpoint. How can this contrast reversal be explained? After all, the drive frequency is the same in both cases, and the red material has a lower loss tangent at the driving frequency.

To shed some light on the situation, we want to examine some time histories. If you've used the example loader, these were enabled. Otherwise, click to tab 3 Simulation Parameters, check the box "Include time histories", set number of histories to 1, and enter 15 for "choose time history points". This gives one time history when the tip is in the middle of the red region. We will want to compare the time histories for the different setpoints.

The time history of force is shown in Figure 28. Note that while the *cantilever deflection* is nearly sinusoidal, the time history of *force* is far from sinusoidal. In other words, if we examine the fourier transform of the force, it contains many higher harmonics (even though the fourier transform of the cantilever would have no significant higher harmonics). This means that the quantity of interest is not the loss tangent of the material at the driving frequency, but the loss tangent over a wide range of driving frequencies. Importantly, the number and relative magnitude of the higher harmonics is different for the two different setpoints, which means that effectively a different frequency range of the materials is being sampled in each case.

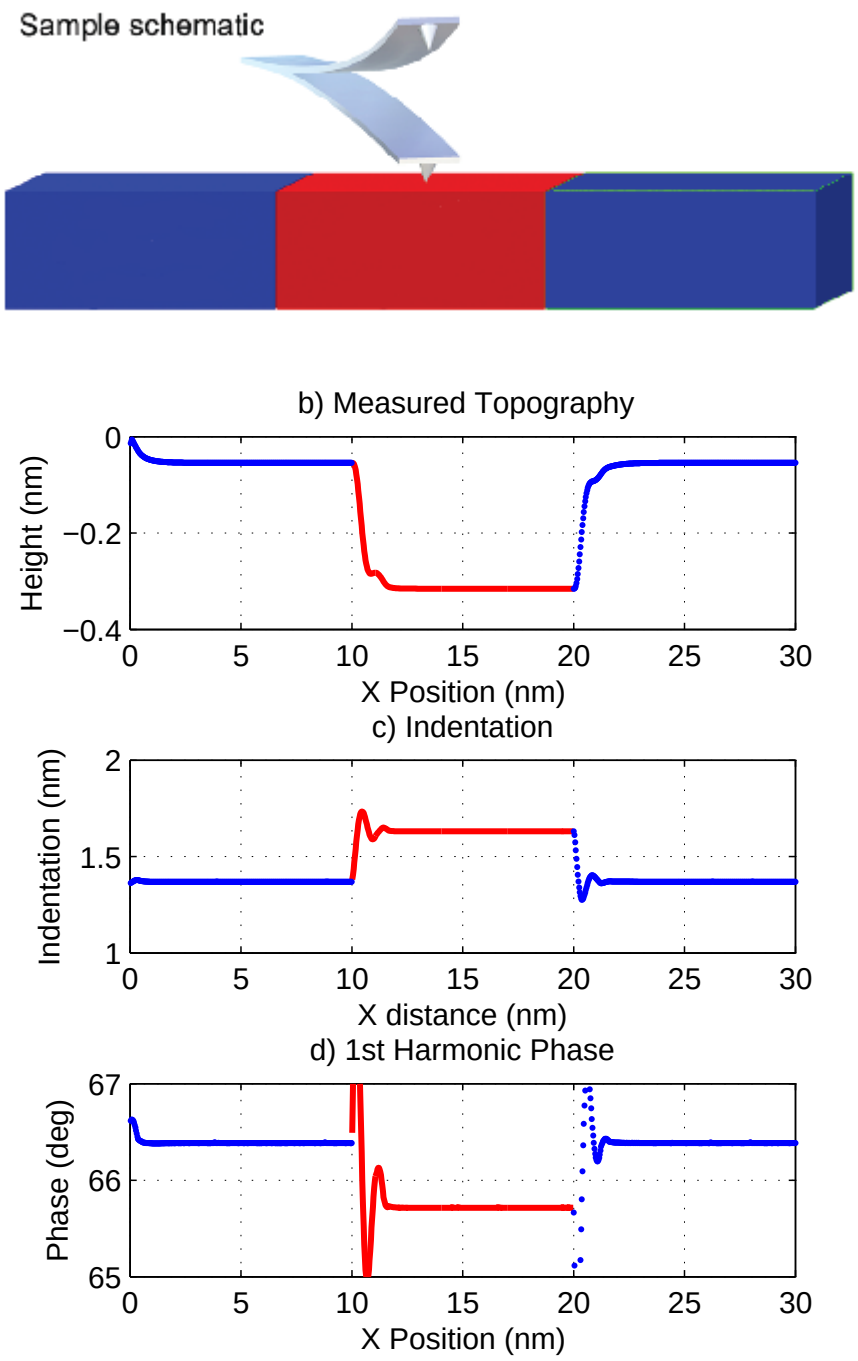

FIG. 25: a) Schematic of sample. There is a region in the middle (the "feature") that has the same height as the surrounding area (the "substrate") but different material properties. b) Measured topography vs. X distance over which the AFM scans. The sample is actually flat so the step in topography is an artifact. c) The indentation, which shows that the measurement error is due to an increased indentation on the softer region. d) The lock-in phase (deg) vs. X distance (nm). (**AMS** Example 2)

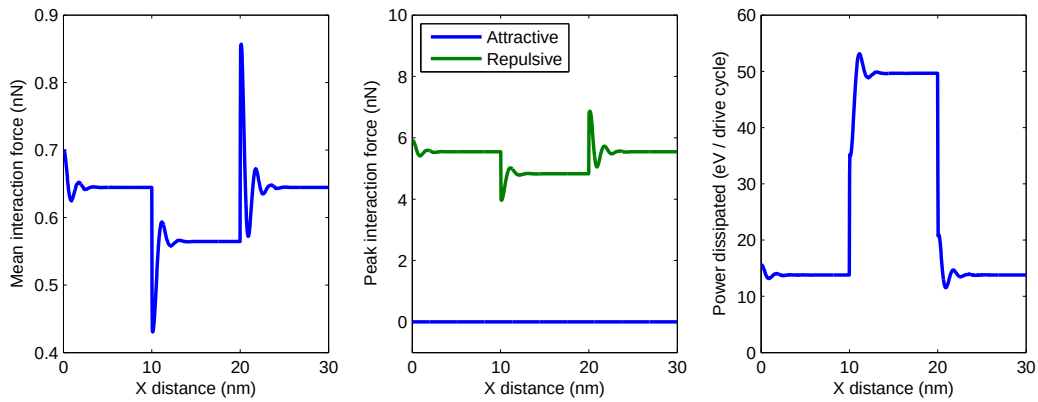

FIG. 26: (a) The mean interaction force (nN) vs. X distance (nm). The magnitude of the average force is affected by the viscoelastic sample damping. (b) Peak attractive and repulsive interaction forces (nN) vs. X distance. (c) The tip-sample energy dissipation (eV / drive cycle) vs. X distance (nm). (**AMS** Example 2)

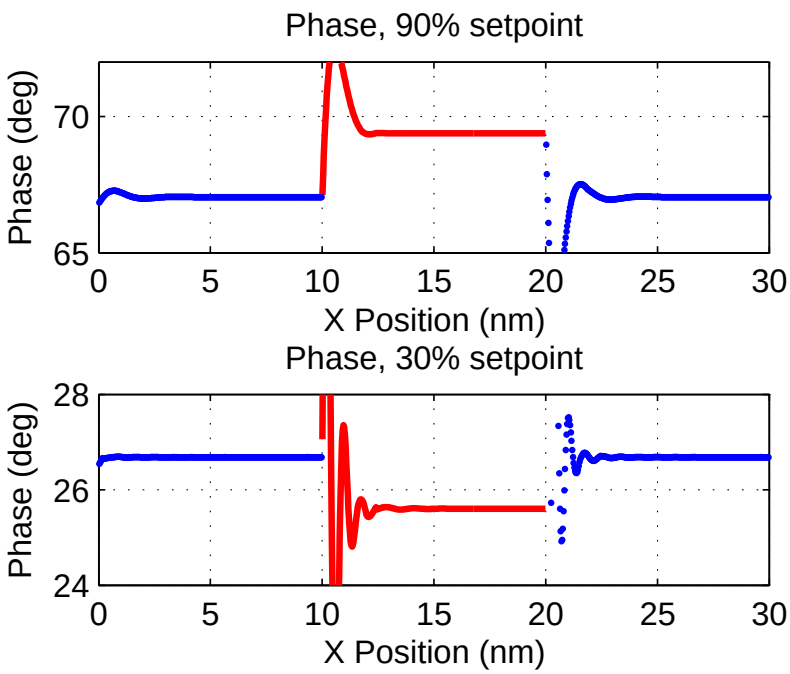

FIG. 27: 1st harmonic phase versus X for two different setpoints when the natural frequency is increased to 200 kHz and the stiffness is raised to 40 N/m. There is now a phase contrast reversal between the different setpoints.

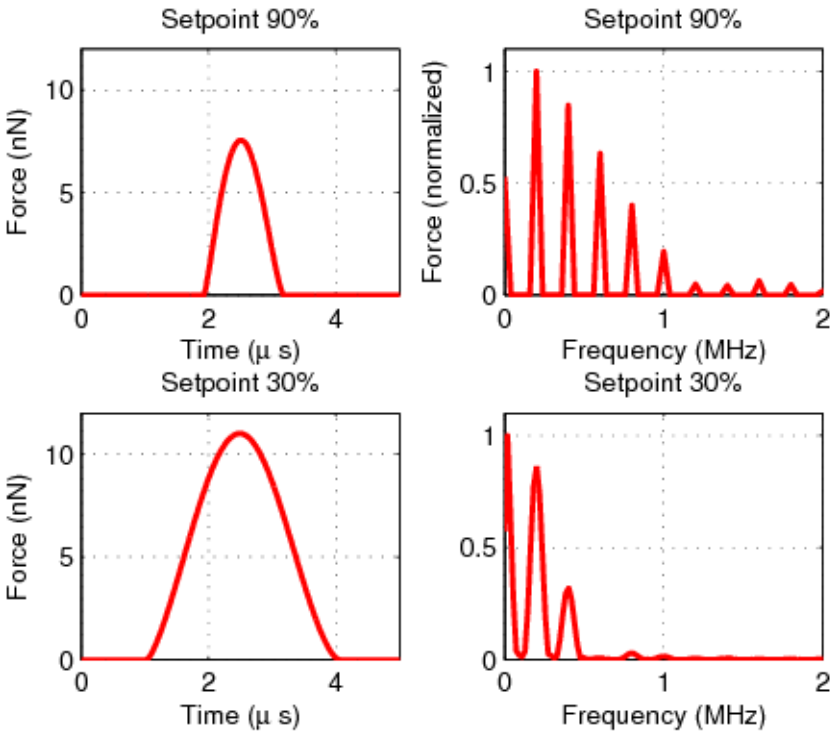

FIG. 28: Time histories of force for the two different setpoints in Figure 27. Also shown in the Fourier transform of the time history. At the higher setpoint, the contact time is shorter, which means higher frequency components. At the lower setpoint, the contact time is longer, which means not as many high frequency components. (**AMS Example 2**)

3. Example 3: Effects of adhesion, Jumps between regimes

In the previous example, the topography error was largely attributed to a difference in indentation caused by a difference in sample elasticity. In this example we demonstrate that even for samples with identical elasticity, there can be topography errors that are not related indentation. This simulation consists of a hard substrate with a small step feature on it. The feature has identical tip-sample interaction properties to the substrate except that the Hamaker constant is slightly smaller. We also explore consequences of the attractive and repulsive regimes introduced in the Amplitude Modulated Approach Curves section. You may wish to work through AMAC example 1 and 2 before trying this example.

You can run the example by choosing "Example 3" from the drop down menu, or by entering the parameters from the table manually. After the simulation runs look at the measured topography, Figure 29. You will note that the red line indicates the true topography and the blue line the measured topography. Clearly there is a significant error.

It will be instructive in sorting this out to consider what really is the effect on tip-sample interaction of changing the Hamaker constant while keeping the intermolecular distance the same? The Force Viewer tool can easily show this. This tool is explained in section III H. For now, we simply present the result in figure 30. We note that for the larger Hamaker constant, the minimum value of force is smaller, although it occurs at the same gap. Also, for a given force that is less than the minimum, say -1 nN, it occurs farther from the sample surface with a larger Hamaker constant. Since tapping mode images at a constant amplitude reduction, and to a rough approximation the same amplitude reduction will happen with a similar force level, we see that we might expect that with a larger Hamaker constant, the cantilever will be farther away from the same surface at the same amplitude reduction.

Now, is there anything that we could do to get a better scan? Examine the mean interaction forces, shown in figure 31. Note that they are negative for the whole scan. That is, we are imaging in an attractive regime. We may guess that if we were to image in an repulsive regime, the effects of the attractive forces may be less important. The proper way to find the repulsive regime would be use the Amplitude Modulated Approach Curves tool (section III A). For now, assume that we'll try to guess a better set of parameters. Lower the setpoint ratio from 0.98 to 0.95 and re-run the simulation. The results should look like Figure 32. This is actually worse than before. Not only is the feature height incorrect, the section of substrate after the feature is incorrect as well. What is going on here? Again, examine the mean interaction forces for a clue, see Figure 33. Note that the substrate section at the begining of the scan has an repulsive mean force while the substrate section at the end of the scan has an attractive mean force. We are now in a bi-stable region, which is even worse.

Again, the proper way to correct this situation is to perform Amplitude Modulated Approach Curves and find a good region for imaging. For now, try the following: raise the Unconstrained Amplitude from 13 nm to 25 nm. The results show now like look figures 34 and 35. The topography error is now much smaller on the step, and the mean interaction forces are repulsive for the whole scan. You'll note, of course, that now we have some overshoot at

the leading edge of the step. This is due to poor controller gains. We briefly discussed controller gains in the next example.

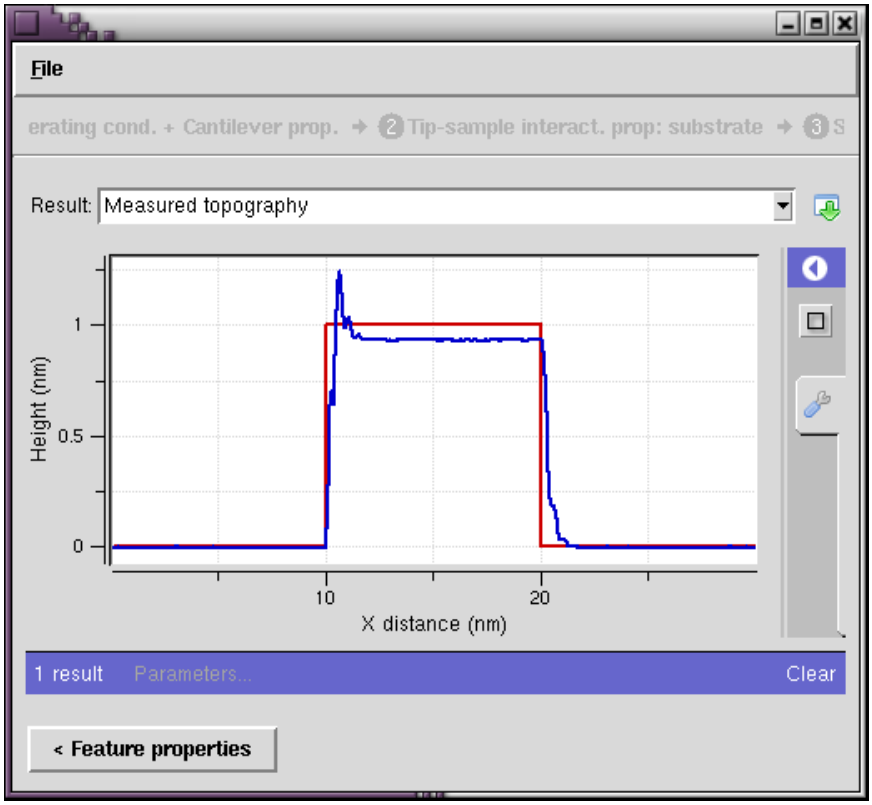

FIG. 29: Measured topography and sample height. (**AMS** Example 3)

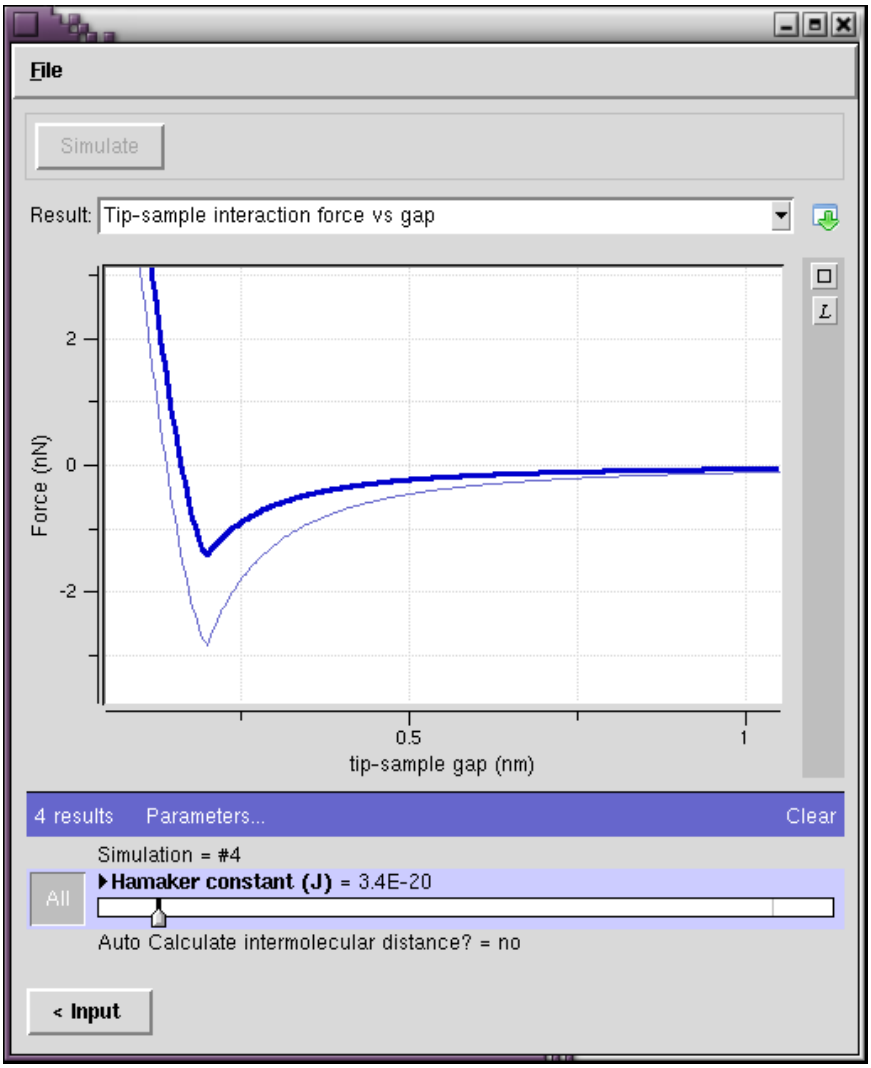

FIG. 30: Tip-sample interaction forces for (**AMS** Example 3). The bold line is A=3.4e-20, the thin line is A=6.8e-20

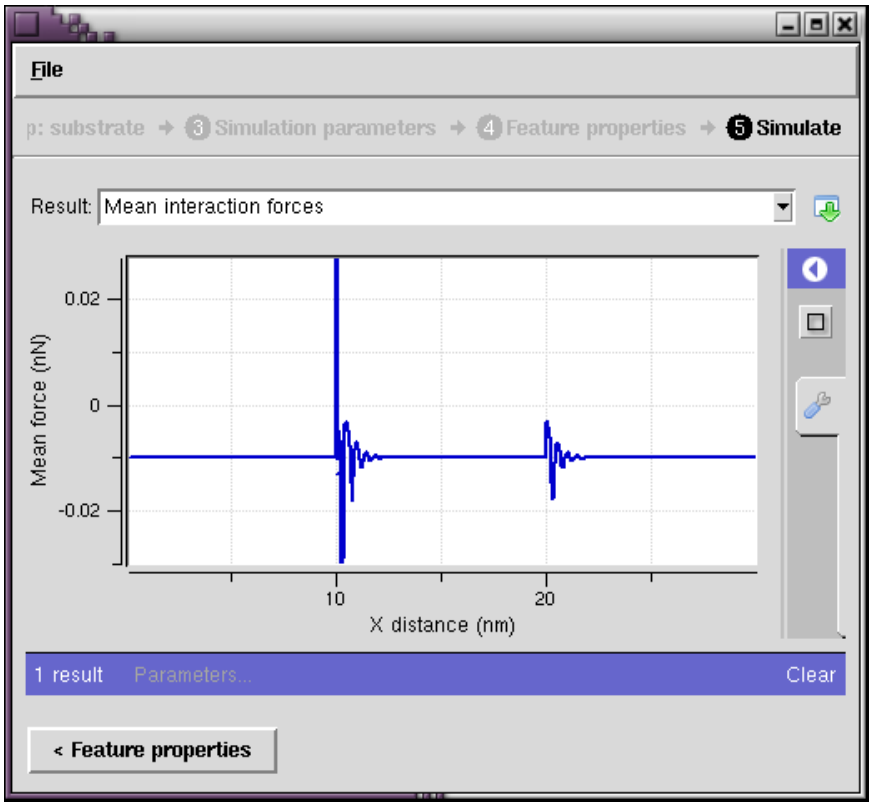

FIG. 31: Mean interaction forces. (**AMS** Example 3)

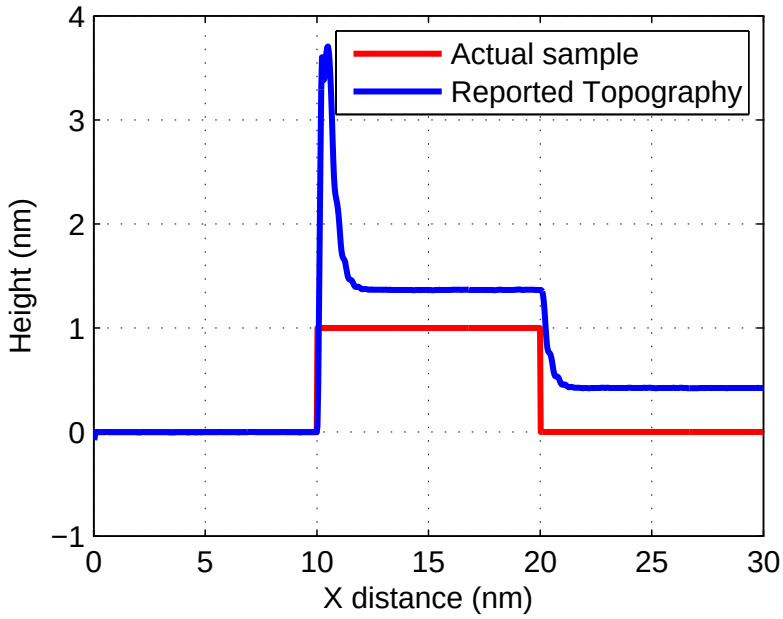

FIG. 32: Measured topography and sample height, with setpoint lowered to 0.65 (**AMS** Example 3)

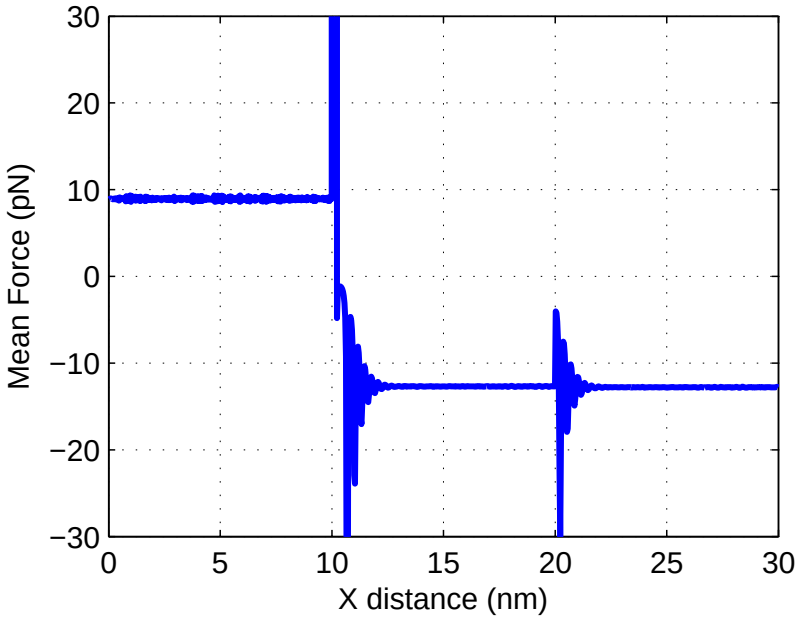

FIG. 33: Mean interaction forces with setpoint lowered to 0.65 (**AMS** Example 3)

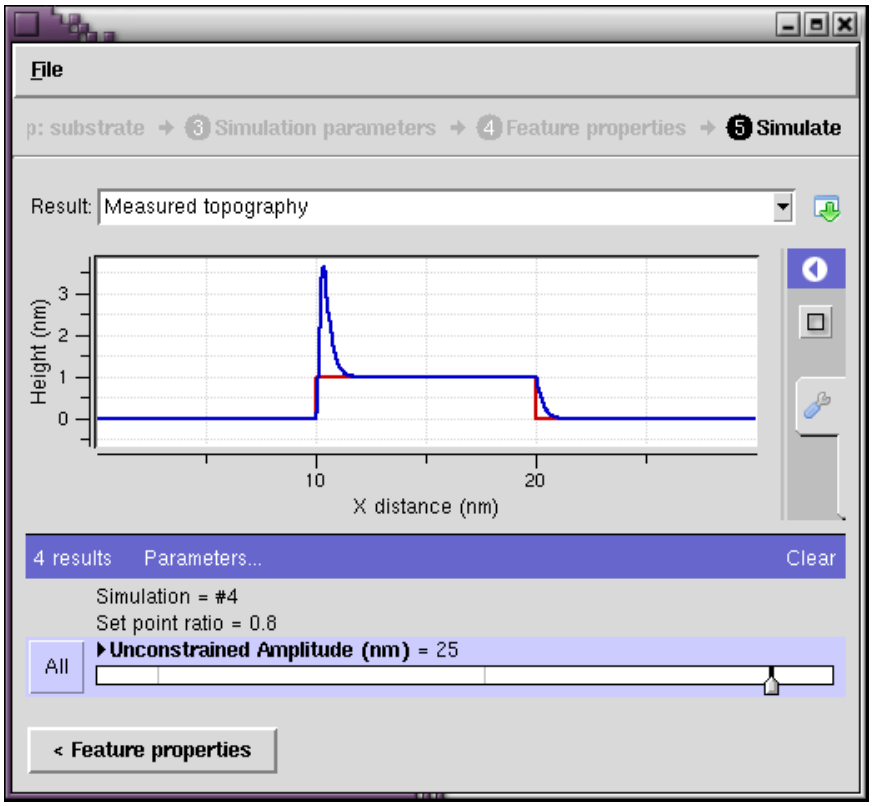

FIG. 34: Measured topography and sample height with unconstrained amplitude raised to 25 nm. (**AMS** Example 3)

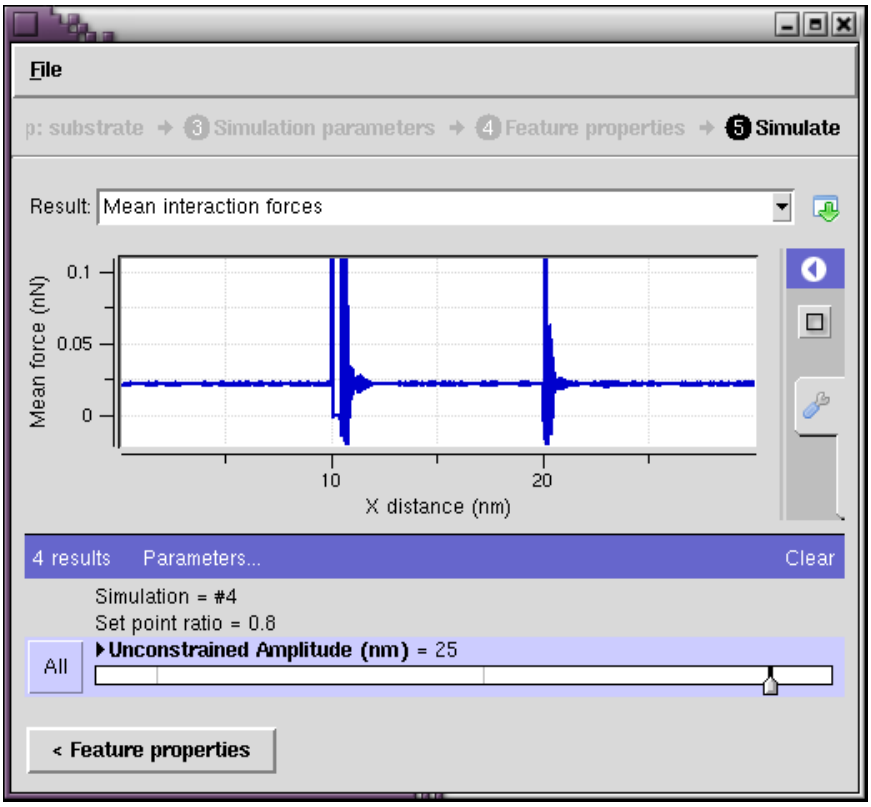

FIG. 35: Mean interaction forces with unconstrained amplitude raised to 25 nm. (**AMS** Example 3)

4. Example 4: Effect of controller gains

In this section we explore the effects of controller gains on the scanning response. There are many factors which affect the response, the largest ones are scanning speed (slower speed = more accurate scan), setpoint ratio, lock-in time constants, and controller gains. In this example we will explore only the controller integral gains.

This example use the same basic parameters from Example 3 but the feature material properties to be the same as the substrate. To run this example, first select Example 4 from the Example loader drop down menu. The initial value of Integral gain will be 0.001. Run this simulation. Then click Input to go back, and enter an integral of 0.002. Repeat for 0.004 and 0.008. Then, examine the topography response (click the All button to overlay the results). If you zoom in, it should look similar to Figure 36, your lines may be different colors. The blue line in this example corresponds to a gain of 0.001. This gain is clearly a little low, it takes awhile for the controller to respond when it hits the step edge. The green line is 0.002. This is a little better. The purple line is 0.004. This response is much quicker, but now there is some overshoot. Finally, the orange line is 0.008. This gain is so high that the controller is on the verge of going unstable, and rings significantly.

If we take this example to the extreme, try entering an integral gain of 0.032. You will note that the transient percent number fluctuates rapidly and does not converge. Eventually, it will give up without ever performing the simulation. This represents the fact that the controller cannot stabilize on the substrate surface and so it cannot even begin the scan (let alone the step edge). You will note that are some hints on stabilizing the controller in the "ErrorMessage" drop down. Conversely, if we enter a value of 0.00001 for the integral gain, the controller will take so long to stabilize on the substrate surface that it will time out.

5. Example 5: Controller Instability

In this example we demonstrate an imaging artifact that can occur on sticky (i.e. highly adhesive) samples. Choose example 5 from the Example loader. Note that this simulation models the substrate with Hertz contact (no adhesion) and the feature with DMT contact (adhesion). When you run the simulation, the measured topography should look like Figure 37. On the feature (between X=25 and X=75), there is a series of sharp spikes. The cantilever appears to be jumping away from the surface for some reason. This is apparently some kind of controller instability. Based on the results in the previous example, we might try to decrease the controller gains. However that will not change the behavior (try it for yourself).

The best way to determine what is going on is to open the Dynamic Approach Curves tool and examine the approach curve for the cantilever and sample parameters. In particular, we should examine the behavior around 70% setpoint ratio that we are using in this example. Perform one run for the substrate (Hertz contact) and one for the sample (DMT). The result should look like 38. On the substrate (red curve) the amplitude is reduced smoothly to zero as the cantilever approaches the surface. But on the sample, the cantilever snaps in to permanent contact with the surface

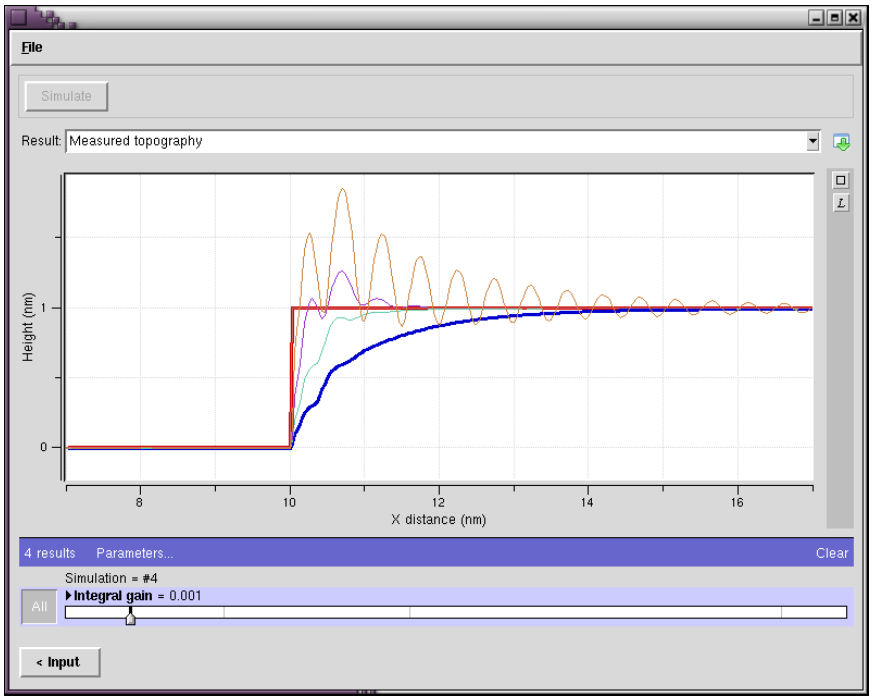

FIG. 36: The effect of integral gain on the measured topography response. (**AMS** Example 4)

at about A=4.5 nm (75% setpoint).

We can now explain the scanning behavior. The cantilever starts far from the surface with a large amplitude. The controller brings the cantilever closer to the surface to reduce the amplitude. However, before the amplitude is reduced to the setpoint of 70%, the cantilever snaps-in and the amplitude jumps to nearly 0. The controller sees that this amplitude reduction has gone too far, and pulls the cantilever away from the sample in order to increase the amplitude. The process then repeats.

There simply is no settings of controller gains or scannin speeds that would make this system stable. In a real experiment, the only two choice would be to raise the setpoint ratio to a point that is stable (e.g. 80%), or to change the free amplitude. Raising the setpoint is simple enough, but the behavior on change the free amplitude may be non-intuitive. Try raising the unconstrained amplitude to 7 nm, and then decreasing it to 5 nm. Which one gives a larger stable region (in terms of amplitude ratio)?

You should find that raising the free amplitude decreases the width of the stable region (i.e. the jump happens at 80% instead of 75) but lowering the free amplitude increases the width of the stable region (i.e. the jump happens at 70% instead of 75). Why should this be? The answer has to do with the stability of dynamic systems, and is somewhat out of the scope of this manual. The curious reader is encouraged to find an introductory text on mechanical vibrations.

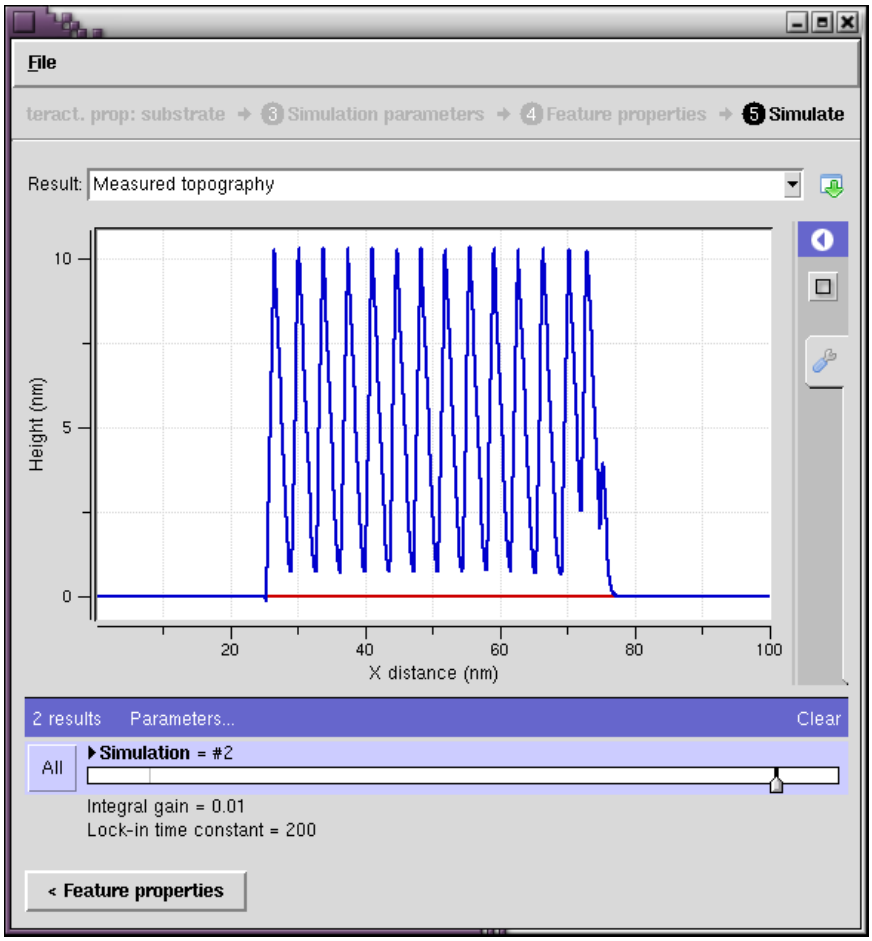

FIG. 37: Measured topography. The large spikes represent a controller instability. (**AMS** Example 5)

C. Amplitude Modulated Approach Curves: Advanced

Microcantilevers are used to image biological and other materials in liquids. The Amplitude Modulated Approach Curves: Advanced (**AMAC: Advanced**) tool was originally developed to simulate the response of an excited microcantilever approaching a sample in liquid; however, it can also be used for multi-mode simulations in air or vacuum. Both the first and second flexural eigenmodes of the cantilever are considered in the simulation (this allows for a better approximation of the cantilever response in liquid).

The following assumptions are made in the **AMAC Advanced** tool:

1. Cantilever dynamics are modeled by the multiple eigenmode model (Eq. 101).

2. Interactions between the tip and the sample are modeled by any one of the models described in Section IV A.

3. The cantilever is either acoustically excited or magnetically excited [25].

4. The cantilever excitation occurs through either a single frequency (conventional) or two-frequencies (bimodal).

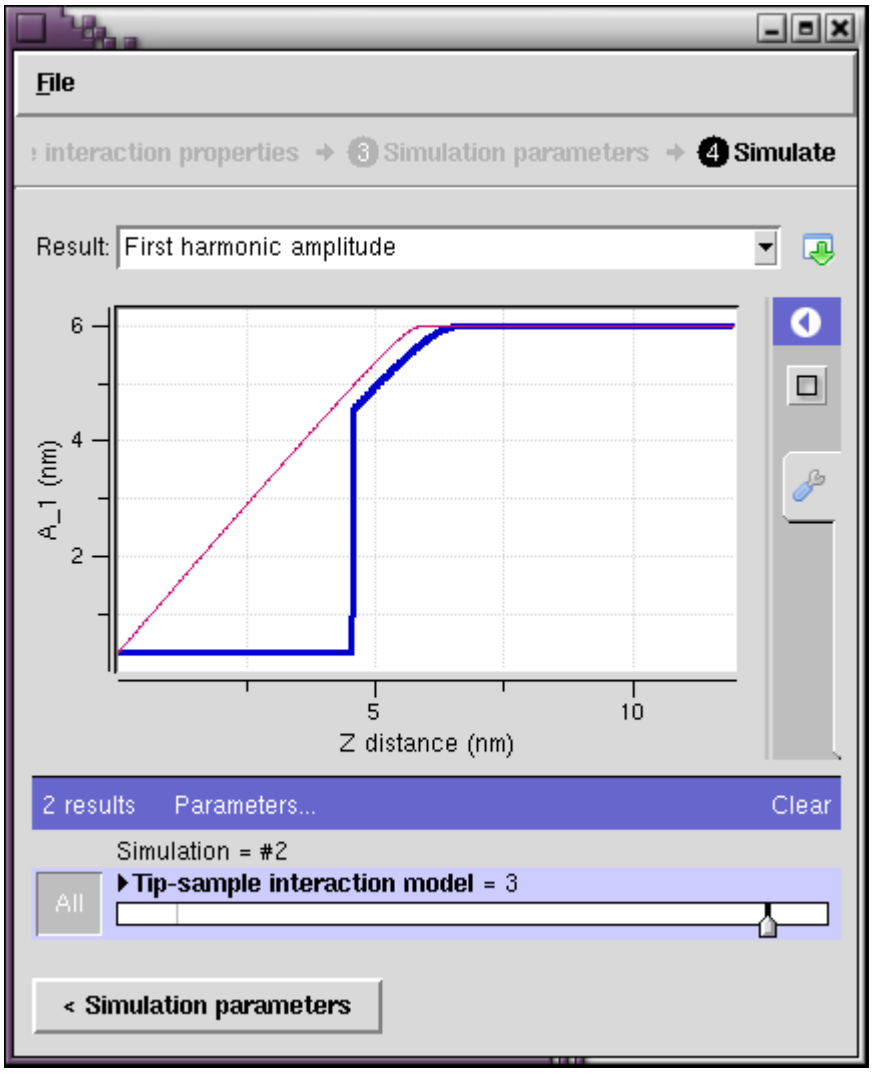

FIG. 38: Approach curves on the substrate (red) and sample (blue). On the sample, the cantilever snaps in to the surface due to the large attractive forces. (**AMS** Example 5)

5. The Z separation between the sample can be reduced or increased, but the cantilever does not move laterally. Inertial and hydrodynamic forces caused by the Z motion are negligible.

This section provides an overview of the outputs of the AMAC: Advanced tool in the form of several example simulations.

TABLE III: Input parameters for AMAC: Advanced examples.

PARAMETER	EX. 1	EX. 2	EX. 3	EX. 4	EX. 5
Operating conditions, cantilever properties					
Choose excitation source	Magnetic	Magnetic	Magnetic	Magnetic	Acoustic
Choose frequency scheme	Single freq.	Two freq.	Single freq.	Two freq.	Two freq.
Number of eigenmodes	2	2	2	2	2
Unconstrained Amplitude (nm)	10	10	20	20	17
Unconstrained Amplitude (2nd drive frq) (nm)	NA	1	NA	1.17	0.56
Auto calculate k_i ($i > 1$)?	no	no	no	no	yes
k_i (N/m)	0.036, 1.4	0.036, 1.4	30, 1200	30, 1200	0.9
Q_i	1.2, 2	1.2, 2	400, 1200	400, 1200	225, 1000
f_i (kHz)	9.3, 72	9.3, 72	350, 2450	350, 2275	48.9, 306.6
f_d (kHz)	9.3	9.3,72	350	350,2275	48.9, 306.6
Tip mass, (m_{tip}/m_c)	0	0	0	0	0
Z approach velocity (nm/s)	20	20	100	100	100
Z range Determination	Autocalc	Autocalc	Autocalc	Autocalc	Specify
Lock-in Time Constant (us)	500	500	NA	NA	200
Tip-sample interaction properties					
Tip-sample interaction model	Hertz	Hertz	Hertz	Hertz	DMT
Tip radius (nm)	30	30	10	10	20
Young's modulus of tip (GPa)	130	130	130	130	130
Poisson's ratio of the tip	0.3	0.3	0.3	0.3	0.3
Intermolecular Distance	NA	NA	NA	NA	0.1
Hamaker constant	NA	NA	NA	NA	4e-20
Young's modulus of sample (GPa)	10	1	1, 5	1, 5	1e-6
Poisson's ratio of the sample	0.3	0.3	0.3	0.3	0.3
Include visco-elastic forces?	none	Kelvin-voigt	none	none	none
Sample viscosity (Pa· s)	NA	100	NA	NA	NA
Simulation parameters					
Number of points plotted	1000	750	500	500	1000
Deflection points per cycle	1000	1000	1000	1000	1000
Plot a higher harmonic?	no	no	yes	no	no
Number of higher harmonics	NA	NA	1	NA	NA
Choose higher harmonics	NA	NA	7	NA	NA
Include time histories	yes	yes	yes	yes	no
Number of time histories	3	1	1	1	NA
Choose amplitude ratio(s)	0.95, 0.9, 0.5	0.9	0.9	0.9	NA
Number of cycles	2	2	2	4	NA
Choose X-axis variable	Amp. ratio	Z-distance	Amp. ratio	Amp. ratio	Amp. ratio

1. Example 1: Multiple impact regimes for a Biolever in liquid

In this example, we will simulate a Biolever approaching a mica sample in a buffer solution and observe oscillations with multiple impacts per oscillation period [26]. We will show how abrupt transitions in the phase correspond to grazing trajectories which indicate multiple impact oscillations. Refer to Table III, Example 1 for the correct input values.

To begin this example, open the **Amplitude Modulated Approach Curves (Advanced)** tool from the **VEDA** tools selection. Wait for the user input window to open (you should start in the *Operating conditions and cantilever properties* tab). Either select "Example 1" from the *Example Loader* dropdown box, or follow these instructions to set the parameters manually: Change the *excitation source* to *Magnetic*. Enter the first and second natural frequencies in *f (kHz)* and excitation frequencies both as comma delimited values: 9.3, 72. Next, click on the *Tip-sample interaction properties* tab. Verify the *Include sample viscoelastic forces* is set to *None*, and change the *Young's modulus of sample (GPa)* to 10. Now, click on the *Simulation parameters* tab. Check the *Include sample of time histories* box. Make sure that the *Number of time histories to collect* is 3, and that the corresponding amplitude ratios are 0.95, 0.9, 0.5. Set the *Number of cycles included in sample* to 2. Finally, click *Simulate* and wait for the simulation to reach completion. The simulation runs in less than one minute.

The simulation records three extractions of deflection/tip-sample interaction time histories. The first corresponds to an amplitude ratio $A_1/A_0 = 0.95$ (see Figure 39a). At this amplitude ratio, single impact oscillations are observed where the tip makes contact with the sample once per oscillation period. Closer to the sample, at an amplitude ratio $A_1/A_0 = 0.9$ (see 39b), double impact oscillations are observed and eventually triple impacts occur are found at $A_1/A_0 = 0.5$ (see Figure 39c).

Looking at the phase of the response (Figure 40), we have identified the precise amplitude ratios where transitions to the indicated multiple impact regime occurs where Gn marks to grazing trajectory which leads to an amplitude branch where n impacts per oscillation occur. Not surprisingly, we can see in Figure 42 and Figure 43 that characteristics of the interaction with the sample (mean force, peak force) are affected by multiple impact regimes.

Figure 43 demonstrates that tip-sample contact time for soft cantilevers in liquids behaves much differently than stiff cantilevers in air (see Figure 13). Inside a given impact regime, contact time is actually decreasing as amplitude ratio decreases. This is happens because of the role momentary excitation of the second eigenmode during tip-sample contact. Secondly, we see that contact time increases nearly stepwise near the beginning of a multiple impact regime, also indicating the importance of second eigenmode dynamics to tip-sample contact for soft cantilevers in liquids.

2. Example 2: Bimodal excitation of a Biolever in a liquid environment

In this example, we will simulate a Biolever being excited at its first two natural frequencies in a liquid environment. Refer to Table III, Example 2 for the correct input values.

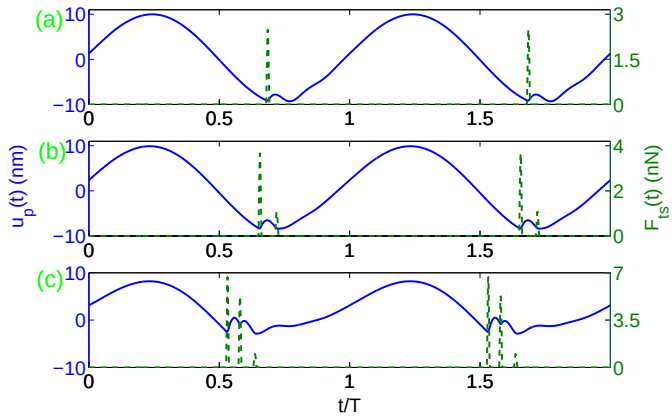

FIG. 39: Photodiode deflection signal $u_p(t)$ and tip-sample interaction force $F_{ts}(t)$ fro two periods of oscillation at amplitude ratios A_1/A_0 of 0.95 (a), 0.9 (b), and 0.5 (c). Each time the cantilever passes a grazing point, an additional impact with the sample is added to the oscillation cycle. (**AMAC Advanced** Example 1)

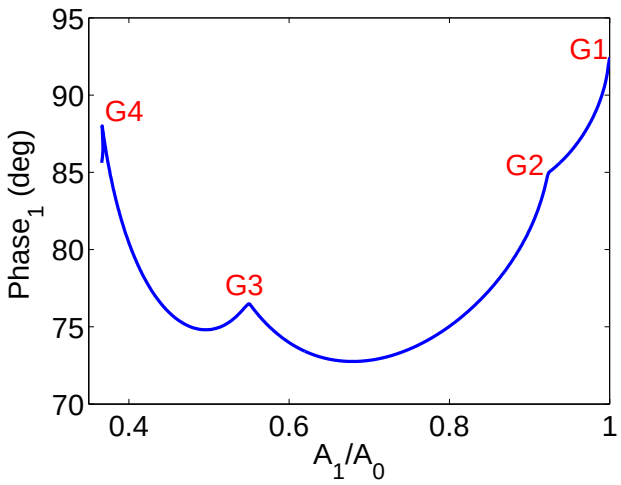

FIG. 40: Phase (deg) of the primary harmonic vs. amplitude ratio A_1/A_0. G1-G4 are grazing points where the cantilever tip contacts the sample at zero velocity (**AMAC Advanced** Example 1).

Because the least common multiple of two drive periods $\omega_{d1} = \omega_1 = 2\pi \cdot 9.3$ kHz and $\omega_{d2} = \omega_2 = 2\pi \cdot 72$ kHz is large, the period of the overall oscillation is long $T = 0.0033$s, which is very long compared to the period of the fundamental drive. This requires a much longer lock-in time constant for a good measurement. In this example, we compare two lock-in time constants: of 500 us and time constant of 5 ms.

To begin this example, open the **AMAC Advanced** tool from the **VEDA** tools selection. Wait for the user input window to open (you should start in the *Operating conditions and cantilever properties* tab). Either select "Example 2" from the *Example Loader* dropdown box, or follow these instructions to set the parameters manually: Change the *excitation source* to *Magnetic* and change the *Frequency scheme* to *two frequencies (bimodal)*. Change the first and second natural frequencies in *f (kHz)* to 9.3, 72, and include two drive frequencies f_d *(kHz)* to 9.3, 72. Set *Z approach velocity (nm/s)* to 20. Uncheck the *Autocalculate Time Constant* box and manually the set *Lockin Time constant* to

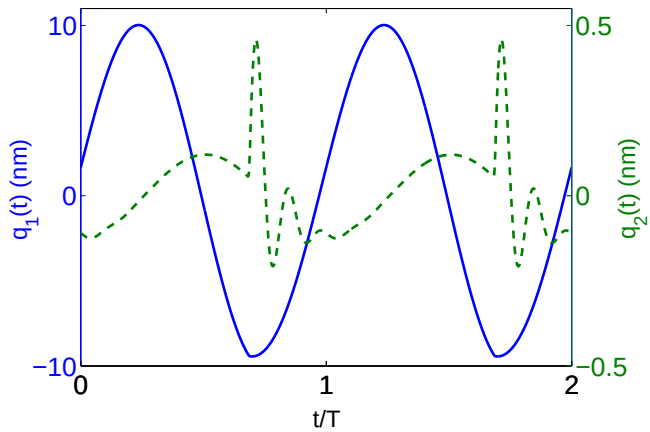

FIG. 41: Response of the first $q_1(t)$ and second $q_2(t)$ eigenmodes tapping at an amplitude ratio $A_1/A_0 = 0.95$. Near times of contact with the sample, the second eigenmode becomes momentary excited and then decays. A slower varying deflection is caused by the excitation force. (**AMAC Advanced** Example 1)

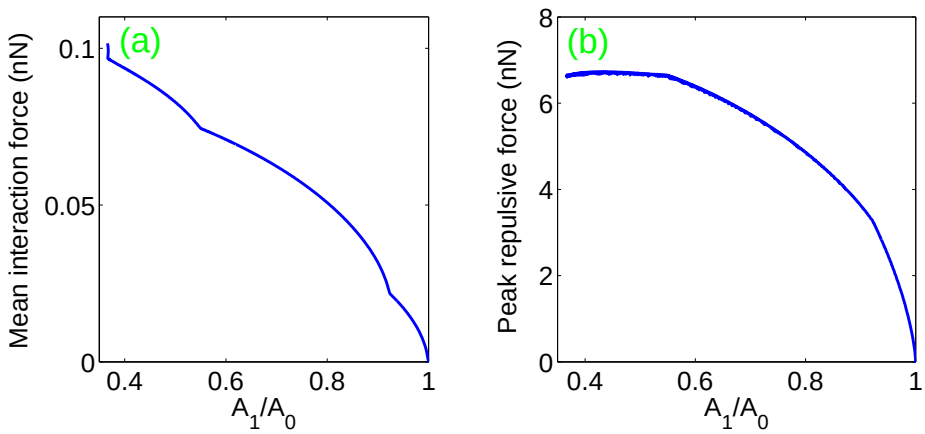

FIG. 42: Mean (a) and peak repulsive (b) interaction forces (nN) vs. amplitude ratio. A sharp change in their trends occurs near the grazing trajectories. (**AMAC Advanced** Example 1)

500 μs. Next, click on the *Tip-sample interaction properties* tab. Set the *Young's modulus of sample (GPa)* to 1. Under the *Non-conservative forces* box, choose *Kelvin-voigt* for the *sample viscoelastic forces* dropdown box and set the *Sample viscosity* $(Pa \cdot s)$ to 100. Now, click on the *Simulation parameters* tab. Make sure the *Include sample of time histories* box is checked. Set the *Number of time histories to collect* to 1, and that the corresponding amplitude ratio is 0.9 only. Set the *Number of cycles included in sample* to 2. Set the *X-axis variable* to *Z-distance (nm)* for this example. At the bottom of this tab, uncheck *Fourier* so that only the lock-in computations are plotted not the Fourier integrals (for clarity in the plots)

Finally, click the *Simulate* button in the lower right-hand corner, and wait for the simulation to reach completion. Once the simulation has completed, click the *Input* button. Open the *Operating conditions and cantilever properties* tab, and change the *Lock-in Time Constant* to 5 ms. Then, click the *Simulate* button again, and wait for the second simulation to reach completion. For this example, each run generally takes less than 1 minute to complete.

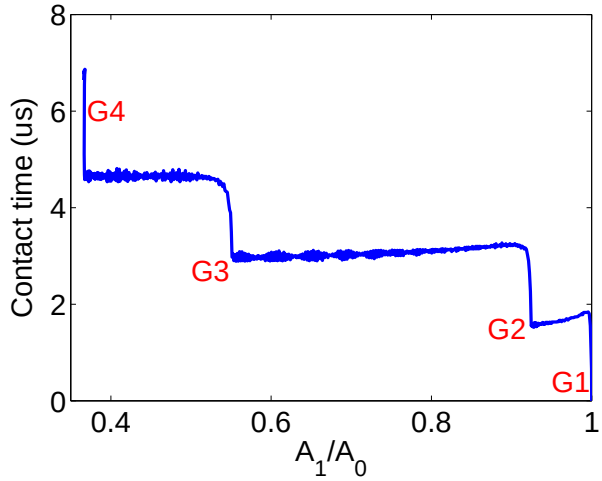

FIG. 43: Contact time (μs) vs. amplitude ratio A_1/A_0. Notice the abrupt change in contact time occurring near each grazing point. (**AMAC Advanced** Example 1)

The amplitudes of the primary and secondary excitations are shown in Figure 44 (a) and (b), respectively, for lock-in time constants of 500 us and 5 ms. Only after increasing the lock-in time constant by an order of magnitude does the amplitude of the second eigenmode converge. The reason for this becomes clear looking at the time history in Figure 45. The second eigenmode interacts sporadically with the sample due to the combination of external forcing excitation and the momentary excitation from the tip-sample interaction. This leads to mixture of single and double impact oscillations occurring at the same amplitude ratio.

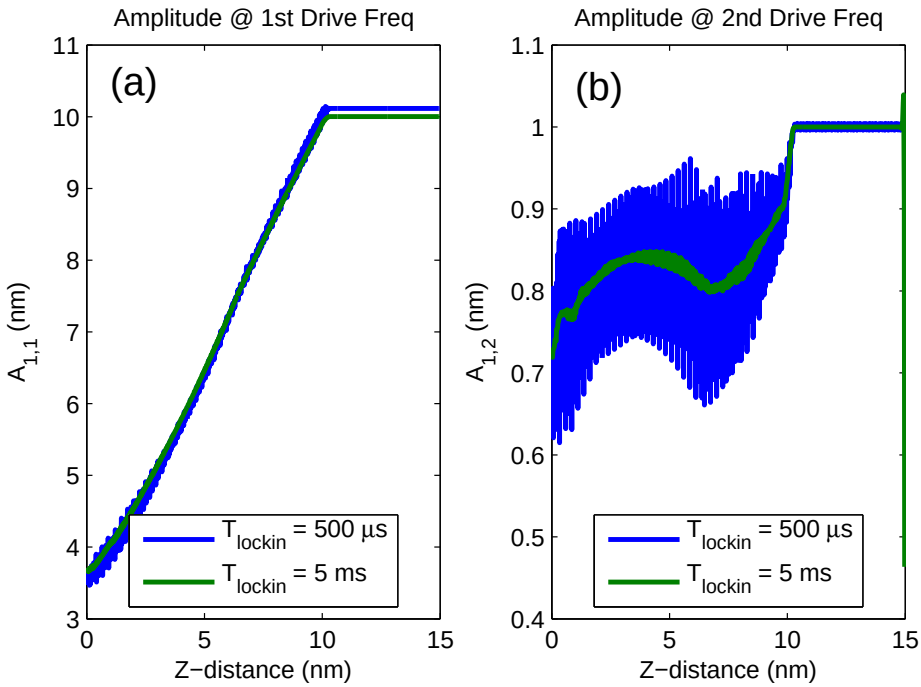

FIG. 44: Amplitude (nm) vs. Z-distance (nm) for the first (*Left*) and second (*Right*) frequencies. Two simulations were performed with two different lock-in time constants: 500 us and 5 ms. (**AMAC Advanced** Example 2)

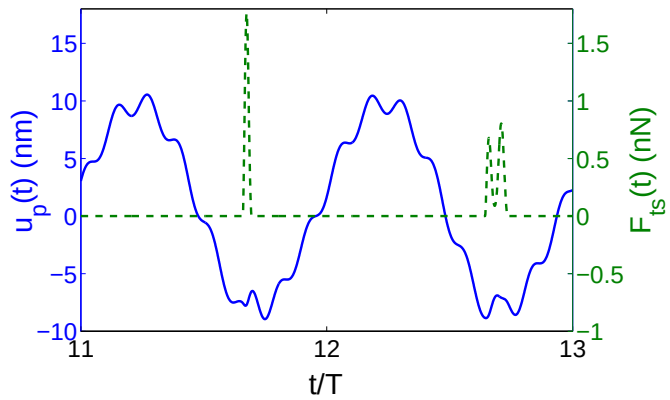

FIG. 45: Photodiode deflection signal $u_p(t)$ and tip-sample interaction force vs. Z-distance (nm) at an amplitude ratio $A_1/A_0 = 0.9$. (**AMAC Advanced** Example 2)

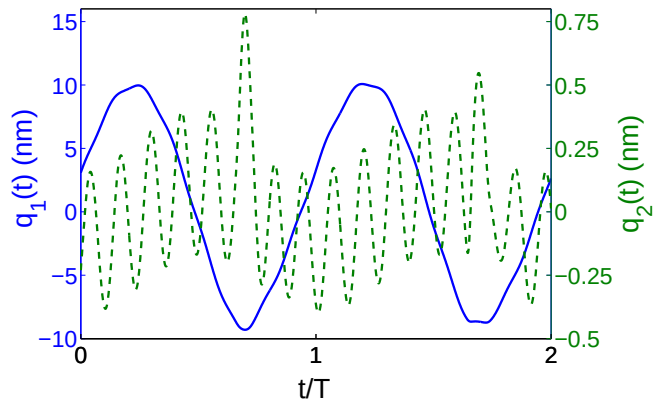

FIG. 46: Response of the first $q_1(t)$ and second $q_2(t)$ eigenmodes of the cantilever at an amplitude ratio $A_1/A_0 = 0.9$. (**AMAC Advanced** Example 2)

3. *Example 3: Internal resonance of a stiff cantilever in air*

In this example, we will simulate internal resonance of a stiff microcantilever in air; this situation is commonly known as "harmonic cantilevers" in the AFM community. Internal resonance is a phenomenon that occurs for special cantilevers in which a higher eigenmode, such as the second flexural eigenmode or the first torsion mode, is very near an integer multiple of the fundamental eigenmode [27–31]. This results in the higher eigenmode being excited by a harmonic of the tip-sample interaction force. Refer to Table III Example 3 for the correct input values for this example.

To begin this example, open the **AMAC Advanced** tool from the **VEDA** tools selection. Wait for the user input window to open (you should start in the *Operating conditions and cantilever properties* tab). Either select "Example 3" from the *Example Loader* dropdown box, or follow these instructions to set the parameters manually: Change the *excitation source* to *Magnetic* and set the *Frequency scheme* to *Single frequency (conventional)*. Set the *First*

frequency amplitude (nm) to 20. Set the eigenmode stiffness values (k_i *(N/m)*), and eigenmode quality factors (Q) to 30, 1200 and 400, 1200, respectively. Change the first and second natural frequencies in (kHz) to 350, 2450, and change *fd (kHz)* to 350. Change the *Z approach velocity (nm/s)* to 100. Next, click on the *Tip-sample interaction properties* tab. Under this tab, change the *Tip radius (nm)* to 10, and make sure the *Young's modulus of sample (GPa)* is set to 1 for the first simulation. On the second run, the *Young's modulus of sample (GPa)* will be changed to 5. Set all non-conservative and forces to "no" or "none". Now, click on the *Simulation parameters* tab. Set the *Number of points plotted* to 500. Check the *Plot a higher harmonic* box, and set the *Number of higher harmonics* to 1. Set the *higher harmonic* to 7 only. Make sure the *Include sample of time histories* box is checked. Set the *Number of time histories to collect* to 1, and that the corresponding amplitude ratio is 0.9 only. Set the *Number of cycles included in sample* to 2. Also, set the *X-axis variable* to *Amplitude ratio* for this example.

Finally, click the *Simulate* button in the lower right-hand corner, and wait for the simulation to reach completion. Once the simulation has completed, click the *Input* button. Open the *Tip-sample interaction properties* tab, and change the *Young's modulus of sample (GPa)* to 5. Then, click the *Simulate* button again, and wait for the second simulation to reach completion. For this example, each run generally takes about seven minutes to complete. This gives a total running time of about 14 minutes.

Figure 47 shows the key difference between internal resonance in air for harmonic cantilevers, which is a steady state resonant effect, and momentary excitation of higher eigenmode for soft cantilevers in liquids shown in Figure 39, which is a transient ring-down effect that occurs because of low quality factors inherent to soft cantilevers in liquids. For harmonic cantilevers in air, which have high quality factors, the second eigenmode develops a steady state *resonant* oscillation shown in Figure 47b.

The second eigenmode is excited by a harmonic of the tip-sample interaction force and therefore contains information about tip-sample interaction and thus the material properties of the sample. Unlike phase contrast in air (See Figure 48), which tells only about variations in dissipative (nonconservative) interactions, the amplitude of the second eigenmode in an internal resonance scheme contains information about conservative interactions. For the two purely elastic samples (conservative tip-sample forces), there is a clear contrast in the amplitude of the second 7th harmonic due to the different elasticities.

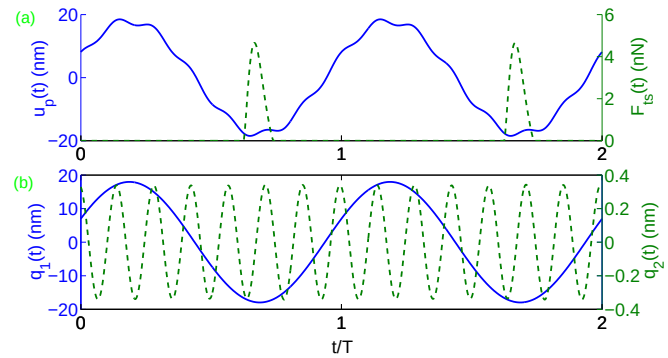

FIG. 47: Internal resonance observed while tapping on a sample of $E = 1$ GPa at an amplitude ratio $A_1/A_0 = 0.9$. (a) Photodiode deflection signal $u_p(t)$ and tip-sample interaction force $F_{ts}(t)$ vs. time t/T at $A_1/A_0 = 0.9$. (b) The first and second eigenmodes at A_1/A_0=0.9. (**AMAC Advanced** Example 3)

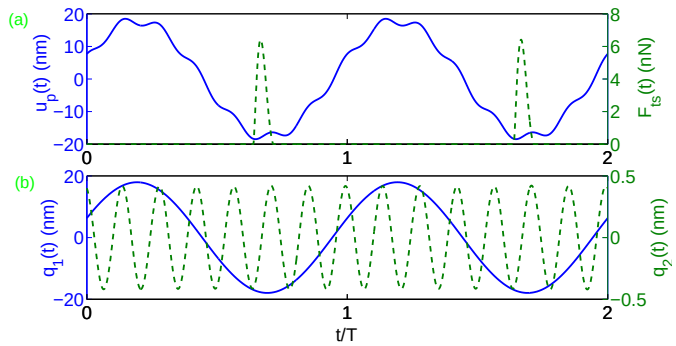

FIG. 48: Internal resonance observed while tapping on a sample of $E = 5$ GPa at an amplitude ratio $A_1/A_0 = 0.9$. Photodiode deflection signal $u_p(t)$ and tip-sample interaction force $F_{ts}(t)$ vs. time t/T at $A_1/A_0 = 0.9$. (b) The first and second eigenmodes responses $A_1/A_0 = 0.9$. (**AMAC Advanced** Example 3)

4. *Example 4: Bimodal excitation in air*

In this example, we will simulate a microcantilever excited in air at its first two natural frequencies. To begin this example, open the **AMAC Advanced** tool from the **VEDA** tools selection. Wait for the user input window to open (you should start in the *Operating conditions and cantilever properties* tab). Either select "Example 4" from the *Example Loader* dropdown box, or follow these instructions to set the parameters manually: Change the *excitation source* to *Magnetic* and set the *Frequency scheme* to *two frequencies (bimodal)*. Set the unconstrained amplitude $A_{0,1}$ *(nm)* to 20 and set the *Second frequency amplitude (nm)* to 1.17. Then, set the equivalent stiffnesses of the eigenmodes k_i *(N/m)*, and eigenmode quality factors Q_i to 30,1200 and 400,1200, respectively. Change the first and second natural frequencies (kHz) and excitation frequencies (kHz) both to $350, 2250$, and change *fd1 (kHz)* to 350. Set *fd2 (kHz)* to 2275. Change the *Z approach velocity (nm/s)* to 100. Next, click on the *Tip-sample interaction properties* tab. Under this tab, change the *Tip radius (nm)* to 10, and make sure the *Young's modulus of sample (GPa)* is set to 1 for the first simulation. On the second simulation, the *Young's modulus of sample (GPa)* will be changed to 5. Set the *Sample viscosity* $(Pa \cdot s)$ to 0. Now, click on the *Simulation parameters* tab. Set the *Number of*

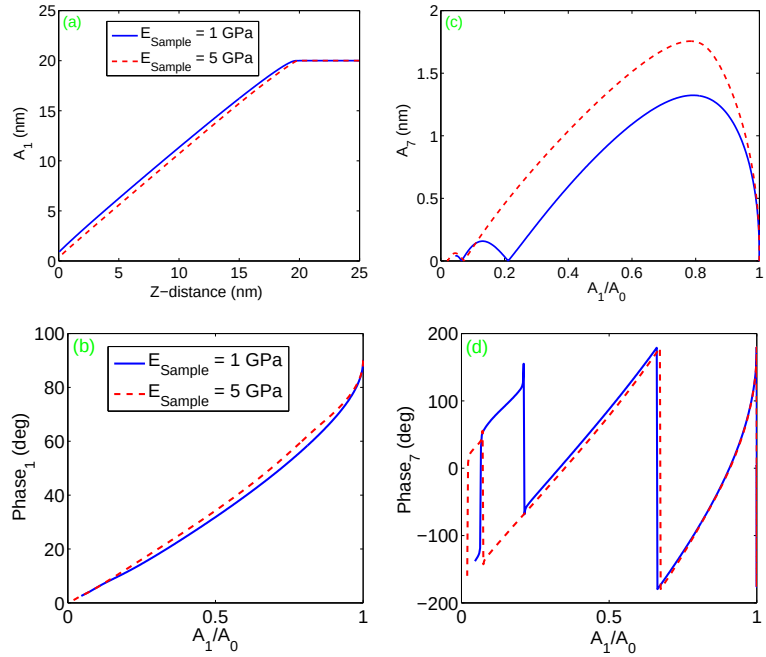

FIG. 49: (a) Amplitude A_1 (nm) or the primary harmonic of the excitation frequency vs Z-distance for two different samples. (b) Phase of the primary harmonic vs amplitude ratio A_1/A_0 where A_0 is the unconstrained amplitude. (c) Amplitude A_7 (nm) and (d) phase (deg) of the 7th harmonic vs amplitude ratio A_1/A_0 for two different samples. (**AMAC Advanced** Example 3)

points plotted to 500. Uncheck the *Plot a higher harmonic* box. Make sure the *Include sample of time histories* box is checked. Set the *Number of time histories to collect* to 1, and that the corresponding amplitude ratio is 0.9 only. Set the *Number of cycles included in sample* to 4. Also, set the *X-axis variable* to *Amplitude ratio* for this example.

Finally, click the *Simulate* button in the lower right-hand corner, and wait for the simulation to reach completion. Once the simulation has completed, click the *Input* button. Open the *Tip-sample interaction properties* tab, and change the *Young's modulus of sample (GPa)* to 5. Again, click the *Simulate* button and wait for the second simulation to complete. For this example, each of the two simulations may take up to 6 minutes to complete for a total running time of about 12 minutes.

Figure 50 shows the waveform, tip-sample interaction, and individual eigenmode responses for the first and second eigenmode. Because of the high quality factors in air, the momentary excitation of the second eigenmode is obviated and the waveform is much less sporadic. However, the signal still does not evolve into a periodic oscillation with respect to the drive frequency. Note the slightly different tip-sample forces shown in Figure 50.

Unlike conventional single frequency tapping-mode, internal resonance, and the first eigenmode of a bimodal scheme, we see that there is phase contrast in the second eigenmode that occurs even for the purely elastic samples (Figure 51). Additionally, the amplitude contrast of the second eigenmode is inverted from internal resonance (see Sec. III C 3, the stiffer sample having a smaller amplitude.)

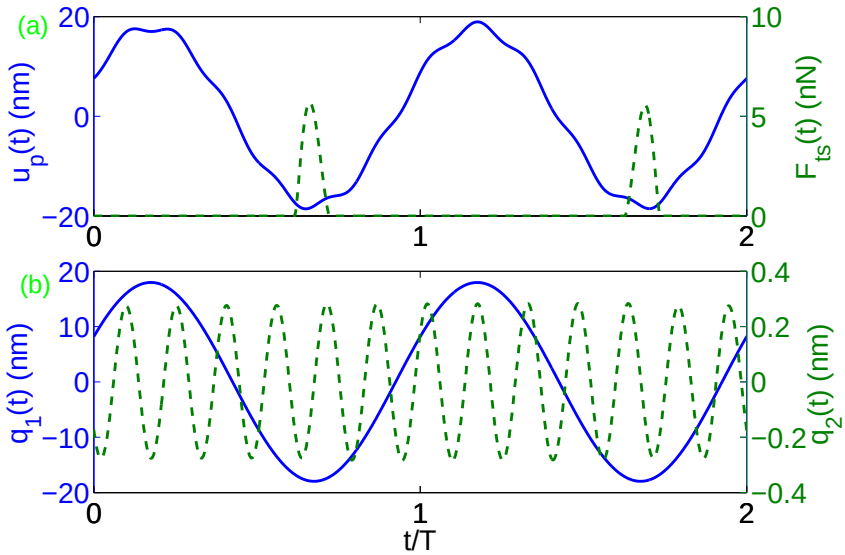

FIG. 50: The cantilever response when approaching a sample of $E = 1$ GPa. (a) Photodiode deflection signal $u_p(t)$ and tip-sample interaction force vs. Z-distance (nm) at $A_{1,1}/A_{0,1}$=0.9, where $A_{1,1}$ is the first harmonic or the primary excitation frequency and $A_{0,1}$ is the unconstrained amplitude at this frequency. (b) The response of first and second eigenmodes at $A_{1,1}/A_{0,1} = 0.9$. (**AMAC Advanced** Example 4)

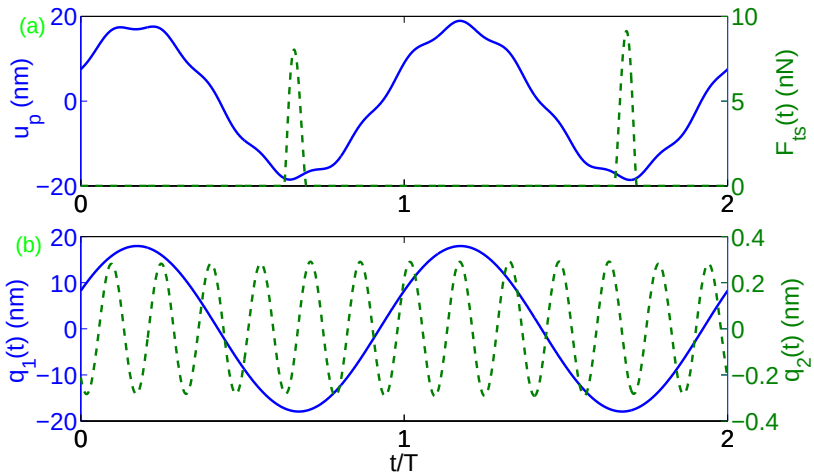

FIG. 51: The cantilever response when approaching a sample of $E = 5$ GPa. (a) Observed tip deflection and tip-sample interaction force vs. Z-distance (nm) at $A_{1,1}/A_{0,1} = 0.9$. (b) The first and second eigenmodes at $A_1/A_0 = 0.9$. (**AMAC Advanced** Example 4)

5. *Example 5: Phase spectroscopy in Bimodal AFM*

This example reproduces the results of [32]. We will attempt to show that bimodal AFM is sensitive to variations in conservative attractive forces. Select example 5 from the dropdown example loader and run the simulation. Then click back to tab 2 and change the Hamaker constant from 4e-20 to 9e-20, and run the simulation. Compare the two different results. In particular look at the 1st and 2nd frequency phase. Note that we are plotting these phases against the 1st frequency amplitude ratio. Then, click back to tab 3, and change the x-axis variable to *2nd frequency*

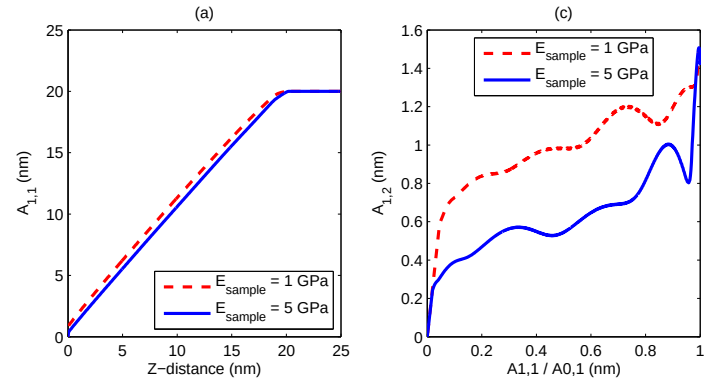
(a)
(c)
$A_{1,1}$ (nm)
Z−distance (nm)
$A_{1,2}$ (nm)
A1,1 / A0,1 (nm)
E_{sample} = 1 GPa
E_{sample} = 5 GPa

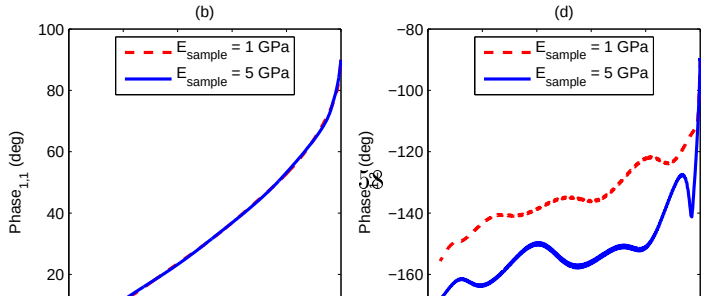
(b)
(d)
$Phase_{1,1}$ (deg)
$Phase_{2,1}$ (deg)
E_{sample} = 1 GPa
E_{sample} = 5 GPa

amplitude ratio. Simulate both Hamaker constants. Examine the two phases now. Your results should look like Figure 53. You should find contrast between the two materials when plotting the cross-mode representation. That is, when you plot 2nd phase against 1st amplitude, or 1st phase against 2nd amplitude, there is contrast between the two material. But when you plot 1st phase versus 1st amplitude, or 2nd phase versus 2nd amplitude, the two materials look identical. Your simulation results will likely show a little more noise than [32]. This is because we have picked a fast approach speed (100 nm/s) in order to keep the simulation time short. Reducing the approach speed will yield cleaner results.

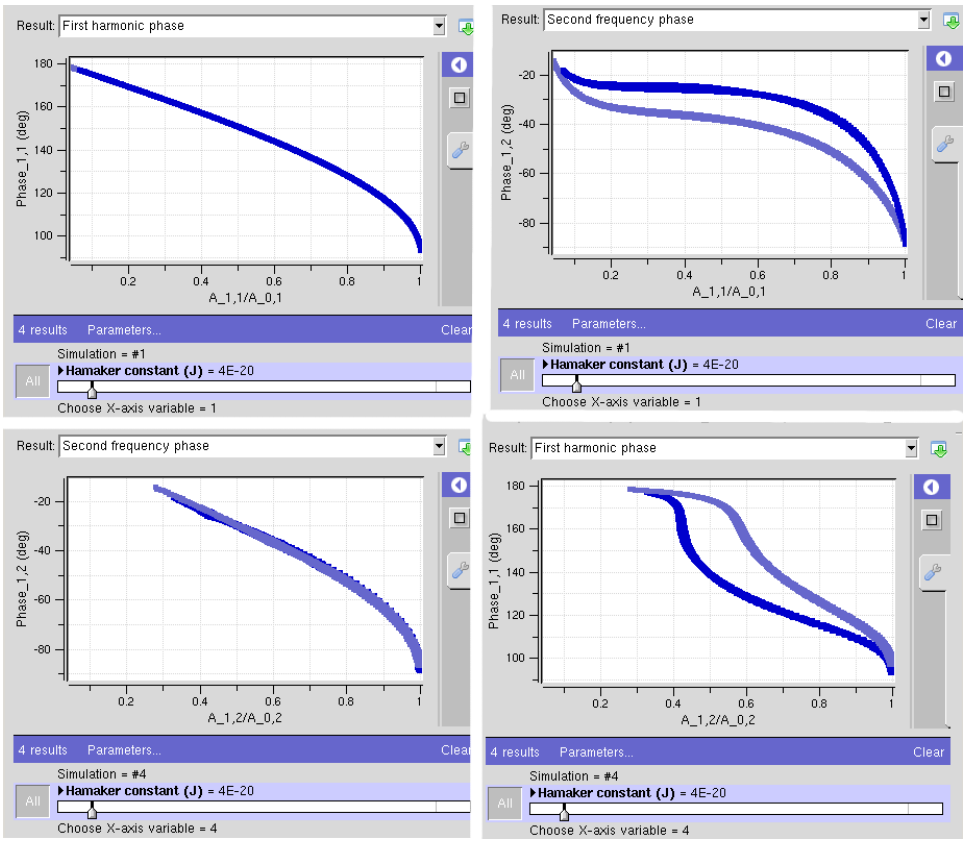

FIG. 53: Demonstration of bimodal sensitivity to conservative material properties. The left column shows the parallel mode representation: 1st phase vs 1st amp and 2nd phase vs 2nd amp. In this representation, both materials have the same result (aside from a small amount of noise). The right column shows the cross-mode representation, 1st phase vs 2nd amp and 2nd phase versus 1st amplitude. In this representation, there is a very clear difference between the two materials. (**AMAC Advanced** Example 5)

D. Amplitude Modulated Scanning (Advanced)

The Advanced Amplitude Modulated Scanning builds upon the Basic Scanning tool in the same way that the Advanced Amplitude Modulated Approach Curves tool builds upon the Basic Amplitude Modulated Approach Curves. Multiple eigenmodes, magnetic excitation, and other advanced features are included. New users should first refer to the examples for the Advanced Amplitude Modulated Approach curves tool and the Basic Amplitude Modulated

Scanning tool. All of the concepts in these tools are directly transferable.

1. Material Contrast in Bimodal AFM

While imaging a two component-blend polymer sample with a tapping mode cantilever in air, what types of material contrast can bimodal AFM give between the two blends? Open the Amplitude Modulated Scanning tool (advanced) and Load Example 1. This will set the parameters for a small step feature on a substrate, initially the feature and the substrate have the same material properties.

Before we run the bimodal case, let's run a plain tapping mode case. Choose "single frequency (conventional)" from the dropdown box "Choose frequency scheme" on tab 1. Run this simulation and look at the topography. By default, the feature has the same material properties as the substrate. Now, click back and change the Feature Young's modulus to 5 GPa on tab 4. Run this simulation. Examine the 1st harmonic phase. Can you see any difference between the phase on the feature and on the substrate?

You should notice two things. First, there is a topography error due to the different stiffness of the feature. Second, there is no phase contrast. Remember, phase in tapping mode depends on the RATIO of dissipative to conservative forces. That ratio is zero for both cases here because there is no dissipative component.

Now, change back to tab 1, and select Bimodal. You'll note that the drive amplitudes and frequencies are already filled in for you. Run this simulation. Examine second frequency amplitude and phase. You should see a very clear contrast between the materials.

Experiment with different combinations of materials. What types of contrasts can you see?

E. Amplitude Modulated Approach curves, steady state solution

THIS SECTION IS STILL UNDER CONSTRUCTION

The basic idea of the tool is described in Ref [33]. This tool uses a completely different method than all of the other tools. Instead of numerically solving the exact equations in time, an single-harmonic steady state version is used. This is less accurate, however in many situations can still provide a reasonable estimate and is an order of magnitude faster than other tools. This was motivated by the desire to simulate polymer surfaces using Attard's model (section IV B 8). This model is computationally intractable for the direct simulation used in the other tools, but runs in a reasonable amount of time with this tool.

The basic options are similar to the other Amplitude Modulated Approach Curves tools. Some exceptions are described below.

First, the excitation frequency is always assumed to be equal to the natural frequency (i.e. on resonance operation). Second, for bimodal operation, the tool needs to compute a number of cycles equal to the lowest common multiple (aka as "winding number") of the two drive periods. E.g. if the second frequency is 6.5 times the first, then the winding number is 2 (i.e. the pattern repeats every 2 cycles of the first frequency and every 13 cycles of the second frequency, because 13/2=6.5). If the ratio is 6.25 then the winding number is 4, and if the ratio is 6.249, then the winding number is 1000 (6249/1000 = 6.249).

To avoid this number being excessive, the second drive frequency is rounded. Two types of rounding are available. The first is ordinary everyday rounding to either 1, 2 or 3 decimal places. For example 6.24 (156/25, winding number 25) could be rounded to 6.2 (31/5 winding number 5). Although this is easy to understand, it may result in a larger than necessary winding number (i.e. a slower simulation).

A more intelligent rounding is available. This looks for a pair integers p, q such that p/q is approximately equal to the desired ratio and q is no more than a specified limit. q is the winding number. E.g. instead of rounding 6.24 down to 6.2 (winding number 5) with ordinary rounding, we could round it up to 6.25, which has a winding number of 4. This results in a simulation that is 20% faster.

You can check the exact frequencies that were used by looking for the "Omega_i (natural frequency)" line in the "Misc internal values" result.

The following examples are available

- Example 1: This is an identical set of parameters to Example 1 from the Basic Amplitude Modulated Approach Curves tool, meant to illustrate the differences between them. You should note that the steady state tool runs an order of magnitude faster, and gets nearly the same result. However, as the amplitude reduction must always be monotonic in this tool, it misses a portion of the curve after the jump from attractive to repulsive mode.

- Example 2: This example illustrates using the tool on a conservative sample, specifically capillary forces

- Example 3: This example illustrates the use of Attard's model in tapping mode, in repulsive regime. Examing the time history plots will show the useful features of Attard's model.
- Example 4: A second example of Attard's model, but this one is performed in an attractive regime. Note in the time histories, the tip does not indent the sample, rather you can see the sample rising up to meet the tip.
- Example 5: This example illustrates the use of bimodal on a conservative sample (Hertz)
- Example 6: This example illustrates the use of Attard's model in bimodal

F. Frequency Sweep

In the process of imaging a sample, an AFM operator would typically use a frequency sweep tuning curve to find a natural frequency (in order to pick an operating frequency), and possibly to measure the quality factor and/or stiffness of the given cantilever. In this case, the frequency sweep performed far from the sample, and frequency response is linear. To study nonlinear interactions with the sample, the cantilever is brought closer to the sample so that the oscillating tip interacts with the sample. The frequency sweep tool in VEDA is able to simulate frequency sweeps while in interacting with the sample. This is useful for gaining understanding of the underlying nonlinear dynamics of AFM as well as understanding the operation of the instrument.

1. *Example 1: Examining the nonlinear resonance response of a microcantilever near HOPG in air*

This example simulates the frequency response of an Olympus diving board cantilever at various distances above HOPG in dry air. The parameters for this simulation are taken from Lee, et al. [7] and are given in Table IV. In this example we will investigate the nonlinear resonance response.

To begin this example, open the **Frequency Sweep** tool from the **VEDA** tools selection. Start in the *Operating conditions and cantilever properties* tab. For *excitation method* choose *Acoustic excitation*, for *Excitation scheme*, choose *Linear ramp*, and uncheck the box *Use setpoint*. Enter the values listed in the table in the respective boxes. Then click the *Tip-sample interaction properties* tab. For *Tip-sample interaction model* select *DMT contact*, and uncheck the box *Auto Calculate intermolecular distance*. Enter the values from the table in the respective boxes. Then click simulate (the defaults in the *Simulation parameters* will be sufficient for this example.

The simulation should take approximately 20s. After the simulation has run, click the input button in the lower left to go back to the inputs. Select the *Operating conditions and cantilever properties* tab and increase the *Unconstrained Amp @ Nat Freq (nm)* from 89.3 nm to 89.4 nm. Click the simulate tab. Repeat this process increasing the unconstrained amplitude by 0.1 nm each time until a maximum of 90.2 nm (total 10 simulation runs).

Then, click the *All* button to the right of the slider bar on the graph window to plot all of the runs on top of each other. Then, click and drag in the plot window to zoom in on the peak of the curves. You should see a result

like in Figure 54. This figure is approximately the same as Fig 9 in Lee, et al., with three exceptions. First, Lee, et al. plotted peak-peak amplitudes while VEDA plots peak amplitudes, so the results are different by a factor of two. Second, Lee, et al. did not use exactly 0.1 nm steps. Finally, the paper was computed using AUTO97, which is able to find unstable branches (the dashed lines in Figure 9 of Lee, et al.). VEDA integrates the differential equation numerically and so only the stable branches can be plotted.

We note the following results about the plot. The lowest curve, representing 89.3 nm amplitude, is approximately the frequency response of a linear single degree of freedom (DOF) oscillator. The separation 90 nm minus the peak amplitude 89.3 nm yields a minimum tip-sample separation of 0.7 nm during the oscillation. At this range the van der Waals forces are almost zero, so there is little non-linear effect. With each successive curve, the minimum tip-sample separation decreases, so now van der Waals forces start to be significant. On each curve, identify the point at which the maximum amplitude occurs. You will notice that these points are decreasing in frequency as amplitude increases. This is characteristic of a *softening* non-linearity (see, for example [34]). At 89.8 nm unconstrained amplitude, the resonant peak will start to move up in frequency. This indicates that the repulsive DMT forces are starting to have some effect. DMT contact forces have a *stiffening* effect. By 90.0 nm unconstrained amplitude, the resonance peak has moved to the right of the original resonant peak. If we draw a line connecting the resonance peaks for each curve, we get the "backbone" curve, which is Figure 8 in Lee, et al.

Let us use VEDA to examine some further features of this phenomena. From the *Result* drop down box, pick *Mean Interaction forces*. Drag *Unconstrained Amp @ Nat Freq* slider bar from left to right to highlight the curves one at a time. It should look something like Figure 55. Notice that as the Unconstrained amplitudes increase, the Mean forces become more and more negative (attractive) until 89.8 nm. At 89.8 nm the mean force is still attractive but it is has started to turn around and come back towards zero. At 90.0 you see that the mean force has become positive (repulsive) for the first time. This is the transition between the so-called **attractive** and **repulsive** imaging regimes.

Of course, in an real experiment we could not observe tip-sample interaction force directly. But we can observe the phase of the response signal. Choose *First harmonic phase* from the drop down box, which will look like Figure 56. For the curves in the attractive regime, note that the phase angle increases (relative to the linear case) as the frequency sweeps through resonance but for the curves in the repulsive regime, the phase angle decreases.

TABLE IV: Input parameters for Frequency sweep examples.

PARAMETER	EXAMPLE 1
Operating conditions, cantilever properties	
Choose excitation source	Acoustic
Excitation scheme	Linear Ramp
Number of eigenmodes	1
Unconstrained Amp. @ Nat. Freq.(nm)	89.3
Auto calculate k_i ($i > 1$)?	no
k_i (N/m)	0.87
Q_i	33.3
Auto calculate Slope calibration?	yes
f_1 (kHz)	44
f_{dstart} (kHz)	43.5
f_{dstop} (kHz)	44.5
Sweep time (s)	0.1
Tip mass, (m_{tip}/m_c)	0
Use setpoint	no
Z distance (nm)	90
Tip-sample interaction properties	
Tip-sample interaction model	DMT contact
Tip radius (nm)	10
Young's modulus of tip (GPa)	130
Poisson's ratio of the tip	0.3
Auto Calculate intermolecular distance?	no
Intermolecular distance (nm)	0.38
Hamaker constant (J)	2.96e-19
Young's modulus of sample (GPa)	10
Poisson's ratio of the sample	0.3
Simulation parameters	
Number of points plotted	1000
Deflection points per cycle	1000

2. *Example 2: Effect of sample Stiffness on non-linear response*

In this example, we will determine the effect of sample stiffness on the non-linear frequency response that we found in the previous example. This example will use the same basic parameter set as Example 1. If you have just run example 1, then hit the "Clear" button in the outputs window to delete the old results and then go back to the Simulation. If you are starting this example fresh, follow the instructions to in Example 1 to input the first set of parameters, or use the Example Loader to get the first set of parameters. Make sure the Unconstrained Amplitude is 90.2 nm. Then in the simulation tab, change the Young's modulus to 5 GPa and hit the "simulate" button. Once the simulation has run, return the to inputs window and change Young's modulus to 10 GPa. Repeat for 15, 20, and 25 GPa.

Hit the "All" button to overlay the results. If you zoom in a little bit, the output window should look like Figure 57. You will notice that the jump-down happens farther to the right for stiffer samples. That is, there is a larger range of frequencies where non-linear effects are important. This is a general trend in AFM: Tip-sample non-linearities are

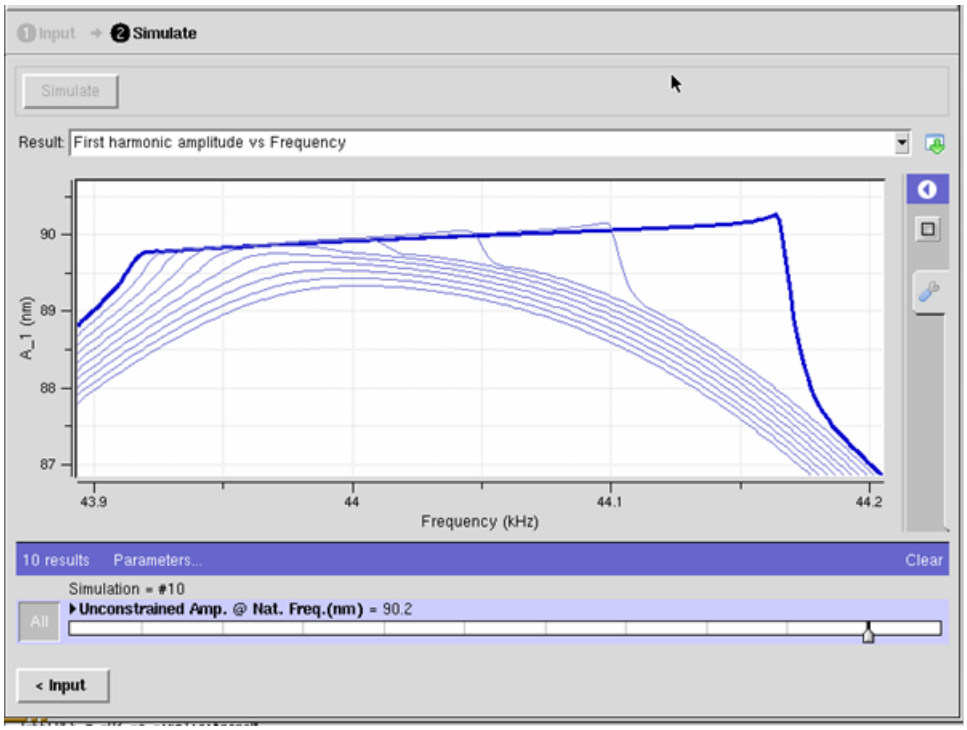

FIG. 54: First harmonic amplitude versus frequency for 10 different unconstrained amplitudes. The series of curves illustrates the softening (due to van der Waals) and then hardening (due to DMT contact) backbone curve (**Frequency Sweep** Example 1)

more pronounced for stiffer samples.

3. *Example 3: Sweep up versus sweep down*

In this example, we will examine the difference between sweep up (starting at a low frequency and gradually increasing the frequency) and sweep down (starting at a high frequency and gradually decreasing the frequency). For a linear system, these two are always identical, but for a non-linear system they may be quite different. This example will use the same basic parameter set as Examples 1 and 2. If you have just run example 1 or 2, then hit the "Clear" button in the outputs window to delete the old results and then go back to the Simulation. If you are starting this example fresh, follow the instructions to in Example 1 to input the first set of parameters, or use the Example Loader to get the first set of parameters. Make sure the Unconstrained Amplitude is 90.2 nm, and set the sample Young's modulus to 15 GPa and hit the "simulate" button. Once the simulation has run, return the to inputs window and reverse fd start and fd stop (i.e. set fd start = 44.5 and set fd stop = 43.5 kHz). Then hit simulate again. Hit the "All" button to overlay the two results.

You will notice that the sweep up and sweep down are close to each other, except for a small region in the middle. If you zoom in on this region, the output window should look like Figure 58. First, examine the responses at 44.2 kHz. At this frequency, the sweep up and sweep down simulations have very different amplitudes. This mean that

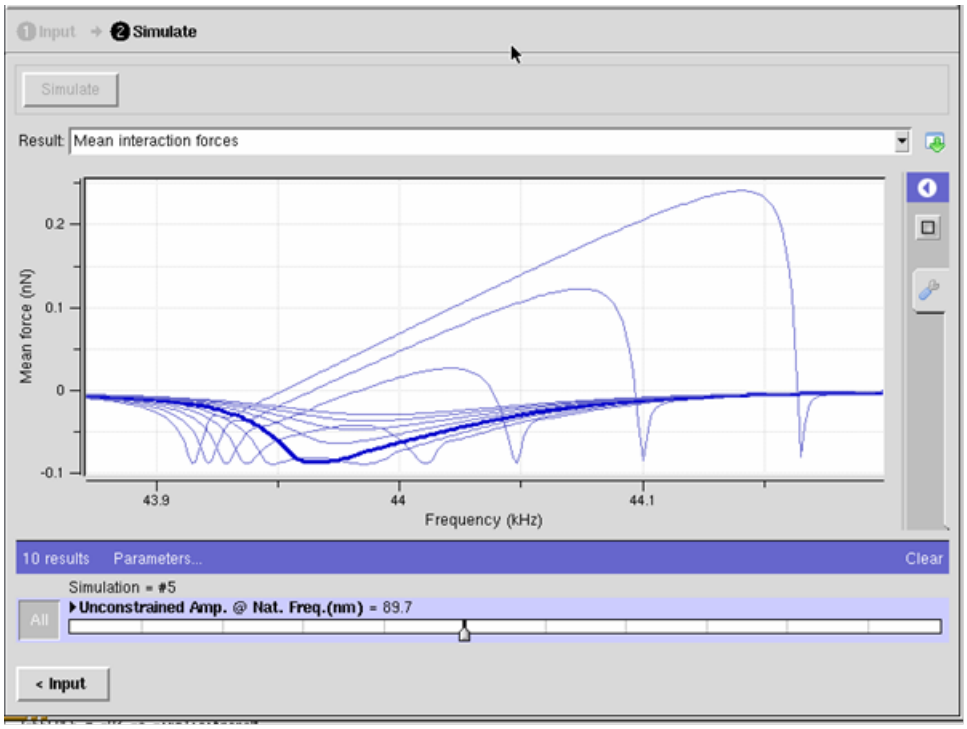

FIG. 55: Mean interaction force versus frequency for 10 different unconstrained amplitudes. The series of curves illustrates the transition from the attractive regime to the repulsive regime (**Frequency Sweep** Example 1)

at this particular combination of Z, unconstrained amplitude, and drive frequency, there are two different possible solutions. Which solution you get depends on the initial conditions (i.e. where you are coming from). Note that this condition, refered to as bi-stability, can be undesirable for imaging. Bi-stabilities are explored more in the Amplitude Modulated Approach Curves examples.

Now, examine the response at 44.3 kHz. There is also a small difference between sweep up and sweep down here. Is this also due to a non-linear effect? No. This is a linear effect due to the fact that we are changing frequency at a fairly rapid rate (change of 1 kHz in 0.1s) so that the system is not quite at steady state. If you were to repeat this simulation but with a sweep time of 0.5s instead, there should be much better agreement at 44.3 kHz, but of course that simulation will take five times longer to run. You might also notice that the jump-downs will be sharper (higher slope) at the slow sweep rate, and might happen at slightly different frequencies.

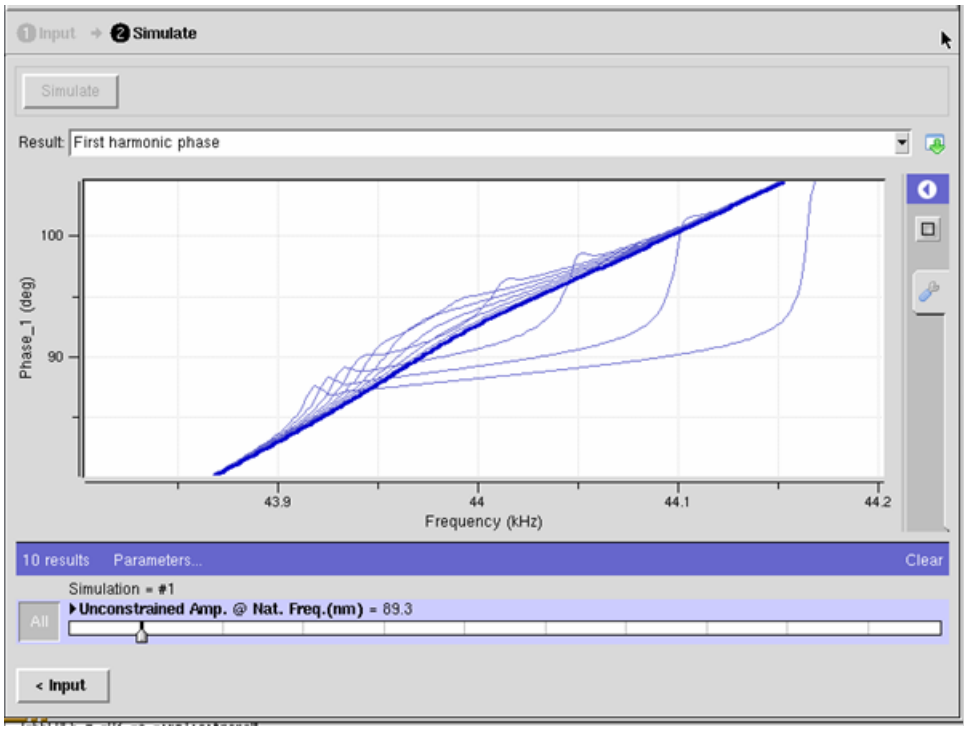

FIG. 56: First harmonic phase versus frequency for 10 different unconstrained amplitudes. The series of curves illustrates the transition from the attractive regime to the repulsive regime (**Frequency Sweep** Example 1)

G. Force Distance Curves

This tool simulates approach and retraction curves between the tip of an unexcited cantilever and a sample.

The following assumptions are unique to the F-Z Curves tool:

1. The cantilever is unexcited (forcing function applied to the cantilever). Any tip deflections would be caused by interactions between the tip and sample only.

2. Interactions between the tip and the sample are modeled by any one of the models described in Section IV A.

3. The Z separation between the sample can be reduced or increased, but the cantilever does not move laterally.

4. Inertial forces caused by the Z motion are negligible (but viscous forces are included)

The curves may be triggered (approach to a specific deflection and then reverse) or untriggered (approach to a specific Z distance and then reverse).

This section provides an overview of the outputs of the F-Z Curves (FZC) tool in the form of several example simulations.

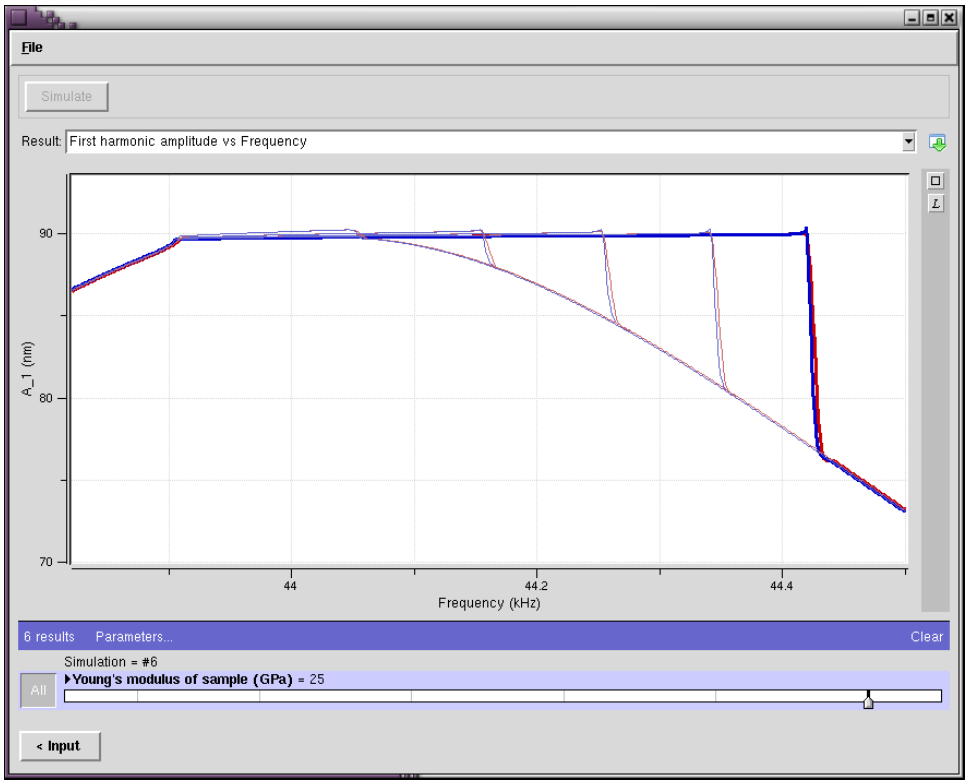

FIG. 57: First harmonic amplitude versus frequency for 5 different sample Young's moduli (**Frequency Sweep** Example 2)

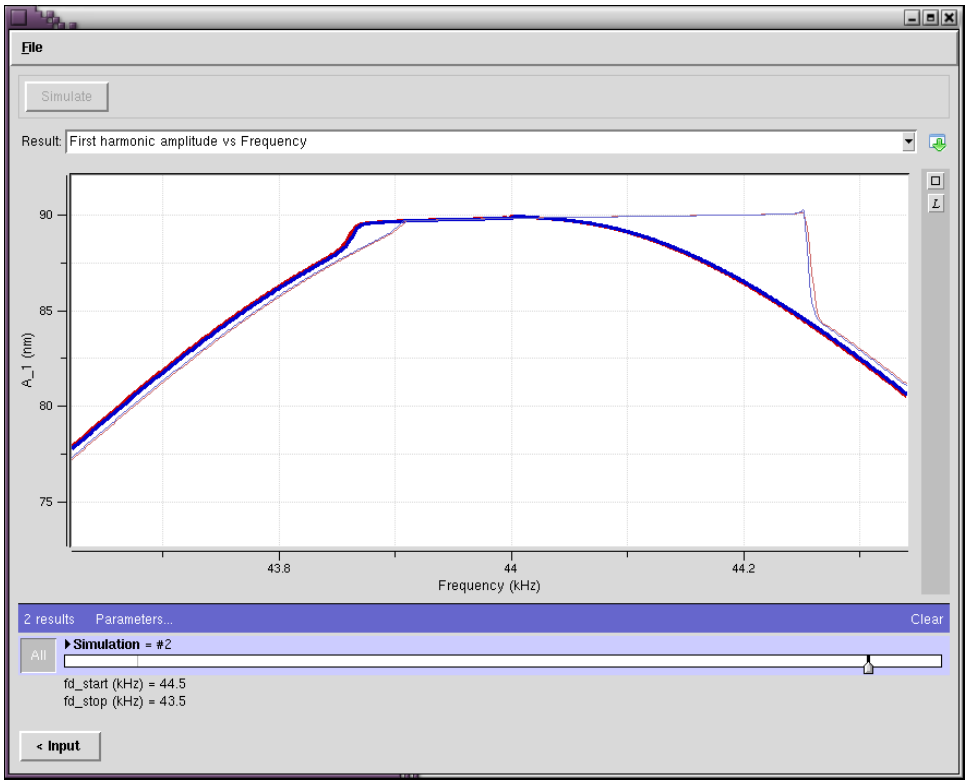

FIG. 58: First harmonic amplitude versus frequency for sweep up versus sweep down (**Frequency Sweep** Example 3)

TABLE V: Input parameters for F-Z Curves examples.

PARAMETER	EXAMPLE 1	EXAMPLE 2
Operating conditions and cantilever properties		
Operating mode	Untriggered, Approach & Retract	
Number of eigenmodes	1	1
Auto calculate k_i $(i > 1)$?	no	no
k_i (N/m)	0.87	0.87
Q_i	33	33
f_i (kHz)	44	44
Tip mass	0	0
Z approach velocity (nm/s)	200	200
Gamma (Z drag)	0	0
Initial Z separation (nm)	10	-5
Final Z separation (nm)	-5	10
Tip-sample interaction properties		
Tip-sample interaction model	DMT contact	JKR
Tip radius (nm)	10	10
Young's modulus of tip (GPa)	130	130
Poisson's ratio of the tip	0.3	0.3
DMT Calculation Options	Enter Adhesion force and Hamaker constant, autocalculate intermolecular distance	NA
van der Waals adhesion force (nN)	1.4167	1.4167
Hamaker constant (J)	$3.4 \cdot 10^{-20}$	NA
Young's modulus of sample (GPa)	1	1
Poisson's ratio of the sample	0.3	0.3
Simulation parameters		
Number of points plotted	1000	1000
Deflection points per cycle	1000	1000

1. Example 1: Approaching and retracting from a sample modeled using DMT contact

The primary experimental observable in this type of experiment is tip deflection versus Z displacement, and this is shown in Figure 59. Typically this deflection is then multiplied by the cantilever static bending stiffness to arrive at tip-sample interaction force versus Z displacement. Since this is a simulation, we have the tip-sample force available to us directly, see figure 60. Note that there appears to be some ringing of the cantilever on snap-in. This is because VEDA is simulating the entire cantilever dynamics in the time-domain, it is not a static solution. Two quantities that are often of interest in force spectroscopy are tip-sample interaction force versus gap and indentation versus Z displacement. In an experiment these would have to be reconstructed from the observed deflection, but since this is a simulation, we have them directly in Figures 61 and 62.

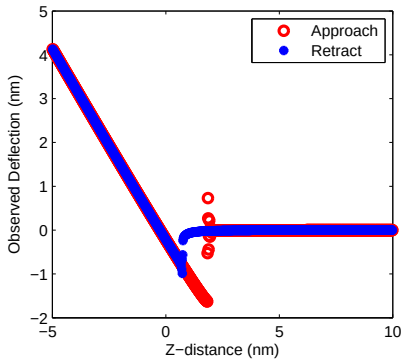

FIG. 59: Observed cantilever tip deflection versus Z-distance for the unexcited cantilever (modeled using DMT contact). (FZ Curves Ex. 1)

2. *Example 2: Approaching and retracting from a sample modeled using JKR*

This example uses the exact same parameters as Example 1, except the sample is modeled using JKR contact instead of DMT. Assuming you have already run example 1, go back to tab 2, change the interaction model to JKR and then simulate again. Compare the results for the two different interaction models. When you examine the cantilever deflection versus Z (Figure 63) you will note that during the approach, the cantilever tip snaps onto the sample later using the JKR model than with the DMT contact model. The reason for this is the discontinuous jump in the force seen in JKR, whereas the DMT contact model utilized an attractive van der Waals force even before the

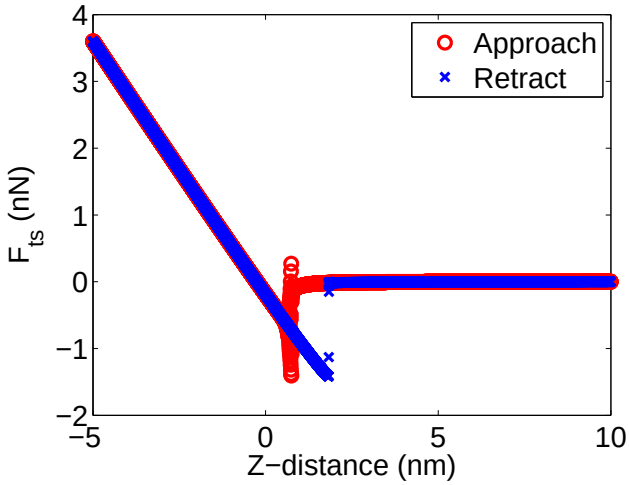

FIG. 60: Tip-sample interaction force versus Z-distance for the unexcited cantilever (modeled using DMT contact). (FZ Curves Ex. 1)

cantilever tip contacts the sample.

3. *Example 3: Approaching and retracting from a sample using Attard's model*

This example demonstrates the use of Attard's model for viscoelasticity (Section IV B 8). As this model is more complex than other models, an additional visualization has been included: a movie showing the interaction of the tip with the sample surface. This is located under "Surface Deformation Movie"

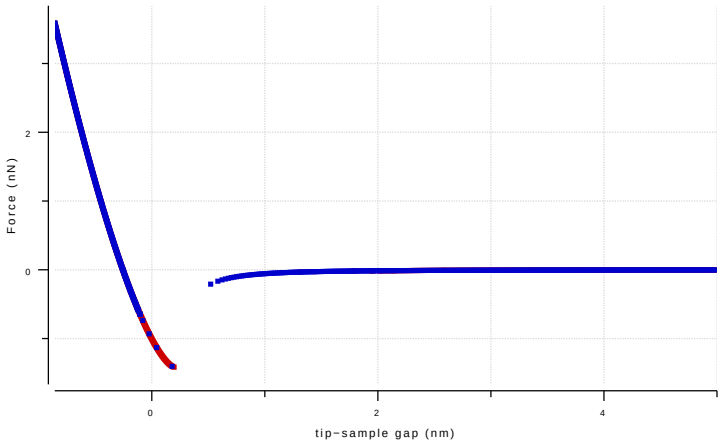

FIG. 61: Tip-sample interaction force versus gap for the unexcited cantilever (modeled using DMT contact). (FZ Curves Ex. 1)

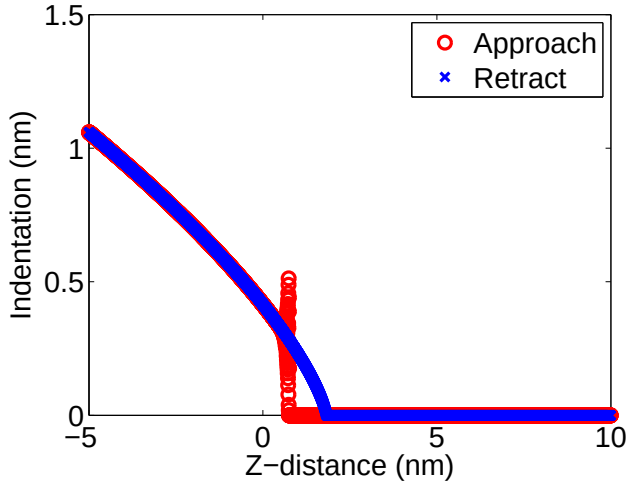

FIG. 62: Tip indentation into sample versus Z-distance for the unexcited cantilever (modeled using DMT contact).(FZ Curves Ex. 1)

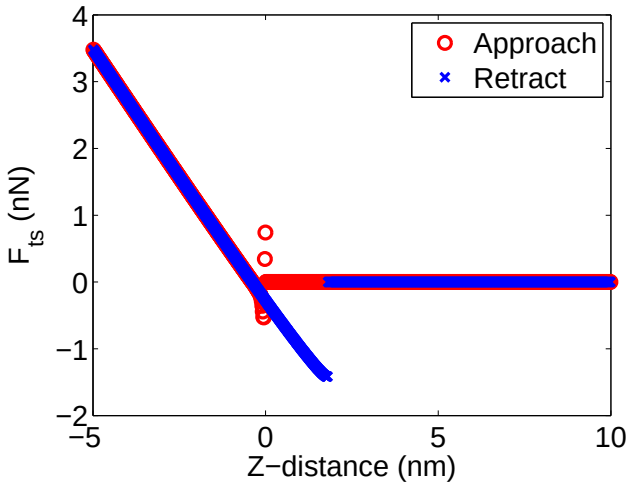

FIG. 63: Tip-sample interaction force versus Z-distance for the unexcited cantilever (modeled using JKR). (FZ Curves Ex. 2)

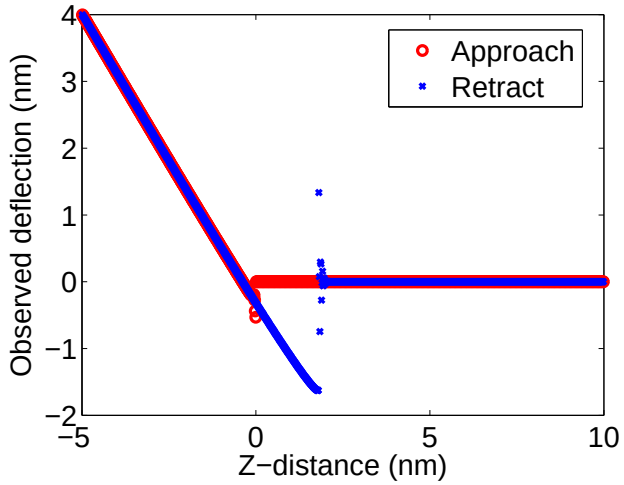

FIG. 64: Observed cantilever tip deflection versus Z-distance for the unexcited cantilever (modeled using JKR).(FZ Curves Ex. 2)

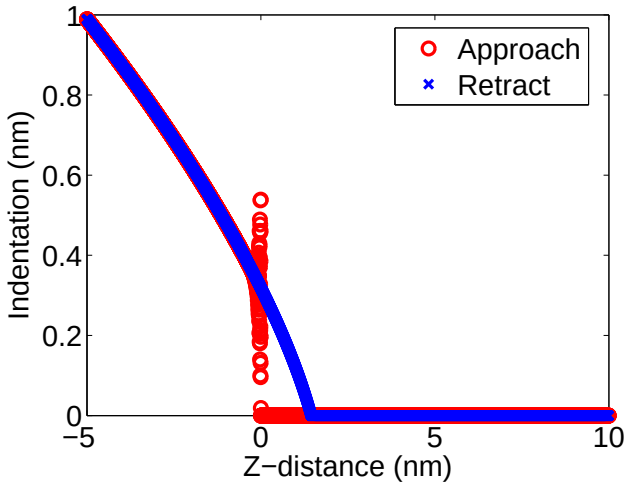

FIG. 65: Tip indentation into sample versus Z-distance for the unexcited cantilever (modeled using JKR).(FZ Curves Ex. 2)

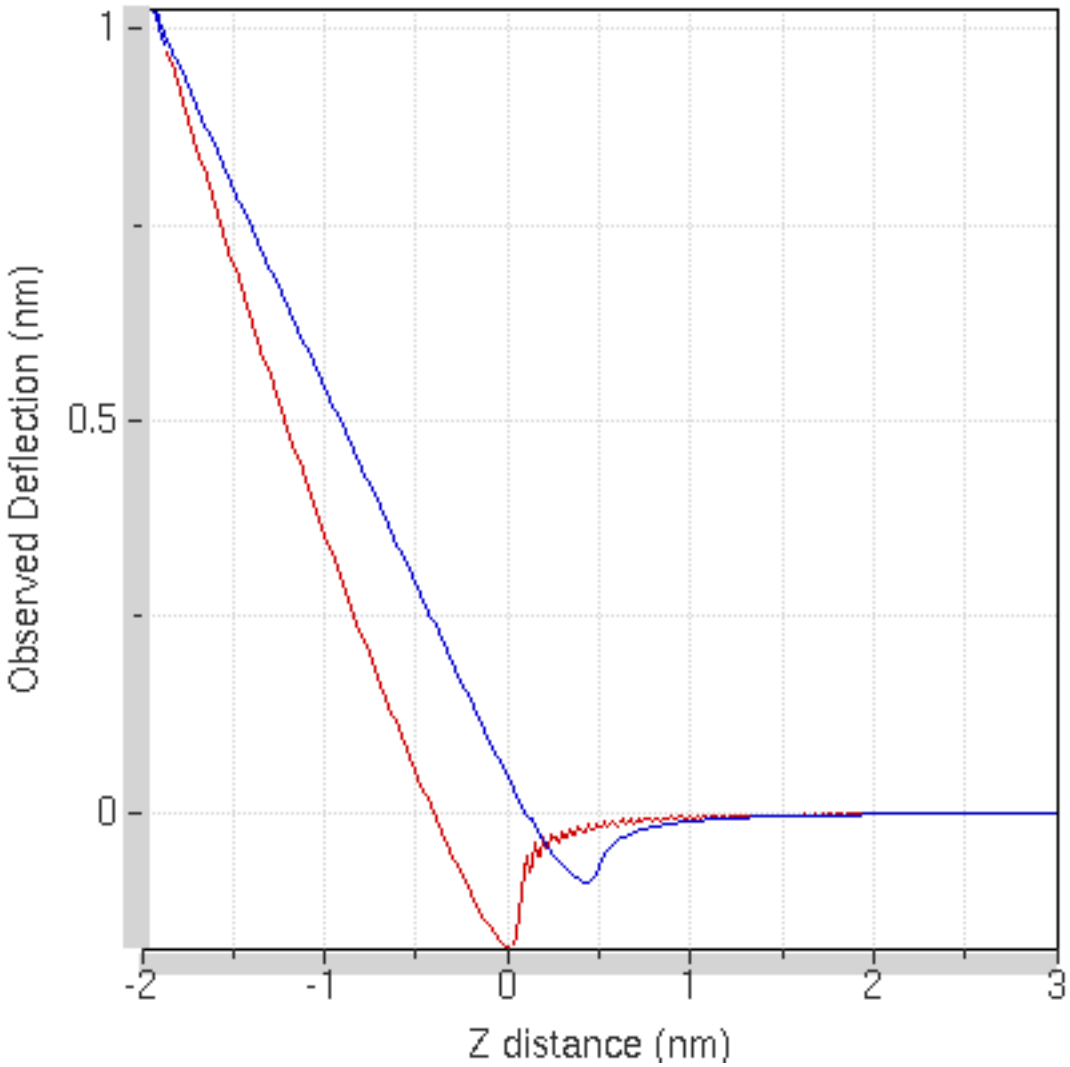

FIG. 66: Observed cantilever deflection vs Z distance for a soft sample modeled using Attard's model (Fz curves Ex 3)

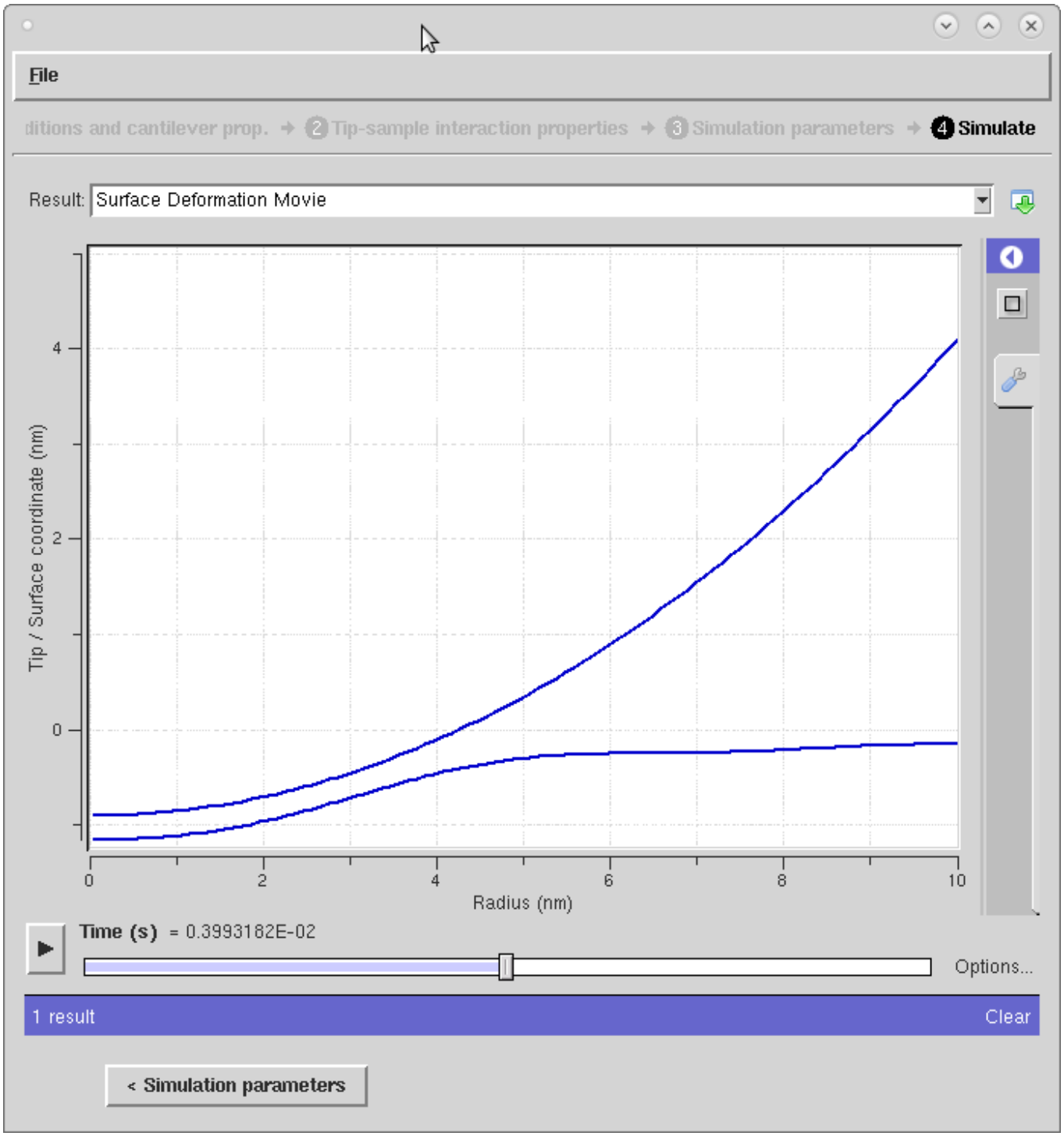

FIG. 67: Surface deformation movie. The top line is the tip and the bottom line is the sample. (Fz curves Ex 3)

H. Force Viewer

In order to run a simulation, it is necessary to specify a tip-sample interaction model. Cartoons of representative tip-sample interaction models are given in section IV A. It is often useful, however, to see the exact tip-sample force vs. gap curve for a specific set of parameters. The F-Z curves tool can be used for this (e.g. Figure 61), however the problem with that tool is that since it simulates the cantilever dynamics, some regions of the F-d curve are not visible. That is, when the cantilever snaps-in or pulls-off, it skips over a region in the F-d curve. The force-viewer tool is utility that does not have this deficiency. It plots the entire F-d curve independent of any cantilever dynamics.

1. *Example 1: DMT Model*

As an example, we shall plot the tip-sample interaction force for the parameter of F-Z curves Example 1. Open the Force Viewer tool from the VEDA tools menu. Enter 5 nm for the starting gap, -0.9 for the final gap. On the Tip-sample interaction tab, enter the parameters from Table V Example 1. Press simulate. You should get an output like Figure 68. Compare this with Figure 61. The two figures should be identical, except Figure 68 contains the entire curve in the area where Figure 61 had a blank spot.

The force viewer also plots the interaction stiffness, which is the first derivative of the interaction force. This is useful for comparision to many small-amplitude spectroscopy theories which calculate interaction stiffness (e.g. [35]). Note that the sign convention on interaction stiffness is typically taken such that a positive interaction stiffness causes a positive shift in resonance frequency. In other words, $k_{int} = -\frac{\partial}{\partial d} F_{ts}(d)$. Versions of VEDA prior to 2.0.19 (Feb 2011) used the opposite sign convention (positive gradient causes negative frequency shift, which is not as commonly used in the literature).

2. *Example 2: Viscoelastic Material Models*

The force viewer tool can also be used to explore non-conservative forces. In this case, the forces when approaching the sample are different than the forces retracting from the sample. In this example, we demonstrate using the tip-sample force viewer to see the forces when a Prony series model is used.

We start with the DMA (Dynamic Mechanical Analysis) data of Read [36] for polypropylene. The raw data is reproduced in Figure 69. This data is specified as E_{loss} and $E_{storage}$ versus frequency, which is typical for DMA data. VEDA cannot directly utilize this type of data. Instead, we must fit the data to one of the constitutive models in section IV A. In this case we use a Prony series (Generalized Maxwell) section IV B 6. The Prony series consists of a set of pairs of modulii G_j and relaxation times τ_j. To do the fit, we specify the τ_j a priori, and then use a least squares fit to calculate the modulii G_j that best fit the data.

In this case we choose to use a seven term series (more terms will fit the data better, but obviously will take longer

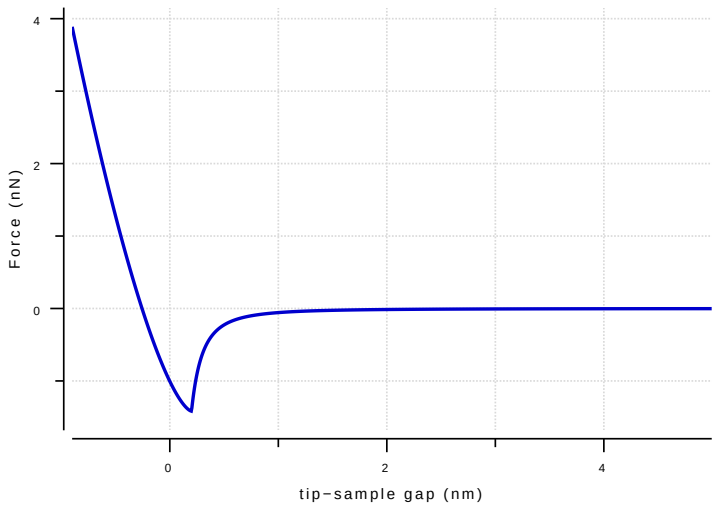

FIG. 68: Tip-sample force versus gap (modeled using DMT). Force Viewer Ex. 1

to simulate). We anticipate running a simulation with a 100 kHz cantilever which will have a contact time of a few microseconds, so we choose the relaxation times equally spaced (on a logarhythmic scale) between 2 ms and 0.1 us, which gives relaxation time spaced above and below the expected contact time. The fit is conducted using lsqcurvefit() command in Matlab. You can use the "Fit Viscoelastic DMA data to Prony Series" tool to do these fits on your own data.

The results are shown in figure 70. As you can tell, the Prony series fits the data reasonable well between 100 Hz and 1 MHz. A better fit could have been obtained with more terms, but this is not bad for an example.

Now we will see the forces that result from indenting this sample. Open the force viewer tool and select Example

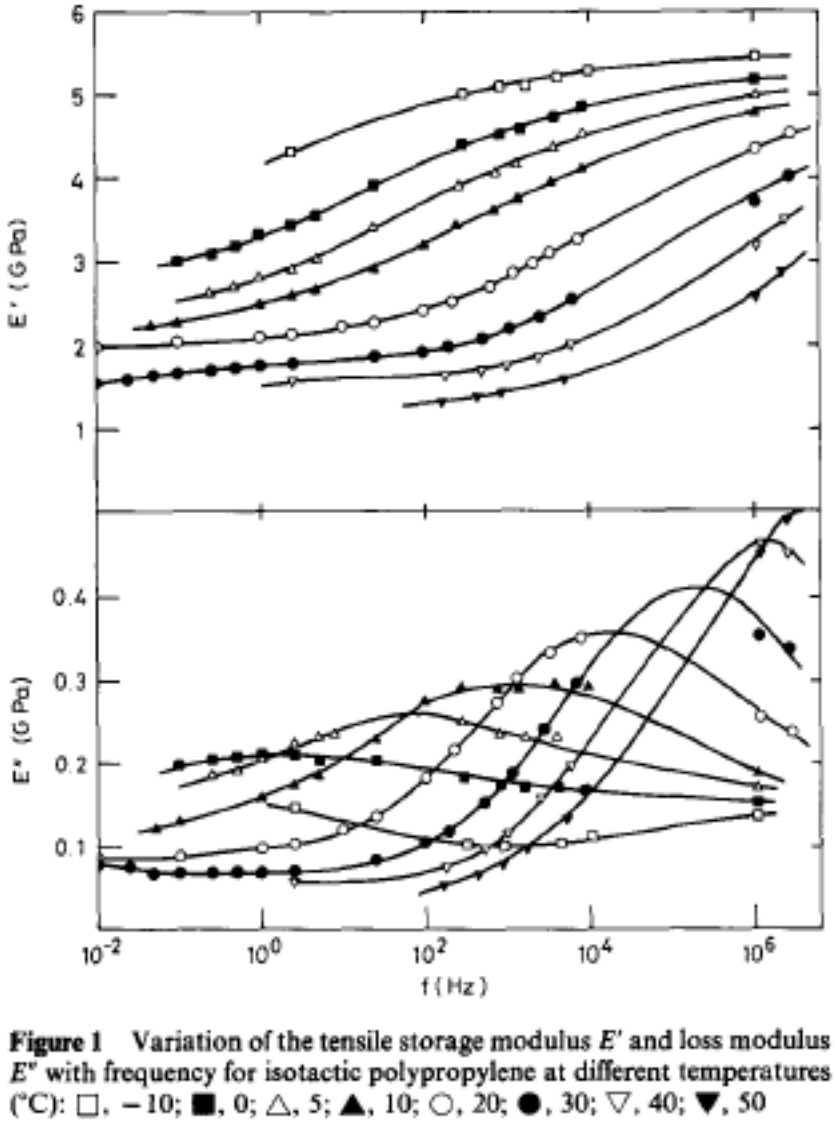

FIG. 69: DMA data from [36] for polypropylene. Force Viewer Ex. 2

2 from the drop down box. You'll note that the Non-conservative velocity option has been set to a sine wave with duration 10 microseconds, and that the initial gap is set just above zero. This approximately simulates a contact time of 10 us. On the tip-sample interaction tab, you'll note that the Prony series coefficients have been filled in at the bottom under Non-conservative forces. Click to simulate a single tap with these parameters. Then, go back to tab 1 and decrease the time from 10 microseconds to 0.1 microsecond and re-run.

The results are shown in Figure 71

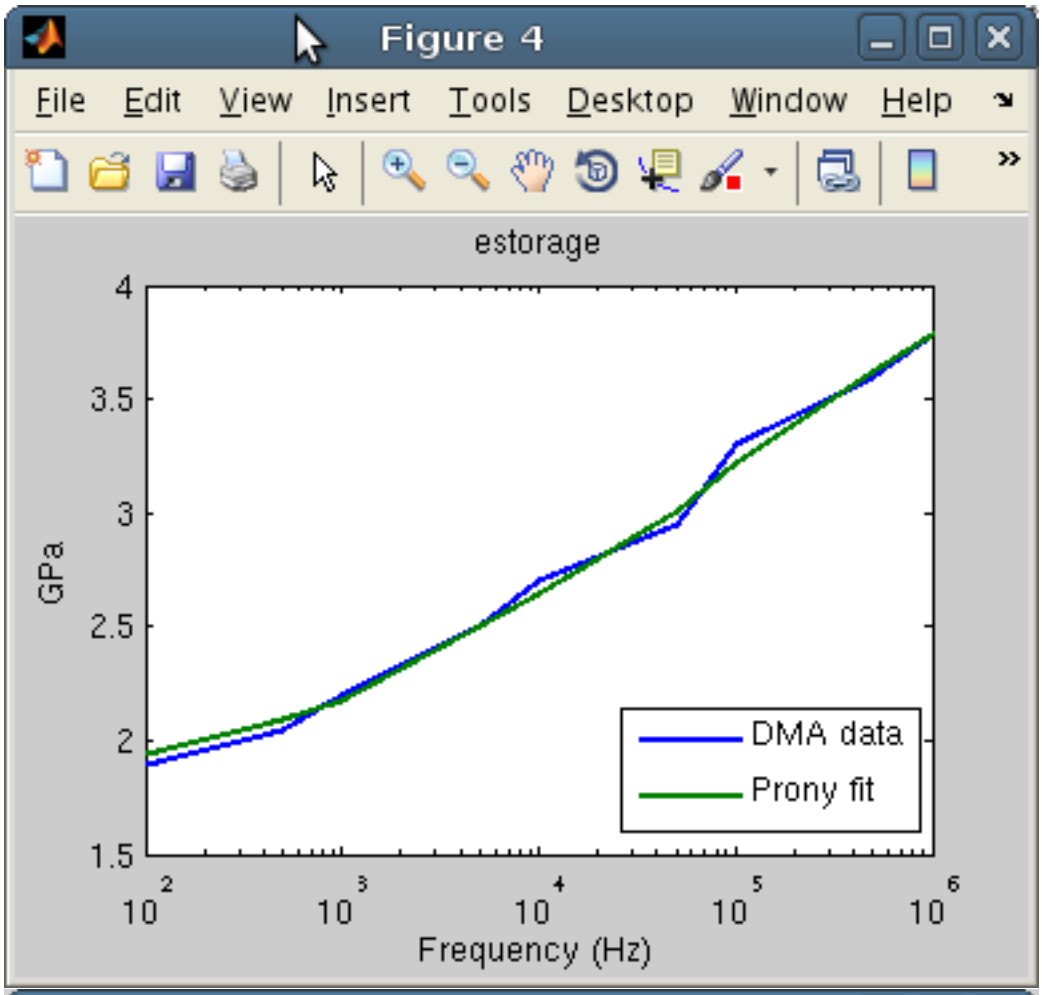
Figure 4
File Edit View Insert Tools Desktop Window Help
estorage
GPa
4
3.5
3
2.5
2
1.5
10^2
10^3
10^4
10^5
10^6
Frequency (Hz)
DMA data
Prony fit

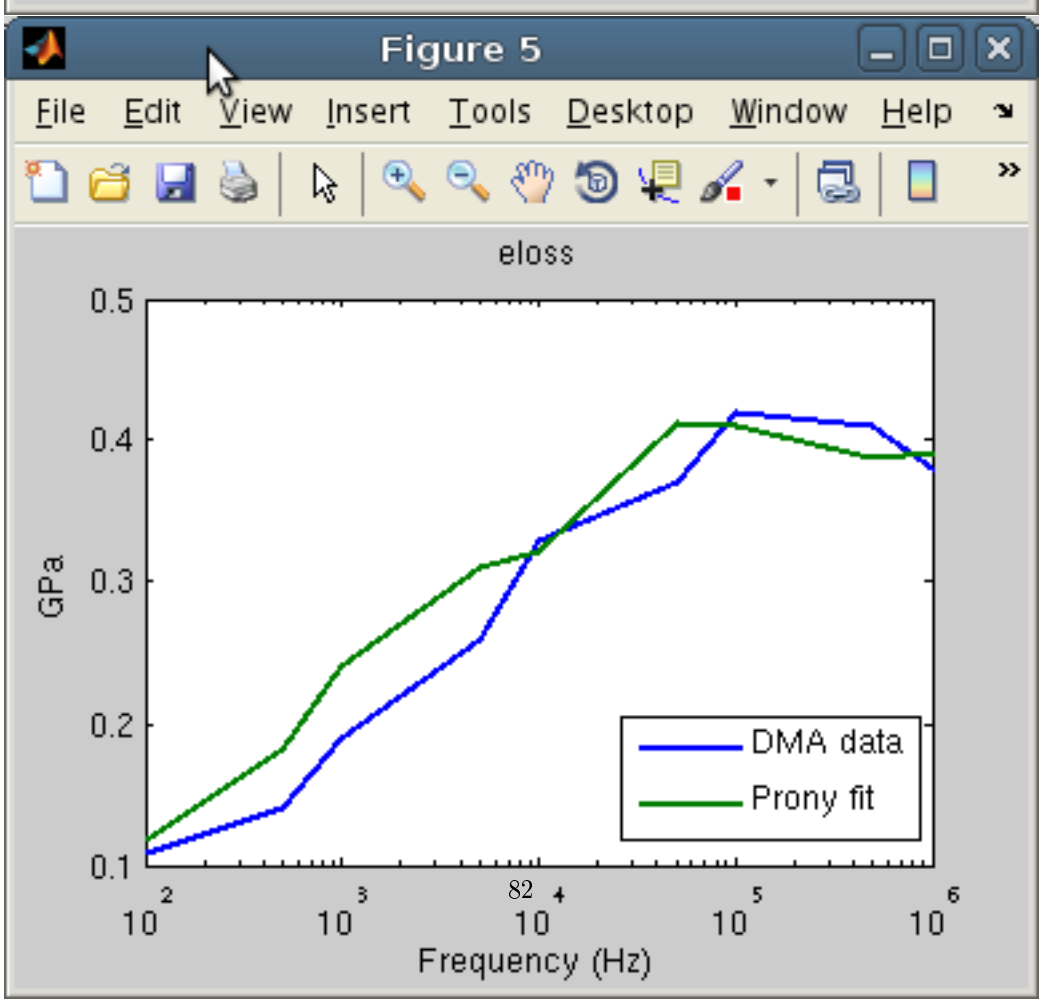
Figure 5
File Edit View Insert Tools Desktop Window Help
eloss
GPa
0.5
0.4
0.3
0.2
0.1
10^2
10^3
10^4
10^5
10^6
Frequency (Hz)
DMA data
Prony fit

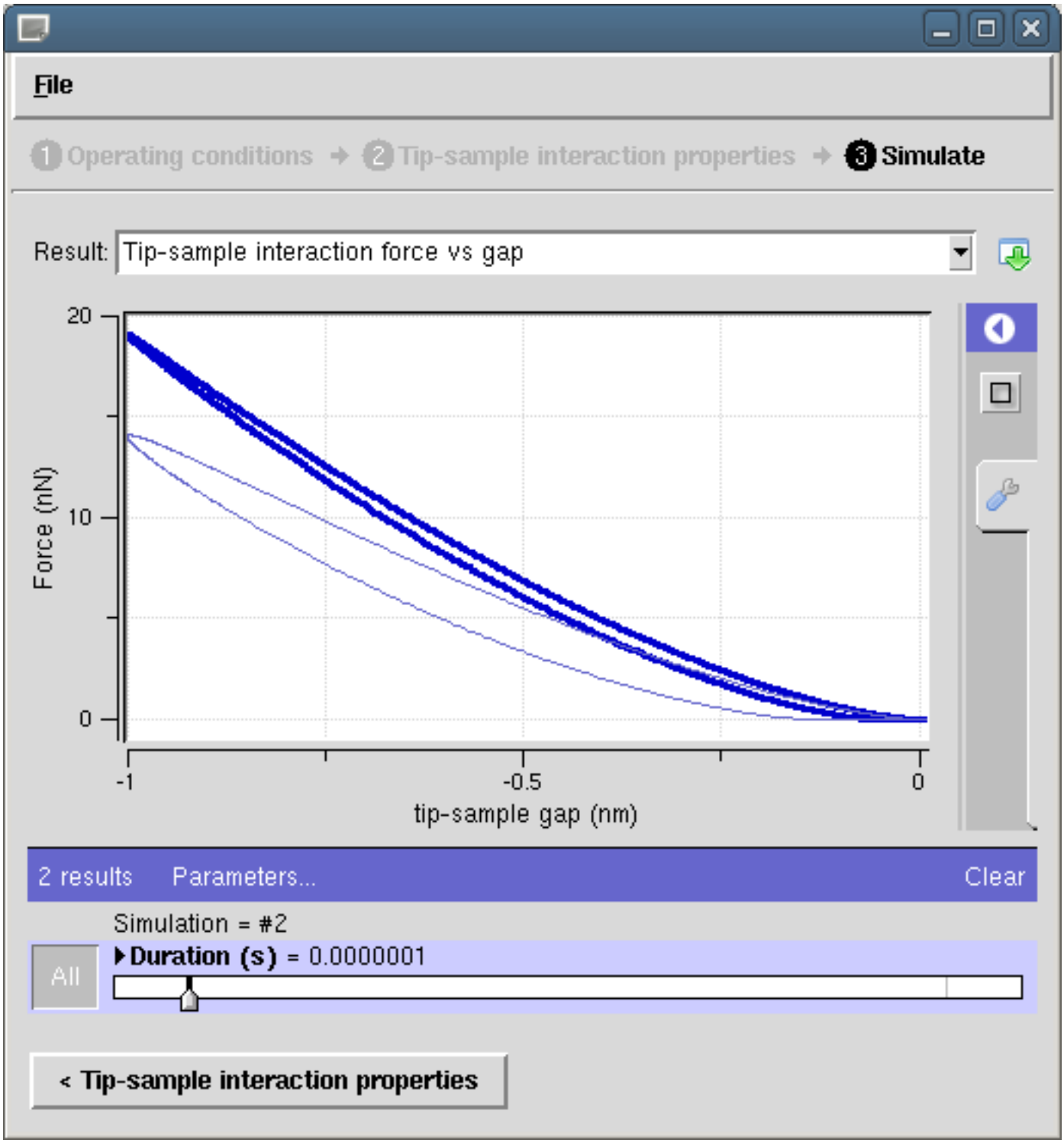

FIG. 71: Simulation of a single tap on a polymer at two different rates. Force Viewer Ex. 2

3. *Example 3: Attard's model*

Compare this model to the Force Distance Curves Tool Example 3 in section III G 3. The tip-sample interaction parameters are identical. For the FZ curves tool, the Z distance is specified, and the tip-sample gap is determined

based on the dynamic deflection of the cantilever. In the force viewer tool, the tip-sample gap is specified a priori. There is no cantilever. In the limit of an extremely stiff cantilever (i.e. zero cantilever deflection) the two tools would give the same result.

I. FM Approach Curves

1. *Approach to a Si facet in UHV*

In this example we simulate the approach of a silicon tip onto a (111) silicon facet. The majority of the parameters are taken from [37]. The only difference is that Nony's controller scheme is slightly different, so we have used controller gains appropriate to VEDA's controller.

Launch the Frequency Modulated Approach Curves tool and enter the parameters shown in Table VI. The majority of the parameters are similar to those in the Amplitude Modulated Approach Curves tool so we will only walk through a few of the parameters.

The Frequency Modulation tab is unique to the FM tools. On it you will find the controller gains for the frequency modulation controllers. Chose Direct Amp/Freq Control yes (see section IV F). We have implemented the method of [38] to automatically calculate gains for the PLL and amplitude controller. Leave this box checked to get a good starting guess for the gains. After the simulation has run, you can see the gains that were calculated in the *Misc. Internal Values* result, and use them as starting values if you want to tweak the controller performance.

The simulation parameters tab contains one difference from the AM tools. For the AM tools, it was possible to plot most variables against either Z displacement or setpoint ratio. For FM, setpoint ratio does not exist because amplitude is constant. Therefore, the options are Z displacement and min gap (also known as the "distance of minimum approach" in the literature). Choose min gap for this simulation to compare with Nony's results.

Hit the simulate button and wait for the simulation to run. Note that this simulation does take several minutes to run. If you are short on time, you can increase the approach speed to 20 nm/s. The results will be slightly off, but the general picture will be okay.

The first thing you should check in any frequency modulation approach curve is the the controller performance. Examine the first harmonic amplitude and first harmonic phase. You will want to verify that the these two parameters stay relatively constant during the approach. The phase is shown in Figure 72. In this case phase is constant to within about 0.1 degree during the majority of the approach and starts to deviate at the very end (where the Morse potential starts changing very rapidly). The amplitude controller also performs well, about 0.1 percent deviation over the entire range. This controller performance should be acceptable. When you start to run your own simulations, always check these two parameters. If the first harmonic amplitude or phase starts to deviate from a straight line, you'll need to tune the controller parameters. If these drop significantly, you may need to increase the gains. If they start a growing oscillation, you may need to decrease the gains. You will need to reconsider the gains any time you change a

parameter, but especially approach speed, quality factor, lock-in parameters, sampling rate, and natural frequencies

Now, examine the FM Feedback results. This contains the two main FM observables. The frequency shift is of most interest. The shape of the frequency shift follows the tip-sample interaction force. In fact, the exact tip-sample interaction force should be recoverable from the frequency shift (see [39]). The other channel is the drive amplitude, which is sometimes called the "apparent dissipation" or sometimes just "dissipation." In this case, the Morse potential is a purely conservative interaction, so there is no actual dissipation there. However, the driving frequency is changing, and the energy dissipation of a simple harmonic oscillator changes with the drive frequency. This is one contribution to the apprent dissipation. A second component is the small phase error we noted before. A phase error indicates that the PLL is not exactly tracking the natural frequency, and when driving off resonance more energy is required. To reduce this error, we could decrease the approach speed to give the PLL more time to react.

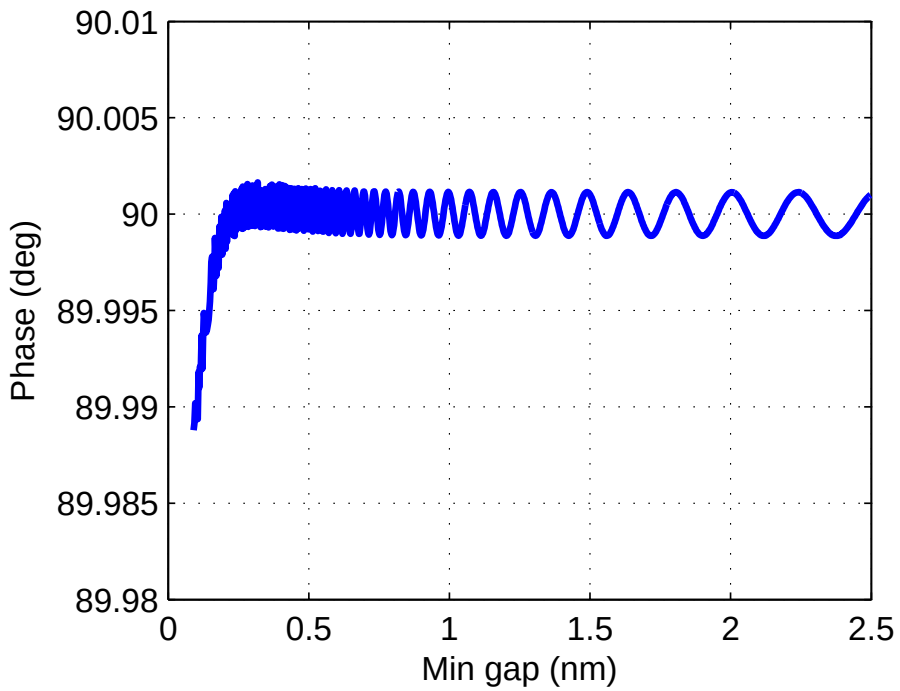

FIG. 72: First harmonic phase versus min gap during the approach curve. The phase stays relatively constant during most of the approach, indicating a good controller. Near the left side of the figure, the change in phase indicates that the controller cannot keep up as well in this region. FMAC Ex. 1

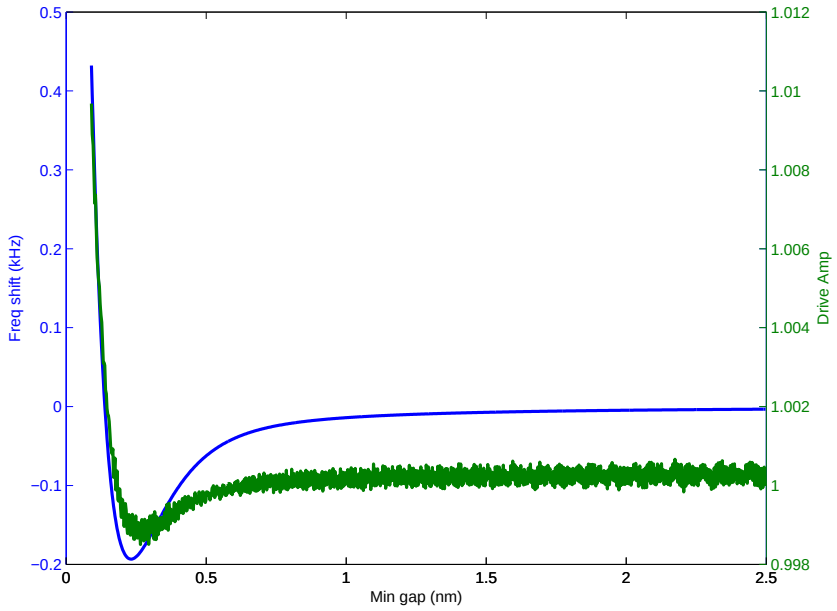

FIG. 73: Frequency shift (blue) and Drive Amplitude (red) (aka apparent dissipation) during the approach curve. FMAC Ex. 1

TABLE VI: Input parameters for Frequency Modulated approach curve examples.

PARAMETER	EXAMPLE 1	EXAMPLE 2
Operating conditions, cantilever properties		
Choose excitation source	Acoustic	magnetic
Choose frequency scheme	Single Frequency	Single Frequency
Number of eigenmodes	1	2
Unconstrained Amp. @ Nat. Freq.(nm)	7.0	1
Auto calculate k_i $(i > 1)$?	no	yes
k_i (N/m)	30	0.6
Q_i	100	3,4
f_1 (kHz)	150	10,70
f_d (kHz)	150	10
Tip mass, (m_{tip}/m_c)	0	0
Approach velocity (nm/s)	2	5
Initial Z separation (nm)	9.5	3
Final Z separation (nm)	7.1	0.5
Choose Lock-in filter order	4th order	2nd order
Lock-in time constant	50 us	1 ms
Sampling frequency (MHz)	0.5	1
Frequency Modulation		
Direct Amp/Phase Control	yes	yes
Autocalculate Controller gains	yes	yes
Tip-sample interaction properties		
Tip-sample interaction model	Morse Potential + van der Waals	Hertz
Tip radius (nm)	5	5
Hamaker constant(J)	1.865e-19	NA
Morse equilibrium position(nm)	0.2357	NA
Morse range(nm)	0.12	NA
Morse depth(J)	3.641e-19	NA
Young's modulus of sample	60	
Poisson's ratio of the sample	0.3	
Include hydration forces	no	yes
Lambda	NA	0.245
Hydration scaling	NA	1.2e7
Non-conservative solvation forces	no	yes
Scaling	NA	1e-5
Decay	NA	0.25
Simulation parameters		
Number of points plotted	1000	
Deflection points per cycle	1000	
Choose x-axis variable	Min gap	
use defaults for all other parameters on this tab		

2. *Approach to mica in liquid*

This example is under construction

J. FM Scanning

The FM scanning tool combines the functionality of the other scanning tools with the frequency modulation discussed under FM Approach Curves. The only additions are that there is now a frequency shift setpoint on tab 2 (you can specify if this should be an attractive or repulsive shift).

It is recommended to use autocalculation of the Amplitude and PLL gains when using this tool. If you wish to use non-default gains, it is suggested that you use the FM Approach curves tool to find stable gains first, then move on to this tool. Otherwise if you have stability problems, it will be difficult to determine if the problem is with your Z (topography) gains or with the FM gains.

There are currently no examples for the FM Scanning tool.

K. Contact Mode Scanning

The contact mode scanning tool simulates one of the earliest and simplest AFM imaging modes. The utility of this tool is that allows understanding the operation of the controller without having to deal with the complexities of dynamic AFM.

1. *Example 1: Tip-sample geometry convolution*

This example illustrates the tip-sample geometry convolution described in section IV H. Select example 1 from the drop down menu. On the tip-sample interaction properties tab, note that we have picked a 5 nm tip radius. The end of the tip is assumed to be spherical. Also, on the feature properties tab, we've picked a sinusoidal feature with height 30 nm and width 35 nm and checked the box for tip-sample convolution.

Click simulate to begin the simulations. When it's done, the result should look like 74. The measured topography (blue) resembles the actual sample geometry (red), but it is just slightly wider. This is a common problem with measuring widths of small features.

Go back to the feature properties tab and reduce the feature width to 25 nm. Repeat the simulation for feature widths of 15, 5, and 1 nm. When you're finished the result should look some like Figure 75. Note that we've turned off the "sample height" plots to improve clarity (click on the triangle to reveal the legend, and uncheck all the red lines). Note that as the feature width decreases, the measured geometry looks less and less like a sinusoid, and more like a rectangle a circle of radius 5 nm on top (draw in dashed line for illustration). In this case, the sample is showing us an image of the tip, instead of the tip showing us an image of the sample!

L. Peak force tapping tool

THIS SECTION IS STILL UNDER CONSTRUCTION

The peak force tapping tool simulates the scanning mode of the same name (https://www.bruker.com/content/bruker/int/en/products-and-solutions/microscopes/materials-afm/afm-modes/peakforce-tapping.html). In this mode, the Z piezo is oscillated at a frequency considerably lower than the cantilever resonance, e.g. 2 kHz for a 100 kHz cantilever. Effectively this collects a series of force-distance

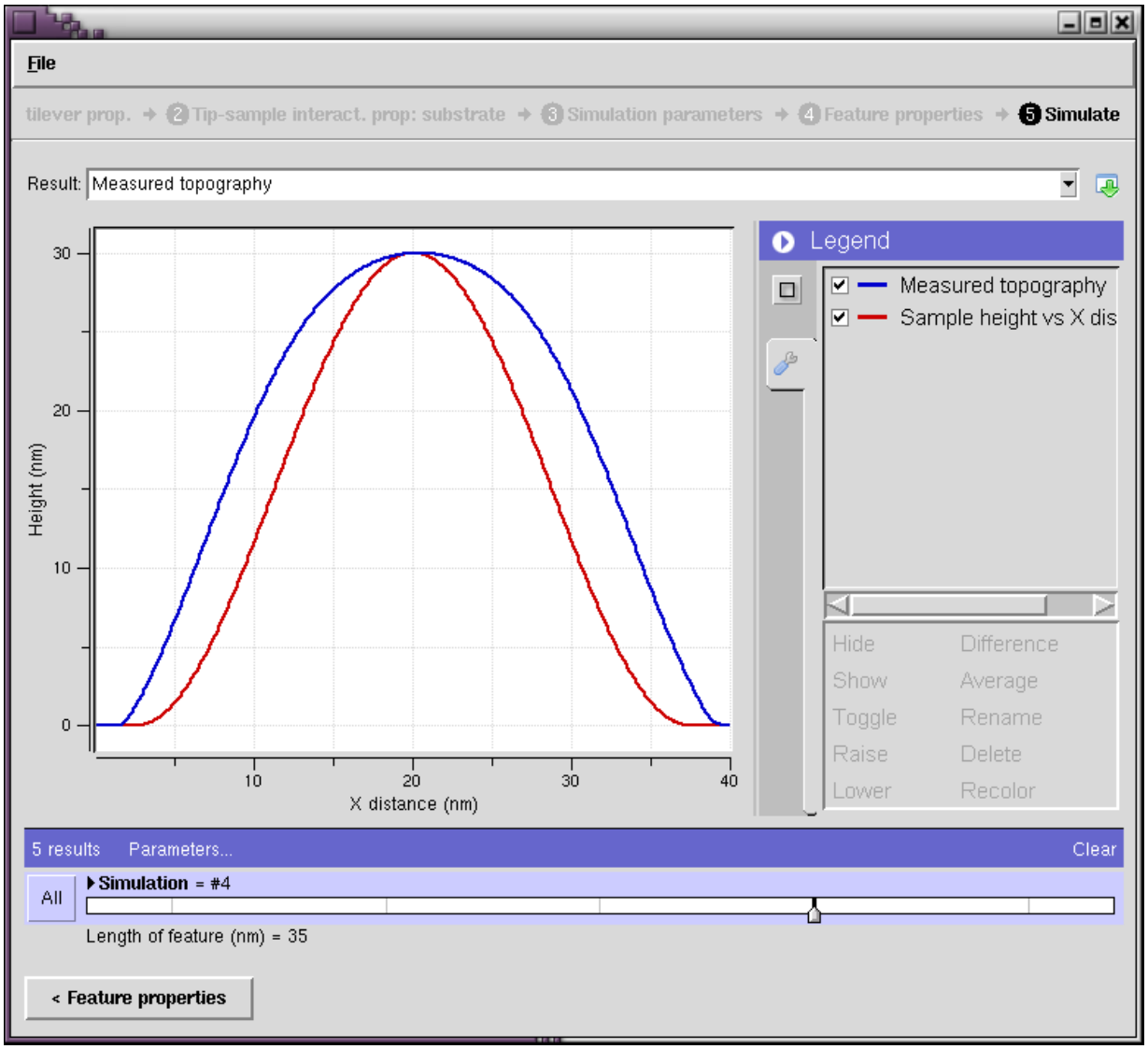

FIG. 74: Measured topography for a 5 nm tip radius compared with the actual sinusoidal feature of width 35 nm. The measured topography resembles the feature, but is just slightly wider.

curves. For each curve, the deflection is processed to extract the peak force, and then a feedback control is used to adjust the mean Z position such that the peak force is constant over the scan.

Major assumptions of this tool:

- In a real AFM, only the deflection is an experimental observable and the force must be reconstructed. This is illustrated in Figure 76. In the quasi-static limit (excitation << resonance frequency), the cantilever behaves as a simple spring F=kx and force is simply deflection times stiffness. For finite excitation frequencies, there will be some steady state dynamic response, but it is fairly easy to filter it out and recover the tip-sample force. As the excitation frequency becomes higher, this reconstruction becomes more difficult. The feedback control in the VEDA peak force tapping tool is directly on the simulated tip-sample force. In other words, it is assumed that the force can be *perfectly* reconstructed from the observed deflection. This will be true only for very low

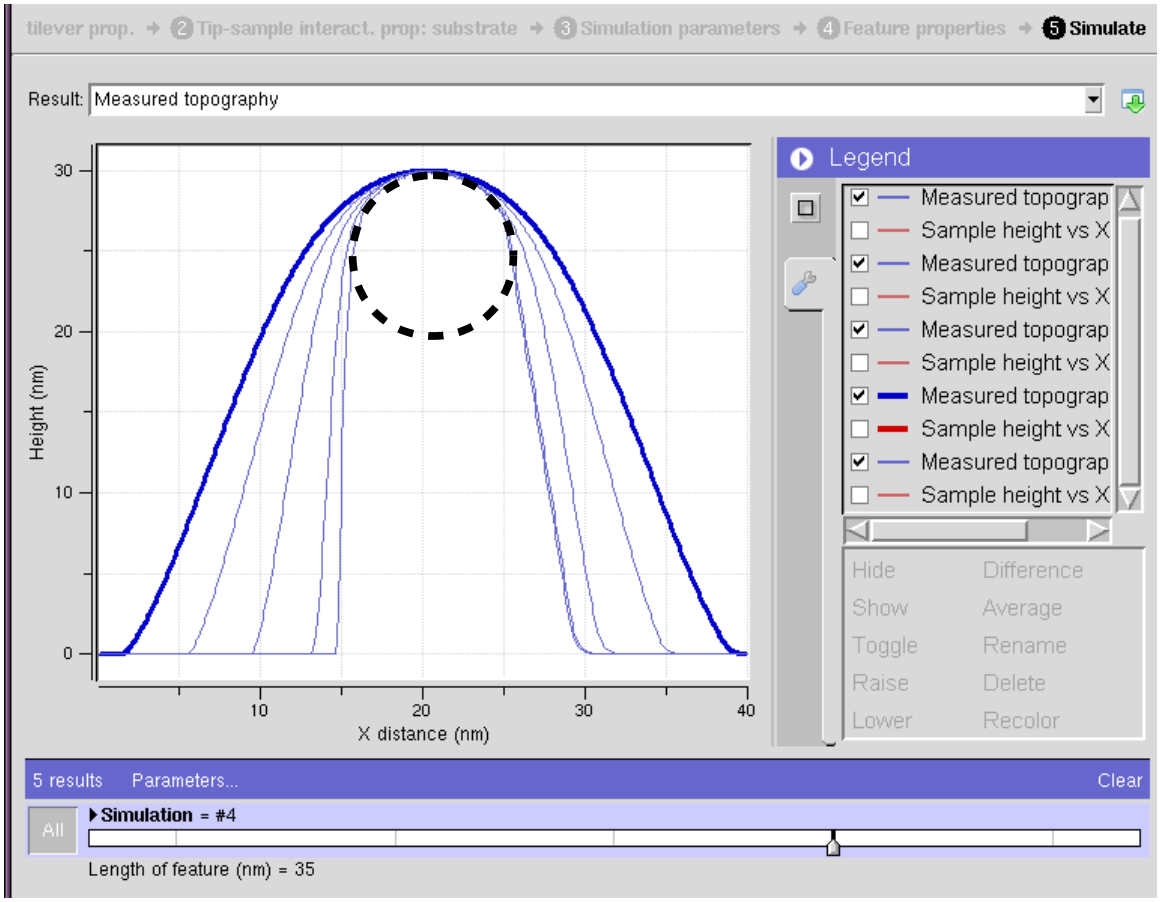

FIG. 75: Measured geometry for a 5 nm tip radius and a sinusoidal feature of successively decreasing widths. For very small features, the measured geometry begins to resemble a circle with a radius of 5 nm - the feature is imaging the tip instead of the tip imaging the feature

excitation frequencies.

1. *Example 1: Peak force tapping on sinusoidal feature, modeled with Hertz contact*

This is a basic example intended to demonstrate the operation of the Peak Force Tapping mode.

2. *Example 2: Flat sample with two different materials, using Attard's model*

This example is similar to the Amplitude Modulated Scanning (basic) Example 2 in section III B 2, in that a flat sample is modeled with two different materials. Whereas that example used a Hertz based viscoelastic contact model, in this example we demonstrate the use of Attard's viscoelastic contact model (section IV B 8).

As Attard's model is more computationally demanding, the scan lines per second has been increased to 10 for this example versus the previous one to keep the run time reasonable. This can be decreased if you want to more realistically simulate a higher resolution scan.

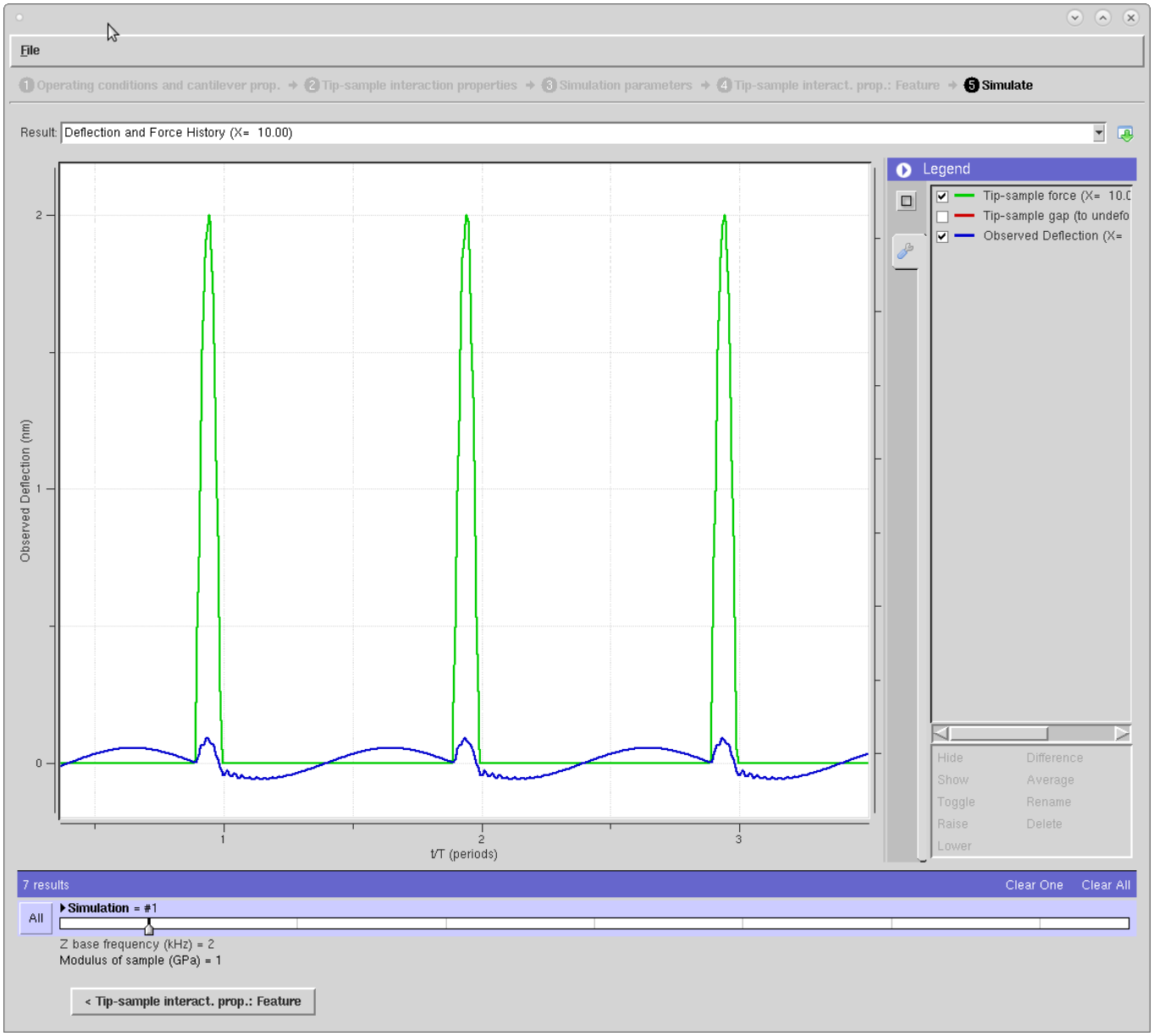

FIG. 76:

M. Jump mode tool

The tool formerly referred to as the "jump mode" tool (which actually just did a single triggered force curve) has been combined into the Force distance curves tool (section III G)

N. Single point tool

Instead of performing an approach curve (or a scan), this tool simply computes a solution at a single point. This is most useful when you want to examine the time histories for a particular Z distance but you do not wish to compute an entire approach curve or scan.

There are currently no examples for this tool

IV. THEORY

In this section, we describe the basic theory behind the various VEDA tools. We develop a general multiple degree-of-freedom (DOF) model for the AFM microcantilever interacting with a sample. This section begins with a description of the tip-sample interaction force model, followed by models for cantilever dynamics, controller dynamics, the DDASKR numerical integration scheme, and tip-sample geometry convolution.

A. Models for tip-sample interaction

VEDA currently offers several options for models for interaction forces between the tip and the sample, including piecewise linear contact, Hertz contact, Derjaguin-Müller-Toporov (DMT), Derjaguin-Landau-Verwey-Overbeek (DLVO) electrostatic double layer forces, Chadwick model for thin membranes and Kelvin-Voigt dissipation. With the exception of the ad-hoc linear contact model, interaction models are based on a spherical tip interacting with an elastic medium. The contact mechanics for these models is strictly valid for a spherical tip interacting with a flat, isotropic, linearly elastic sample surface and will continue to hold so long as the features of the sample are sufficiently larger than the tip radius. However, when interacting with nanostructures that are of the similar size as the tip, the contact mechanics model is not adequate.

1. *Piecewise linear contact*

The piecewise linear contact model, the simplest of the models described here, is an ad-hoc model which is often applied to small indentations of small shell-like structures such as viral capsids, hollow microtubules or carbon nanotubes. This model will be applicable when Van der Waals or electrostatic forces are negligible (e.g. in high ionic concentration buffer solutions). This model is useful for simple simulations and to compare sample stiffness directly to cantilever stiffness. For a contact stiffness (force gradient) k_{ts}^{rep} and tip-sample gap d, the piecewise linear contact model is

$$F_{ts}(d) = \begin{cases} 0, & d > 0 \\ -k_{ts}^{rep} d, & d \leqslant 0 \end{cases} \tag{2}$$

where $d = 0$ is the sample surface.

2. *Piecewise linear attractive/repulsive contact*

The piecewise linear attractive/repulsive model is the next more complex model. A linear attractive gradient is added to the repulsive gradient. This model is useful for simple simulations and to compare sample stiffness directly to cantilever stiffness, but when van der Waals or electrostatic forces are not completely negligible. For a contact

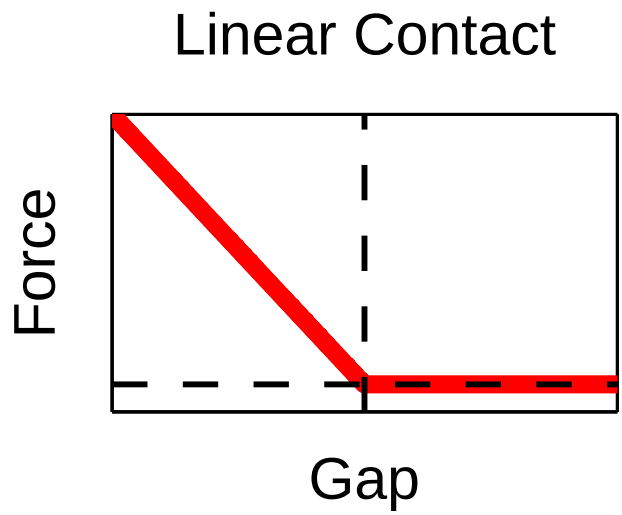

FIG. 77: Tip-sample force versus gap for the piecewise linear contact model.

stiffness (force gradient) k_{ts}, gap between the tip and sample d, attractive gradient k_a, and maximum adhesion force F_{ad}, the piecewise linear attractive/repulsive contact model is

$$F_{ts}(d) = \begin{cases} 0, & d \geq L_0 \\ k_a(d - L_0), & 0 < d < L_0 \\ F_{ad} - k_{ts}d, & d \leq 0 \end{cases} \tag{3}$$

where $d = 0$ is the sample surface. The adhesion force is given by $F_{ad} = k_a L_0$, where L_0 is the length of the attractive gradient.

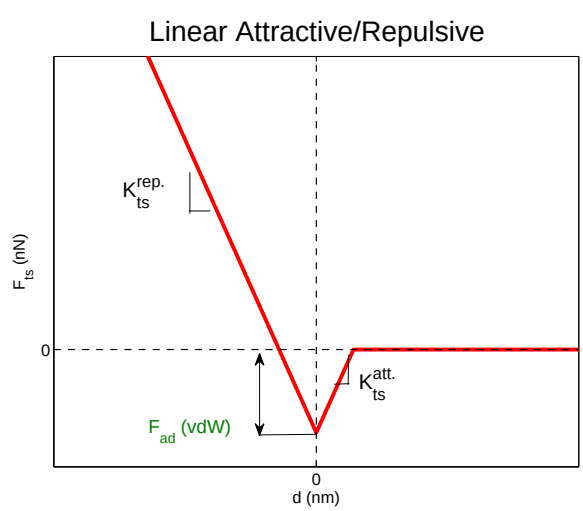

FIG. 78: Tip-sample force versus gap for the piecewise linear attractive/repulsive contact model.

3. Hertz contact

The Hertz contact model considers an elastic sphere indenting an elastic half-space [40], For a tip-sample gap d (sample surface is located at $d = 0$), the model may be written as

$$F_{ts}(d) = \begin{cases} 0, & d > 0 \\ \frac{4}{3}E^*\sqrt{R}(-d)^{3/2}, & d \leqslant 0 \end{cases} \tag{4}$$

$$E^* = \left[\frac{1-\nu_{tip}^2}{E_{tip}} + \frac{1-\nu_{sample}^2}{E_{sample}}\right]^{-1}. \tag{5}$$

where, R is the radius of the tip, E and ν are elastic Young's moduli and Poisson's ratios and E^* is the effective elastic modulus between the tip and the sample system. This model is reasonable under conditions when van der Waals, electrostatic, and chemical forces are negligible compared to the repulsive elastic interaction such as in high ionic concentration buffer solutions.

Technically, this model is actually not for a spherical tip, but for a paraboloid tip. The paraboloid is a good approximation to a sphere when the tip radius is larger than the contact radius (i.e. when the indendation is not too large).

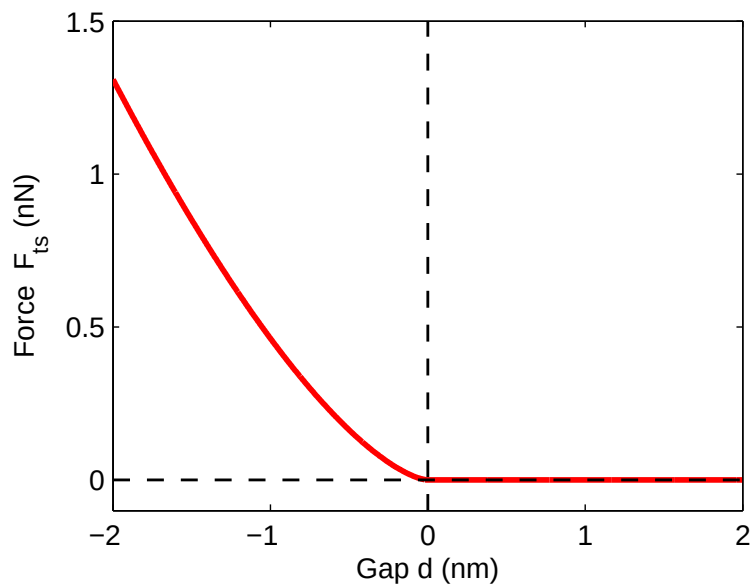

FIG. 79: Example Tip-sample force versus gap for the Hertz contact model. The example shown is for E^*=110 MPa and tip radius R=10 nm

For a rigid tip, we could also write $E^* = E_{sample}/\{1-\nu_{sample}^2\}$, then for a linear elastic material [41] shear modulus is expressed in terms of Young's modulus and Poisson's ratio as $G = E/2(1+\nu)$. Thus an alternative form of the Hertz force is

$$F_{ts}(d) = \begin{cases} 0, & d > 0 \\ \frac{8G}{3(1-\nu)}\sqrt{R}(-d)^{3/2}, & d \leqslant 0 \end{cases} \tag{6}$$

4. Hertz contact conical tip

The previous model is for a paraboloid tip (or a large sphere). For a conical tip with opening angle θ, the equation becomes

$$F_{ts}(d) = \begin{cases} 0, & d > 0 \\ \frac{2E^* \tan(\theta)}{\pi}(-d)^2, & d \leqslant 0 \end{cases} = \begin{cases} 0, & d > 0 \\ \frac{4G \tan(\theta)}{(1-\nu)\pi}(-d)^2, & d \leqslant 0 \end{cases} \tag{7}$$

This is generally only valid for large θ (for small θ the material will plastically yield at the apex of the cone). Note that some authors define the angle θ as the angle between the cone surface and the sample (the exterior angle), while we have choose the opening angle of the cone (the interior angle). The difference is whether $\tan(\theta)$ appears in the numerator or denominator.

5. Derjaguin-Müller-Toporov (DMT) contact model

The Derjaguin-Müller-Toporov (DMT) contact model [42] includes attractive, noncontact van der Waals forces [40, 43] combined with Hertz contact forces [40] and is valid for low adhesion, relatively stiff contacts when operated in air or vacuum and under very dry conditions. Even at low humidities, capillary condensation can occur between the tip and sample which is not included in this model. The results therefore may not be applicable for extremely compliant, highly adhesive contacts. For a tip-sample gap d, where $d = a_0$ (the intermolecular distance) is the sample surface, the DMT model can be written as

$$F_{DMT}(d) = \begin{cases} -\frac{HR}{6d^2}, & d > a_o \\ -\frac{HR}{6a_0^2} + \frac{4}{3}E^*\sqrt{R}(a_0 - d)^{3/2}, & d \leqslant a_0 \end{cases} \tag{8}$$

where H is the Hamaker constant, R is the radius of the tip, E and ν are elastic moduli and Poisson's ratios and E^* is the effective elastic modulus between the tip and the sample system defined in Eq. (4). For $d > a_0$ the tip experiences van der Waals forces. At $d \leqslant a_0$ the van der Waals force saturates and Hertz contact forces begin.

6. Derjaguin-Landau-Verwey-Overbeek electrostatic double layer forces

For simulation in liquid environments where salt buffer concentrations are low to moderate, we have taken the model from [44], which combines Derjaguin-Landau-Verwey-Overbeek (DLVO) model for electrostatic double layer

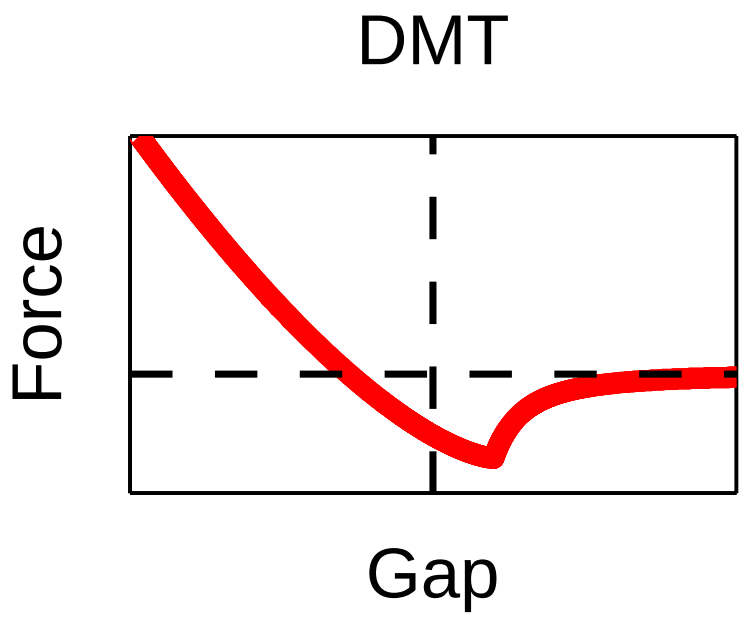

FIG. 80: Tip-sample force versus gap for the DMT contact model.

forces and DMT short-range forces (IV A 5). For a tip-sample gap $d = 0$, where the sample surface is located at $d = a_0$, the conjunction of DMT and DLVO models can be written as

$$F_{DLVO+DMT}(d) = \begin{cases} \frac{4\pi R}{\epsilon\epsilon_0 K_D}\sigma_T\sigma_S e^{-K_D d} - \frac{HR}{6d^2}, & d > a_0 \\ \frac{4\pi R}{\epsilon\epsilon_0 K_D}\sigma_T\sigma_S e^{-K_D a_0} - \frac{HR}{6a_0^2} + \frac{4}{3}E^*\sqrt{R}(a_0 - d)^{3/2}, & d \leqslant a_0 \end{cases} \tag{9}$$

$$E^* = \left[\frac{1-\nu_{tip}^2}{E_{tip}} + \frac{1-\nu_{sample}^2}{E_{sample}}\right]^{-1}.$$

where H is the Hamaker constant, R is the radius of the tip, E and ν are elastic moduli and Poisson's ratio's and E^* is the effective elastic modulus between the tip and the sample system, $1/K_D$, ϵ_0, ϵ, σ_T and σ_S are Debye length, the permittivity of free space, the dielectric constant of the medium, the surface charge density of the tip, and the surface charge density of the sample, respectively.

7. *Johnson-Kendall-Roberts (JKR) contact model*

The Johnson-Kendall-Roberts (JKR) model [45] predicts a hysteretic adhesion due to the necking of the sample. JKR and DMT contact models, which both derive from Hertzian elastic theory, have been shown to be limiting cases of Maugis theory [46]. While DMT applies to stiff samples with low adhesion, JKR applies to soft, compliant surfaces and allows the sample to "neck" in the presence of an adhesive load. The JKR contact model is nonconservative and includes a dependency of the history of the tip-sample contact. The JKR model can be written compactly through the use of a mode variable m describing the state of the tip-sample contact [47]. Let $m = 1$ signify contact with the sample and $m = 0$ otherwise. Accordingly, the JKR model can be expressed as

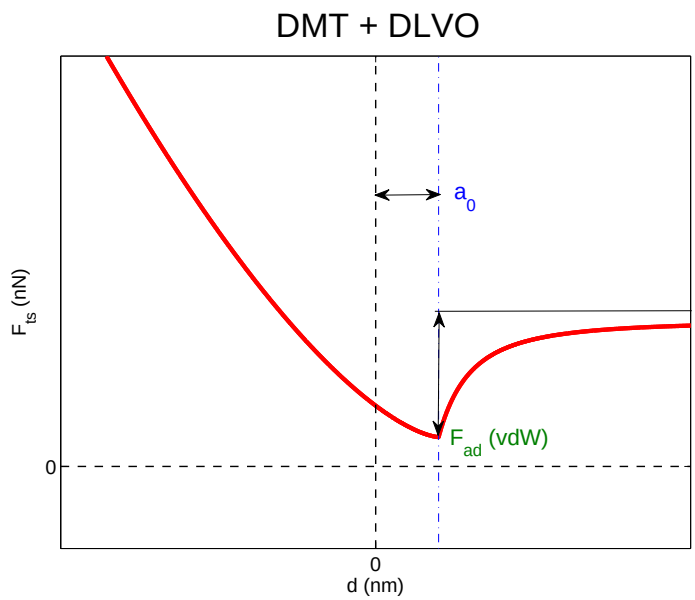

FIG. 81: Tip-sample force versus gap for the DLVO contact model. Note that if F_{ad} is used as an input, it is used to calculate the intermolecular distance a_0 considering the van der Waals forces only (neglecting the double layer forces). This is why F_{ad} appears as a relative measurement in the figure (and *not* as the absolute adhesion force)

$$F_{ts}(a,m) = \begin{cases} 0, & m = 0 \\ \frac{4E^* a^3}{3R} - \sqrt{8\pi W_{JKR} E^* a^3}, & m = 1 \end{cases} \tag{10}$$

where $W_{JKR} = 2F_{ad}/3\pi R$ is the work of adhesion, F_{ad} is the adhesion force, a is the contact radius that is described implicitly as

$$d = -\frac{a^2}{R} + \sqrt{\frac{2\pi W_{JKR} a}{E^*}} \tag{11}$$

where the critical gap $d_{crit} = \sqrt{2\pi W_{JKR} a_{crit}/E^*} - a_{crit}^2/R$ is the distance at which the contact terminates, and $a_{crit} = (\pi R tip^2 W_{JKR}/8E^*)^{1/3}$ is the corresponding contact radius. While approaching in noncontact (m=0), contact occurs at $d = 0$ where the mode variable changes to $m = 1$. Upon retraction from the sample, tip-sample contact persists until $d > d_{crit} > 0$. At this point, the tip and sample separate and there is an abrupt transition from contact to noncontact. Note that the representation of the JKR model in Eq. 10 permits a trajectory which passes through the d_{crit} boundary where the tip remains in noncontact with the sample while departing from the sample. This dependence on the history of the gap between the tip and sample makes the mode variable necessary to describe this model.

8. *Chadwick theory for thin membranes*

Chadwick theory [48] models the indentation of an elastic sphere interacting with a thin incompressible membrane that is supported on a rigid substrate, when the thickness of the layer is small relative to the contact area. The

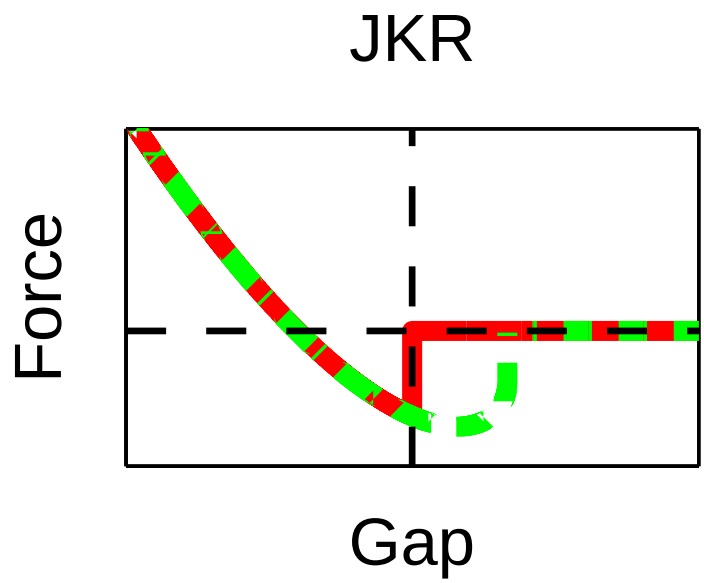

FIG. 82: Tip-sample force versus gap for the hysteretic JKR contact model. While the tip is approaching the sample, interaction forces are zero until contact is made at $d = 0$. While the tip is retracting from the sample, contact persists for $d > 0$ where the sample necks in the presence of adhesive forces. At $d = d_{crit}$ an abrupt transition from contact to noncontact occurs.

Chadwick model is expressed as

$$F_{membrane}(d) = \begin{cases} 0, & d > 0 \\ \frac{2\pi E^* R d^2}{3h}, & d \leqslant 0 \end{cases} \tag{12}$$

where the membrane has a thickness h and the membrane surface is located at $d = 0$, R is the radius of the tip, E^* is the effective elastic modulus between the tip and the sample system Equation (5). The model above assumes that the membrane slips without friction on the substrate. Ref [48] gives an equation for the case when the membrane is bonded to the substrate, but this is not implemented.

9. *Hertz contact with bottom effect correction for thin samples, (Dimitriadis et al, Gavara & Chadwick)*

The Hertz contact model section IV A 3 assumes the sample is a half-space, which is suitable when the thickness of the sample is very large. When the sample is extremely thin, the theory of section IV A 8 is applicable. When the sample thickness is an intermediate between these two, another theory is needed.

For a rigid spherical indenter, and an incompressible ($\nu = 0.5$) sample, Ref [49] gives the following formula:

$$F(d) = \begin{cases} 0, & d > 0 \\ \frac{16E}{9} R^{1/2} \delta^{3/2} [1 + 0.884\chi + 0.781\chi^2 + 0.386\chi^3 + 0.0048\chi^4], & d \leqslant 0 \end{cases} \tag{13}$$

where $\chi = \sqrt{R\delta}/h$, the membrane has a thickness h and the membrane surface is located at $d = 0$, R is the radius of the tip.

The model above assumes that the membrane slips without friction on the substrate. This reference also gives an equation for the case when the membrane is bonded to the substrate, but this is not implemented.

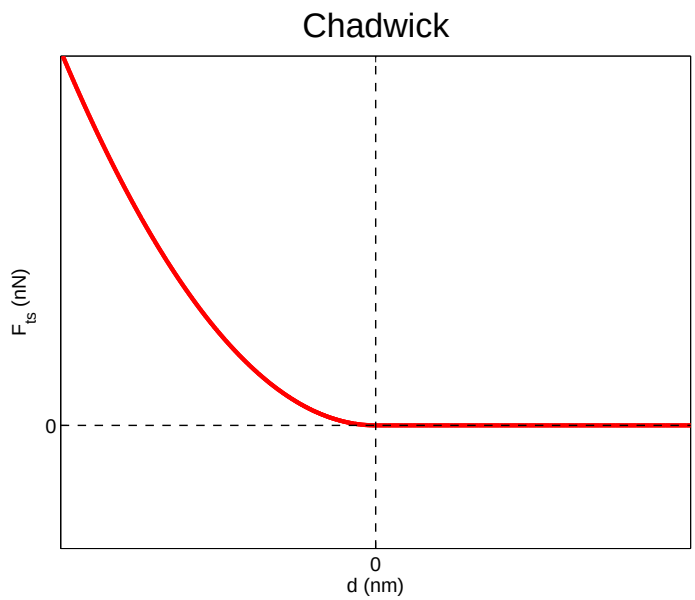

FIG. 83: Tip-sample force versus gap for the Chadwick contact model.

For a conical indenter (again rigid tip and incompressible sample), Ref [50] gives the formula, also referred to as the Bottom Effect Cone Corrected model

$$F(d) = \begin{cases} 0, & d > 0 \\ \frac{8E\tan\theta\delta^2}{3\pi}[1 + 1.7795\frac{2\tan\theta}{\pi^2}\frac{\delta}{h} + 16(1.7795^2)\tan^2\theta\frac{\delta^2}{h^2}], & d \leqslant 0 \end{cases} \tag{14}$$

10. Lennard-Jones Potential + van der Waals

The Lennard-Jones Potential is commonly used to describe interatomic forces. It is often used in non-contact FM AFM to describe short range forces between the atoms on the tip and atoms on the sample. Van der Waals forces may be added to describe the long range forces between the atoms in the bulk of the tip and the bulk of the sample (e.g. [51]) This interaction model is only adequate for the attractive regime. It does not model contact forces well. Therefore it should only be used for non-contact FM AFM. It should not be used for tapping mode AFM or any operation in repulsive regime. The force is given by

$$F_{LJ}(d) = -\frac{HR}{6d^2} + \frac{12E_0}{r_0}\left[\left(\frac{r_0}{d}\right)^{13} - \left(\frac{r_0}{d}\right)^{7}\right] \tag{15}$$

where H is the Hamaker constant, R is the tip radius, E_0 is the binding energy, r_0 is the equilibrium distance, and d is the tip-sample gap.

11. Viscoelastic contact models

The description of viscoelastic contact models grew so big that it was convenient to give it a separate subsection. Please see section IV B.

12. Morse Potential

The Morse potential is similar to the Lennard-Jones potential and is also used in combination with van der Waals for FM AFM [37]. The same conditions apply. The force is given by:

$$F(d) = -\frac{HR}{6d^2} + \frac{2U_0}{\lambda}\left[\exp(\frac{r_c-d}{\lambda}) - \exp(\frac{2r_c-2d}{\lambda})\right] \tag{16}$$

where H is the Hamaker constant, R is the tip radius, U_0 is the depth, r_c is the equilibrium distance, λ is the range, and d is the tip-sample gap. An example is shown in figure 84.

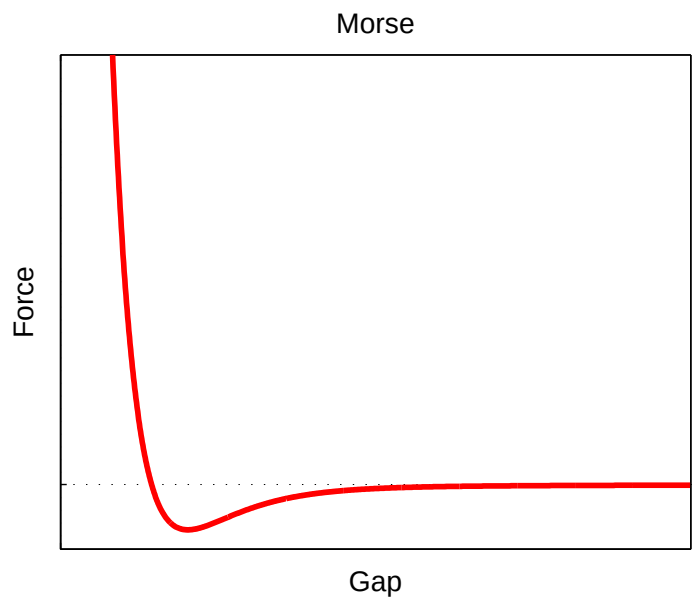

FIG. 84: Tip-sample force versus gap for the Morse potential.

13. Long range electrostatic forces (noncontact)

VEDA includes two different models for the long range electrostatic force between a sphere and a plane. The first is from [52].

$$F(d) = -4\pi\varepsilon_0 \frac{\varepsilon - 1}{\varepsilon + 1} \frac{R_{tip}^2}{d^2} V_{tip}^2 \tag{17}$$

where ε_0 is the permittivity of free space, ε is the local dielectric constant, d the tip-sample distance, R_{tip} is tip radius and V_{tip} is the potential difference between the tip and sample $V_{tip} = V_{DC} - \phi_{surface} + V_{AC}\cos(\omega_{AC}t)$ where V_{DC} , $\phi_{surface}$, V_{AC} , ω_{AC} are the applied DC bias voltage, surface potential, applied AC bias voltage, and bias frequency, respectively.

Note that this model has the same functional form $(1/d^2)$ as the van der Waals component of DMT contact. However, DMT contact assumes that the van der Waals force saturates at some finite distance away from the sample. This model does not include any contact forces and the forces will not saturate. If the tip-sample gap ever becomes zero, the simulation will halt with an error.

When using an applied AC bias voltage, you may wish to make use of the higher harmonics outputs to see the cantilever oscillation amplitude at the frequency of the bias voltage oscillation (and twice that frequency). Remember that the higher harmonics are specified relative to the cantilever (e.g. piezo) driving frequency.

An example is shown in Figure 85 (for pure DC bias).

The second model is from [53]

$$F_{total}(d) = \frac{4\pi}{(\pi - \theta_{lever})^2}\varepsilon\varepsilon_0 V_{tip}^2 \left(ln\left(\frac{d - \frac{\delta}{2} + h}{d + \frac{\delta}{2}}\right) - sin\left(\frac{\theta_{tip}}{2}\right)\frac{h - \delta}{\left(d - \frac{\delta}{2} + h\right)}\frac{d - \frac{\delta}{2}}{d + \frac{\delta}{2}}\right) - \frac{HR}{6d^2} \tag{18}$$

Where the lever is characterized by its length l, width w, and angle θ_{lever} with respect to the sample surface. The tip is a truncated cone of height h and opening angle θ_{tip} that ends smoothly in a paraboloidal tip apex of radius r. Additionally, δ is the height of the truncated part of the cone and is given by the relation $\delta = \frac{r}{\tan^2\left(\frac{\theta_{tip}}{2}\right)}$, and the final term is a van der Waals force on the tip.

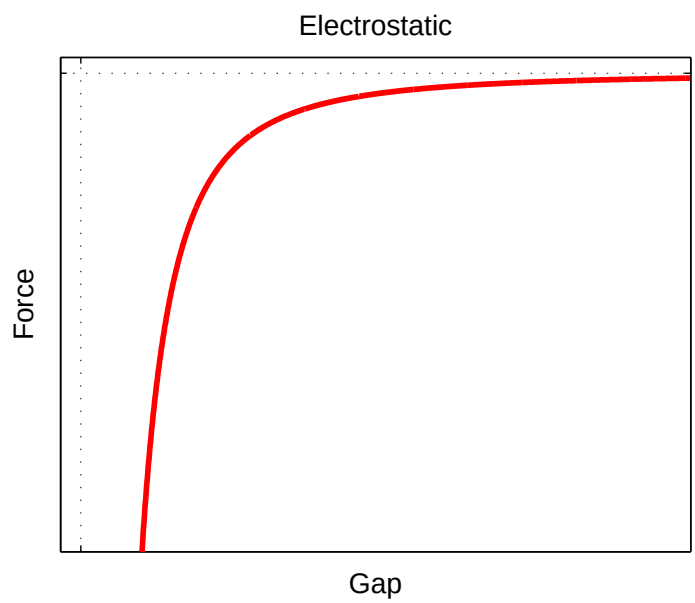

FIG. 85: Tip-sample force versus gap for the electrostatic model of [52], equation (17)

14. Capillary forces

When a tip comes into contact with a sample in the presence of moist air, a liquid capillary can form between them. When the tip retracts, the capillary neck breaks. This process causes a hysteretic, non-conservative force. The model used in VEDA is from Kober et al. [54]. The hysteretic force in this model can be added on top of the other contact models. The force is given by:

$$F_{cap}(d,m) = \begin{cases} 0, & m = 0 \\ \frac{2\Delta E}{D_0^2}(d - D_0), & d \geq a_0, m = 1 \\ F_{ad,cap}, & d < a_0, m = 1 \end{cases} \tag{19}$$

where $d = a_0$ is the DMT intermolecular distance (set to 0 for Hertz model), $d = D_0$ is the distance at which the neck breaks, ΔE is the energy dissipated per hysteretic cycle, $F_{ad,cap}$ is the force jump when the capillary neck forms $F_{ad,cap} = \frac{2\Delta E}{D_0^2}(a_0 - D_0)$ and m is a state variable defined as follows: When $m = 0$ the capillary neck is "off" and when $m = 1$ the capillary neck is "on". When $d < a_0$, then m is set to 1. When $d > D_0$, then m is set to 0. At all other times, m retains its value from the previously computed point.

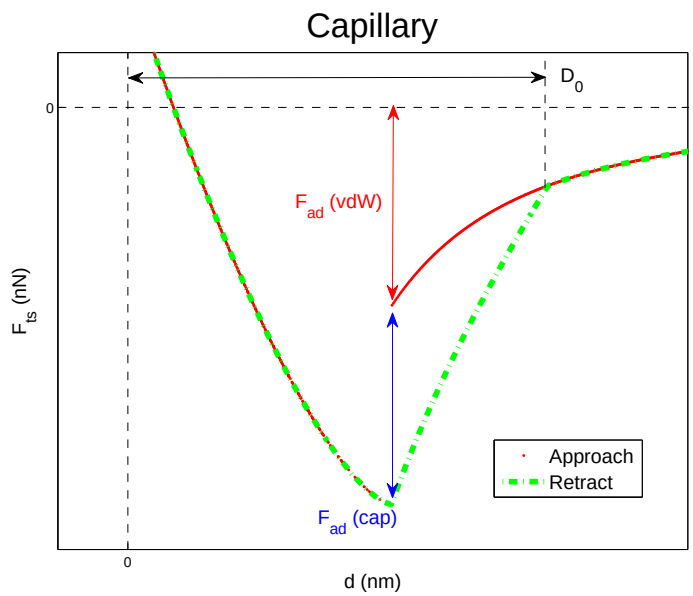

FIG. 86: Tip-sample force versus gap for the Capillary model. Note that the capillary forces are shown on top of a DMT contact model, but could just as easily be added to Hertz, Linear contact, etc.

15. Molecular recognition forces: Worm like chain model

When a functionalized vibrating tip approaches to the sample surface of interest and ligand binds to specific recognition sites, a molecular bonding force will be detected, modifying the microcantilever dynamics [55, 56]. When the tip intermitently interacts with the sample surface and recognition occurs, a transient reduction in oscillation

amplitude is observed with no change in actual sample topography. Specific recognition forces (forces between ligand thetered at a tip and a sample surface recognition sites) will be modeled using the worm like chain (WLC) model [57, 58]:

$$F_{WLC}(d) = \begin{cases} 0, & d < 0 \\ 0, & d \geq 0, m = 0 \\ -\frac{k_B T}{L_P}\left[\frac{1}{4\left(1-\frac{d}{L_0}\right)^2} - \frac{1}{4} + \frac{d}{L_0}\right], & d \geq 0, m = 1 \end{cases} \tag{20}$$

In which: d is the tip-sample gap (where d=0 is the sample surface), k_B is the Boltzmann's constant, L_P is the persistance length, L_0 is the contour length, T is the temperature, and m is a mode variable indicating if the chain is attached to the tip or not. The transitions are that the chain form (m goes from 0 to 1) at $d = 0$, and the chain break (m from 1 to 0) at at pre-specified distance $d = L_r$. The distance L_r can be choosen such that the bond ruptures at a particular force. This transition behavior is an approximation for ease of computation. In reality the bond rupture will be controlled by a stochastic process where there is a certain probability of the bond breaking at a given force level. This is a reasonable approximation because for many applications, the tip sample forces stay well below the bond rupture force (i.e. the chain never breaks).

16. *Solvation forces: conservative*

Solvation forces have to do with an ordering of liquid molecules near a solid-liquid interface [43]. This can give rise to a so-called oscillatory force with a period approximately equal to the molecule diameter, as well as a monotonic background force known as a hydration force. An example oscillatory force is shown in Figure 87 and is given by a simple decaying cosine [43].

In VEDA, we use the model of [59] which attempts to include the effect of a shaped tip by slicing the tip into several parts and calculating the force on each part:

$$F(d) = \sum_{k=0}^{N} 2\pi r^2(z_k) k_B T \rho \cos\left(\frac{2\pi(z_k + d)}{\sigma}\right) \exp\left(-\frac{z_k + d}{\sigma}\right) \tag{21}$$

where z_k denoted the height of the kth slice of the tip (we assume a spherical tip here), and σ is a decay length. With one slice, the model reduces to the simple model of [43] above. Note that we have adopted the conservative part of this model only. See below for the non-conservative part.

Similarly, [59] gives a hydration force of

$$F(d) = \sum_{k=0}^{N} 2\pi r^2(z_k) p_h \exp\left(-\frac{z_k + d}{\lambda}\right) \tag{22}$$

where λ is decay lengths. Versions of VEDA prior to 2.0.27 (Jan 2012) used this model. However, with some algebra it can be shown that this sum does not converge. In other words, as the number of slices is increased, the force increases without bound. Further, using the Derjaguin approximation [60], if the energy per unit area of two flat surfaces is given by $w(d) = \exp(-d/\lambda)$, then the integrated force over the entire tip is proportional to $\exp(-d/\lambda)$ regardless of the tip shape. Therefore, versions of VEDA starting from 2.0.27 use the following for the hydration force:

$$F(d) = 2\pi r^2 p_h \exp\left(-\frac{d}{\lambda}\right) \tag{23}$$

(i.e. the same equation as before but with N=1)

In the results of [59], λ and σ were found to be approximately the diameter of the liquid molecules (e.g. around 0.25 nm for water). However, [43] suggests that λ could be as much as 1 nm for hydophilic surfaces in water, and as much as 2 nm for hydrophobic surfaces in water. The user is suggested to consult the literature for the specific system you are interested in. p_h is an empirically determined constant.

Normally, the solvation forces saturated at $d = 0$. However, this means that the gradient is discontinuous there, which may be non-physical. When the "enforce continuous gradient" option is checked, the solvation forces continue at act even below $d = 0$. This should only be used for stiff samples for which indentation is small. For soft samples this option is not useful.

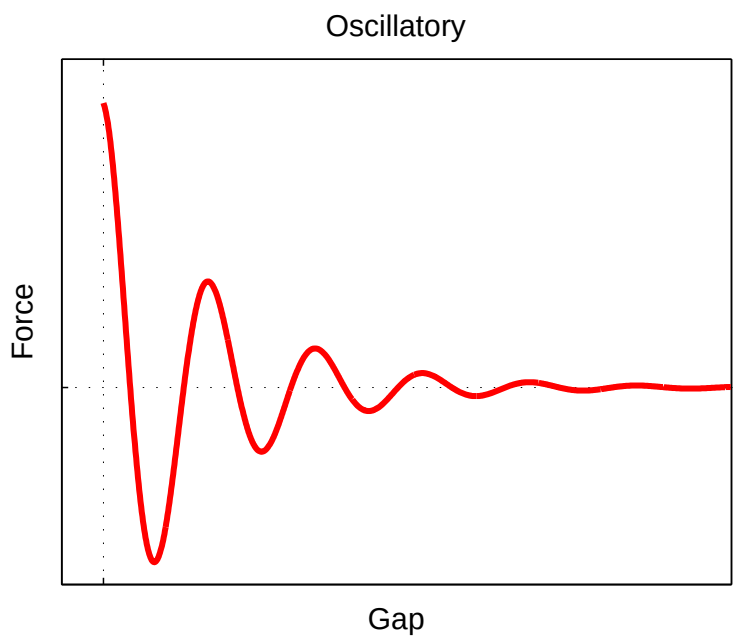

FIG. 87: Tip sample interaction force versus gap for oscillatory forces

17. Solvation forces: non-conservative

[59] suggested that the non-conservative solvation force was proportional the conservative solvation force at any given separation. This leads to an oscillatory non-conservative force. However, more recent works such as [61] have suggested that the non-conservative part of the solvation forces should be monotonic. For simplicity, we adopt only a monotonic model. Specifically

$$F_{ts}(d,\dot{d}) = \begin{cases} c\dot{d}e^{-\frac{d}{\lambda}} & d > 0 \\ c\dot{d} & d < 0 \end{cases},$$

where c is an empirically determined scaling constant (kg/s) and λ is a decay length (on the order of the liquid molecule diameter).

Previous versions of VEDA, (prior to 2.0.33 June 2012, and including the recent journal publication [23]) had the viscosity decay smoothly to zero as the tip indents the sample. However, that was somewhat ad-hoc. The present assumption that the viscosity saturates to a constant value at contact is more physically justifiable. The assumption that even when the tip and sample are in contact, there is still a region just outside the contact area where liquid molecules are being squeezed. It is similar to the assumption in the DMT model that attractive forces saturate when the tip and sample contact. The difference between the previous model and the present model is trivially small for stiff samples. This is because the indentations are typically small on stiff samples, and the velocities are small when the tip and sample are in contact.

18. Magnetic dipole-dipole interactions

The magnetic dipole-dipole interactions are from [62]. The tip is modeled as a sphere, and the sample is modeled as a spheric superparamagnetic material coated with a thin layer of non-magnetic material. The tip is assumed to be directly above the particle (this makes the model most useful for approach curve simulations and not as useful for scanning simulations).

$$F_{ts}(d) = \frac{-3\mu_0 m_p m_t}{\pi(d + R/2 + d_m/2 + \delta)^4}$$

where μ_0 is the permeability of free space, m_p is the magnetic model of the particle, R is the tip radius, d_m is the effective magnetic radius of the particle, and δ is the thickness of the nonmagnetic layer.

19. Tip-sample squeeze film damping

Reynold's squeeze film damping has been proposed to act in liquid AFM between tip and sample at small separation distances [35]. It can be described by a damping coefficient given by

$$\gamma = 6\pi\eta\frac{R_{tip}^2}{d} \tag{24}$$

so that the force is simply

$$F = 6\pi\eta\frac{R_{tip}^2}{d}\dot{d} \tag{25}$$

This model obviously has a problem at d=0. In VEDA we therefore propose the following correction

$$F_{ts}(d,\dot{d}) = \begin{cases} 6\pi\eta\frac{R_{tip}^2}{d}\dot{d}, & d > a_0 \\ 6\pi\eta\frac{R_{tip}^2}{a_0}\frac{d}{a_0}\dot{d}, & 0 < d < a_0 \\ 0, & d < 0 \end{cases}$$

20. Surface Energy Hysteresis

Surface energy hysteresis is a catch-all term for a large number of physical processes that cause the energy of forming a solid-solid interface to be greater that the energy of destroying the interface. For these processes, the total energy dissipation will depend only on the total contact area formed, not on the tip velocity. Ref. [?] suggests a tip sample interaction model including surface energy hysteresis. The model was based on a DMT model. In the original formulation, the attractive and repulsive parts are handled separately (the attractive part was called "long-range dissipative interfacial interactions"). Using a slightly different notation, they can be combined into one expression as follows

$$F_{ts,app}(d) = \begin{cases} -\frac{HR}{d^2} & d > a_0 \\ \frac{4}{3}E^*\sqrt{R}(a_0-d)^{3/2} - \frac{HR}{a_0^2}, & d < a_0 \end{cases}$$

$$F_{ts,ret}(d) = \begin{cases} -\frac{(H+4\pi\gamma a_0^2)R}{d^2} & d > a_0 \\ \frac{4}{3}E^*\sqrt{R}(a_0-d)^{3/2} - \frac{HR}{a_0^2} - 4\pi R\gamma, & d < a_0 \end{cases}$$

$$F_{ts}(d,\dot{d}) = \begin{cases} F_{ts,app}(d), & \dot{d} < 0 \\ F_{ts,ret}(d), & \dot{d} > 0 \end{cases}$$

We note that this model includes only a single parameter γ, which is the change in surface energy (J/m^2) between approach and retract , to describe the strength of the hysteresis. Ref. [?] had two parameters, one for $d < a_0$ and a separate one for $d > a_0$. Although that is a more general case than our model, it means that the force described by that model is not necessarily continuous at $d = a_0$. We have restricted ourselves only to the case where the force is continuous.

This model has been shown to match several features of experimental energy dissipation measurements well, and it is well suited to analysis (e.g. the method of averaging). However, for numerical simulation it can present a problem. The switch between the approach and retract forces happens instantaneously. This means that the force is discontinuous at the switch, which is clearly non-physical. This may cause difficulties for the differential equation solver, and it can also introduce non-physical high frequency oscillation of the cantilever.

Therefore, we suggest a modification which allows the force to be continuous everywhere. Initially, $\dot{d} < 0$ and $F_{ts}(d) = F_{ts,app}(d)$. If, at time $t = t_0$ and $d = d_0$, the velocity switches sign from $\dot{d} < 0$ to $\dot{d} > 0$, then the force for time $t > t_0$ is defined as $F_{ts}(d) = F_{ts,ret}(d) + (F_{ts,app}(d_0) - F_{ts,ret}(d_0))\, e^{-(d-d_0)/\lambda}$, where λ is a decay length (we use 0.1 nm typically). In other words, when the velocity switches, the current trajectory is smoothly transitioned into the new trajectory. The difference between the current and new trajectories decays exponentially.

The above definition is sufficient for single frequency AFM (e.g. tapping mode). However, for bimodal AFM, it is possible that the velocity might reverse two (or more) times, and the second reversal might happen before the transition to the new trajectory is complete. Therefore, we instead use this definition: If the velocity reverses at time $t = t_0$ and $d = d_0$, then then let F^* be the force at time t_0. Then the force for time $t > t_0$ is defined as $F_{ts} = F_{ts,m}(d) + (F^* - F_{ts,m}(d_0))\, e^{(-d-d_0)/\lambda}$, and m equals either *app* or *ret*, depending on which direction the velocity has switched to. This allows an arbitrary number of reversals at arbitrary distances, while still always maintaining continuity of the forces.

21. Non-smoothness of the interaction force models

Note that all the tip-sample interaction models above describe interaction forces that are mostly continuous with respect to the tip-sample gap d. However at the critical gap value ($d = 0$ or $d = a_0$) when the repulsive force model begins, the F_{ts} vs. d curve becomes non-smooth. This is important because performing numerical simulations of tip motion with non-smooth interactions creates the possibility of errors creeping in due to the choice of the numerical integration scheme. In VEDA we do not artificially smooth out such forces but rather retain them in their ideal form and instead rely on specialized numerical integration schemes to deal with such non-smooth forces.

B. Tip samples interaction: Viscoelasticity

An elastic material is one where the stress (forces) at time t depends only on the strain (displacements) at time t, and does not depend on the rate of strain, or on any past history of the strain. For example, a steel spring could be considered as an elastic body. A viscous material, on the other hand, is one in which the stresses are dependent on only on the strain rate (velocity). For example, most common liquids such as water or oil. Many materials, however, display some mixture of viscous and elastic response. That is, the stresses may depend both on the current strain as well as the strain rate and the past history of the strain. This is called viscoelasticity.

There are several different continuum models for viscoelasticity, which can be combined with the tip-sample interaction models above in a few different ways. The three common classical elements are shown in Figure 88.

In the next section, we describe viscoelasticity based on the linear contact model. Then, we give several sections describing viscoelasticity based on the Hertz contact model.

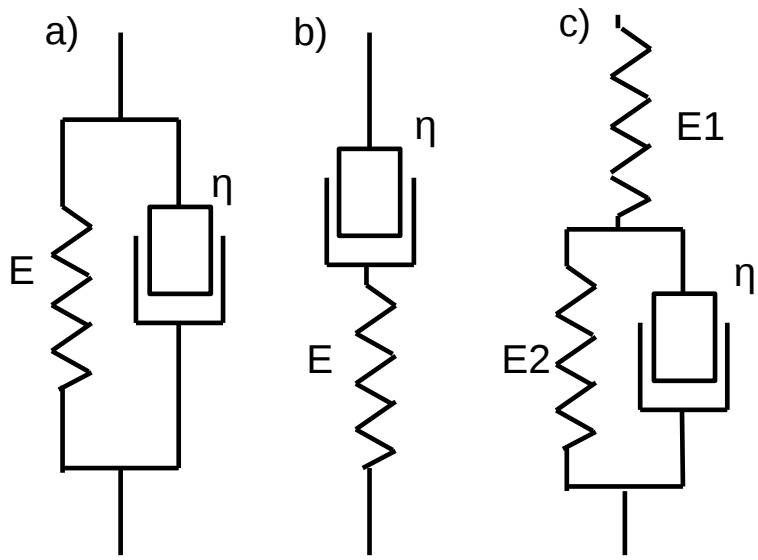

FIG. 88: The three classical viscoelastic elements. (a) the Kelvin-voigt model, a spring and a damper in parallel. (b) the Maxwell model, a spring and a damper in series, (c) the three element model (delayed elasticity), a spring in series with a Kelvin-voigt element

1. *Viscoelasticity based on Linear Contact*

The linear contact model was described in IV A 1. In this model, the tip-sample interaction force is represented by a simple spring. To extend this model to viscoelasticity, we simply add linear dashpots (and possibly some extra springs). The dashpot can be combined in with the spring in several different ways (i.e. series versus parallel). The Kelvin-Voigt viscoelastic dissipation model assumes a spring in parallel with a damper. This model is applicable when the relaxation time of the material is very short (compared to the tip-sample contact time).

A naive implementation of this model would be to simply add the spring and dashpot forces. Let η be the damping coefficient in N-s/m. Then the force is given by:

$$F_{ts}(d) = \begin{cases} 0, & d > 0 \\ -k_{ts}^{rep} d - \eta \dot{d}, & d < 0 \end{cases} \tag{26}$$

This referred to in VEDA as the "Ad-hoc kelvin-voigt" model (for linear contact) and this was the default model prior to 2.0.22 (Aug 2011). However, there is a problem with this model: for very viscous samples the total force can go negative, which is non-physical. The linear contact model does not include any attractive forces, so the tip

should leave contact with the sample instead of the force going negative. Therefore, we introduce an extra condition as follows:

$$F_{ts}(d) = \begin{cases} 0, & d > 0 \\ -k_{ts}^{rep} d - \eta \dot{d}, & -k_{ts}^{rep} d - \eta \dot{d} > 0 \\ 0, & \text{otherwise} \end{cases} \tag{27}$$

The condition on the second line prevents the force from being negative. For the linear attractive/repulsive model (section IV A 2), the condition is modified to allow the force to go negative up to the adhesion force. This condition is, admittedly, somewhat ad-hoc, but the linear model is ad-hoc to begin with. The Hertz contact based models (described below) have a more rigorously developed viscoelastic theory.

The biggest problem with this model is that the viscous force is discontinuous. Immediately upon entering contact the force can be huge. If you have convergence problems with this model, try to using another model (or Hertz contact) instead

It may be instructive to compute the energy dissipated per cycle for this model in the case of permanent contact with the sample. $W = \oint F_{ts}(d, \dot{d}) dd = \int_0^{2\pi/\omega} F_{ts}(d, \dot{d}) \dot{d} dt$ Assume a sinusoidal $d = A\cos(\omega t)$. Then

$$W = -\int_{\pi/\omega}^{2\pi/\omega} \eta(\omega A \sin(\omega t))^2 dt = \frac{\pi}{2} \eta \omega A^2. \tag{28}$$

Note that this term includes ω. The energy loss per cycle depends on the frequency, thus this is classified as a rate dependent dissipation model.

For linear contact, we can also formulate the response for the three element model. This consists of two springs and one dashpot arranged as in 88. We can derive the force as follows: Let the compression of spring 1 be d_1 and force in spring 1 be $k_1 d_1$. Then let then compression of the spring-dashpot pair be d_2 and the force is $F_2 = k_2 d_2 + \eta \dot{d}_2$. Then, the two contraints on the system are the overall displacement of the system $d = d_1 + d_2$ and the force in each set is the same $F = F_1 = F_2$. Using these conditions, we arrive at a governing differential equation

$$k_1 d(t) = (k_1 + k_2) d_2(t) + \eta \dot{d}_2 \tag{29}$$

which can be solved for d_2

$$d_2(t) = \frac{k_1}{\eta} \mathrm{e}^{-\frac{t(k_1+k_2)}{\eta}} \int_0^t d(\tau) \, \mathrm{e}^{\frac{(k_1+k_2)\tau}{\eta}} d\tau \tag{30}$$

From this and $F_2 = k_2 d_2 + \eta \dot{d}_2$, the force can be found. This model has the advantage that the force is not discontinuous upon contact, unlike the Kelvin-voigt model. For a sinusoidal excitation $d(t) = A\sin(\omega t)$, this is solved

to yield $d_2(t) = k_1 A\left(-\eta\omega\cos(\omega t) + (k_1+k_2)\sin(\omega t)\right) / \left(k_1^2 + 2k_1k_2 + k_2^2 + \omega^2\eta^2\right)$, which leads to the loss tangent being $\tan\delta = \frac{k_1\eta\omega}{k_1k_2+k_2^2+\omega^2\eta^2}$.

It is also possible to use other viscoelastic consitutive equations with the linear contact model (e.g. maxwell, generalized maxwell) but we have not done so here.

2. Hertz contact based viscoelasticity, Kelvin-Voigt

For the Hertz (and related) tip-sample interaction models, the force calculation is more complex than for linear contact. The elastic Hertz formulas in section IV A 3 were derived by calculating the area of contact between the tip and the sample that would occur for a given indentation. From the contact area, a contact force can be computed. Therefore to calculate the viscoelastic response, we must take the contact area into account. We start with the simple Kelvin-voigt model and then extend to other models in subsequent sections.

Before describing the full Kelvin-voigt model, we also briefly mention the *ad-hoc* Kelvin-voigt model. This was the model used in VEDA prior to version 2.0.22 (Apr 2010), and it has been used in the literature several times (for example [63, 64]). The model is deriving by assuming that the viscoelastic material's contact area and sample deformation are related to the identation by the exact same formula as in the purely elastic problem. This leads to the combined elastic plus viscous force being

$$F_{ts}(d,\dot{d}) = \begin{cases} 0, & d > 0 \\ \frac{4}{3}E^*\sqrt{R}(-d)^{3/2} - \eta\dot{d}\sqrt{-Rd}, & d \leqslant 0 \end{cases} \tag{31}$$

However, there are two problems with this model. First, if $\dot{d}$ and η are large, then it is possible for F_{ts} to be negative. But the Hertz contact model should not include any attractive forces, so this is non-physical. Put another way, as the tip withdraws, the deformed sample does not return to its original condition instantly, but it takes some time to relax because of the viscoelasticity. If the tip withdraws too fast, then it may completely pull away from the sample before $d = 0$. However, the ad-hoc model cannot account for this. Essentially, if the tip pulls away quickly, the ad-hoc model is applying an attractive force to slow it down and forcing it to withdraw only as fast as the sample can relax.

The reason that the model has this error is the assumption that the contact area and indentation were related by the same formulas as in the elastic case. The correct formula take into account a different relation between them. According to the so called "correspondance principle" if the solution to an elastic problem is known, then the solution to the corresponding viscoelastic solution is found by replacing the shear modulus G with a viscoelastic operator appropriate to the material [41]. Therefore, in the standard contact mechanics theory [65, 66], the solution for viscoelastic contact is found by taking the Hertz formula $F = \frac{4}{3}E^*\sqrt{R}d^{3/2} = \frac{8}{3(1-\nu)}G\sqrt{R}d^{3/2}$ and replacing G with a convolution integral

$$F(t) = \frac{8}{3(1-\nu)}\sqrt{R}\int_0^t \psi(t-\tau)\frac{d}{d\tau}d^{3/2}(\tau)d\tau \tag{32}$$

where ψ is the stress relaxation operator for the linear viscoelastic material in question. This operator describes the stress in the material if a step change in strain is applied. For the Kelvin-voigt model, this is:

$$\psi(t) = G + \eta\delta(t) \tag{33}$$

where δ is the Dirac delta. That is to say, a step change in strain is a delta function in strain rate, and in the Kelvin-voigt model the visous portion of the stress is directly proportional to strain rate. Another way to say this is that the stress relaxes instantly after the load is applied. The delta function in (33) makes the convolution integral (32) particularly simple to evaluate. We have merely $F(t) = \frac{4}{3}E^*\sqrt{R}d^{3/2} - \frac{2\eta}{1-\nu}\dot{d}\sqrt{-Rd}$. This is similar to the ad-hoc model. However, there is one caveat. This theory only applies when the contact area is increasing (i.e. when the tip is going down into the sample).

When the contact area is decreasing (tip is withdrawing), the theory of [67] must be used. The first step is to find the value of t_1 that satisfies the formula

$$\int_{t_1(t)}^t \psi(t-\tau)\frac{\partial}{\partial\tau}d(\tau)d\tau = 0 \tag{34}$$

When this formula is satisfied, the contact area (i.e. radius of the circle of contact) at time t_1 and time t will be the same. For Kelvin-Voigt, we substitute (33) in and use the properties of Dirac delta [note: A commonly given definition of the Dirac delta is $\int_{-\infty}^{\infty}\delta(x)dx = 1$. In this case we are integrating over a smaller interval so we need the definition $\int_0^{\infty}\delta(x)dx = 1/2$] to find:

$$G\left(d(t) - d(t_1)\right) + \frac{1}{2}\eta\dot{d}(t) = 0 \tag{35}$$

and then re-arrange:

$$d(t_1) = d(t) + \frac{1}{2}\frac{\eta}{G}\dot{d}(t) \tag{36}$$

Thus, we can find t_1 by simply looking backwards through the indentation history to find the time at which this value of indentation occured. Now that we know t_1, we can find the force from (32), except we must change the limits of integration to

$$F(t) = \frac{8}{3(1-\nu)}\sqrt{R}\int_0^{t_1} \psi(t-\tau)\frac{d}{d\tau}d^{3/2}(\tau)d\tau \tag{37}$$

Therefore, we can write the entire force model as:

$$F(d,\dot{d},t) = \begin{cases} 0 & m=0 \text{ (not in contact)} \\ \frac{8}{3(1-\nu)}\sqrt{R}\int_{t_0}^{t} \psi(t-\tau)\frac{d}{d\tau}d^{3/2}(\tau)d\tau, & m=1, \dot{d}<0 \text{ (indentation increasing)} \\ \frac{8}{3(1-\nu)}\sqrt{R}\int_{t_0}^{t_1} \psi(t-\tau)\frac{d}{d\tau}d^{3/2}(\tau)d\tau, & m=1, \dot{d}>0 \text{ (indentation decreasing)} \end{cases}$$

Where m is a mode variable that keeps track of if the tip is in contact or not. The non-contact to contact transition ($m=0$ to $m=1$) happens when tip-sample gap transitions when $d<0$. The contact to non-contact transition ($m=1$ to $m=0$) happens when either $d>0$ or $t_1<t_0$, where t_0 is the time at which the non-contact to contact transition occurred,

Now, for Kelvin-voigt, we know that $t_1<t$, so the Dirac delta simplifies and we have merely $F(t)=\frac{4}{3}E^*\sqrt{R}d(t_1)^{3/2}$. But, we already know $d(t_1)$ from (36). Therefore, it is not necessary that we actually find t_1. We can use

$$F(t) = \frac{4}{3}E^*\sqrt{R}(d(t)+\frac{1}{2}\frac{\eta}{G}\dot{d}(t))^{3/2}$$

Thus, the entire force model is:

$$F_{ts}(d,\dot{d}) = \left\{ \begin{array}{ll} 0, & m=0 \\ \frac{4}{3}E^*\sqrt{R}(-d)^{3/2} - \frac{2}{(1-\nu)}\eta\dot{d}\sqrt{-Rd}, & m=1, \dot{d}<0 \\ \frac{4}{3}E^*\sqrt{R}(-d-\frac{1}{2}\frac{\eta}{G}\dot{d})^{3/2} & m=1, \dot{d}>0, \end{array} \right\}$$

The tip first contacts the sample ($m=0$ to $m=1$ transition) the first time that $d<0$, and contact is broken ($m=1$ to $m=0$ transition) when either $d>0$ or $-d-\frac{1}{2}\frac{\eta}{G}\dot{d}<0$. An example force curve is shown in Figure 89.

These models assume that the sample can be approximated by a semi-infinite half-space. Also, the tip is assumed to be rigid (i.e. the modulus of the tip is assumed to be much higher than the modulus of the sample).

Viscoelastic forces are not applicable to models not based on Hertz contact (e.g. Morse or Lennard-Jones potential models).

Finally, we have not yet described how to take into account any attractive forces. In VEDA we include only a simple ad-hoc implementation of a DMT like attractive force model with the viscoelastic models. The assumptions are that 1) there is no energy dissipation when the tip is no touching the sample. 2) the sample does not neck. 3) the attractive forces saturate at a fixed value ($F_{ad}=-HR/(6a_0^2)$) below $d=a_0$. In this case we can simply add the van der Waals forces directly to the viscoelastic forces.

$$F_{ts}(d,\dot{d}) = \left\{ \begin{array}{ll} 0, & m=0 \\ \frac{4}{3}E^*\sqrt{R}(-d)^{3/2} - \frac{2}{(1-\nu)}\eta\dot{d}\sqrt{-Rd}, & m=1, \dot{d}<0 \\ \frac{4}{3}E^*\sqrt{R}(-d-\frac{1}{2}\frac{\eta}{G}\dot{d})^{3/2} & m=1, \dot{d}>0, \end{array} \right\} + \left\{ \begin{array}{ll} -\frac{HR}{6d^2}, & d>a_o \\ -\frac{HR}{6a_0^2}, & d\leqslant a_0 \end{array} \right\}$$

If the sample necks (i.e. deforms even when tip and sample are not in contact), then this model will not be applicable. In that case a DMT contact is not applicable and a JKR type contact is more relevant. However, Viscoelasticity in conjunction with JKR contact is based on an entirely different set of theory which is significantly more complicated, and is not available currently in VEDA.

For reference, we also give the creep compliance function for Kelvin-voigt

$$\phi(t) = \frac{1}{G}\{1 - e^{-t/T}\} \tag{38}$$

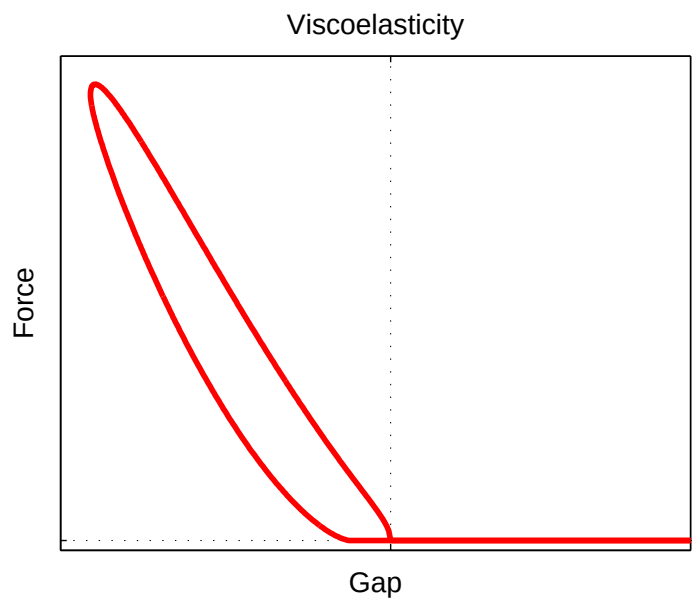

FIG. 89: Example Tip-sample force versus gap for a Kelvin-voigt viscoelastic model

3. Viscoelasticity conical tip

The previous section was for a parabolic ("spherical") tip. For a conical tip, Eq (34) still holds, but in analogy to section IV A 4, Eq (32) must be replaced with

$$F(t) = \frac{4\tan(\theta)}{(1-\nu)\pi}\int_0^t \psi(t-\tau)\frac{d}{d\tau}d^2(\tau)d\tau = \frac{8\tan(\theta)}{(1-\nu)\pi}\int_0^t \psi(t-\tau)d\dot{d}d\tau \tag{39}$$

4. Maxwell viscoelasticity

The Maxwell model for viscoelasticity is a spring in series with a dashpot. This model is applicable when the relaxation time of the material is very long (compared to the tip-sample contact time). In this case the stress relaxation function is [65]

$$\psi(t) = Ge^{-t/T} \tag{40}$$

where $T = \eta/G$ is the relaxation time of the material.

In this case, the convolution integral of equation (32) is not easy to evaluate in closed form and must be done numerically. Also, we must find t_1 explicitly. This makes the evaluation of the Maxwell model significantly slower than the Kelvin-voigt model. However, the constant G can be pulled out the equation and then rewritten in terms of reduced modulus

$$F(t) = \frac{4}{3}E^*\sqrt{R}\int_0^t \exp(\frac{\tau - t}{T})\frac{d}{d\tau}d^{3/2}(\tau)d\tau \tag{41}$$

and simplified

$$F(t) = 2E^*\sqrt{R}\int_0^t \exp(\frac{\tau - t}{T})\sqrt{d}\dot{d}d\tau \tag{42}$$

We can also find [41] for this model

$G_{storage} = \frac{G\omega^2T^2}{1+\omega^2T^2}$, $G_{loss} = \frac{G\omega T}{1+\omega^2T^2}$, $\tan\delta = \frac{1}{\omega T} = \frac{G}{\eta\omega}$

which is the opposite loss tangent behavior as Kelvin-voigt.

5. *Three element model*

The standard three element model is a spring in series with a Kelvin-voigt element. The stress relaxation function is [65]

$$\psi(t) = \frac{G_1}{G_1 + G_2}\{G_2 + G_1\exp(-t/T_\sigma)\} \tag{43}$$

where $T_\sigma = \eta/(G_1 + G_2)$ is the stress relaxation time. The creep compliance is [68][69]

$$\phi(t) = \frac{1}{G_1} + \frac{1}{G_2} * \{1 - \exp(-t/T_\epsilon)\} \tag{44}$$

where $T_\epsilon = \eta/G_2$ is the creep retardation time. When T_σ is very short (compared to the contact time), this model reduces to the Kelvin-voigt model. When T_σ is very long, this model reduces to the maxwell model. When T_σ is on the same order as the contact time, this model exhibits behavior that the Kelvin-voigt and maxwell models cannot capture.

Useful relationships for the three-element model are:

$$G_{storage}(\omega) = \frac{G_1 G_2}{G_1 + G_2} + \frac{G_1^2}{G_1 + G_2} \frac{\tau^2 \omega^2}{1 + \tau^2 \omega^2} \tag{45}$$

$$G_{loss}(\omega) = \frac{G_1^2}{G_1 + G_2} \frac{\tau \omega}{1 + \tau^2 \omega^2} \tag{46}$$

$$\tan \delta(\omega) = \frac{\omega \tau G_1}{G_2 + G_2 \tau^2 \omega^2 + G_1 \tau^2 \omega^2} \tag{47}$$

The maximum $\tan \delta$ is

$$\tan \delta(\omega) = \frac{sqrt(G_1 + G_2) G_2 G1}{2(G_1 + G_2) G_2} \tag{48}$$

The formulas can also be written as

$$\psi(t) = G_\infty + (G_0 - G_\infty) \exp(-t/T) \tag{49}$$

where

$$G_0 = \psi(0) = \frac{G_1}{G_1 + G_2} \{G_2 + G_1 \exp(0)\} = \frac{G_1 (G_1 + G_2)}{G_1 + G_2} = G_1$$

, and

$$G_\infty = \lim_{t \to \infty} \psi(t) = \frac{G_1}{G_1 + G_2} \{G_2 + G_1 \exp(-t/T)\} = \frac{G_1 G_2}{G_1 + G_2}$$

Going the other way

$$G_2 = \frac{G_\infty G_0}{G_0 - G_\infty}$$

Also

$$T_\epsilon = T_\sigma \frac{G_0}{G_{inf}}$$

Useful relationships in the frequency domain are:

$$G_{storage}(\omega) = G_\infty + (G_0 - G_\infty)\frac{\tau^2\omega^2}{1+\tau^2\omega^2} \tag{50}$$

$$G_{loss}(\omega) = (G_0 - G_\infty)\frac{\tau\omega}{1+\tau^2\omega^2} \tag{51}$$

6. Generalized Maxwell Model. Prony Series

The three element model still lacks sufficient generality to describe all materials. In reality, there is not one relaxation process, but multiple relaxation processes occuring simultanously [70]. To describe this, the Generalized Maxwell model includes multiple Maxwell elements in parallel. The stress relaxation function is:

$$\psi(t) = G_\infty + \sum_j G_j \exp(-t/T_j) \tag{52}$$

where G_∞ is the modulus after the material is fully relaxed. The summation is known as a Prony series. An alternative description is

$$\psi(t) = G_0 - \sum_j G_j\{1 - \exp(-t/T_j)\} \tag{53}$$

Where G_0 is the initial modulus before any relaxation ($G_0 = G_\infty + \sum_j G_j$) We implement the first form in VEDA. Useful relationships for the Prony series are (http://polymerfem.com/polymer_files/Prony_Series_Conversion.pdf)

$$G_{storage}(\omega) = G_\infty + \sum_j \frac{G_j\tau_j^2\omega^2}{1+\tau_i^2\omega^2} \tag{54}$$

$$G_{loss}(\omega) = \sum_j \frac{G_j\tau_j\omega}{1+\tau_i^2\omega^2} \tag{55}$$

The creep compliance function for the generalized Maxwell model is not easy to write down in closed form, but it can found [71]. There is also a generalized Kelvin-voigt model, consisting of a number of elements in series. For generalized kelvin-voigt, the creep compliance function can be easily written directly, but the stress relaxation function is difficult to find (but not impossible). Because the formulation of the equations here requires the stress relaxation function, we do not implement a generalized Kelvin-voigt model in VEDA. If you need to simulate a model described by generalized Kelvin-voigt, we suggest that you find the stress relaxation function for it, and then convert to an equivalent generalized Maxwell model.

7. Dynamic elastic modulus

The properties of viscoelastic materials are often described using a concept called "dynamic elastic modulus". The traditional Young's modulus is replaced with a "storage modulus" that describes conservative response and a "loss modulus" that describes energy dissipation. Unfortunately, there is currently no good way to directly use these storage and loss modulii in VEDA. If you have storage and loss modulus data versus frequency for a material of interest, you must fit the data to a Prony series and then perform the simulation using the Generalized maxwell model. More details will be added to this section in future releases.

8. Spatial discretization models (Attard)

The above several subsections dealt with the extension of the elastic Hertz contact problem to a viscoelastic material. This theory is satisfactory in many cases, however, there are two big limitations:

- The numerical calculations are only reasonable for the situation where the contact area increases monotonically to a single maximum and then decreases monotonically to zero. This usually the case for standard tapping mode. However, for bimodal AFM, the contact area may have any number of minima and maxima during a single tap. Although [67] has provided analytical expressions for these situations, they are too complicated to be practically useful (requiring numerical integration followed by numerical differentation followed by numerical integration).
- There is no good way to couple attractive forces into the solution. Some authors have extended the JKR contact model to viscoelastic materials, but again there may be issues with non-monotonic contact areas.

Therefore, in addition to the Hertz-based models, we have also implemented another viscoelastic model into VEDA. This model is based on the work of [72, 73]. This is an entirely different approach. It is more akin to a finite element or boundary element method than a contact mechanics problem. We discrete the sample surface with a mesh, and then solve for the deflection and pressure at each point explicitly. This removes all assumptions about the relations between contact area, indentation, and force, and allows the use of arbitrary attractive forces.

We start with an axisymmetric elastic halfspace. If the pressure distribution $P(r)$ is specificed, then the vertical deformation $u(r)$ can be computed from:

$$u(r) = \frac{-1}{\pi E^*} \int \frac{P(s)}{|\mathbf{r} - \mathbf{s}|} d\mathbf{s} \tag{56}$$

where $1/E^*$ is the reduced elasticity (Attard has used $2/E^*$ for reduced elasticity instead). Let the separation between the tip and the surface be given by $h(r) = d + \frac{r^2}{2R} - u(r)$, where d is the tip-sample gap at the center of tip,

$r^2/2R$ specifies a parabolic tip shape. Let $p(z)$ be a potential (such as lennard-jones) specifying the pressure between two infinite plates at a separation of z. Then, eq 56 becomes

$$u(r) = \frac{-1}{\pi E^*} \int \frac{p(h(s))}{|\mathbf{r}-\mathbf{s}|} d\mathbf{s} = \frac{-1}{\pi E^*} \int \frac{p(d + \frac{s^2}{2R} - u(s))}{|\mathbf{r}-\mathbf{s}|} d\mathbf{s} \tag{57}$$

This is a non-linear integral equation for u (the pressure depends on the deformation, but the deformation depends on the pressure). It could be solved by Newton-Rhapson or another numerical method. For a viscoelastic problem, apply the correspondence principle:

$$u(r,t) - u(r,0) = \int_0^t \frac{-1}{\pi E(t-t')} \int \frac{\dot{p}(h(s,t'))}{|\mathbf{r}-\mathbf{s}|} d\mathbf{s} dt' \tag{58}$$

Whereas the elastic case involved the solution of an integral equation that is non-linear in u, the viscoelastic case involves solving a differential-integral equation that is *linear* in u. Taking a time derivative on both sides gives

$$\dot{u}(r,t) - \dot{u}(r,0) = \frac{-1}{\pi} \int_0^t \left(\frac{d}{dt} \frac{1}{E(t-t')} \right) \left(\int \frac{\dot{p}(h(s,t'))}{|\mathbf{r}-\mathbf{s}|} d\mathbf{s} \right) dt' + \frac{-1}{\pi E(0)} \int \frac{\dot{p}(h(s,t))}{|\mathbf{r}-\mathbf{s}|} d\mathbf{s} \tag{59}$$

Assume that $1/E(t)$, which is the creep compliance, represents a three element model:

$$\frac{1}{E(t)} = \frac{1}{E_\infty} + \frac{E_\infty - E_0}{E_\infty E_0} e^{-t/\tau}$$

then $1/E(0) = 1/E_0$ and $\frac{d}{dt}(1/E(t-t')) = -\frac{1}{\tau}\frac{E_\infty - E_0}{E_\infty E_0} e^{-t/\tau}$, from which we get

$$\dot{u}(r,t) - \dot{u}(r,0) = \frac{-1}{\pi} \int_0^t \left(-\frac{1}{\tau} \frac{E_\infty - E_0}{E_\infty E_0} e^{-t/\tau} \right) \left(\int \frac{\dot{p}(h(s,t'))}{|\mathbf{r}-\mathbf{s}|} d\mathbf{s} \right) dt' + \frac{-1}{\pi E_0} \int \frac{\dot{p}(h(s,t))}{|\mathbf{r}-\mathbf{s}|} d\mathbf{s} \tag{60}$$

Then, comparing back to eq 58, we recognize a pattern. Add and subtract $1/E_\infty$

$$\dot{u}(r,t) = \frac{1}{\pi\tau} \int_0^t \left(\frac{E_\infty - E_0}{E_\infty E_0} e^{-t/\tau} + \frac{1}{E_\infty} - \frac{1}{E_\infty} \right) \left(\int \frac{\dot{p}(h(s,t'))}{|\mathbf{r}-\mathbf{s}|} d\mathbf{s} \right) dt' + \frac{-1}{\pi E_0} \int \frac{\dot{p}(h(s,t))}{|\mathbf{r}-\mathbf{s}|} d\mathbf{s} \tag{61}$$

which yields

$$\dot{u}(r,t) = \frac{1}{\pi\tau} \int_0^t \left(\frac{1}{E(t)} - \frac{1}{E_\infty} \right) \left(\int \frac{\dot{p}(h(s,t'))}{|\mathbf{r}-\mathbf{s}|} d\mathbf{s} \right) dt' + \frac{-1}{\pi E_0} \int \frac{\dot{p}(h(s,t))}{|\mathbf{r}-\mathbf{s}|} d\mathbf{s} \tag{62}$$

Therefore we can rearrange and rename:

$$\dot{u}(r,t) = \frac{-1}{\tau} \left(u(r,t) - u_\infty(r,t) \right) - \frac{1}{\pi E_0} \int \frac{\dot{p}(h(s,t))}{|\mathbf{r}-\mathbf{s}|} d\mathbf{s}$$

$$u_\infty(r,t) = \frac{-1}{\pi E_\infty} \int \frac{p(h(s,t))}{|\mathbf{r}-\mathbf{s}|} d\mathbf{s}$$

where u_∞ represents the surface position that would result if the pressure distribution were fixed at its current value and then the sample is allowed to relax for an infinite amount of time. But we also have

$$\dot{p}(h(r,t)) = p'(h(r,t)) \left(\dot{d}(t) - \dot{u}(r,t)\right)$$

and also considering the formula (14) from [74], we have

$$\dot{u}(r,t) = \frac{-1}{\tau}\left(u(r,t) - u_\infty(r,t)\right) - \frac{1}{E_0} \int p'(h(s,t)) \left(\dot{d}(t) - \dot{u}(s,t)\right) k(r,s) s ds \tag{63}$$

where $k(r,s)$ is given by

$$k(r,s) = \begin{cases} \frac{4}{\pi r} K(s^2/r^2), & s < r \\ \frac{4}{\pi s} K(r^2/s^2), & s > r \end{cases} \tag{64}$$

where $K(m)$ is the complete elliptical integral of the first kind with modulus m. Note that Eq. 64 is the same as formula (15) from [74] except a typo has been corrected. We precompute k to save time. Because the combination $k(r,s)s$ always appears together, we precompute it together. So define $\kappa(r,s) = k(r,s)s$

$$\dot{u}(r,t) = \frac{-1}{\tau}\left(u(r,t) - u_\infty(r,t)\right) - \frac{1}{E_0} \int p'(h(s,t)) \left(\dot{d}(t) - \dot{u}(s,t)\right) \kappa(r,s) ds \tag{65}$$

Attard implies that he uses an iterative solver. In practice this seems to be slow (at least, for the typical problem sizes we have considered of 50 - 200 radial points) . Iterative solvers could potentially be faster for larger problems.. If we discretize the integral in 63 into N points, (with Δr_j accounting for non-uniform spacing, and accouting for trapezoidal integration)

$$\dot{u}_i = -\frac{1}{\tau}\left(u(r_i,t) - u_\infty(r_i,t)\right) - \frac{1}{E_0} \sum_{j=1}^{N} (\Delta r_j) p'(h(r_j,t)) \left(\dot{d}(t) - \dot{u}(r_j,t)\right) \kappa(r_i,r_j) \tag{66}$$

Note that there is a singularity in $k(r,s)$ at $r = s$. However, the integral has a finite area. Therefore the value of $\kappa(r_i,r_j)$ at $i = j$ can be calculated according to [75]. Defining the matrix J as

$$J_{ij} = \frac{2}{E_0} (\Delta r_j) p'(h(r_j,t)) \kappa(r_i,r_j) - \delta_{ij}$$

where δ is kroneker delta, and defining the vector b

$$b_i = \frac{1}{\tau}\left(u(r_i,t) - u_\infty(r_i,t)\right) + \frac{1}{E_0}\sum_j (\Delta r_j) p'(h(r_j,t))\dot{d}(t)\kappa(r_i,r_j)$$

where u_∞ can also be discretized $u_\infty = -\frac{1}{E_\infty}\sum_{j=1}^{N}(\Delta r_j)p(h(r_j,t))\kappa(r_i,r_j)$

Then we get the simple linear equation

$$b_i = J_{ij}\dot{u}_i \tag{67}$$

which is easily solved directly.

After inverting the matrix, we have a system of ordinary differential equations, which can be solved using the same differential equation solver as used for the cantilever dynamics. Inversion of the matrix will obviously take some time, but as long as the number of points is kept small, the problem can be solved in a reasonable time.

The solution time of Eq 67 can be further reduced by performing a Fourier transform and truncating the highest order terms. Specifically, let $u(r_i,t) = \sum_{k=1}^{M} a_k(t)cos(\pi k r_i/R)$, where R is the radial extent of the computational domain, and M is the number of Fourier basis function ($M \leq N$), so then $\dot{u}(r,t) = \sum_{k=1}^{M} \dot{a_k}(t)cos(\pi k r_i/R)$. Substituting into the above, we obtain

$$b_i = J_{ij}\sum_{k=1}^{N}\dot{a_k}(t)cos(kr_i/R)$$

or

$$b_i = J_{ij}C_{ik}\dot{a}_k \tag{68}$$

where $C_{ik} = cos(\pi k r_i/R)$ is the Fourier transform matrix. If $M = N$, then Eq 68 is solvable by Gaussian Elimination just as Eq 67. However, for time savings, we desire $M < N$. Therefore Eq 68 is over constrained, and we solve it in the least squares sense

$$C_{ik}^T b_i = C_{ik}^T J_{ij} C_{ik}\dot{a}_k \tag{69}$$

This approach is similar to that described in [33], but is better conditioned numerically.

For further time savings, the model is not solved when the tip is so far away from the sample that the force is nearly zero. By default, the cutoff is 4 nm. This is user adjustable.

For all other VEDA models, when output plots refer to "tip sample gap", it is referenced to the equilibrium position of the *undeformed* sample surface. This was appropriate as the deformation of the sample surface was not tracked as

indepedent variable. For Attard's model, the deformation of the surface is tracked independently. Plots that refer to "gap" still refer to the undeformed surface, not the deformed surface. The deformed position at the center of the tip (i.e. $u(0,t)$) is output separately.

Finally, for this model, movies of the tip interacting with the sample can be produced to visual the interaction. These are available in Force Distance Curves tool, and when time histories are selected in another of the other tools.

C. Models for cantilever dynamics

This section is devoted to modeling the dynamics of the continuous cantilever beam as it interacts with a sample. A continuous beam is represented by an infinite DOF system, where each DOF corresponds to an eigenmode of the beam. Any numerical simulation of a cantilever beam involves an approximate truncated DOF model where only a finite number of eigenmodes are retained. In conventional dAFM in air or vacuum where the excitation frequency is near the resonance of the first eigenmode, a single DOF (point-mass) model is appropriate [76]. However, soft cantilevers in liquid environments [44], internal resonance [27–31, 77], or bimodal excitation [78, 79] will require two or more DOFs. In what follows, we first discuss the characteristics of the equivalent point-mass model [80] for a single eigenmode, followed by classic Bernoulli-Euler beam theory for a cantilever beam with tip mass and solve for the dispersion relationship for the eigenvalues and normal eigenmodes. Using the normal eigenmodes as a basis, we show how the standard Galerkin discretization method can produce the equivalent point-mass model or a more general multiple DOF model.

1. *The equivalent point-mass model*

Figure 90 illustrates the concept of the equivalent point-mass model. A single eigenmode of the cantilever beam can be represented as an equivalent point-mass model describing the dynamics of the tip interacting with a sample [26]. The continuous cantilever beam has a linear mass density ρ_c, elastic modulus E_c, area moment of inertia I_c and length L_c. For the ith eigenmode $u_i(x,t) = \Phi_i(x)q_i(t)$, the equivalent point-mass model has an equivalent mass m_i and stiffness k_i. Depending on the excitation source (i.e., acoustic or magnetic), there is also a specific equivalent forcing. The damping of the point-mass oscillator is characterized by a measured quality factor.

Before proceeding with a rigorous mathematical derivation, let us consider a simple physical concept. For the time being, all we need to know about continuous vibrations is that vibrations of a continuous beam may be decomposed into eigenmodes; each of which represents one DOF of an infinite DOF system. Accordingly, each eigenmode can be represented as an equivalent point mass model [80]. In doing so, we must ensure that the kinetic T and potential V energy of the eigenmode $u_i(x,t) = \Phi_i(x)q_i(t)$ are equal respectively equal to the kinetic and potential energy of the point-mass model for a given state $(u_i(L_c,t), \dot{u}_i(L_c,t))$ of the probe *tip*. From the condition on the kinetic energy on the ith eigenmode is

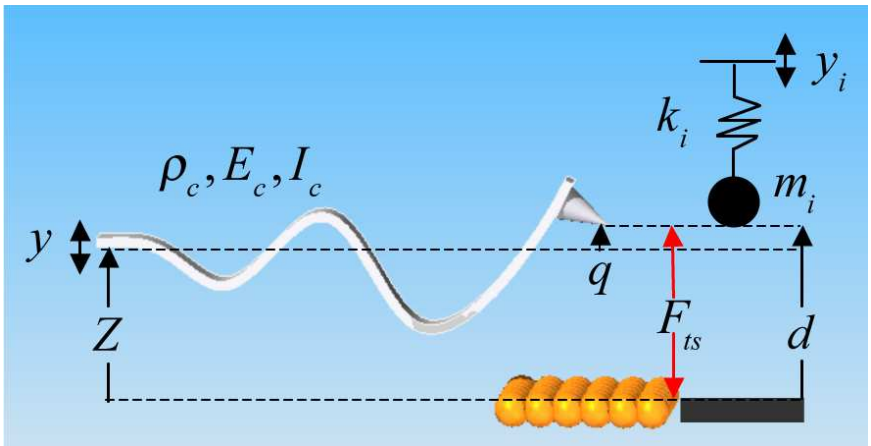

FIG. 90: (a) Schematic of a continuous AFM microcantilever with acoustic (piezo) excitation and (b) the equivalent point-mass model. The continuous microcantilever distributed mass, ρ_c, Young's modulus, E_c, area moment, I_c, and length, L_c. The point-mass has equivalent stiffness, k_i, and equivalent mass, m_i, and is driven by an equivalent base motion y_i. Both oscillators have identical kinetic and potential energy for a given state of tip motion $(q, \dot{q})$. Furthermore, in both models, the tip-sample interaction force, $F_{ts}(d)$, is identical.

$$\frac{1}{2}\int_0^{L_c} \rho_c[\dot{u}_i(x,t)]^2 dx + \frac{1}{2}m_{tip}[\dot{u}_i(L_c,t)]^2 = \frac{1}{2}m_i[\dot{u}_i(L_c,t)]^2 \tag{70}$$

where ρ_c is the linear mass density and m_i is the equivalent mass. Substituting $u_i(x,t) = \Phi_i(x)q_i(t)$ into Eq. 70, we find

$$m_i = \rho_c \int_0^{L_c} \left[\frac{\Phi_i(x)}{\Phi_i(L_c)}\right]^2 dx + m_{tip} \tag{71}$$

Eq. 70 holds for any arbitrary scaling of $\Phi_i(x)$, however, logically we can define a unique scaling of the eigenfunction such that $\overline{\Phi}_i(x) = \Phi_i(x)/\Phi_i(L_c)$ (i.e., the eigenfunctions are normalized such that the deflection at the tip is unity in every mode). Consequently, the generalized coordinates q_i now correspond to the deflection of the tip in the ith eigenmode and the equivalent mass is unique.

Similarly, the potential energy can be written as

$$V = \frac{1}{2}\int_0^{L_c} E_c I_c[u_i''(x,t)]^2\, dx = \frac{1}{2}k_i[u_i(L_c,t)]^2 \tag{72}$$

Substituting $u_i(L_c,x) = \overline{\Phi}_i(x)q_i(t)$ into Eq. 72

$$k_i = E_c I_c \int_0^{L_c} \left[\overline{\Phi}_i''(x)\right]^2 dx \tag{73}$$

One can use the principle of virtual work to derive the equivalent forcing.

In the following sections, we will provide a full derivation of a general multiple DOF model starting from classical Bernoulli-Euler beam theory. This process is guided by the principle that each eigenmode must be represented by an equivalent point-mass model in the final discretized multiple DOF model.

2. Bernoulli-Euler beam model

The classical Bernoulli-Euler beam model is applicable to small deflections of slender, uniform beams. Here, we develop a model for the dynamics of the AFM probe from Bernoulli-Euler beam theory. In this section we have assumed:

1. The AFM probe is a diving-board type cantilever that can be modeled in theory as a slender, uniform, and rectangular beam.
2. Deflection amplitudes of the cantilever tip are very small relative to the cantilever length.
3. A probe tip located at the free-end of the cantilever has a small but finite mass and negligible rotational inertia. This assumption hinges on the fact that most tips are conical or pyramidal, and should have relatively small rotational inertia about their bases.
4. All of the damping comes from hydrodynamic forces, and internal damping of the cantilever is negligible.

The most general partial differential equation (PDE) governing the small deflections of the cantilever beam for either an acoustic (base) excitation or a magnetic excitation [81] according to classical Bernoulli-Euler beam theory for small deflections in a ground-fixed (inertial) frame is as follows

$$\rho_c \ddot{w}(x,t) + F_{hydro}(\dot{w}(x,t)) + E_c I_c w''''(x,t) = F_{ts}(d,\dot{d})\delta(x - L_c) + F_{mag}(t), \tag{74}$$

where x is the axial coordinate along the cantilever's longitudinal axis, L_c is the length, dots represent temporal derivatives, primes are derivatives with respect to x, F_{hydro} is the hydrodynamic force and ρ_c, E_c, I_c are the linear density, elastic modulus and area moment of inertia respectively. The absolute deflection, $w(x,t) = Z(t)+y(t)+u(x,t)$, is composed of the separation from the sample, $Z(t)$, the acoustic excitation $y(t)$, and the deflection in the non-inertial frame attached to the base $u(x,t)$, F_{mag} represents a uniformly distributed magnetic excitation. If the cantilever is acoustically excited, F_{mag} is set to zero. Otherwise, $y(t) = 0$ if the cantilever is magnetically excited. The tip-sample interaction force $F_{ts}(d,\dot{d})$ (see Sec. IV A), and $\delta(\cdot)$ is the Dirac delta distribution.

The boundary conditions are:

$$u(0,t) = 0\ , \quad u'(0,t) = 0\ , \quad u''(L_c,t) = 0\ , \tag{75}$$

$$E_c I_c u'''(L_c,t) = m_{tip}\ddot{w}(L_c,t) = m_{tip}(\ddot{u}(L_c,t) + \ddot{y}(t) + \ddot{Z}(t)). \tag{76}$$

Typically in dAFM, a photodiode measures the bending angle $u'(L,t)$ and infers the deflection $u(L,t)$ relative to the base, therefore, we proceed to model the dynamics of the cantilever in the non-inertial, moving frame attached to

the cantilever's base. The equation of motion (Eq. 74) in the non-inertial frame attached to the moving base is:

$$\rho_c \ddot{u}(x,t) + F_{hydro}(\dot{u}(x,t) + \dot{y}(t) + \dot{Z}(t)) + E_c I_c u''''(x,t) = F_{ts}(d, \dot{d})\delta(x - L_c) - \rho_c \ddot{y}(t) + F_{mag}(t). \tag{77}$$

Regarding F_{hydro}, we assume that the Reynold's number is low so that force due to $\dot{u}(x,t)$, $\dot{y}(t)$, $\dot{Z}(t)$ can be treated by linear superposition. Also because of the low Reynold's number, we expect the damping force to have a linear dependence velocity. Now $\dot{Z}(t)$ will typically have much lower frequency content than $\dot{u}(x,t)$ or $\dot{y}(t)$, so we allow difference coefficients. Thus, $F_{hydro}(\dot{u}(x,t) + \dot{y}(t) + \dot{Z}(t)) = \gamma_f \dot{u}(x,t) + \gamma_f \dot{y}(t) + \gamma_d \dot{Z}(t)$. An empirical correlation for γ_d can be found in [82] while γ_d will be discussed later.

Henceforth, allow

$$F(x,t) = -\rho_c \ddot{y}(t) - \gamma_f \dot{y}(t) - \gamma_d \dot{Z}(t) + F_{mag}(t) \tag{78}$$

to represent the excitation of the driving force per unit length of the cantilever. Note while the velocity of the Z-piezo motion $\dot{Z}(t)$ is nonzero when scanning and its acceleration $\ddot{Z}(t)$ is also nonzero while scanning, it is reasonable to assume $\dot{Z}(t) \ll \dot{y}(t)$ and $\ddot{Z}(t) \ll \ddot{y(t)}$. Therefore, in the scanning tool we neglect hydrodynamic and inertial forces due to $Z(t)$. In the F-Z Curves and the approach curves tools, $\gamma_d \dot{Z}(t)$ is included while $\rho_c \ddot{Z}(t)$ is neglected (for those tools $\ddot{Z}(t)$ would only be non-zero at the very beginning and end of the approach anyway). In the frequency sweep tool, Z is constant so these effects are not relevant.

3. *The dispersion relationship and normal eigenmodes*

Our goal is to truncate the infinite DOF model represented by the PDE in Eq. 79 single or multiple DOF model describing the dynamics of the dAFM probe tip in the non-inertial frame. The truncation is achieved by a Galerkin discretization of the governing PDE using the normal eigenmodes as a basis.

We can derive the dispersion relationship and normal eigenmodes of the cantilever by neglecting the nonconservative forces (i.e., damping or tip-sample interactions) and external forcing. Under such conditions, Eq. 79 reduces to

$$\rho_c \ddot{u}(x,t) + E_c I_c u''''(x,t) = 0. \tag{79}$$

The solution process for solving Eq. 79 follows the standard separation of variable approach. In doing so, we make the substitution $u(x,t) = \Phi(x)q(t)$ into Eq. 79, yielding

$$\frac{\ddot{q}(t)}{q(t)} = -\frac{E_c I_c}{\rho_c} \frac{\Phi''''(x)}{\Phi(x)}. \tag{80}$$

The only way for Eq. 80 to hold for all time and x is for the right and left sides to be constant which we will call ω^2. This yields two ordinary differential equations (ODEs) for the temporal and spatial components of $u(x,t)$. The ODE describing the temporal component $q(t)$ becomes

$$\ddot{q}(t) + \omega^2 q(t) = 0, \tag{81}$$

which has a solution of general form

$$q(t) = A\sin\omega t + B\cos\omega t. \tag{82}$$

The spatial component $\Phi(x)$ is governed by

$$\Phi''''(x) - \left(\frac{\alpha}{L_c}\right)^4 \Phi(x) = 0, \tag{83}$$

where α is defined for convenience by

$$\alpha^4 \equiv \rho_c \omega^2 L_c^4 / E_c I_c \tag{84}$$

The solution to Eq. 83 has a general form

$$\Phi(x) = c_1 \sin\left(\frac{\alpha_i x}{L_c}\right) + c_2 \cos\left(\frac{\alpha_i x}{L_c}\right) + c_3 \sinh\left(\frac{\alpha_i x}{L_c}\right) + c_4 \cosh\left(\frac{\alpha_i x}{L_c}\right) \tag{85}$$

The general form of $\Phi(x)$ is decided by the boundary conditions. Since we are considering the unforced problem in this section, the boundary conditions 75 reduce to:

$$u(0,t) = 0\ , \quad u'(0,t) = 0\ , \quad u''(L_c,t) = 0\ , \quad u''(L_c,t) = 0\ , \quad E_c I_c u'''(L_c,t) = m_{tip}\ddot{u}(L_c,t). \tag{86}$$

Substituting $u(x,t) = \Phi(x)q(t)$ into Eq. 86 and realizing $\ddot{q} = -\omega^2 q(t)$ (Eq. 81), we find

$$\Phi(0) = 0\ , \quad \Phi'(0) = 0\ , \quad \Phi''(L_c) = 0\ , \quad E_c I_c \Phi'''(L_c) + \omega^2 m_{tip}\Phi(L_c) = 0. \tag{87}$$

Substituting the general form of $\Phi(x)$ (Eq. 85) in the first and second boundary conditions, we quickly find $c_2 = -c_4$ and $c_1 = -c_3$. Eliminating c_3 and c_4 from the remaining two boundary conditions, and then using Eq. (84) we are left with two equations and two unknowns:

$$\begin{bmatrix} \sin\alpha + \sinh\alpha, & \cos\alpha + \cosh\alpha \\ \cos\alpha + \cosh\alpha - \overline{m}_{tip}\alpha(\sin\alpha - \sinh\alpha), & -\sin\alpha + \sinh\alpha - \overline{m}_{tip}\alpha(\cos\alpha - \cosh\alpha) \end{bmatrix} \begin{pmatrix} c_1 \\ c_2 \end{pmatrix} = \begin{pmatrix} 0 \\ 0 \end{pmatrix} \tag{88}$$

where $\overline{m}_{tip} = m_{tip}/m_c$ is the non-dimensional tip mass where $m_c = \rho_c L_c$ is the mass of the cantilever beam. The nontrivial solutions to Eq. 88 are found by taking the determinant of the matrix which yields the dispersion relationship:

$$\cos\alpha\cosh\alpha + 1 + \overline{m}_{tip}\alpha(\cos\alpha\sinh\alpha - \sin\alpha\cosh\alpha) = 0. \tag{89}$$

Eq. 89 supports a countably infinite number of solutions α_i, each of which correspond to an eigenmode. The general solution takes the form $u(x,t) = \sum_{i=1}^{\infty} \Phi_i(x) q_i(t)$ where the eigenfrequencies of the ith eigenmode are given by $\alpha_i^4 = \rho_c \omega_i^2 L_c^4 / E_c I_c$ and the eigenfunction $\Phi_i(x)$ is found by eliminating c_2 using the first three boundary conditions in Eq. 88, which leaves an arbitrary scaling c_1 for the entire eigenfunction. Choosing $c_1 = 1$, we have

$$\Phi_i(x) = \sin\left(\frac{\alpha_i x}{L_c}\right) - \sinh\left(\frac{\alpha_i x}{L_c}\right) - \sigma_i\left[\cos\left(\frac{\alpha_i x}{L_c}\right) - \cosh\left(\frac{\alpha_i x}{L_c}\right)\right] \tag{90}$$

where $\sigma_i = \frac{\sin\alpha_i + \sinh\alpha_i}{\cos\alpha_i + \cosh\alpha_i}$. Note that the eigenfunction in Eq. 90 is identical to the simple cantilever beam (without tip mass). The effect of the particle mass located at the free-end has only modified the eigenvalues α_i according to Eq. 89.

While $\overline{m}_{tip}$ is fairly small (around 10% for many commercial levers), these values of tip mass can still have a profound effect on higher eigenmodes in dAFM applications. As tip mass is added to the cantilever, the outer-most node of higher eigenmodes gradually move towards the tip. When a node is close to the free-end, large amounts of kinetic and potential energy are present for small deflections of the tip in that eigenmode. This results in large stiffnesses and masses of the higher eigenmodes [80]. The first eigenmode, which contains no nodes, is not affected significantly by the tip mass.

4. The Galerkin discretization

Now that we know the eigenfunctions $\Phi_i(x)$, we can use them as a basis for a Galerkin discretization of Eq. 79. In particular, we will use the unique scaling of the eigenmode $\overline{\Phi}_i(x)$ to ensure that energy is preserved when taking the inner product. Note that the cantilever beam with tip mass is a self-adjoint system with orthogonal eigenmodes [83]

$$\int_0^{L_c} \overline{\Phi}_i(x)\overline{\Phi}_j(x)dx = \begin{cases} -\bar{m}_{tip}, & \text{for } \; i \neq j \\ \mu_i, & \text{for } \; i = j \end{cases} \tag{91}$$

where μ_i is the portion of the cantilever equivalent mass resulting from the beam mass (not including the tip mass). If the tip mass is zero, $\mu_i = 1/4$; however, if it is nonzero, the higher eigenmodes are affected, and therefore μ_i are affected.

The Galerkin discretization is performed by substituting $u(x,t) = \sum_{j=1}^{\infty} \overline{\Phi}_j(x) q_j(t)$ into Eq. 79, and taking the inner product with $\overline{\Phi}_i(x)$ as follows

$$\int_0^{L_c} \overline{\Phi}_i(x) \left(\rho_c \sum_{j=1}^{\infty} \overline{\Phi}_j(x)\ddot{q}_j(t) + \gamma_f \sum_{j=1}^{\infty} \overline{\Phi}_j(x)\dot{q}_j(t) + E_c I_c \sum_{j=1}^{\infty} \overline{\Phi}_j''''(x) q_j(t) = F(x,t) \right) dx. \tag{92}$$

or

$$\rho_c \sum_{j=1}^{\infty} \int_0^{L_c} \overline{\Phi}_i(x)\overline{\Phi}_j(x)dx\ddot{q}_j(t) + \gamma_f \sum_{j=1}^{\infty} \int_0^{L_c} \overline{\Phi}_i(x)\overline{\Phi}_j(x)dx\dot{q}_j(t) + E_c I_c \sum_{j=1}^{\infty} \int_0^{L_c} \overline{\Phi}_i(x)\overline{\Phi}_j''''(x)dx q_j(t) = \int_0^{L_c} \overline{\Phi}_i(x)F(x,t)dx. \tag{93}$$

Also substitute the sum into the boundary conditions (87)

$$\begin{gathered} \Phi(0) = 0\ , \quad \Phi'(0) = 0\ , \quad \Phi''(L_c) = 0 \\ E_c I_c \sum_{j=1}^{\infty} \overline{\Phi}(L_c)_j'''(x) q_j(t) = m_{tip}(\sum_{j=1}^{\infty} \overline{\Phi}(L_c)_j(x)\omega_j^2 q_j(t) + \ddot{y}(t) + \ddot{Z}(t)) \end{gathered} \tag{94}$$

We integrate the stiffness term by parts [83]

$$\sum_{j=1}^{\infty}\left(E_cI_c\int_0^{L_c}\overline{\Phi}_j''''(x)\overline{\Phi}_i(x)dx\right)=\sum_{j=1}^{\infty}\left(E_cI_c\overline{\Phi}_j'''(x)\overline{\Phi}_i(x)|_0^{L_c}-E_cI_c\overline{\Phi}_j''(x)\overline{\Phi}_i'(x)|_0^{L_c}+E_cI_c\int_0^{L_c}\overline{\Phi}_i''(x)\overline{\Phi}_j''(x)dx\right) \tag{95}$$

From the boundary conditions (Eq. ??), $\overline{\Phi}_j''(x)\overline{\Phi}_i'(x)|_0^{L_c}=\cancel{\overline{\Phi}_j''(L_c)}\overline{\Phi}_i'(L_c)-\overline{\Phi}_j''(0)\cancel{\overline{\Phi}_i'(0)}=0$. Also, from the boundary conditions (Eq. ??): $\sum_{j=1}^{\infty}\left(E_cI_cq_i(t)\overline{\Phi}_j'''(x)\overline{\Phi}_i(x)|_0^{L_c}\right)=\sum_{j=1}^{\infty}\left(E_cI_cq_i(t)\left[\overline{\Phi}_j'''(L_c)\Phi_i(L_c)-\overline{\Phi}_j'''(0)\cancel{\overline{\Phi}_i(0)}\right]\right)=m_{tip}\left(\sum_{j=1}^{\infty}\ddot{q}_j(t)+\ddot{y}+\ddot{Z}\right)$. Note the last term in Eq. 95 is the equivalent stiffness (Eq. 73), which can be shown to be diagonal. Substitute these results into Eq. 93

$$\sum_{j=1}^{\infty}\left(\rho_c\int_0^{L_c}\overline{\Phi}_i(x)\overline{\Phi}_j(x)dx+m_{tip}\right)\ddot{q}_j(t)+\gamma_f\sum_{j=1}^{\infty}\int_0^{L_c}\overline{\Phi}_i(x)\overline{\Phi}_j(x)dx\dot{q}_j(t)+E_cI_c\int_0^{L_c}[\overline{\Phi}_j''(x)]^2dxq_j(t)=$$
$$\int_0^{L_c}\overline{\Phi}_i(x)F(x,t)dx-m_{tip}\left(\ddot{y}+\ddot{Z}\right) \tag{96}$$

Then the orthogonality relation in Eq. 91 can be used to simplify the mass terms:

$$\left(\rho_c\int_0^{L_c}\overline{\Phi}_i^2(x)dx+m_{tip}\right)\ddot{q}_i(t)+\gamma_f\sum_{j=1}^{\infty}\int_0^{L_c}\overline{\Phi}_i(x)\overline{\Phi}_j(x)dx\dot{q}_i(t)+E_cI_c\int_0^{L_c}[\overline{\Phi}_i''(x)]^2dxq_i(t)=$$
$$\int_0^{L_c}\overline{\Phi}_i(x)F(x,t)dx-m_{tip}\left(\ddot{y}+\ddot{Z}\right). \tag{97}$$

At this point, note that the damping terms still have off-diagonal elements if m_{tip} is non-zero. Thus the damped eigenmodes are not diagonal in the basis of undamped eigenmodes. Equivalently speaking, the modal equations we have developed are coupled. However, in VEDA, we neglect the off diagonal terms and work with uncoupled equations. This is valid for the following reasons: in air, the damping is very small, and therefore it has little overall effect on the eigenmodes, and the undamped and damped eigenmodes are nearly identical. In liquid, the off-diagonal terms are small compared to the on-diagonal terms, therefore we can neglect them. Finally, we obtain the desired result

$$\left(\rho_c\int_0^{L_c}\overline{\Phi}_i^2(x)dx+m_{tip}\right)\ddot{q}_i(t)+\left(\gamma_f\int_0^{L_c}\overline{\Phi}_i^2(x)dx\right)\dot{q}_i(t)+\left(E_cI_c\int_0^{L_c}[\overline{\Phi}_i''(x)]^2dx\right)q_i(t)=$$
$$\int_0^{L_c}\overline{\Phi}_i(x)F(x,t)dx-m_{tip}\left(\ddot{y}+\ddot{Z}\right) \tag{98}$$

We can rearrange Eq. ?? to include experimentally observable parameters, such as ω_i and the quality factor Q_i, to obtain

$$\frac{\ddot{q}_i(t)}{\omega_i^2}+\frac{\dot{q}_i(t)}{\omega_iQ_i}+q_i(t)=\frac{F_{ts}(d,\dot{d})}{k_i}+\frac{F_i(t)}{k_i} \tag{99}$$

where F_i is the equivalent forcing or excitation of the ith eigenmode (which includes the tip mass inertial loading) and $d=Z+y(t)+\sum_1^N q_i(t)$ is the instantaneous gap between the tip and the sample and N is the number of eigenmodes (DOFs) retained in the model. The dependence of the tip-sample interaction on the tip-sample gap d

and its rate $\dot{d}$ couples the response of all eigenmodes 1 through N together. For example, consider a two-eigenmode model ($N = 2$) for a magnetically excited cantilever ($y(t) = 0$) and a conservative tip-sample interaction potential of the type $F_{ts} = F_{ts}(d)$ where $d = Z + q_1 + q_2$ [44]. In this case, the two-eigenmode model can be expressed as

$$\begin{aligned} \frac{\ddot{q}_1(t)}{\omega_1^2} + \frac{\dot{q}_1(t)}{\omega_1 Q_1} + q_1(t) &= \frac{F_{ts}(Z + q_1 + q_2)}{k_1} + \frac{F_1(t)}{k_1} \\ \frac{\ddot{q}_2(t)}{\omega_2^2} + \frac{\dot{q}_2(t)}{\omega_2 Q_2} + q_2(t) &= \frac{F_{ts}(Z + q_1 + q_2)}{k_2} + \frac{F_2(t)}{k_2} \end{aligned} \tag{100}$$

The form of $F_i(t)$ will vary depending on the source (magnetic or acoustic) and the frequency scheme (single or multifrequency excitation). This is discussed in Sec. IV C 7.

5. *The non-dimensional multiple degree-of-freedom model*

For the purposes of the simulation, it becomes essential to nondimensionalize Eq. 99 by characteristic length and time scales to avoid a loss of precision during numerical integration. We nondimensionalize time according to $\tau = t\Omega$, where Ω is an arbitrary scaling frequency. For good numerical practices, Ω is chosen to make characteristic time scales, such as oscillation period, on the order of unity. Common choices for the scaling frequency are ω_d or ω_1. Similarly, the spatial coordinates are nondimensionalized by according to $\overline{q} = q/\Lambda$, where Λ is an arbitrary length scale chosen to make characteristic length scales, such as amplitude, on the order of unity. One common choice is $\Lambda = A_0$, where A_0 is the unconstrained amplitude. Allowing primes to denote $d/d\tau$, the nondimensional equation of motion is expressed as

$$\overline{q}_i''(\tau) + \frac{\Omega_i}{Q_i}\overline{q}_i'(\tau) + \Omega_i^2 \overline{q}_i(\tau) = \frac{\Omega_i^2}{k_i}\left[\overline{F}_{ts}(\overline{d}, \overline{d}') + \overline{F}_i(\tau)\right] \tag{101}$$

where $\Omega_i = \omega_i/\Omega$ and $\overline{d} = d/\Lambda$. For convenience, we have also the scaled forces $\overline{F}_i = F_i/\Lambda$ and $\overline{F}_{ts} = F_{ts}/\Lambda$.

6. *The photodiode signal*

Since most commercial AFMs utilize the photodiode optical-lever technique, which measures the bending angle and attempts to infer the cantilever deflection, our simulations designed to reproduce the photodiode signal. After properly calibrating the cantilever based on the first eigenmode deflection, as explained in [44], the photodiode deflection signal is

$$\overline{u}_p(\tau) = \sum_{i=1}^{N} \chi_i \overline{q}_i(\tau) \tag{102}$$

where $\chi_i = \overline{\Phi}_i'(\overline{x})/\overline{\Phi}_1'(\overline{x})|_{\overline{x}=1}$. Note we have assumed that the laser is focused at the free end. Also, note that the higher eigenmodes are naturally amplified by this measurement. When the user specifies an unconstrained amplitude A_0, it is referring to the amplitude of $\overline{u}_p(\tau)$. If instead the true deflection is desired (such as would be obtained with

an interferometer measurement instead of a photodiode), the user can specify this in the GUI ("output type" near the bottom of the "operating conditions and cantilever properties" tab).

As a side note, a standard experimental method is to calibrate χ using a static F-z curve. This gives the static bending χ_s whereas in dynamic AFM we typically need the 1st eigenmode mode χ_1. For zero tip mass, $\chi_1 \approx 1.09\chi_s$, and $\chi_s \propto \frac{3}{2L}$ (rad/m) where L is the length of the cantilever. This relation is for an infintessimal laser spot size exactly at the free end.

7. Excitation sources and schemes

In this section, we discuss various models for the excitation $\overline{F}_i$ including magnetic excitation, acoustic excitation, photothermal excitation, and briefly multiple frequency excitations. In liquid environments, where quality factors are small, the source of cantilever excitation becomes particularly important. For standard operation in ambient or vacuum, the excitation source is not critical.

An excitation by an external magnetic field is the simplest to model. Two different types of magnetic excitation in common use. One is referred to as Lorentz force actuation [84] (such as Asylum's i-Drive). This works by running an time-varying electrical current through a wire loop on the cantilever. When a constant external magnetic field is applied, this generates a uniform force distribution on the cantilever such that $f(x,t) = f_{mag}\cos\omega_d t$. Then from the general form of the equivalent forcing, we find that the modal force on the ith eigenmode has the form

$$\overline{F}_i^{mag}(\tau) = \overline{F}_{mag}\beta_i \cos\Omega_d\tau \tag{103}$$

where $\overline{F}_{mag} = f_{mag}L_c/\Lambda$, f_{mag} is load distribution, ω_d is the drive (excitation) frequency and $\beta_i = \int_0^1 \overline{\Phi}_i(\overline{x})\overline{x}$. The first few values of β_i are 0.391, -0.217, 0.127, -0.091 for i =1,2,3,4.

The other common method is to make the cantilever a permanent magnet. This could be either with a thin coating of a magnetic material (such as Agilent's MAC mode), or a small magnetic particle glued to the cantilever. Then a time-varying external magnetic field is applied. The most common case is when the external magnetic field is perpendicular to the axis of magnetization of the cantilever [85, 86]. In this case the magnetic field effectively creates a torque on the cantilever, which leads to the same modal force on each eigenmode. In other words

$$\overline{F}_i^{mag}(\tau) \propto \overline{F}_{mag}\cos\Omega_d\tau \tag{104}$$

The difference between these two types of magnetic excitation is small compared to the difference between magnetic and other modes. Note: Versions of VEDA prior to Feb 2012 did not correctly distinguish these two types of excitation. There was just a "magnetic" excitation which was a uniform force.

From Eq. 101, the transfer function for either of these types of magnetic forcing is given by

$$G_i^{mag}(j\overline{\Omega}_d) \equiv \frac{\overline{A}_i(j\overline{\Omega}_{d,i})}{\overline{F}_i(j\overline{\Omega}_{d,i})/k_i} = \left[1 - \overline{\Omega}_{d,i}^2 + j\overline{\Omega}_{d,i}/Q_i\right]^{-1} \tag{105}$$

$$\overline{U}_p(L_c, j\overline{\Omega}_{d,i}) = \overline{F}_{mag} \sum_{i=1}^{N} \chi_i \beta_i G_i^{mag}(j\overline{\Omega}_{d,i})/k_i. \tag{106}$$

and

$$\overline{F}_{mag} = \overline{A}_0 \left\{ \left| \sum_{i=1}^{N} \chi_i \beta_i G_i^{mag}(j\overline{\Omega}_{d,i}) \right| \right\}^{-1} \tag{107}$$

The forcing term is:

$$\frac{\Omega_i^2}{k_i} \overline{F}_i(\tau) = \frac{\Omega_i^2}{k_i} \overline{F}_{mag} \beta_i \tag{108}$$

For an acoustic (base) excitation, the force is:

$$\overline{F}_i^{AC}(\tau) = -\frac{k_i}{\Omega_i^2} \left(\frac{\beta_i + \overline{m}_{tip}}{\mu_i + \overline{m}_{tip}} \right) \overline{y}_{,\tau\tau}(\tau) - \frac{k_i \beta_i}{\Omega_i \mu_i Q_i} \overline{y}_{,\tau}(\tau). \tag{109}$$

where $\mu_i = \int_0^1 \overline{\Phi}_i^2(\overline{x}) d\overline{x}$, $\beta_i = \int_0^1 \overline{\Phi}_i(\overline{x}) d\overline{x}$ and $\overline{x} = x/L_c$. Considering harmonic excitation $\overline{y}(\tau) = \overline{A}_{base} \cos \Omega_d \tau$, where $\Omega_d = \omega_d/\Omega$ is the drive (excitation) frequency, the force becomes For an acoustic excitation, the transfer function is

$$G_i^{AC}(j\overline{\Omega}_{d,i}) = \frac{\overline{A}(j\overline{\Omega}_{d,i})}{\overline{y}(j\overline{\Omega}_{d,i})} = \frac{\overline{\Omega}_{d,i}^2 \left(\frac{\beta_i + \overline{m}_{tip}}{\mu_i + \overline{m}_{tip}} \right) - \frac{j\overline{\Omega}_{d,i}}{Q_i} \left(\frac{\beta_i}{\mu_i} \right)}{1 - \overline{\Omega}_{d,i}^2 + j\overline{\Omega}_{d,i}/Q_i} \tag{110}$$

where $\overline{\Omega}_{d,i} = \omega_d/\omega_i$. In the case of multiple frequency excitations $\overline{\Omega}_{d,i}^{(j)} = \omega_d^{(j)}/\omega_i$. Also, define N_i^{AC} to be the numerator or G_i^{AC}, then an acoustic forcing term is given by

$$\frac{\Omega_i^2}{k_i} \overline{F}_i(\tau) = \overline{A}_{base} \Omega_i^2 |N_i^{AC}(j\overline{\Omega}_{d,i})| \cos \left[\Omega_d \tau - \angle N_i^{AC}(j\overline{\Omega}_{d,i}) \right] \tag{111}$$

where $\angle N_i^{AC}(j\Omega_d) = \text{atan2}\left[-\text{Im}\{N_i^{AC}(j\Omega_d)\}, \text{Re}\{N_i^{AC}(j\Omega_d)\} \right]$. The base amplitude is calculated from the specified unconstrained amplitude $\overline{A}_0$ by

$$\overline{A}_{base} = \overline{A}_0 \left\{ \left| \sum_{i=1}^{N} \chi_i(L_c) G_i^{AC}(j\overline{\Omega}_{d,i}) \right| \right\}^{-1}. \tag{112}$$

The hydrodynamic force due to Z piezo motion, assuming a constant velocity $\dot{Z}(t) = v_{aprch}$ (see section IV C 2), is

$$F_i^Z = \int_0^{L_c} \overline{\Phi}_i(x) dx \left(-\gamma_d \dot{Z} \right) = v_{aprch} \beta_i \gamma_d \tag{113}$$

The equivalent forcing is:

$$\overline{F}_i^Z = \frac{\Omega_i^2}{\Lambda k_i} v_{aprch} \beta_i \gamma_d = \frac{\Omega_i^2}{k_i} \overline{v}_{aprch} \Omega \beta_i \gamma_d \tag{114}$$

where $\overline{v}_{aprch} = v_{aprch}/\Omega\Lambda$.

Multiple frequency excitations are also possible. The theoretical considerations are the same as described for each frequency excitation, and an unconstrained amplitude at each frequency must be specified. For instance, a two frequency (ω_{d1}, ω_{d2}) magnetic excitation will take the form

$$\overline{F}^{mag}(\tau) = \left(\frac{F_{mag}^{(1)} \Omega_i^2}{k_i \Lambda} \int_0^{L_c} \overline{\Phi}_i(x) dx \right) \cos \Omega_d^{(1)} \tau + \left(\frac{F_{mag}^{(2)} \Omega_i^2}{k_i \Lambda} \int_0^{L_c} \overline{\Phi}_i(x) dx \right) \cos \Omega_d^{(2)} \tau \tag{115}$$

For modes in which the drive frequency is fixed (e.g. tapping mode), the above excitation schemes are sufficient to capture most of the relevant dynamics. However, for modes in which the drive frequency can vary (e.g. frequency modulation), there are additional considerations. For acoustic excitation, the base motion $\overline{y}(\tau)$ may not be constant with frequency, but may have a depedence $\overline{y}(\tau) = \overline{A}_{base}(\Omega_d)\cos\Omega_d\tau$ (where $\overline{A}_{base}$ is complex valued - the amplitude and phase may change with frequency). In VEDA, we include a simple model whereby $\overline{A}_{base}(\Omega_d)$ is given by a single degree of freedom oscillator - the user gives a natural frequency and quality factor.

We also include a model for photothermal excitation which has a frequency dependence as well. Photothermal excitation is quite complex [87, 88]. We include only a very simplified model here. First, we assume that the laser spot is positioned in a location on the cantilever where it excites mainly the first eigenmode and the excitation of the other eigenmodes is negligible. Second, we assume that both the magnitude and phase of the excitation force change linearly with frequency. That is, we assume $F_1^{pt} = F_{pt}c_1(\bar{\Omega}_{d,1} - 1)\cos(\Omega_d\tau + c_2(\bar{\Omega}_{d,1} - 1))$, where c_1 and c_2 are constants, and $F_i^{pt} = 0$ for $i = 2, 3, 4\cdots$

8. *Self-excitation models (BETA testing)*

We include a simplified version of the self-excitation configuration used by [89]. This feature should be considered a beta test. There may be bugs or errors in it.

The self-excitation is usable in Amplitude Modulated approach curves (advanced), amplitude modulated scanning (advanced), and the new "Amplitude modulated single Z" tool. To use the feature, for the box "choose frequency scheme", change it from "single frequency" to "self-excitation".

I suggest that you make use of the time history outputs (on "simulation parameters" tab). This will allow you to see the cantilever deflection and applied force as a function of time so that you can see how I am doing the gain and saturation, and how the cantilever responds to the force.

Because this is still in beta testing, there are a few limitations:

1) We only implemented the self-excitation for magnetic drive. For acoustic (piezo) drive it is more complicated because we must keep track of both the base position and the forces. For air (high Q), the magnetic drive and the acoustic drive will give the same answer anyway so it does not matter. For liquids, acoustic and magnetic is very different.

2) [89] suggests that the phase delay between the motion of the base and the modal forcing on the cantilever provides a natural phase delay and that a phase shifter is not strictly necessary. However, per above, we use only a magnetic force that is assumed to act instantly. Therefore it may be necessary to introduce a phase delay. However, we have actually not implemented a true phase shifter, but a rather a simple time delay. That is, we read the cantilever motion, wait a specified amount of time, and then output the force. For air (high Q), the cantilever motion will be dominated by a single harmonic anyway, so this delay is fine. For liquids (low Q), the cantilever motion may include

higher harmonics. In this case the time delay might not represent your physical system.

3) Finally, the output is reported using a lock-in amplifier model that has a center frequency as the "driving frequency", even though the self-excitation may stabilize on a solution that is not exactly at the first natural frequency. Therefore you may need a wide bandwidth on the lock-in amplifier to get the correct amplitude signal (and the phase signal might not be defined very well). In the future, we might want to use an RMS measurement of amplitude, or use a Phase-locked-loop to track the self-excitation frequency.

So essentially, the current implementation should work fairly well for simulations in air. For simulations of liquid (Q $<$ 10) it may not work as well.

9. *Extensions to triangular and other non-standard geometries*

While the discretized models in this section are derived for rectangular beams, the results provide a reasonable approximation for triangular cantilevers and other geometries under standard operating conditions and as long as the quality factors are sufficiently large ($Q_1 \gtrsim 20$) - a condition that is typically met for cantilevers oscillating in ambient conditions. By standard operating conditions, we mean that a single drive frequency is tuned to the natural frequency of the fundamental eigenmode ($\omega_d = \omega_1$), and the natural frequencies of higher eigenmodes do not lie within integer multiples of the fundamental. In this case, if $Q_1 \gtrsim 20$, only the fundamental eigenmode will contribute significantly to the cantilever dynamics. The motion of the base of the cantilever should be very small in the case of acoustic excitation, and one can show the difference between magnetic and acoustic excitation sources is negligible. Also, the photodiode deflection $u_p(t)$ is approximately the response of the fundamental eigenmode $q_1(t)$. Finally, for non-rectangular geometries, calibration of the stiffness k_1 may require thermal calibration methods to insure accurate predictions [80, 90].

D. Models for lock-in amplifiers and noise

In dynamic AFM (both amplitude modulated and frequency modulated), the controller's objective is to maintain a constant tip amplitude as the AFM cantilever probes the sample in the presence of tip-sample interaction forces. To do this, an accurate measurement of the amplitude is needed.

In commercial AFMs, the amplitude of the photodiode signal is generally measured using a lock-in amplifier. A lock-in multiplies the photodiode signal with the drive (reference) signal or possibly a higher harmonic of the drive signal. Since both of these signals are approximately sinusoidal, resulting in a signal of the form $(A\sin(\omega t))2\sin(\omega t) = A - A\sin(2\omega t)$. Then a low pass filter is used to remove the 2ω component leaving only the constant A component. The choice of the low-pass filter time constant involves a trade-off between a quick time-domain response of the filter and noise rejection. With a long filter time constant, the filter will average over many drive cycles and thus give a clean signal. However, it will take the filter longer to respond to a change in the signal. With a short filter time constant,

the filter will average over fewer drive cycles and thus response is much quicker, but noise and even nonlinearities, such as the higher harmonics, may distort the measurement. In the current version of VEDA, you can choose from either a 1st, 2nd or 4th order Butterworth filter with various choices of time constant. Random noise can also be added directly to the deflection signal to simulate measurement shot noise.

Another way to compute the amplitude is by a Fourier transform over a specified number of oscillation cycles and then extracting the amplitude at the drive frequency. This method usually has better noise rejection than the lock-in method. Therefore, comparing the amplitude and phase as measured by the fourier integral to the amplitude and phase as measured by the lock-in can often serve as an indicator of whether the choosen lock-in model is good. But there are two situations where the fourier integral method performs worse than a lock-in. The integral needs to be computed over an integer number of drive cycles to avoid spectral leakage. For fixed frequency tools this is not a problem, but for frequency modulation where the frequency can changes at every step it is not always possible to get an integer number of drive cycles. Additionally, in certain oscillation regimes (e.g. chaos) it is impossible. In this cases the Fourier integrals may be unreliable.

For the tools which use feedback control, VEDA will plot both the Fourier transform amplitude and the lock-in amplitude. But, only the lock-in amplitude is used for feedback control (this is a difference from previous versions, which did not have a lock-in model and thus used the Fourier analysis for feedback control). The basic versions of some tools plot only one method or the other to avoid unecessarily complicating the ouput for begining users.

E. Models for AM controller dynamics

In Amplitude Modulated (AM) AFM, when the response amplitude deviates from the desired amplitude, the Z displacement is adjusted accordingly and recorded as the sample topography.

For scanning simulations, we choose a simple proportional-integral (PI) controller to maintain the desired amplitude. A block diagram of the feedback scheme is shown in Figure 91 This is the typical controller used in most commercial AFM instruments today. More specifically, the feedback parameter is the amplitude error, e, which is defined as:

$$e = A_1/A_0 - A_{sp} \tag{116}$$

where A_1 and A_{sp} are the current amplitude of the primary harmonic and the set-point amplitude ratio respectively. Based on the amplitude error, the Z displacement from the sample is adjusted according to:

$$\Delta Z(t_n) = \left(-K_P e(t_n) - \frac{K_I}{f_s} \sum_{i=1}^{i=n} e(t_i) \right) \tag{117}$$

where, K_P and K_I are the proportional and integral gain constants, f_s is the sampling frequency, and $t_n = n/f_s$. Note, the controller used in versions 2.0.6 and forward is slightly different than previous controllers. You will need slightly different gains to achieve the same response (the previous controller had an extra integrator block in Figure

91 so that "proportional" control was effectively integral control, and "integral" controller was effectively a double integral control.)

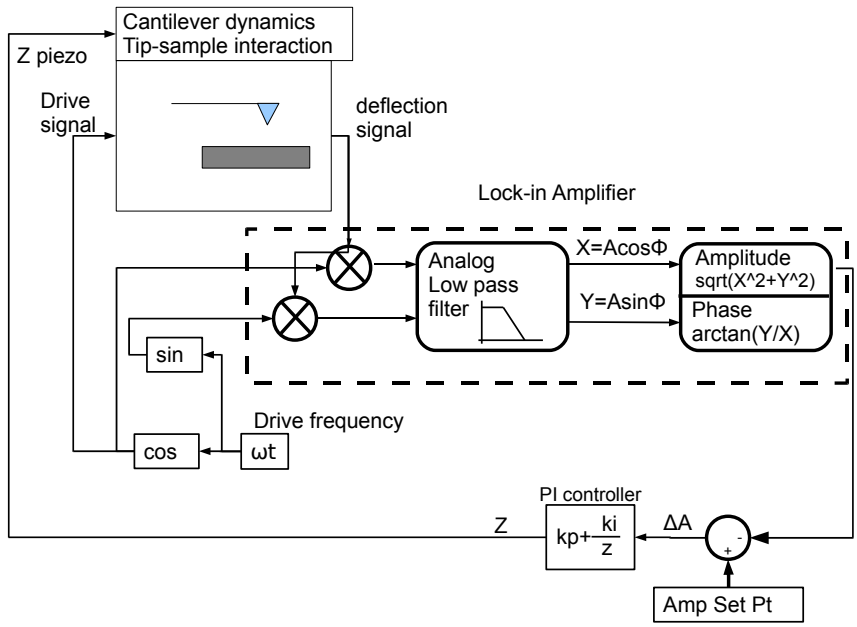

FIG. 91: Feedback control block diagram used in AM simulation

F. Models for FM controller dynamics

The controller scheme for frequency modulated (FM) AFM is significantly more complicated. A block diagram is shown in Figure 92. Three separate controllers are used. First, a Phase Locked Loop (PLL) is used to adjust the drive frequency. As the tip interacts with the sample, attractive forces will effectively make the system softer and lower the resonant frequency. Repulsive forces will effectively make the system stiffer and increase the resonant frequency. The PLL changes the drive frequency to follow the resonant frequency so that the cantilever is always driven at resonance. Then, an second controller is used to increase the driving force (either magnetic force for magnetic drive or base amplitude for acoustic drive) to maintain a constant amplitude. Finally, a Z controller adjusts the height in order to keep the frequency shift from the PLL constant.

Some commercial AFMs use a different scheme. Since ϕ is nearly 90 degrees when the controller is operating properly, and since $\cos(\phi) \approx \phi$ and $\sin(\phi) \approx 1$ when ϕ is nearly 90 degrees, $Y \approx A$ and $X \approx A\phi$. Thus, some AFMs use the X and Y channels in the feedback controllers, skipping the step of computing true amplitude and phase. This generally does not make much difference to the results for properly tuned controllers. VEDA allows simulating both conditions.

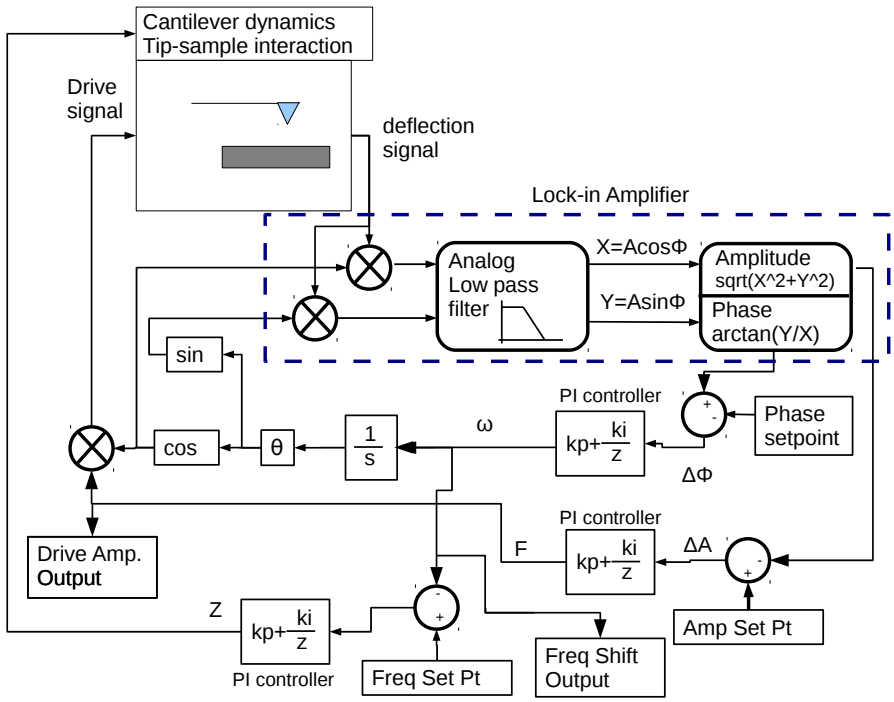

FIG. 92: Feedback control block diagram used in FM simulation

G. Numerical integration scheme

In this section, we describe the numerical integration algorithms, which allow a relative tolerance of $10^{-}9$, that are implemented in all VEDA simulation tools, and why such an approach is necessary. As described earlier, the tip-sample interaction models discussed in Section IV A describe non-smooth interaction forces. Smoothing the interaction forces or using conventional integration routines to integrate the non-smooth forces cannot predict accurately the tip vibration response. In order to accurately integrate the non-smooth interaction forces, a DDASKR routine with a root-finding algorithm based on DASPK differential algebraic equations (DAEs) software package (DASPK, UCSB) is used [91–95]. Conventional integration routines cannot accurately and efficiently deal with the non-smooth interaction forces. Figure 93 compares schematically the DDASKR integration routine and the conventional integration routines. In Figure 93, the upper region represents the van der Waals regime (noncontact) and the lower region represents the contact regime, where the tip of the cantilever is said to be in contact with the sample surface according to the DMT contact model (Eq. 8).

Among the conventional integration routines, fixed time-step integration routines (Figure 93) integrate using the interaction model in noncontact from A to F, even though F is already in the contact region, and then use the contact interaction model to integrate from F to G. Adaptive time-step integration routines tend to reduce the time-step close to the boundary. Figure 93 indicates that adaptive time-step routines integrate from A to D with the noncontact interaction model, and then integrate from D to E with the contact model. Adaptive time-step routines still cannot

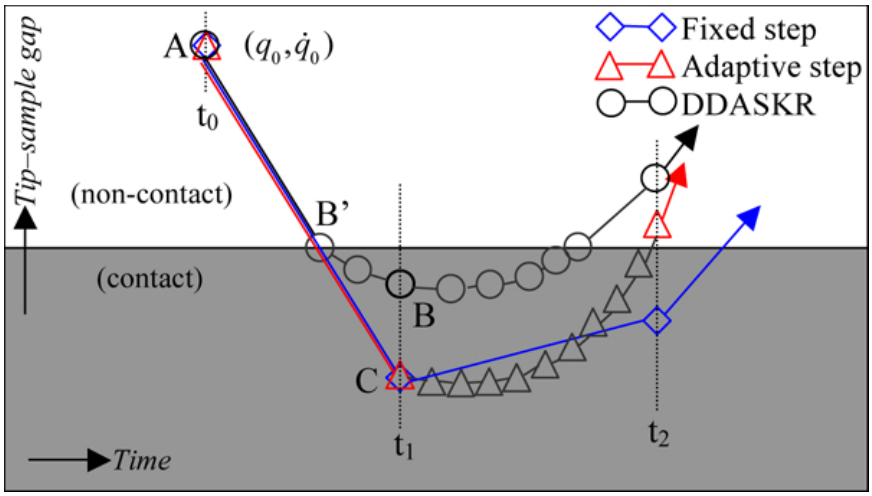

FIG. 93: Comparison between DDASKR and conventional integration routines.

detect the position of the boundary in order to integrate around the boundary. Unless extremely small time-steps are chosen, conventional integration routines cannot accurately integrate the non-smooth interaction forces.

The DDASKR routine uses a root finding algorithm to detect the sample boundary, allowing for easy implementation of non-smooth or discontinuous interaction forces. The DDASKR routine can detect the boundary between two regions (contact and noncontact), and implement the noncontact interaction model to integrate from A to the boundary position B, then apply the contact interaction model to integrate from B to C.

H. Tip-sample geometry convolution

Scanning simulations also include the option to simulate image artifacts due to the finite size of the probe tip. However, we stress that such approximations consider only geometry [18] and do not account for differences in the tip-sample interaction potential itself or any resulting nonconservative interactions. Figure 94 illustrates the actual tip-sample surface h and geometrically convolved surface h^*. For continuous functions h^* may be determined algebraically; however, since the scanning tool includes the option of a sharp discontinuous step, the convolved surface is found by iteration. Not surprisingly, we find that the tip geometry has a substantial effect on the measured topography for sample features on the same order or smaller than the tip radius.

I. Energy outputs

To analyze AFM dynamics (e.g. to understand the meaning of phase contrast), it is often convenient to work with the energy balances and compute the energy coming in and out of the oscillating cantilever through different channels. In order to compute this in the VEDA simulations, we begin with the equations of motion with all terms having units of force ((99) with terms re-arranged).

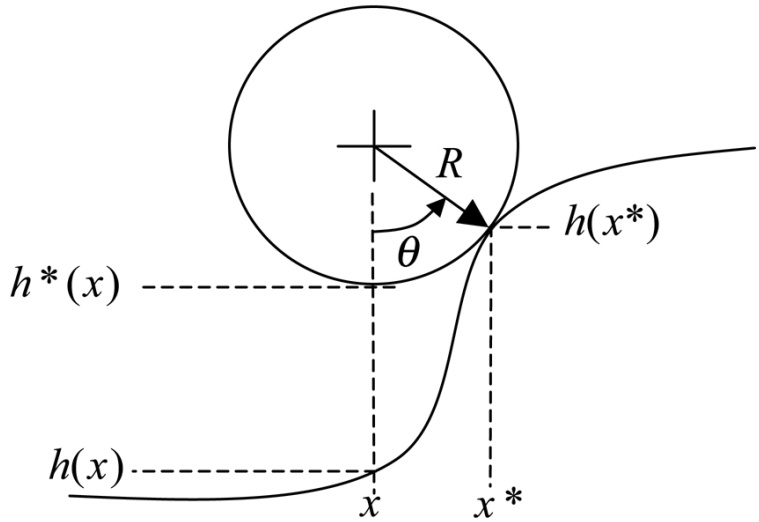

FIG. 94: Geometric approximation for imaging artifacts due to finite probe tip sizes. For the actual sample height, h, at a position x, a convolved sample height, h^*, is observed at position x due to a contact with the sample at position x^*.

$$\frac{k_i\ddot{q}_i}{\omega_i^2} + \frac{k_i\dot{q}_i}{\omega_i Q_i} + k_i q_i = F_{ts}(d,\dot{d}) + F_i(t)$$

then, in order to compute the work done by the different forces, we take a path integral around one deflection cycle

$$\oint \frac{k_i\ddot{q}_i}{\omega_i^2}\cdot dq_i + \oint \frac{k_i\dot{q}_i}{\omega_i Q_i}\cdot dq_i + \oint k_i q_i \cdot dq_i = \oint F_{ts}(d,\dot{d})\cdot dq_i + \oint F_i(t)\cdot dq_i \tag{118}$$

We can parameterize the path integral by time, with T as the period of one drive cycle:

$$\int_0^T \frac{k_i\ddot{q}_i}{\omega_i^2}\dot{q}_i dt + \int_0^T \frac{k_i\dot{q}_i}{\omega_i Q_i}\dot{q}_i dt + \int_0^T k_i q_i \dot{q}_i dt = \int_0^T F_{ts}(d,\dot{d})\dot{q}_i dt + \int_0^T F_i(t)\dot{q}_i dt \tag{119}$$

Or

$$\int_0^T \frac{k_i\ddot{q}_i}{\omega_i^2}\dot{q}_i dt + E_{med,i} + \int_0^T k_i q_i \dot{q}_i dt = \int_0^T F_{ts}(d,\dot{d})\dot{q}_i dt + E_{drive,i}$$

where $E_{med,i} = \int_0^T \frac{k_i\dot{q}_i}{\omega_i Q_i}\dot{q}_i dt$, and $E_{drive,i} = \int_0^T F_i(t)\dot{q}_i dt$. The above can be rewritten as

$$\frac{1}{2}\int_0^T \frac{k_i}{\omega_i^2}\frac{d}{dt}\dot{q}_i^2 dt + E_{med,i} + \frac{1}{2}\int_0^T k_i \frac{d}{dt}q_i^2 dt = \int_0^T F_{ts}(d,\dot{d})\dot{q}_i dt + E_{drive,i}$$

From which we can immediately recognize the kinetic and potential energy terms for each eigenmode:

$$\int_0^T \frac{d}{dt}E_{kin,i}dt + E_{med,i} + \int \frac{d}{dt}E_{pot,i}dt = \int_0^T F_{ts}(d,\dot{d})\dot{q}_i dt + E_{drive,i}$$

Using the fundamental theorem of calculus

$$E_{kin,i}(T) - E_{kin,i}(0) + E_{med,i} + E_{pot,i}(T) - E_{pot,i}(0) = \int_0^T F_{ts}(d,\dot{d})\dot{q}_i dt + E_{drive,i}$$

and renaming

$$\Delta E_{kin,i} + E_{med,i} + \Delta E_{pot,i} = \Delta E_{tot,i} + E_{med,i} = \int_0^T F_{ts}(d,\dot{d})\dot{q}_i dt + E_{drive,i}$$

Then we give the term $E_{prop,i} = \int_0^T F_{ts}(d,\dot{d})\dot{q}_i dt$ the name "energy propagation", which represents the work done by the tip-sample interaction forces on the ith eigenmode. So then the final energy balance for the ith mode is:

$$\Delta E_{tot,i} + E_{med,i} = E_{prop,i} + E_{drive,i}$$

For periodic motion at steady state, the eigenmode will have no overall change in energy during the drive cycle: $\Delta E_{tot,i} = 0$. So merely:

$$E_{med,i} = E_{prop,i} + E_{drive,i} \tag{120}$$

In some cases, a term of interest is the total energy lost due to tip-sample dissipation. This is defined as $E_{ts} = -\int_0^T F_{ts}(d,\dot{d})\dot{d}dt$. For magnetic excitation (and assuming $\dot{Z} \ll 1$), $\dot{d} = \sum \dot{q}_i$ from which we can rewrite $E_{ts} = -\sum_i E_{prop,i}$. Thus it is sometimes convenient to re-write the energy balance as:

$$E_{med,i} + \sum_{j\neq i} E_{prop,j} + E_{ts} = E_{drive,i} \tag{121}$$

But for acoustic mode, $\dot{d} = \dot{y} + \sum \dot{q}_i$, so there is an additional term $E_{bs} = \int_0^T F_{ts}(d,\dot{d})\dot{y}dt$ which we refer to as "base sample work". Then $E_{ts} = -\sum_i E_{prop,i} - E_{bs}$ and the energy balance for acoustic mode is:

$$E_{med,i} + \sum_{j\neq i} E_{prop,j} + E_{ts} + E_{bs} = E_{drive,i} \tag{122}$$

Finally, for comparison to published work it is often useful to plot Anczykowski's formula [96] for energy dissipation in tapping mode, which is:

$$P = \frac{1}{2}\frac{k\omega_0}{Q_{cant}}[A_0 A\sin(\phi) - A^2\frac{\omega}{\omega_0}] \tag{123}$$

Note that this formula was originally described as calculating the tip-sample energy dissipation. In actuality it computes energy lost from the first harmonic, which could also be energy going to other harmonics / eigenmodes. If you actually want to see tip-sample energy dissipation, VEDA computes that directly. Use this formula only for comparison to published work that has used this formula.

Finally, it is also useful to have measures of the conservative stored energy. The typical quantity used in the AFM literature is called the virial. The virial for the ith eigenmode is calculated as follows [32]

$$V_i = \frac{1}{T}\int_0^T F_{ts}(d,\dot{d})q_i(t)dt$$

This is similar to the energy dissipation equation except that the velocity has been replaced by displacement. Also, the 1/T term indicates that this is the time-averaged conservative work over the cycle, as opposed to the dissipation where we are reporting the sum total dissipation over the cycle. In VEDA we numerically calculate the virial for each eigenmode and then report the summed virial for all eigenmodes.

Note: earlier versions of VEDA had a bug which caused the reported value of dissipation to be higher than the actual value by a factor of 2π. This bug was corrected in version 2.1.11 (September 2014)

V. HOW GET HELP

If you encounter a bug, the following options are available:

- Open a support ticket on nanohub (https://nanohub.org/support/ticket/new) which will be directed to the VEDA development team
- Report the issue on the VEDA mailing list (https://engineering.purdue.edu/ECN/mailman/listinfo/veda-list)

If you have a question on how to use a particular tool or feature, the following options are available:

- Ask a question on the VEDA mailing list (https://engineering.purdue.edu/ECN/mailman/listinfo/veda-list)
- Ask the question on the nanohub Questions page https://nanohub.org/resources/veda/questions

If you have an idea for a new tool or feature, the following options are available:

- Suggest the idea on the VEDA mailing list (https://engineering.purdue.edu/ECN/mailman/listinfo/veda-list)
- Suggest the idea on the nanohub Wishlist page: http://nanohub.org/resources/14139/wishlist

VI. CHANGELOG

- Version 2.2.2 May 2021. This version fixed crashes in the Force Viewer and Force Distance curves tools related to viscoelastic material models. A new example was also added to the Force Viewer tool
- Version 2.2.1, April 2021
  - The former "jump mode" tool has been combined with the "force distance curves" tool. The "jump mode" tool really only did a single triggered force curve anyway. The new tool has the option to pick triggered or untriggered curves.
  - The Force Distance Curves tool now chooses the number of simulation time steps more intelligently, and speed should be improved for complex models like Attard's model.
  - Rounded triangle and sine waves are now options for the Force Distance Curves tool
  - The Peak Force Tapping tool is significantly improved and no longer considered in "beta testing".
  - Time history outputs in scanning tools are now labeled with the actual exact X value when the time history started (which in some situations may be slightly different than the requested value).
  - Sample topography is now included in the time history output for scanning tools.
  - Movies of the sample deformation are now available for Attard's model for Force Distance Curves tool, and AM Approach Curve Steady State Solution tool (when time histories are enabled). These movies were previously available only in the Force Viewer tool.
- Version 2.2.0, 9 December 2020. The major development in this version was the introduction of a new tool Amplitude Modulated Approach Curves using a Steady State solution, described in Section III E, which uses a completely different numerical approach than the rest of the VEDA tools. The motivation behind this tool was to allow simulations with the Attard model (section IV B 8), which are prohibitively slow using the normal tools. However, it can be used with any tip-sample interaction model. The assumptions behind this tool make it only valid for high Q environments (air & vaccuum).

VII. ACKNOWLEDGEMENTS

We would like to thank the National Science Foundation's Network for Computational Nanotechnology (NCN) for financial support of VEDA for the first year of development. We would also like to thank Mark Lundstrum, Don and Carol Scifres Distinguished Professor and Director of NCN for his personal interest and support of this work. We are grateful to Prof. Ron Reifenberger and his students for their interest and fruitful discussions which aided in the development of VEDA. Finally we would like to thank the nanoHUB development team for their assistance and Prof. Linda Petzold et al. for making available as a shared resource their DDASKR integration routine[94].

VIII. APPENDIX: INPUT PARAMETERS AND OPTIONS

Here we provide a reference for all input parameters and options VEDA simulations. All parameters have unique definitions but may appear in multiple tools. Most parameters are introduced in Section IV.

Attractive force gradient: The slope of the attractive force. This is used only in the linear attractive/repulsive mode.

Auto Calculate intermolecular distance?: If this box is checked, the intermolecular distance parameter a_0 used in the in DMT and DMT+DLVO models will be automatically calculated from the van der Waals Adhesion force, the tip radius, and the Hamaker constant. If this box is unchecked the van der Waals Adhesion force will be calculated from the intermolecular distance, the tip radius, and the Hamaker constant. In either case, the relevant relation is $F_{ad} = \frac{HR}{6d^2}$.

Auto calculate alpha? If this box is checked, the dispersion (section IV C 3) for an Euler-Bernoulli beam are calculated from the given tip mass. When it is unchecked, you can enter your own values. Use the default unless you are certain you know what you are doing.

Auto calculate k_i $(i > 1)$?: If this box is checked, the stiffnesses for the higher eigenmodes will be auto calculated from the stiffness for the 1st eigenmode, based on the theoretical formulas for a rectangular cantilever (taking into account the tip mass). If this box is not checked, you must enter a stiffness for each mode.

Auto calculate Slope calibration?: If this box is checked, the slope calibrations for higher eigenmodes will be auto calculated based on the theoretical formulas for rectangular cantilevers (including tip mass). If this box is unchecked, you need to enter slope calibrations for each eigenmode. (Note: most users should leave this box checked).

Choose amplitude ratio(s): The amplitude ratio(s) A_1/A_0 at which to save and plot time history data (deflection, tip-sample force, eigenmodes, phase space). A_1 is the amplitude of the primary harmonic of the excitation frequency and A_0 is the unconstrained amplitude (far from the sample). These A_1/A_0 values must be comma-separated, and the number of values entered must be equal to the number of time histories to collect. This option is only available if the *Include time histories* box is checked.

Choose frequency scheme: Choose between a single frequency excitation (conventional) and two frequency excitation (bimodal).

Choose X-axis variable: Choose whether to plot simulation and time-history data against Z-distance or against amplitude ratio (A_1/A_0)

Choose excitation source: The method used in vibrating the cantilever. Excitation choices include acoustic (base) excitation and magnetic excitation as discussed in Section IV C 7.

Choose higher harmonics: The higher harmonics of the drive frequency for which to plot the amplitude and phase. These higher harmonics must be comma-separated. The number of comma-separated values must be equal to the number of higher harmonics requested.

Critical gap, D_0 (nm): The gap at which the hysteretic capillary force goes to zero. This item is used only with the capillary forces.

Debye length (mum): The Debye length of the ionic fluid within which the dAFM experiment is performed. For deionized water, this value is $1\ \mu m$ [43]. This parameter is only used with the DMT (Derjaguin-Müller-Toporov) [42] + DLVO (Derjaguin-Landau-Verwey-Overbeek) [97] tip-sample interaction model.

Deflection points per cycle: The number of points to be plotted in each time-history graph. The default of 1000 should be sufficient for most simulations, however, this can be verified after running a simulation by viewing the time history data (See Example 1). If the tip-sample interaction history is not acceptably smooth, the user should increase this parameter.

Dielectric constant: The dielectric constant of the solution in which the cantilever is immersed. This parameter is only used with the DMT (Derjaguin-Müller-Toporov) [42] + DLVO (Derjaguin-Landau-Verwey-Overbeek) [97] tip-sample interaction model.

Direct Input of Base Amp / Mag Force : When this box is unchecked, the base amplitude (acoustic drive) or modal forces (other drives) are calculated based on the cantilever parameters and unconstrained amplitudes you entered. When this box is checked, you can directly enter the base amplitude or modal force. Don't use this unless you are sure you know what you are doing.

Drive Freq (kHz): Excitation or drive frequency. Normally, this frequency is identical to the first natural frequency of the cantilever in conventional setups.

Energy dissipated, dE (eV): This is the energy loss during one oscillation cycle using the capillary force model.

Example tip-sample interaction properties This drop down box will automatically populate the tip-sample interaction properties with example properties.

Excitation scheme: (used only in the frequency sweep tool) Choose Linear Ramp Frequency Sweep to generate a continuously changing frequency. Choose Stair Step Frequency Sweep to break the frequency range up into a series of discrete frequency points, one per output point. For a large number of output points, these two are

approximately equivalent. The stairstep is most appropriate for comparing to the results of an experiment that uses a stairstep excitation. The linear ramp is most appropriate for comparing to an analytical theory.

f **(kHz):** Natural frequency of the chosen cantilever eigenmode.

f_1 **(kHz):** Natural frequency cantilever's fundamental eigenmode.

f_i **(kHz):** Cantilever natural frequencies (eigenmode frequencies). Each comma-separated natural frequency corresponds to a cantilever eigenmode (in order). The number of comma-separated values must equal the number of eigenmodes.

f_d **(kHz):** Excitation or drive frequency. Normally, this frequency is identical to the first natural frequency of the cantilever in conventional setups. For a two frequency (bimodal) simulation, enter in two comma delimited values for the first and second (higher frequency) excitations.

f_{dstart} **(kHz):** The starting excitation (drive) frequency of a frequency sweep (used only in the Frequency Sweep tool).

f_{dstop} **(kHz):** The end frequency of the frequency sweep. Note, for sweep up entering $f_{dstart} < fd_{stop}$ and for a sweep down enter $fd_{start} > fd_{stop}$.

Feature height (nm): The height of the feature can be either negative or positive corresponding to a protrusion or depression in the substrate. For the sinusoid, this parameter refers to the peak-to-peak amplitude.

Final Z separation (nm): The final distance from the substrate to the cantilever base. This parameter is only available when the *Specify Z range* box is checked. In order to run a retraction simulation, enter values for $Z_{initial}$ and Z_{final} such that $Z_{initial} < Z_{final}$.

Hamaker constant (J): The Hamaker constant of the tip-sample interaction. The Hamaker constant is used to predict attractive van der Waals forces between the tip and the sample. This parameter depends on the tip material, the sample material, and the surrounding media [43]. This parameter is only used with the DMT contact (Derjaguin-Müller-Toporov) [42] and DLVO+DMT tip-sample interaction models.

Impact: Check the box to include one or more impact Poincare plots in the output. A Poincare plot which plots state-space variables of the cantilever vibration against each other. An impact plot contains data points which are generated each time the tip and sample just reach contact.

Include capillary forces?: Check this box to include non-conservative capillary forces according to Kober et al.'s model [54]. Enter values for *Critical gap* and *Energy dissipated* to use this feature.

Include geometric convolution: Check the box to include effects of the tip-sample geometry convolution.

Include time histories: Check the box if you would like to generate time-history plots (deflection, tip-sample force, eigenmodes, phase space) at specific amplitude ratios. Normally the tools plot peak force values and extract amplitudes and phase directly from the simulated data. Users may wish to access the time history data as well. Using this option, the user is allowed to plot a sample of the cantilever deflection and tip-sample interaction histories and eigenmode responses. Enabling this feature requires the *number of cycles* and the desired *[Choose] amplitude ratio(s)*.

Include visco-elastic forces?: To include non-conservative, viscoelastic tip-sample interaction forces choose the desired constitutive model from the drop-down list. Choices include Kelvin-Voigt, Maxwell, etc. Each model requires different properties, which are listed immediately below this box.

Initial Z separation (nm): The initial Z displacement from the substrate to the cantilever base. This parameter is only available when the *Specify Z range* box is checked. In order to run a retraction simulation, enter values for $Z_{initial}$ and Z_{final} such that $Z_{initial} < Z_{final}$.

Integral gain: This controller setting determines the Z displacement proportional to the integral or cumulative amplitude error, which eliminates steady state errors (Eq. 117). A suitable value for this parameter may vary according to the cantilever, tip-sample force properties, and lock-in time constant.

Intermolecular distance (nm): The intermolecular distance of the sample material. This parameter is only used with the DMT contact (Derjaguin-Müller-Toporov) [42] and DMT+DLVO tip-sample interaction models.

Jump Feedback level (nm): The observed cantilever deflection at which the Z piezo will reverse.

k **(N/m):** Cantilever stiffness of the fundamental eigenmode.

k_i **(N/m):** Cantilever eigenmode stiffness. Each comma-separated value for stiffness corresponds to a cantilever eigenmode (in order). The number of comma-separated values must equal the number of eigenmodes.

Length of feature (nm): This refers to the length of the base of the geometrical feature being imaged by the AFM.

Length of trapezoid top (nm): This parameter is enabled when the user selects the trapezoid feature.

Lock-in time constant (mus): This parameter determines the nearest integer number of cycles over which the amplitude error signal is computed by Fourier transform. This parameter is included to mimic the action of a lock-in amplifier with most commercial instruments.

Membrane thickness (nm): The thickness of a membrane loosely-bound to a stiff substrate. This parameter is only used with the Chadwick tip-sample interaction model.

Nat Freq (kHz): Cantilever natural frequency of the first eigenmode.

Number of cycles: The number of periods for which to save and plot time-history data (deflection, tip-sample force, eigenmodes, phase space). Although, it should be noted that the number of cycles included in the time history sample will affect computation time. This option is only available if the "Include sample of time histories" box is checked.

Number of eigenmodes: The number of cantilever eigenmodes to be included in the simulation.

Number of higher harmonics: The number of higher harmonics of the first natural frequency for which to plot the amplitude and phase. This option is only available when the "Plot a higher harmonic?" box is checked.

Number of Poincare plots: Enter the number of desired Poincare sections. For each Poincare section, a unique abscissa and ordinate set of state-space variables should be chosen.

Number of points plotted: This is the number of points contained in each plot. This values of this parameter may be increased if the user is interested in abrupt features in the results.

Number of time histories: The number of sets of time history plots to generate corresponding to specified amplitude ratios A_1/A_0. This option is only available if the *Include sample of time histories* box is checked.

Output plots: This is a group of options that is given in some of the advanced tools. This gives the user the option of disabling some of the standard output plots. Disabling unwanted plots can slightly speed up computation time. Most users will not need this option and can leave all of the boxes checked.

Plot a higher harmonic?: Check the box if you would like to plot the amplitude and phase of higher harmonics of the drive frequency.

Poincare sections In some of the advanced tools, the user is given the option of generating Poincare plots. These are turned off by default. Two types of Poincare plots are available: stroboscopic (one point per drive cycle) and impact (one point every time the tip impacts the sample). For each plot, the user must enter the state-space variables for the axes. Odd numbers are the displacements of each eigenmode (1 = first eigenmode, 3 = second eigenmode, etc) while even numbers are the velocities of each eigenmode. Entering 0 for x-axis will plot total tip-sample displacement and 0 for y-axis will plot total relative tip-sample velocity.

Poisson's ratio of the sample: The Poisson's ratio of the sample. This parameter is used in all tip-sample interaction models except for the two linear contact models. The Poisson's ratio is a material property that relates a uni-axial strain induced in a specific direction due to a stress applied in the orthogonal direction.

Poisson's ratio of the tip: The Poisson's ratio of the cantilever tip material. This parameter is used in all tip-sample interaction models except for the two linear contact models.

Proportional gain: This controller setting determines the Z displacement proportional to the amplitude error signal (Eq. 4). A suitable value for this parameter may vary according to the cantilever, tip-sample force properties, and *lock-in time constant*.

Q: The quality factor of the fundamental eigenmode. The quality factor is a measure of the "sharpness" of the resonance peak.

Q_i: Cantilever eigenmode quality factor. Each comma-separated quality factor corresponds to a cantilever eigenmode (in order). The number of comma-separated values must equal the number of eigenmodes. In theory, if the user knows the quality factor for the first eigenmode they can predict higher modes depending on the source of dissipation, however, this is not always straightforward. For information on how to approximate the quality factor theoretically of higher eigenmodes, please see [98]. The quality factors of different eigenmodes can be measured easily from either the thermal spectrum or tuning curves of the cantilever. The quality factor of the cantilever eigenmode is an indication of the damping acting on the probe. Originally, the quality factor was defined as the gain at resonance. However, many authors have chosen to adapt the approximation $Q \approx 1/2\zeta$, which is done in VEDA.

Sample stiffness (N/m): The effective stiffness of the tip-sample contact. This parameter is only used with the Linear contact tip-sample interaction model. The sample stiffness is used to determine the tip-sample interaction force when the cantilever tip and the sample are in contact.

Sample viscosity (Pa*cdot* s): The viscosity of the sample. A nonzero sample viscosity is the only cause for any energy dissipation considered by this simulation tool. This parameter can be used with all tip-sample interaction models. The non-conservative, viscoelastic, tip-sample interactions are predicted by the Kelvin-Voigt model. To enable this interaction, check the 'Include visco-elastic forces' check box.

Sampling frequency: The sampling frequency determines the number of points of tip oscillation waveform computed per cycle of oscillation.

Scan lines per second: The rate at which the AFM moves across the sample. *Lines per second* $\cdot$ *scan Length* $=$ *scan velocity*.

Scan size (length) (nm): The entire length of the substrate, including the geometric feature.

Select a geometric feature: Choose the geometry of the feature to be scanned using the AFM. Options include a step change in height (a rectangle), a trapezoid, a sinusoid, or a cylinder (half-circle).

Set point ratio: The ratio of the first harmonic of the cantilever deflection signal while tapping to the unconstrained amplitude.

Signal/Noise ratio (dB): Enter the ratio of the initial cantilever amplitude to noise amplitude in dB ($S/N\ (dB)\ =\ 20 \cdot \log_{10}(S/N)$).

Slope Calibration 2 - Slope Calibration n: Comma-separated values for the slope calibration (Chi) starting with the 2nd eigenmode.

Specify material properties: Check the box to specify separate material properties of the feature (which can be different than the rest of the substrate (sample).

Specify Z range: Check the box if you would like to specify the initial and final Z displacements of the base. In order to run a retraction simulation, enter values for $Z_{initial}$ and Z_{final} such that $Z_{initial} < Z_{final}$. Enabling this feature requires an *initial Z displacement* and a *final Z displacement*. Leave the box unchecked to have VEDA guess a starting and final Z displacement (the guess is usually fairly good for most tip-sample interaction models, but may not be good for models with long range forces such as DLVO)

Stroboscopic: Check the box to include 1 or more stroboscopic Poincare plots in the output. A Poincare plot which plots state-space variables of the cantilever vibration against each other. A stroboscopic plot contains data points which are generated at regular periods in the cantilever oscillations.

Surface charge density (sample) (C/m^2): The surface charge density of the sample. This parameter is only used with the DMT (Derjaguin-Müller-Toporov) [42] + DLVO (Derjaguin-Landau-Verwey-Overbeek) [97] tip-sample interaction model.

Surface charge density (tip) (C/m^2): The surface charge density of the cantilever tip. This parameter is only used with the DMT (Derjaguin-Müller-Toporov) [42] + DLVO (Derjaguin-Landau-Verwey-Overbeek) [97] tip-sample interaction model.

Sweep time (s): The time duration of the frequency sweep from the starting frequency to the stopping frequency (used only in the Frequency Sweep tool).

Tip mass: The mass of the cantilever contact tip as a fraction of the rectangular beam mass (without the tip).

Tip radius (nm): The radius of the cantilever tip which contacts the sample. This parameter is used in all tip-sample interaction models except the two linear models. The manufacturer typically specifies the radius of the probe tip of the cantilever.

Tip-sample interaction model: The model used to simulate the interaction forces between the cantilever tip and the sample. Several models are available: Linear contact, Linear attractive/Repulsive contact, Hertz contact, DMT contact (Derjaguin-Müller-Toporov) [42], DMT + DLVO (Derjaguin-Landau-Verwey-Overbeek) [97] interactions, JKR contact, and Chadwick contact. See section IV A for discussion of the different models.

Unconstrained Amplitude (nm): The unconstrained amplitude (far from the sample) of the photodiode deflection signal $u_p(t)$ for the *primary* drive (excitation) frequency. In the case of the single-frequency (conventional), this is the only unconstrained amplitude. In the case of two-frequency (bimodal), a second unconstrained amplitude is specified.

Unconstrained Amplitude (2nd drive frq) (nm): (For two-frequency (bimodal) schemes only) The unconstrained amplitude (far from the sample) photodiode deflection signal $u_p(t)$ for the *secondary* drive (excitation) frequency. Used only in two-frequency (bimodal) schemes.

Unconstrained Amp. @ Nat. Freq.(nm): (Used only in the frequency sweep tool) The unconstrained amplitude (far from the sample) photodiode deflection signal $u_p(t)$ when driven at the first natural frequency (NOT the start frequency of the frequency sweep).

Use setpoint: (frequency sweep only) If this box is unchecked, you need to enter a Z displacement for the frequency sweep. If this box is checked, then VEDA will pick a Z displacement based on approaching to a particular setpoint. Notes: 1) the setpoint ratio is calculated based on the first natural frequency, regardless of the starting frequency, and 2) for some combinations of operating conditions, the program may not be able to find a Z displacement that satisfies the setpoint. This may happen if the cantilever snaps-in to the surface. In this case you will need to set the Z displacement manually.

van der Waals Adhesion force (nN): The adhesion force is the force that is required to remove the tip of the cantilever from the sample surface. It is also known as the "pull-off" force. This positive quantity can be found experimentally from a static force-distance curve:

$$F_{ad} = |k_c w^*|$$

where, k_c is the static bending stiffness of the cantilever, and w^* is the deflection of the tip at the "pull-off" location as the cantilever is withdrawn from the surface. The adhesion force can also be calculated from the surface energy γ, which is known for many tip-sample material combinations [5, 43] :

$$F_{ad} = 4\pi R_{tip}\gamma$$

where R_{tip} is the radius of the probe tip.

X-axis: Concerning the Poincare plots, these are comma-separated values representing the abscissa variable for each of the plots. For the tip-sample gap, choose 0. Otherwise the odd numbers correspond to the deflections of each of the eigenmodes of the cantilever. For instance, 1 corresponds to q_1, 3 corresponds to q_2, and 5 corresponds to q_3.

Y-axis: Concerning the Poincare plots, these are comma-separated values representing the ordinate variable for each of the plots. For the derivative of the tip-sample gap with respect to time, choose 0. Otherwise the even numbers correspond to the velocities of each of the eigenmodes of the cantilever. For instance, 2 corresponds to q_1', 4 corresponds to q_2', and 6 corresponds to q_3'.

Young's modulus of sample (GPa): The elastic modulus of the sample. This parameter is used in all tip-sample interaction models except the linear contact model. The Young's modulus (or elastic modulus) of the sample is material property that will affect the magnitude of the contact forces the most. The Young's modulus of the tip is usually much larger than that of the sample, making the Young's modulus of the sample the critical parameter in determining contact stiffness.

Young's modulus of tip (GPa): The elastic modulus of the cantilever tip material (for silicon (Si), $E \approx 130$ GPa). This parameter is used in all tip-sample interaction models except Linear contact. The Young's modulus (or elastic modulus) of the is material property that will affect the magnitude of the contact forces, however, the Young's modulus of the tip is typically much larger than that of the sample, making the Young's modulus of the sample the critical parameter.

Z approach velocity (nm/s): The Z approach velocity refers to the average speed at which the base of the micro-cantilever approaches the sample. More concisely $|\dot{Z}(t)|$. A reasonable approximation of this parameter in the experimental setup is found simply by taking the distance of approach (the difference between the and dividing by the time of approach. An appropriate approach speed has much to do the with settling time of the probe $\tau = \omega/2Q$ and the lock-in time constant.

Z displacement (nm): The gap between the sample and the base of the cantilever. If the base is excited (acoustic excitation) then Z displacement refers to the *average* gap between the base of the cantilever and the sample. See the schematic in Section II.

IX. APPENDIX: INSTALLING AND USING VEDA ON YOUR LOCAL MACHINE

VEDA has been designed to run in your web browser through www.nanohub.org, a website run by the Network for Computational Nanotechnology. Some advanced users, however, may wish to install VEDA on their local machines. The advantages of this are: 1) ability to run VEDA without Internet access (at a conference perhaps), 2) ability to load and save input and output files, 3) ability to perform multiple batch runs (e.g. several of the author's publications have included data from several hundred runs that were done in a batch process). Also, VEDA is open source so some users may wish to make custom modifications

The following is an instruction on how to install and use VEDA on your local machine.

A. Installing Rappture on your machine

Step 1) VEDA requires the Rappture libraries, which are designed for Intel x86 Linux (and 32bit PPC or Intel Mac OS X). Therefore the full version VEDA will only run on Linux or MacOS and cannot be run on Windows. Some limited functionality is available on Windows, but it requires some extra effort. See Appendix X for details. The remainder of this chapter will focus on Linux or MacOS.

Go to https://nanohub.org/infrastructure/rappture/wiki/Downloads and follow the provided installation instructions to install Rappture on your machine (recommend to use the binary distribution, only download the source code distribution if the binaries do not work for you).

B. Installing VEDA on your local machine: pre-compiled binaries

Once rappture is installed, now you can install VEDA. There are two options. The easy way is to use the pre-compiled binaries. These are provided for only for Intel x86 Linux. They are statically linked, so they should work with almost any Linux distribution. If the pre-compiled binaries don't work, see the next section for compilation instructions. Follow these steps:

- To download, go to https://nanohub.org/resources/veda, click on "supporting documents" (not download - that takes you to the source code), and download veda-binaries.zip (or a similarly named file).
- Unzip in a convenient location
- Add the VEDA bin/ directory to your path.
- To run the GUIs, change to the rappture/ directory. Each tool has a separate sub-directory. Switch to the subdirectory of the tool you want to run (e.g. fzcurves) and run the command 'rappture' (assuming that the rappture binaries got added to your path in the previous step). Rappture will find the tool.xml file in that directory and load it. You can then enter your parameters exactly as on the website.

- Alternatively, type 'rappture -tool FILENAME', where FILENAME is the complete path to one of the tool.xml files (e.g. 'rappture -tool /apps/veda/rappture/adac/tool.xml')

C. Installing VEDA on your local machine: Compiling from source

Read this section only if you can't use the pre-compiled binaries (described above) for some reason.

1) You will need a FORTRAN 90 compiler. Intel FORTRAN and gfortran (v 4.2 or later) are fully tested and supported. g95 should probably work as well, but we will not guarantee it to work. Most linux distributions will have a gfortran package available (e.g. "apt-get install gfortran") but if not download it from http://gcc.gnu.org/fortran/ . GNU make is also required. Also you'll need development versions of a few libraries if you don't typically compile programs on your machine (libstdc++6-4.3-dev, libexpat1-dev, zlib1g-dev)

2) Download the latest VEDA source code from https://nanohub.org/resources/adac (the download link is fairly small, and is hidden right under the "launch tool" button). Uncompress the file to some convenient directory on your machine.

- Alternatively, if you have subversion, you can check out the sources directly with "svn checkout https://nanohub.org/tools/veda/svn/trunk veda" (this will put the sources in a folder called "veda"). The advantage of this method is that you can quickly update when newer versions are released with just "svn update", instead of downloading and unzipping a file every time.

3) Within the VEDA directory, change to the src/ directory and execute 'make F77=gfortran install" if using gfortran, or 'make F77=g95 install' if using g95, or just 'make install' if using Intel fortran. This will compile the binaries and install them in the bin/ directory.

D. Using VEDA on your local machine

First, let us introduce the concept of how VEDA interacts with the rappture libraries. The data flow as used on www.nanohub.org is like this:

1) The tool.xml specifies all GUI elements 2) rappture reads the tool.xml file, displays the GUI, takes your user input, and then generates a driver.xml file. driver.xml has the exact same structure as tool.xml, except that specific values are filled in for each parameter instead of the default values. 3) The driver.xml file is then sent to the az_ddaskr executable. This program reads the the driver.xml, performs the actual computation, and then outputs a run.xml file. 4) rappture reads the run.xml file and displays the data. This is illustrated graphically in Figure 95.

You can follow this process exactly on your local machine if you want. Simply change directories to the directory that contains the tool you want and type "rappture". The GUI will automatically come up and display that tool. Note that the directories all have abbreviated names. The tools associated with each directory are listed in Table VII.

Directory	Tool
adac	Amplitude Modulated Approach Curves (advanced)
dac	Amplitude Modulated Approach Curves (basic)
fixedpoint	Single Point
forceViewer	Tip-sample force viewer
fzcurves	Force Distance Curves
jump	Jump Mode (i.e. triggered F-z curves)
scan_contact	Contact Mode Scanning
scanbasic	Amplitude Modulated Scanning (basic)
scanning	Amplitude Modulated Scanning (advanced)
freqsweep	Frequency Sweep (basic)
freqadv	Frequency Sweep (advanced)
fmac	Frequency Modulated Approach Curves
fmscan	Frequency Modulated Scanning
forcemod	Force Modulation Scanning (beta testing)
peakforcebasic	Peak Force Tapping (beta testing)

TABLE VII: The directory names under rappture/ and the corresponding tool names

But you have more options. For example, you can

A) Save the run.xml file and view it later. If you do multiple runs, you'll notice that a bunch of files will be created with names like run1271692464.xml. You can pick out the ones you want, rename them to something more memorable, (e.g. run-carbonnanotube1.xml) and move to another directory if you want. Then to see the file later, using rappture's rerun comment (e.g. "rerun run-carbonnanotube1.xml"). This just lets you view the data, you can't use it as a starting point for future simulations. That is, if you press Input to go back to the parameters list, and type in some new parameters, and then hit Simulate, it still only shows the original computation.

Note: the rappture version rappture-Linux-i686-20081010 had a couple of significant bugs in the rerun program. Make sure that you use rappture-Linux-i686-20091009.tar.gz or later

B) Save the driver.xml file and use it as a starting point for future simulations. Normally rappture deletes the driver.xml files after the simulation is finished. There are three options to get a driver file. First, if you hit "Abort" while a simulation is running, rappture won't delete the driver file. Look in the directory for a file named something like driver14516.xml. You can later restart that simulation using "rappture -tool driver14516.xml". Second, you can take an existing driver.xml file and edit it in a text editor (replace the values between the <current></current> tags) Finally, there is a little script that will create a driver file from a run file. It is in the VEDA src directory and the usage is "run_to_driver.pl < run1271692464.xml > driver1.xml" (you need to have Perl installed for this).

C) View the results without using the rappture GUI. The run.xml is, as the name implies, an XML file, so any standard XML parser can read the data file. Example matlab scripts are provided in the bin/ directory (you will need the "sed" package installed for this script). You could come up with a similar program for Java or C++ or what have you.

D) Once you have a driver file that has the parameters you like, you don't actually need the GUI anymore. For example, if you have a file driver1.xml, you can run "az_ddaskr driver1.xml" and it will run the computation and generate a run file. You can later view the run file with "rerun" if you wish.

E. Running batch simulation / parameter studies

Running batch simulations is one option that is available when you run VEDA on your local machine that is not available on the nanohub website.

1. *Running multiple jobs in serial on a single machine.*

The file param-explore.pl in the bin/ directory automates the process of generating and running multiple jobs. (you need to have Perl installed for this to work).

It starts from a template file you provide, and then generates and runs them one at a time as illustrated in Figure 96. This is suitable for running multiple jobs on a single machine one at a time.

You will need to generate two files. The first is the runs file. This should be a text file with each line containing the full parameter set for one run. Each line should be a comma separated list of parameter=value. For example, to make 4 runs with different values of two parameters you might use this file:

PARAM_E = 100, PARAM_nu = 10

PARAM_E = 100, PARAM_nu = 100

PARAM_E = 10, PARAM_nu = 10

PARAM_E = 10, PARAM_nu = 100

The names of the parameters are completely arbitrary. They can be any name you want. The use of the prefix PARAM is not necessary, but recommended to make it easy to recognize what is a parameter in your template file.

The second file that you need is the template file is an xml driver file except that some of the inputs have been replaced by tags. For example, there is a line in the driver file that normally looks something like this

```
<number id="Etip">
<about>
<label> Young's modulus of tip (GPa)</label>
</description> </about>
<default>130</default>
<current>90</current>
</number>
```

You want to edit this file and replace the number inside the <current> line with your tag from the runs file. For example:

```
<number id="Etip">
<about>
```

<label> Young's modulus of tip (GPa)</label>

</description> </about>

<default>130</default>

<current>PARAM_E</current>

</number>

As the param-explore.pl file goes through the runs, it will replace PARAM_E in this file with the values that you have given it in the runs file. Note, this is a literal text substitution. Make sure that the tag names you pick don't occur anywhere else in the file. E.g. If you pick something like 'o' for your parameter instead of 'PARAM_E', the param-explore.pl would replace every 'o' with a number, e.g.

<number id="Etip">

<ab100ut>

<label> Y100ung's m100dulus 100f tip (GPa)</label>

</description> </ab100ut>

<default>130</default>

<current>100</current>

</number>

which is probably not what you want. Hence the suggestion to use a unique prefix like PARAM_. Also, the script will do simple math on any line where a replacement is made. e.g. if TAG_Z=10, then <current>TAG_Z + 10</current> would be replaced with <current>20</current>.

Once you have these two files, just type

param-explore.pl runs.txt template.xml ~/bin/az_ddaskr

replacing 'runs.txt' with the name of your runs file, template.xml with the name of your template file, and replacing ~/bin/az_ddaskr with the pathname of where you installed the VEDA executable. This will then run all of the files, and generate sequentially numbered output files: output1.out, output2.out, output3.out, etc. Once they have all been generated, you can post-process them using the GUI (e.g. "rerun output*"), or by reading them into matlab (use the rappture_reader_multi.m matlab script in the bin/ directory).

2. *Running multiple jobs in parallel on several machines*

For multiple machines in parallel, follow the instructions above, with one exception. We want to generate all of the driver.xml files on one machine, but we don't want to run yet. Therefore, in the param-explore.pl script, instead of the VEDA executable, give it a dummy executable. For example

param-explore.pl runs.txt template.xml touch

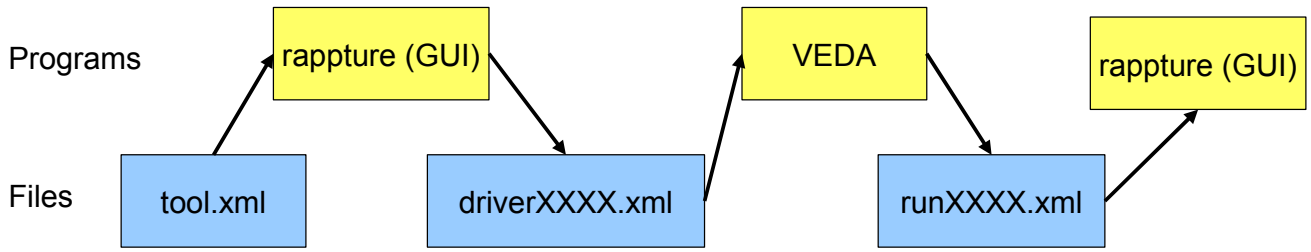

FIG. 95: The flow of data between the various files and programs.

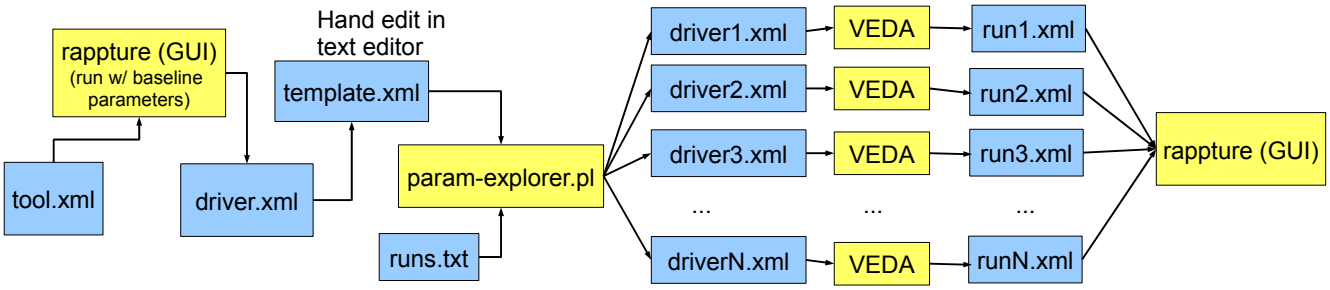

FIG. 96: The flow of data when used batch simulations. The multiple VEDA runs may optionally be managed by a batch queueing system (such as Condor or PBS)

param-explore will then generate all of the driver.xml files, but not actually run them. You can then use any standard batch system (e.g. Condor from http://www.cs.wisc.edu/condor/) to execute VEDA on the resulting driver.xml files. VEDA is statically linked against the rappture libraries, so you need only copy the az_ddaskr file to the compute nodes, you do not need to install rappture on them.

X. APPENDIX: USING VEDA ON A WINDOWS MACHINE

This appendix details the steps necessary to run VEDA on a Windows machine. Currently, the GUI features are not available, so all input is by hand editing the xml input files, and all post-processing has to be by reading the results files into another program such as Matlab or Excel.

A. Compiling the rappture libraries on Windows

We have successfully compiled rappture on windows using the Cygwin package. It may be possible to use other compilers, but we have not tried them. Below is how we did it (note that these instructions are written assuming some knowledge of how to compile programs)

- Install Cygwin from www.cygwin.com

- In addition to the basic install, select the following packages: binutils, expat, libexpat-devel, gcc-core, gcc-fortran, gcc-g++, libncurses-devel, make, time, zlib-devel (the installer will automatically select any dependencies).
- Download the latest source code from https://nanohub.org/infrastructure/rappture/wiki/Downloads (get just the rappture-src package, we have not yet tested the rappture-runtime package).
- Ignore the compilation instructions on the rappture web page. we won't be building the full package, just the libraries.
- open a cygwin bash shell window and change to the directory where you downloaded the rappture archive. Unzip it and change into to the directory
- you'll need to make a few hacks to the 'configure' script. Specifically, replace the line "#define HAVE_GETTIMEOFDAY 1" with "#undef HAVE_GETTIMEOFDAY".
- Then execute the following commands:
  - export CFLAGS=-D_WIN32
  - ./configure –disable-gui –without-tclsh –without-ffmpeg
  - cd src/core
  - make
  - cd ../core2/
  - make
  - cd ..
  - mkdir /apps/rappture/lib
  - cp core/librappture.a core2/librappture2.a /apps/rappture/lib

We got errors such as "make: o: Command not found", and "recipe for target 'librappture' failed'. These can be ignored as long as the librappture.a and librappture2.a files are created.

B. Compiling VEDA on Windows

The directions for compiling VEDA on Linux in section IX C apply with the following additional notes:

- We recommend you install the cygwin 'gcc-fortran' package, which installs gfortran. We are not able to get g95 compiler to work with cygwin. The Intel fortran compiler has not yet been tested on cygwin.

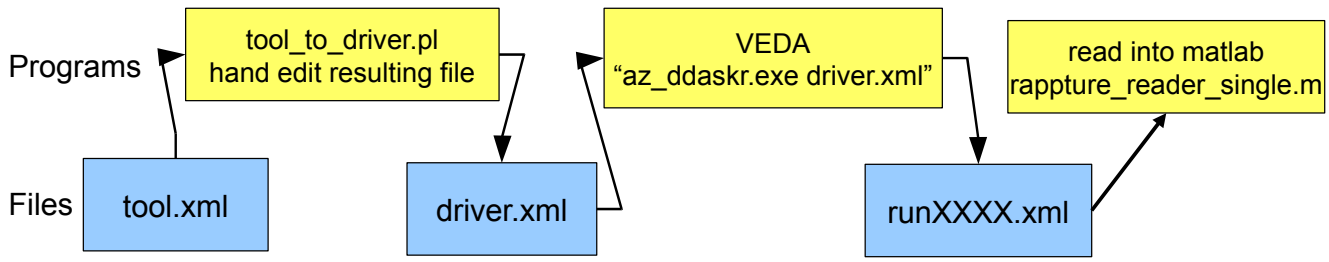

FIG. 97: The data flow when using VEDA on Windows without the GUI. Compare to figure 95.

C. Using VEDA on Windows

Using VEDA on Windows follows most of the general principles for running it on Linux, as described in sectiosn IX D and IX E. The difference is that the GUI is not available to you. Therefore, you'll need to make three changes

1. As described above, normally the rappture GUI takes a tool.xml file and generates a driver.xml. Since the GUI is not available, you will need to do this yourself. Use the tool_to_driver.pl file found in the bin/ directory. (i.e. "tool_to_driver.pl < tool.xml > driver.xml". This will generate a driver file will all of the parameters set to their default value. You will need Perl installed to make this work (can be installed from www.perl.org)

2. To change values from their defaults, you will need to hand edit the driver.xml file. If you are familar with the GUI layout of the tools, it should be easy to locate the various settings within the driver.xml file by searching for key words. You will want to edit the values in the <current> tags (not the <default> tag).

3. You will not be able to use the GUI to post-process your results. We recommend reading the values into matlab using the rappture_reader_single.m file located in the bin/ directory.

This data flow is illustrated schematically in Figure 97.

[1] Binnig, G., Quate, C. F., and Gerber, C. (1986) Atomic force microscope. *Phys. Rev. Lett. 56*, 930–933. I

[2] Martin, Y., Williams, C., and Wickramasinghe, H. (1987) Atomic force microscope force mapping and profiling on a sub 100-a scale. *Appl. Phys. 61*, 4723–4729. I

[3] Albrecht, T., Grutter, P., Horne, D., and Rugar, D. (1991) Frequency-modulation detection using high-q cantilevers for enhanced force microscope sensitivity. *Appl. Phys. 69*, 668–673. I

[4] Garcia, R. and Perez, R. (2002) Dynamic atomic force microscopy methods. *Surf. Sci. Rep. 47*, 197–301. I

[5] Garcia, R. and San Paulo, A. (1999) Attractive and repulsive tip-sample interaction regimes in tapping-mode atomic force microscopy. *Phys. Rev. B 60*, 4961–4967. III A 1, III A 1, III A 2, VIII

[6] Hu, S. Q. and Raman, A. (2006) Chaos in atomic force microscopy. *Phys. Rev. Lett. 96*, 036107.

[7] Lee, S. I., Howell, S. W., Raman, A., and Reifenberger, R. (2002) Nonlinear dynamics of microcantilevers in tapping mode atomic force microscopy: A comparison between theory and experiment. *Phys. Rev. B 66*, 115409. III F 1

[8] Rutzel, S., Lee, S. I., and Raman, A. (2003) Nonlinear dynamics of atomic-force-microscope probes driven in lennard-jones potentials. *Proc. Roy. Soc. A 459*, 1925–1948. I

[9] Garcia, R. and San Paulo, A. (2000) Dynamics of a vibrating tip near or in intermittent contact with a surface. *Phys. Rev. B 61*, 13381–13384.

[10] Anczykowski, B., Kruger, D., and Fuchs, H. (1996) Cantilever dynamics in quasinoncontact force microscopy: Spectroscopic aspects. *Phys. Rev. B 53*, 15485–15488.

[11] Haugstad, G. and Jones, R. R. (1999) Mechanisms of dynamic force microscopy on polyvinyl alcohol: region-specific non-contact and intermittent contact regimes. *Ultramicroscopy 76*, 77–86. I

[12] Salapaka, M. V., Bergh, H. S., Lai, J., Majumdar, A., and McFarland, E. (1997) Multi-mode noise analysis of cantilevers for scanning probe microscopy. *J. Appl. Phys. 81*, 2480–2487. I

[13] Stark, R. W., Drobek, T., and Heckl, W. M. (1999) Tapping-mode atomic force microscopy and phase-imaging in higher eigenmodes. *Appl. Phys. Lett. 74*, 3296–3298.

[14] Minne, S. C., Manalis, S. R., Atalar, A., and Quate, C. F. (1996) Contact imaging in the atomic force microscope using a higher order flexural mode combined with a new sensor. *Appl. Phys. Lett. 68*, 1427–1429. I

[15] Montelius, L. and Tegenfeldt, J. O. (1993) Direct observation of the tip shape in scanning probe microscopy. *Appl. Phys. Lett. 62*, 2628–2630. I

[16] Ramirez-Aguilar, K. A. and Rowlen, K. L. (1998) Tip characterization from afm images of nanometric spherical particles. *Langmuir 14*, 2562–2566.

[17] Velegol, S. B., Pardi, S., Li, X., Velegol, D., and Logan, B. E. (2003) Afm imaging artifacts due to bacterial cell height and afm tip geometry. *Langmuir 19*, 851–857.

[18] Villarrubia, J. S. (1997) Algorithms for scanned probe microscope image simulation, surface reconstruction, and tip estimation. *J. Res. Natl. Inst. Stand. Technol. 102*, 425–454. I, IV H

[19] Ashhab, M., Salapaka, M. V., Dahleh, M., and Mezic, I. (1999) Dynamical analysis and control of microcantilevers. *Automatica 35*, 1663–1670. I

[20] Schitter, G., Menold, P., Knapp, H. F., Allgower, F., and Stemmer, A. (2001) High performance feedback for fast scanning atomic force microscopes. *Rev. Sci. Instrum. 72*, 3320–3327.

[21] El Rifai, O. M. and Youcef-Toumi, K. (2007) On automating atomic force microscopes: An adaptive control approach. *Cont. Eng. Prac. 15*, 349–361. I

[22] Melcher, J., Hu, S., and Raman, A. (2008) Invited article: Veda: A web-based virtual environment for dynamic atomic force microscopy. *Rev. Sci. Instrum. 79*. I

[23] Kiracofe, D., Melcher, J., and Raman, A. (2012) Gaining insight into the physics of dynamic atomic force microscopy in complex environments using the veda simulator. *Review of Scientific Instruments 83*, 013702. I, IV A 17

[24] Hu, S. (2007) Ph.D. thesis (Purdue University). 1, 4

[25] Xu, X. and Raman, A. (2007) Comparative dynamics of magnetically, acoustically, and brownian motion driven micro-cantilevers in liquids. *J. Appl. Phys. 102*, 034303. II C, 5, 3

[26] Melcher, J., Xu, X., and Raman, A. (2008) Multiple impact regimes in liquid environment dynamic atomic force microscopy. *Appl. Phys. Lett. 93*, 093111. III C 1, IV C 1

[27] Sahin, O., Quate, C. F., Solgaard, O., and Atalar, A. (2004) Resonant harmonic response in tapping-mode atomic force microscopy. *Phys. Rev. B 69*, 165416. III C 3, IV C

[28] Sahin, O., Yaralioglu, G., Grow, R., Zappe, S. F., Atalar, A., Quate, C., and Solgaard, O. (2004) High-resolution imaging of elastic properties using harmonic cantilevers. *Sensor Actuat. A-Phys. 114*, 183–190.

[29] Sahin, O. (2007) Harnessing bifurcations in tapping-mode atomic force microscopy to calibrate time-varying tip-sample force measurements. *Rev. Sci. Instrum. 78*.

[30] Sahin, O., Magonov, S., Su, C., Quate, C. F., and Solgaard, O. (2007) An atomic force microscope tip designed to measure time-varying nanomechanical forces. *Nature Nanotechnology 2*, 507–514.

[31] Sahin, O. (2008) Time-varying tip-sample force measurements and steady-state dynamics in tapping-mode atomic force microscopy. *Phys. Rev. B 77*. III C 3, IV C

[32] Lozano, J. R. and García, R. (2009) Theory of phase spectroscopy in bimodal atomic force microscopy. *Physical Review B 79*, 014110. III C 5, III C 5, IV I

[33] Rajabifar, B., Jadhav, J. M., Kiracofe, D., Meyers, G. F., and Raman, A. (2018) Dynamic afm on viscoelastic polymer

samples with surface forces. *Macromolecules 51*, 9649–9661. III E, IV B 8
[34] Jordan, D. W. and Smith, P. (1999) *Nonlinear Ordinary Differential Equations*. (Oxford University Press). III F 1
[35] deBeer, S., Ende, D., and Mugele, F. (2010) Dissipation and oscillatory solvation forces in confined liquids studied by small-amplitude atomic force spectroscopy. *Nanotechnology 21*, 325703. III H 1, IV A 19
[36] Read, B. E. (1989) Mechanical relaxation in isotactic polypropylene. *Polymer 30*, 1439 – 1445. III H 2, 69
[37] Nony, L. and Baratoff, A. (2006) Noncontact atomic force microscopy simulator with phase-locked-loop controlled frequency detection and excitation. *Phys. Rev. B 74*, 235439. III I 1, IV A 12
[38] Kilpatrick, J. I., Gannepalli, A., Cleveland, J. P., and Jarvis, S. P. (2009) Frequency modulation atomic force microscopy in ambient environments utilizing robust feedback tuning. *Rev. Sci. Inst. 80*, 23701. III I 1
[39] Sader, J. E. and Jarvis, S. P. (2004) Accurate formulas for interaction force and energy in frequency modulation force spectroscopy. *Appl. Phys. Lett. 84*, 1801–1803. III I 1
[40] Butt, H. J., Cappella, B., and Kappl, M. (2005) Force measurements with the atomic force microscope: Technique, interpretation and applications. *Surf. Sci. Rep. 59*, 1–152. IV A 3, IV A 5, IV A 5
[41] Mase, G. and Mase, G. (1999) *Continuum mechanics for engineers*. (CRC). IV A 3, IV B 2, IV B 4
[42] Derjaguin, B., Muller, V., and Toporov, Y. (1975) Effect of contact deformations on adhesion of particles. *Journal Colloid Interface Sci. 53*, 314–326. IV A 5, VIII
[43] Israelachvili, J. (1985) *Intermolecular and Surface Forces*. (Academic Press). IV A 5, IV A 16, IV A 16, IV A 16, IV A 16, VIII
[44] Basak, S. and Raman, A. (2007) Dynamics of tapping mode atomic force microscopy in liquids: Theory and experiments. *Appl. Phys. Lett. 91*, 064107. IV A 6, IV C, IV C 4, IV C 6
[45] Johnson, K., Kendall, K., and Roberts, A. (1971) Surface energy and contact of elastic solids. *Proc. Roy. Soc. A 324*, 301. IV A 7
[46] Maugis, D. (1992) Adhesion of spheres - the jkr-dmt transition using a dugdale model. *J. Colloid Interface Sci. 150*, 243–269. IV A 7
[47] Dankowicz, H. and Paul, M. R. (2009) Discontinuity-induced bifurcations in systems with hysteretic force interactions. *Proc 9th Bienial Conf Engr Sys and Anal* pp. 633–641. IV A 7
[48] Chadwick, R. S. (2002) Axisymmetric indentation of a thin incompressible elastic layer. *SIAM J. Appl. Math. 62*, 1520–1530. IV A 8, IV A 8
[49] Dimitriadis, E. K., Horkay, F., Maresca, J., Kachar, B., and Chadwick, R. S. (2002) Determination of elastic moduli of thin layers of soft material using the atomic force microscope. *Biophysical journal 82*, 2798–2810. IV A 9
[50] Gavara, N. and Chadwick, R. S. (2012) Determination of the elastic moduli of thin samples and adherent cells using conical atomic force microscope tips. *Nature nanotechnology 7*, 733. IV A 9
[51] Hölscher, H., Schwarz, A., Allers, W., Schwarz, U. D., and Wiesendanger, R. (2000) Quantitative analysis of dynamic-force-spectroscopy data on graphite(0001) in the contact and noncontact regimes. *Phys. Rev. B 61*, 12678–12681. IV A 10
[52] Xu, L. and Salmeron, M. (2001) *Nano-Surface Chemistry*, ed. Rosoff, M. (Marcel Dekker Inc), pp. 243–287. IV A 13, 85
[53] Gil, A., Colchero, J., Gomez-Herrero, J., and Baro, A. (2003) Electrostatic force gradient signal: resolution enhancement in electrostatic force microscopy and improved kelvin probe microscopy. *Nanotechnology 14*, 332. IV A 13
[54] Kober, M., Sahagun, E., Fuss, M., Briones, F., Luna, M., and Saenz, J. J. (2008) Adhesion hysteresis in dynamic atomic force microscopy. *Physica Status Solidi - Rapid Research Letters 2*, 138–140. IV A 14, VIII
[55] Hinterdorfer, P., Baumgartner, W., Gruber, H. J., Schilcher, K., and Schindler, H. (1996) Detection and localization of individual antibody-antigen recognition events by atomic force microscopy. *Proceedings of the National Academy of Sciences 93*, 3477–3481. IV A 15
[56] Stroh, C., Wang, H., Bash, R., Ashcroft, B., Nelson, J., Gruber, H., Lohr, D., Lindsay, S. M., and Hinterdorfer, P. (2004) Single-molecule recognition imaging microscopy. *Proceedings of the National Academy of Sciences of the United States of America 101*, 12503–12507. IV A 15
[57] Bustamante, C., Marko, J., Siggia, E., and Smith, S. (1994) Entropic elasticity of lambda-phage dna. *Science 265*, 1599–600–. IV A 15
[58] Fuss, M., Sahagún, E., Köber, M., Briones, F., Luna, M., and Sáenz, J. (2009) Phase contrast in simultaneous topography and recognition imaging. *Ultramicroscopy 109*, 1189 – 1192. IV A 15
[59] Jeffery, S., Hoffmann, P. M., Pethica, J. B., Ramanujan, C., Özer, H. O., and Oral, A. (2004) Direct measurement of molecular stiffness and damping in confined water layers. *Physical Review B 70*, 054114. IV A 16, IV A 16, IV A 16, IV A 17
[60] Butt, H., Graf, K., Kappl, M., and Wiley, J. (2003) *Physics and chemistry of interfaces*. (Wiley-VCH). IV A 16
[61] Kaggwa, G. B., Kilpatrick, J. I., Sader, J. E., and Jarvis, S. P. (2008) Artifact-free dynamic atomic force microscopy reveals monotonic dissipation for a simple confined liquid. *Applied Physics Letters 93*, 011909. IV A 17
[62] Rasa, M., Kuipers, B., and Philipse, A. (2002) Atomic force microscopy and magnetic force microscopy study of model colloids. *Journal of colloid and interface science 250*, 303–315. IV A 18
[63] Garcia, R., Gomez, C. J., Martinez, N. F., Patil, S., Dietz, C., and Magerle, R. (2006) Identification of nanoscale dissipation processes by dynamic atomic force microscopy. *Phys. Rev. Lett. 97*, 016103. IV B 2
[64] Melcher, J., Carrasco, C., Xu, X., Carrascosa, J., Gómez-Herrero, J., José de Pablo, P., and Raman, A. (2009) Origins of phase contrast in the atomic force microscope in liquids. *Proceedings of the National Academy of Sciences 106*, 13655. IV B 2
[65] Johnson, K. L. (1985) *Contact Mechanics*. (Cambridge University Press). IV B 2, IV B 4, IV B 5
[66] Lee, E. H. and Radok, J. R. M. (1960) The contact problem for viscoelastic bodies. *Journal of Applied Mechanics 27*, 438–444. IV B 2

[67] Ting, T. C. T. (1966) The contact stresses between a rigid indenter and a viscoelastic half. *Journal of Applied Mechanics.* IV B 2, IV B 8
[68] Mainardi, F. and Spada, G. (year?) Creep, relaxation and viscosity properties for basic fractional models in rheology. IV B 5
[69] Kelley, P. A. (year?) Mechanics lecture notes: An introduction to solid mechanics. IV B 5
[70] Nielsen, L. and Landel, R. (1994) *Mechanical properties of polymers and composites.* (CRC Press). IV B 6
[71] Park, S. and Schapery, R. (1999) Methods of interconversion between linear viscoelastic material functions. part i—a numerical method based on prony series. *International Journal of Solids and Structures 36*, 1653–1675. IV B 6
[72] Attard, P. (2001) Interaction and deformation of viscoelastic particles. 2. adhesive particles. *Langmuir 17*, 4322–4328. IV B 8
[73] Attard, P. (2001) Interaction and deformation of viscoelastic particles: Nonadhesive particles. *Physical Review E 63*, 061604. IV B 8
[74] Attard, P. and Parker, J. L. (1992) Deformation and adhesion of elastic bodies in contact. *Physical Review A 46*, 7959. IV B 8, IV B 8
[75] Attard, P. (2000) Interaction and deformation of elastic bodies: origin of adhesion hysteresis. *The Journal of Physical Chemistry B 104*, 10635–10641. IV B 8
[76] Rodriguez, T. R. and Garcia, R. (2002) Tip motion in amplitude modulation (tapping-mode) atomic-force microscopy: Comparison between continuous and point-mass models. *Appl. Phys. Lett. 80*, 1646–1648. IV C
[77] Balantekin, M. and Atalar, A. (2005) Enhanced higher-harmonic imaging in tapping-mode atomic force microscopy. *Appl. Phys. Lett. 87*, 243513. IV C
[78] Proksch, R. (2006) Multifrequency, repulsive-mode amplitude-modulated atomic force microscopy. *Appl. Phys. Lett. 89.* IV C
[79] Lozano, J. R. and Garcia, R. (2008) Theory of multifrequency atomic force microscopy. *Phys. Rev. Lett. 1.* IV C
[80] Melcher, J., Hu, S., and Raman, A. (2007) Equivalent point-mass models of continuous atomic force microscope probes. *Appl. Phys. Lett. 91*, 053101. IV C, IV C 1, IV C 3, IV C 9
[81] Han, W., Lindsay, S., and Jing, T. (1996) A magnetically driven oscillating probe microscope for operation in liquids. *Appl. Phys. 69*, 4111–4113. IV C 2
[82] Janovjak, H., Struckmeier, J., and Muller, D. J. (2005) Hydrodynamic effects in fast afm single-molecule force measurements. *Eur. Biophys. J. Biophy. 34*, 91–96. IV C 2
[83] Merirovitch, L. (1997) *Principals and Techniques of Vibrations.* (Prentice Hall, New Jersey). IV C 4, IV C 4
[84] Buguin, A., Du Roure, O., and Silberzan, P. (2001) Active atomic force microscopy cantilevers for imaging in liquids. *Applied Physics Letters 78*, 2982. IV C 7
[85] Han, W. H., Lindsay, S. M., and Jing, T. W. (1996) A magnetically driven oscillating probe microscope for operation in liquids. *Appl. Phys. Lett. 69*, 4111–4113. IV C 7
[86] Penedo, M. and Luna, M. (2011) Enhanced efficiency in higher modes excitation for afm in liquids by means of magnetostrictive actuation. IV C 7
[87] Ramos, D., Tamayo, J., Mertens, J., and Callega, M. (2006) Photothermal excitation of microcantilevers in liquids. *Journal of Applied Physics 99*, 124904. IV C 7
[88] Pini, V., Tiribilli, B., Gambi, C., and Vassalli, M. (2010) Dynamical characterization of vibrating afm cantilevers forced by photothermal excitation. *Physical Review B 81*, 54302. IV C 7
[89] Basso, M., Paoletti, P., Tiribilli, B., and Vassalli, M. (2008) Modelling and analysis of autonomous micro-cantilever oscillations. *Nanotechnology 19*, 475501. IV C 8, IV C 8
[90] Hutter, J. L. and Bechhoefer, J. (1993) Calibration of atomic-force microscope tips. *Rev. Sci. Instrum. 64*, 1868–1873. IV C 9
[91] Brenan, K., Campbell, S., and Petzold, L. R. (1989, republished by SIAM, 1996) *Numerical Solution of Initial Value Problems in Differential Algebraic Equations.* (Elsevier, New York). IV G
[92] Ascher, U. M. and Petzold, L. R. (1998) *Computer methods for ordinary differential equations and differential-algebraic equations.* (SIAM), pp. 3 – 305.
[93] VanKeken, P. E., Yuen, D. A., and Petzold, L. R. (1995) Daspk: A new high order and adaptive time-integration technique with applications to mantle convection with strongly temperature- and pressure-dependent rheology. *Geophys. Astrophys. Fluid Dyn. 80*, 57–74.
[94] Brown, P. N., Hindmarsh, A. C., and Petzold, L. R. (1994) Using krylov methods in the solution of large-scale differential-algebraic systems. *SIAM J. Sci. Compu. 15*, 1467–1488. VII
[95] Landman, U. and Luedtke, W. D. (1991) Nanomechanics and dynamics of tip substrate interactions. *J. Vac. Sci. Technol. B 9*, 414–423. IV G
[96] Anczykowski, B., Gotsmann, B., Fuchs, H., Cleveland, J. P., and Elings, V. B. (1999) How to measure energy dissipation in dynamic mode atomic force microscopy. *Appl. Surf. Sci. 140*, 376–382. IV I
[97] Derjaguin, B. and Landau, L. (1945) Theory of stability of highly charged liophobic sols and adhesion of highly charged particles in solutions of electrolytes. *Zhurnal Eksperimentalnoi I Teoreticheskoi Fiziki 15*, 663–682. VIII
[98] Basak, S., Raman, A., and Garimella, S. V. (2006) Hydrodynamic loading of microcantilevers vibrating in viscous fluids. *J. Appl. Phys. 99*, 114906. VIII